Spectroscopic Analysis and Characterisation of Cosmetic Powders

A thesis submitted in fulfilment of requirements for the degree of Doctor of Philosophy

Elizabeth Kulikov

Bachelor of Science (Applied Chemistry) (Honours)

School of Applied Science

RMIT University

October 2013

Declaration

I certify that except where due acknowledgement has been made, the work is that of the author alone; the work has not been submitted previously, in whole or in part, to qualify for any other academic award; the content of the thesis is the result of work which has been carried out since the official commencement date of the approved research program; any editorial work, paid or unpaid, carried out by a third party is acknowledged; and, ethics procedures and guidelines have been followed.

Elizabeth Kulikov

03/10/2013

Acknowledgements

I would like to first and foremost thank my supervisor, Professor Mike Adams, whose guidance and support throughout my PhD candidature, has enabled me to achieve my final goals. I am extremely grateful for your encouragement and sharing your extensive knowledge and skills with me.

A special thanks to my second supervisor, Associate Professor Kay Latham for her advice and expertise and encouragement throughout my research project.

I would like to thank the following University staff that have helped me in various ways throughout my time at RMIT, Mr. Karl Lang, Mr. Frank Antolasic, Mrs. Zara Holman, Mrs. Nadia Zakhartchouk, Ms. Ruth Cerpriano, Mrs. Dianne Mileo and Dr. Lola Suarez Barranco.

I am very grateful to my fellow PhD students for their constant understanding and support but also being there to have a laugh. To Kat Fortig, Vivian Li, Andrew Basile and Nicholas Nola, you have made my time at RMIT all the more enjoyable. I must give a big thanks to Fiona Charalambous and Rahul Ram, who gave me confidence and guidance when it was most needed. I thank you both for encouraging me believe I had the ability to undertake my PhD.

To my wonderful girls, thank you for your constant support and encouragement. Thanks for showing an interest in my research and counting on your friendships when I'm feeling stressed. I can always turn to you girls to make me smile.

I cannot express enough appreciation to my boyfriend, Eldon Abbott. I thank him for his patience, support and editing skills.

This thesis is dedicated to my parents, Christine Kulikov and Fred Kulikov and siblings Catherine and Simon. Thanking you for your continued support on my long endeavour. Even

though they may not completely understand my work, they have never once questioned or discouraged me from pursuing an education in science.

Publications

Published

- **Classification and discrimination of some cosmetic face powders using XRF spectrometry with chemometric data analysis,** *X-Ray Spectrometry, Volume 41, Issue 6, 2012, pp.410-415.* Elizabeth Kulikov, Kay Latham and Michael J. Adams.

In Preparation

- **X-ray (Fluorescence and Diffraction) Analysis of Cosmetic Powders**
- **Infrared Characterisation of Cosmetic Powders**

Table of Contents

List of Figures

List of Tables

Abstract

The material components of 39 cosmetic foundation powders, 23 being mineral-based and 17 traditional-based formulations, have been studied by X-ray Fluorescence (XRF), X-ray powder Diffraction (XRD) and spectroscopic analysis in the visible region, and mid and near-infrared regions. Chemometric applications including Principal Component Analysis (PCA), 2D correlation and multivariate curve resolution techniques have been applied to data to aid in interpretation and classify samples based on similarities and differences in formulations.

The composition of mineral and traditional-based foundation powders was found to be quite different. Traditional formulations comprised of talc and, in some cases, calcium carbonate, while mineral-based samples contained larger amounts of mica. Some samples, denoted by their producers as mineral samples, were subsequently classified as traditional as they contained talc in their formulations.

2D correlation applied across two spectroscopic methods highlights positive correlating spectral features between techniques. Elemental concentrations produced through XRF analysis, were correlated with XRD data. In this manner XRF data successfully aided the interpretation of XRD data and confirmed components that could be represented by a single element in their component phases, in particular, zinc oxide, bismuth oxychloride and titanium dioxide.

FTIR (Fourier Transform Infrared Spectroscopy) analysis of samples in the mid and near infrared regions provided information on the structural and chemical composition of foundation samples. Correlation of XRD data and spectral data in the mid-infrared region confirmed the presence of talc, kaolin, calcium carbonate and mica in samples.

In general, mineral-based samples could be discriminated based on manufacturer, but traditional-based samples could not. The techniques and data analysis methods developed and applied here could be of benefit to the analysis of other complex, solid samples.

Chapter 1: Introduction

1.1 History of Cosmetics

Cosmetics have been used since mankind's earliest days. There has long been a desire by individuals to improve their appearance and artificially enhance their sexual attraction and the cosmetics trade and industry have a long history [1]. Make-up has been used to enhance facial colour since before 4000BC. The Ancient Egyptians led the way in cosmetic production, developing innovative formulations for their beauty needs. They decorated their eyes with green, white and black make-up. The use of black eye liners, known as kohls, was very popular, and was used to emphasise the eyes [2]. Kohl was generally made of galena or lead sulphide. It was believed that eye make-up could ward off bad spirits and improve eye-sight [3]. One of the first known eye shadows was the green ore malachite ($CuCO_3.Cu(OH)_2$) but Egyptians also used a finely ground form of antimony trisulfide to darken their eye-lids and give lustre to their eyes [4]. Other studies have identified two natural lead-based compounds: crushed ore of galena (PbS) and cerrussite ($PbCO_3$) present in Egyptian powders dating from between 2000 and 1200BC. Other components were laurionite (PbOHCl) and phosgenite ($Pb_2Cl_2CO_3$). Since neither is naturally occurring, it is assumed that the Egyptians synthesised these compounds using wet chemistry [5]. In prehistoric times, colour was used by man in cave paintings. The skin was coloured either as a camouflage or to provoke fear in an enemy. Various civilisations throughout history have used cosmetics in their customs, in particular body paints. The Australian aborigines daubed their faces with white clay and wore wreaths made of flowers and feathers. The North American Indians, decorated their bodies with brightly coloured war paints [6]. Make-up was not for common use amongst the public

in Ancient times. In ancient Greece and Rome, only the political elite and wealthy used such products [1]. Among the many things that the Romans used were white lead and chalk to whiten their skin.

Like the Ancient Egyptians, kohl was used as make-up for the eyes. Hair dye was popular and ranged from blonde to dark brown, according to the prevailing trends [6].

By the nineteenth century, the use of cosmetics was widespread throughout Europe. The church condoned its use, as it was primarily used by prostitutes and only acceptable for theatre. A pale face was desired as it defined an individual's place in society. Those with pale skin were associated with the upper class and differed from those in the working class that were more exposed to the European sun. Thus, the higher class women of European society, attempted to lighten their skin to emphasise their delicacy and femininity. White lead paint was used, which also may have contained arsenic. Cheeks were stained with rouge comprised of red ochre and vermilion, a naturally occurring mercuric oxide. The trend of using toxic chemicals to promote beauty, continued throughout the nineteenth century. Eventually, lead was replaced with zinc oxide for the whitening effect. The absence of regulations of the use and manufacture of cosmetics led to many negative side effects. The whitening of the skin through lead-based cosmetics caused deformities, blindness and even death [3].

1.2 Typical modern formulations

Today, cosmetic preparations are commonplace consumer products and are used to help correct flaws and improve the appearance of human skin [1]. Cosmetic ingredients are listed in the International Cosmetic Ingredient Dictionary and Handbook, with over 10,000 individual chemicals that are, or have been, used in cosmetic production [7].

The cosmetic, toilet and fragrance industry can be divided into five main categories: skin care, hair care, make-up, fragrances and personal hygiene. Make-up products have global sales of around $22.5 billion annually and can be categorised into four groups as illustrated in Figure 1.1 [8]. Make-up preparations generally refer to products used on various parts of the face [1]. Applied to the skin's surface, to hide blemishes and give the skin an overall smooth finish, foundations (in the form of liquid, mousse, cream, loose or pressed powder) are used in conjunction with concealers, bronzers and blushes. The eye area focuses on contouring products to emphasise and highlight features with coloured eye shadows (cream, powder or pencil), varying shades of eye-liners and mascara to highlight lashes [1]. Finally, a variety of colours of lipsticks, lip-liners, glosses and lip balm conditioners can be applied to the lips.

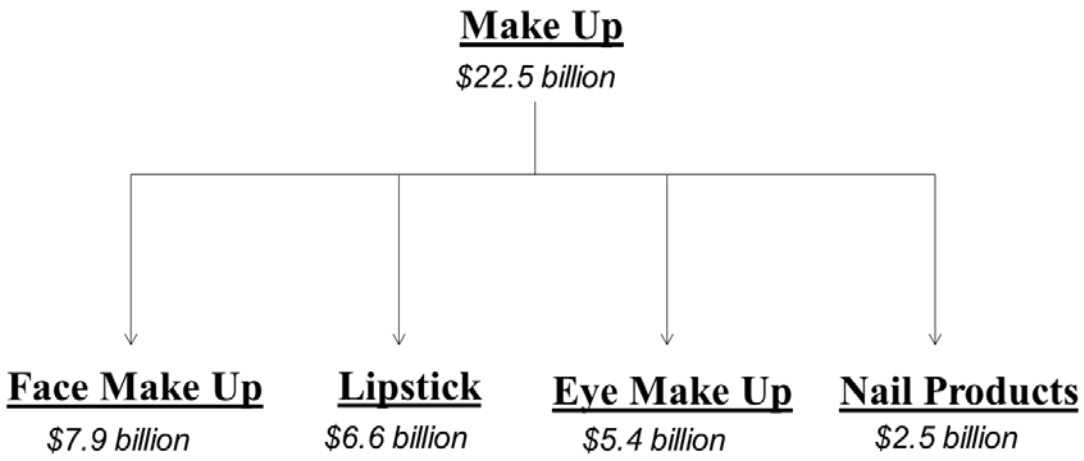

Figure 1.1 Classification of Make-up Products and global market figures based on sales in 2001 [8].

Laws and legislation concerning regulations for consumer products vary worldwide. In Australia, cosmetic products must meet the definition of cosmetic in Australia under the Industrial Chemicals (Notification and Assessment) Act 1989, which states that a cosmetic is ‘any substance or preparation intended for placement in contact with any external part of the human body’. Ingredients used in cosmetic production are monitored by the NICNAS

(National Industrial Chemicals Notification and Assessment Scheme) as they are classed as industrial chemicals, even those that are described as naturally occurring. This act ensures that products do not contain chemicals prohibited for use and meet restrictions specified for chemicals used in cosmetics. Ingredients must comply with changed legislative requirements and new cosmetic ingredients are subjected to notification and assessment (NICNAS Cosmetic Guidelines 2007). All cosmetic products must follow trade practice regulations (Consumer Product Information Standards- Cosmetics Regulations 1991) that require the product ingredients to be listed on the container or the product itself, in descending order calculated by either mass or volume [9]. There are also allowed processes in which certain methods are only to be used when producing both organic and non-organic ingredients for cosmetic formulations.

One of the most widely used class of cosmetic products is foundation powder. In 2001, the Global Cosmetics reports indicated that make up products constituted roughly 18% of the total global market for cosmetics, with $7.9billion of sales for face make-up alone [8]. Foundation powders consist of a mixture of inorganic oxides (typically iron, titanium and zinc) in a base of clay minerals (usually kaolinite with mica and occasionally talc) that serve several important functions necessary to produce a quality consumer product [1]. The various properties that a foundation powder must have to be considered a good product include; ability to cover the skin, hide shine and blemishes, readily spread over the skin, adhere to the face, absorb oils and perspiration and give a smooth finish [10]. The ability of face powders to display these properties lies in the materials used and their physical properties (particle size and shape, surface area, texture, colour and brightness) and chemical properties (surface chemistry and charge) [11]. Table 1.1 shows the composition of loose and pressed foundation powders. Loose and pressed powder samples have similar raw materials; however, pressed

powders contain organic binders. Binders can consists of a combination of various components such as fats, waxes and polymer powders to aid in ingredient compression and adhesion [12].

Table 1.1 Typical composition of foundation powders [6&12].

Raw Materials	**Loose Powder**	**Pressed Powder**
Talc	quantum satis	quantum satis
Mica (%)	10	10
Texture Agents (%)	15-35	15-35
Mineral Pigments (%)	<2	<10
Pearls (%)	<5	<5
Binder (%)	None	3 to 8

Traditionally, these cosmetics are made from clay materials such as talc and kaolin. Talc (hydrated magnesium silicate ($Mg_3Si_4O_{10}(OH)_2$)), aids in skin adhesion and provides water repellency, as well as absorbing and holding fragrances. It is odourless and can be easily milled, becoming a bright white powder. A good grade of talc, should be white and free of potential impurities such as carbonates, water soluble iron and asbestos. Variations in the shape and particle morphology of talc affect properties such as, covering powder and wettability [11]. Generally, the smaller the particle size the smoother it will be, but if talc is ground too fine, it begins to have a gritty feel [6].

Kaolin (hydrated aluminium silicate ($Al_2Si_2O_5(OH)_4$)) imparts and maintains a smooth, matte appearance, preventing the product from caking. There are three different groups of clays that are classified as kaolin, kaolinite, nacrite and dickite, all having similar chemical formulae.

Kaolin is added for its grease resistant and perspiration absorbent properties. Kaolin has a moderate covering power and the grade used (white colour to a pale creamy colour) contributes to the face powder tint [13]. It has a characteristic earthy taste and clay like odour when wet. It has a relatively low surface area but has the ability to absorb small molecular substances [11]. Kaolinite and talc are extensively used in the formulation of various cosmetic products. They serve as a base or excipient, and must comply with a number of textural and compositional requirements and have specific technical properties. Lopez-Galindo et al. have reviewed the technical and safety specifications of clays used in pharmaceutical and cosmetic products [11]. Sericite, a naturally fine-grained form of mica ($KAl_2(AlSi_3O_{10})$) is used to impart a shine within the powder [12].

Inorganic pigments used include zinc oxide and titanium dioxide for whiteness and iron oxides for red, brown and other earth tones. There are three basic shades of iron oxides: yellow (hydrated ferrous oxide, $FeO \cdot nH_2O$), red (ferric oxide, Fe_2O_3) and black (which is a mixture of both yellow and red iron oxides) [14]. Zinc oxide is present in moderately low levels and is often incorporated into products due to its astringent health benefits such as soothing properties to the skin as well as sun protection, by filtering and reflecting UV rays [6]. Titanium dioxide also acts as a natural sunblock and is three times a better covering agent than zinc oxide [13]. Other ingredients used, such as calcium carbonate, give a matte finish, zinc and magnesium stearates for binding and water proofing properties may be included and boron nitride which attributes application properties such as skin feel and texture [10, 12].

So-called mineral foundations are relatively new products to the cosmetic industry and are becoming increasingly popular as an alternative to traditional formulations. They have wide appeal due to their use of so-called ‘natural’ ingredients and associated health benefits to the

skin. There are many claims with these new mineral based formulations. Manufacturers claim that they contain anti-inflammatory properties to calm irritated skin. They are oil-free, causing no pore blockages and give a light weight feel, making them suitable for individuals with sensitive and allergy-prone skin. Mineral foundation powders essentially use many of the same chemicals found in traditional formulas, but it is the ingredients they do not contain that contributes to their skin-friendly benefits. Cosmetics are expected to do more than add colour and cover skin imperfections, but should also contain ingredients such as sunscreens and emollients to nourish and protect their skin [8]. Today most makeup preparations have new and improved ingredients that include sunscreens. As public environmental awareness has increased, items seen as safe for the environment are perceived as healthy for users. This philosophy has driven a trend toward increased use of natural products.

Mineral foundations are often referred to as being ‘chemical free’ as they purport to contain no potential skin irritants such as fragrances, talcs, dyes or preservatives [1]. However, formulations vary considerably and there is often little and confusing information regarding what constitutes a ‘mineral’ foundation. Although the safety and effectiveness of cosmetic products are regulated worldwide, laws and regulations vary greatly between countries, often making it impossible for a global industry to be selling the same product [14]. Concerns lie with those manufacturers who do not specify whether they solely contain natural, pure minerals. According to the Australian Trade Practices, ‘naturally occurring’ ingredients are those that are unprocessed in their natural state or only extracted by manual, mechanical, gravitational means, dissolution in water, or heating to remove uncombined water, without any chemical change. For example, bismuth oxychloride is a known skin irritant but is often incorporated into mineral formulations as it is classed as a mineral even though it is not a natural mineral but is a by-product of lead processing. Bismuth oxychloride was originally

developed in cosmetics as a non-toxic alternative to lead carbonate and is in common use [15].

There is no requirement for listing the proportion of each ingredient within a product. The exact composition is not easily determinable from the product labelling and may only be known by the manufacturer [8]. The Australian Government ensures that all ingredients in cosmetic products are classed as industrial chemicals, even those described as 'naturally occurring'. To ensure that all products are safe for workers, the environment and use by consumers, the Australian Government assess the ingredients used in the manufacture and importation of cosmetics in Australia.

1.3 Analytical Methods

It has only been in the last century that science has been applied to the characterization of cosmetic products. Cosmetic preparations typically consist of complex mixtures of many components, and a wide variety of analytical methods must be employed to identify and fully characterise an unknown material. The analysis of ancient cosmetics is extensive [16-19]. Ancient Egyptian burial tombs have been found to have cosmetic powders, preserved in stone vases, reeds and wooden containers [20]. In most cases, the chemical analysis of ancient cosmetic remains is essential in understanding the customs of everyday life in those times and the chemical processes involved in the production. One method that has been extensively used for the characterisation of cosmetics found in ancient civilisations is infra-red spectroscopy. Diffuse reflectance FT-IR is highly effective in providing information concerning the chemical composition and structure of cosmetic foundation powders. It is a fast, non-destructive technique with simple sample preparation. Vibrational spectroscopic techniques, FT-IR and Raman spectroscopy, have been used as complementary methods for

the identification of clay minerals and inorganic pigments. Cosmetic containers frequently found in Ancient Egypt burial sites, have been analysed using FT-IR, not only for its high detectivity of both organic and mineral components, but also due to the non-destructive nature of the technique when dealing with such delicate samples. Chemical analysis of these samples is undertaken to give a greater understanding of their production process, and, in general, for the chemical knowledge and practices in antiquity [21]. The use of FT-IR and near-infrared (NIR) are also effective in the quality control of cosmetic mixtures. In particular, the determination of components in cosmetic mixtures, combined with multivariate spectral processing chemometric techniques to ensure acceptable levels of each component have been used in cosmetic preparations [22].

X-ray diffraction is another non-destructive technique used to investigate the composition of cosmetic formulas. Analysis of cosmetics using XRD is not extensive but because certain ingredients used in cosmetics are highly crystalline it is an ideal method for identification. Ancient Egyptian makeup has been analysed using X-ray powder diffraction not only to identify galena (PbS) as a major ingredient but also identify structural parameters to help in the interpretation of the manufacturing process applied by ancient Egyptians to produce eye makeup [20].

Although there are relatively few published reports on the elemental analysis of cosmetic powders, neutron activation and X-ray methods are most commonly referenced due to their non-destructive nature and their ability to examine the sample without prior dissolution. Thus Kanias has reported the analysis for iron and zinc in cosmetic products including eye shadows and face powders using instrumental neutron activation (INAA) [23]. This author has also applied the technique to trace element analysis, including determination of the lanthanide elements, in cosmetic powders [24]. Using INAA the trace elemental analysis of nail polishes

as a potential source of contamination in analysing nail clippings has been examined by Favaro et al. [25].

Kawauchi et al, reported the measurement of titanium dioxide in cosmetic products with XRF spectrometry [26]. Cosmetic traces are sometimes found as evidence on clothing, crime scene surfaces, etc. They can be successfully analysed using XRF techniques [27] and the elemental profile may be useful in identifying samples made by different manufacturers. Misra et al. successfully applied EDXRF (Energy Dispersive XRF) to the analysis of cosmetic evidence in nail polishes [28]. The evidential value of cosmetic foundation powder smears in forensic casework was reviewed by Gordon and Coulson. Fifty-three different foundation samples from 15 manufacturers were collected with the aim of determining the most discriminating method for the comparison of transferred foundation with samples obtained from a known source in forensic casework [29]. The authors employed statistical analysis of multidimensional, continuously variable elemental data from the SEM-EDX (Scanning Electron Microscope-Energy Dispersive X-ray Spectroscopy) results. Common elements found in foundations included Al, Si, S, Cl, K, Ti and Fe. The forensic analysis of cosmetic face powders was examined by Greenhough, who used a range of analytical techniques including FTIR, SEM and mass spectrometry to characterize 27 samples [30].

Various cosmetic products have been used as evidence in forensic cases. Lipstick smears are often encountered in forensic laboratories

1.4 Project Aims

The aim of this project is to investigate some appropriate analytical techniques, and develop new analysis methodologies, to characterise the inorganic composition of cosmetic foundations. To date, there are few reports in the public domain regarding the chemical analysis of mineral cosmetic foundations and, hence, little background information for

consumers relating to product authenticity and techniques for classification. There is little information for consumers regarding the nature and purpose of materials used in the production process. In addition, characterisation and classification of such samples produces reference work which may be useful for chemists in understanding the science involved in developing new products [31]. Cosmetic foundations are composed of a combination of inorganic oxides and clay minerals. The most common analytical techniques employed for the analysis of such materials are spectroscopic methods. The techniques employed in this work for analysis, included; X-Ray Fluorescence for quantitative multi-elemental analysis, X-Ray Powder Diffraction to investigate the structural information on the crystalline content and vibrational spectroscopy mid-infrared and near-infrared methods to confirm chemical composition and structure of cosmetic foundations.

Interpretation of data is aided by the application of appropriate chemometric analysis techniques, such as principal component analysis, discriminant and cluster analysis, and 2D correlation to identify similarities and differences between samples.

Combining the information provided by the different analytical instruments and with the aid of chemometric interpretation we can essentially answer the following research questions:

1. To what extent can we quantitatively describe the composition of cosmetic foundations and can we identify a single substrate from its chemical composition, and hence, identify the manufacturer?
2. What classification techniques can be applied for successful comparison of two samples to see whether they come from the same or similar source?

Various analytical techniques were selected to investigate the composition of cosmetic powders. Full characterisation was required; therefore techniques had to provide a range of

qualitative and quantitative analysis methods. Due to the complexity of analysis and size of samples, techniques were carefully chosen as to their non-destructive nature. This was an important factor, as no change could be made to chemical composition of the sample. Crystalline structure may be damaged in the sample preparation and presentation process, and the sample had to be maintained for analysis over all analytical methods. The analytical techniques selected provide elemental analysis, phase analysis, chemical composition and colour determination.

1.5 References

1. Westmore M., *Camouflage and Makeup Preparations*, Clinics in Dermatology, Elsevier Science, 2001. **19**: p.406-412
2. Gamberini M, Baraldi C, Palazzoli F, Ribechini E and Baraldi P., *MicroRaman and infrared spectroscopic characterization of ancient cosmetics*, Vibrational Spectroscopy, 2008, **47**: p.82-90.
3. C. Hawks, *Cosmetic & Cosmetology*, World Technologies, New Delhi, **2012**.
4. A. D. Hardy, R. Vaishnaw, S. S. V. Al-Kharusi, H. H. Sutherland, M. A. Worthing, *Composition of eye cosmetics (kohls) used in Oman*, Journal of Ethanopharmacology, 1998, **60**(3): p.223-234.
5. P. Walter, P. Martinetto, G. Tsoucaris, R. Brniaux, M. A. Lefebvre, G. Richard, J. Talabot, E. Dooryhee, *Making make-up in Ancient Egypt, Nature*, 1999, **397**: p.483-484.
6. H. Butler, W. A. Poucher, *Poucher's perfumes, cosmetics and Soaps (9th Ed.)*, Kluwer Academic Publishers, Boston, **2000**.
7. W. F. Bergfeld, D. V. Belsito, J. G. Marks, F. A. Anderson, *Safety Ingredients used in Cosmetics*, Journal of American Academy of Dermatology, 2005, **52**(1): p.125-132.

8. S. Kumar, *Exploratory analysis of global cosmetic industry: major players, technology and market trends*, Technovation, 2005, **25**: p.1263-1272.
9. Australian Trade Practices- Consumer Product Information Standards (Cosmetics) Regulations 1991- http://www.comlaw.gov.au/Details/F2008C00244 -Date accessed: 29/03/2012.
10. Balsam, S., Gershon, Rieger and Strianse, *Cosmetics: Science and Technology. Vol. 1*, John Wiely & Sons Inc, **1972**.
11. A. Lopez-Galindo, C. Viseras, P. Cerezo, *Compositional, technical and safety specifications of clays to be used as pharmaceutical and cosmetic products*, Applied Clay Science, 2007, **36**: p.51-63.
12. J. E. Kogel, N. C. Trivedi, J. M. Baerker, S. T. Krukowski, *Industrial Minerals & Rocks- Commodities, Markets and Uses (7th Ed.)*, SME, Colorado, **2006**.
13. A. Kozlowski, *The Chemistry and Manufacture of Cosmetics (4th Ed.)*, Allured Books, **2008**.
14. S. Amparo, C. Alberto, *Analysis of Cosmetic Products*, Elsevier, Oxford, UK, **2007**.
15. J. E. KIogel, N. C. Trivedi, J. M. Barker, S. T. Krukowski, *Industrial Minerals and Rocks (7th Ed.)*, Soc Mining, Metallurgy and Exploration, Cororado, USA, **2006**.
16. P. Walter, P. Martinetto, G. Tsoucaris, R. Brniaux, M. A. Lefebvre, G. Richard, J. Talabot, E. Dooryhee, *Making make-up in Ancient Egypt*, Nature, 1999, **397**: p.483-484.
17. R. L. Frost, P. A. Williams and W. Martens, *Raman spectroscopy of the minerals boleite, cumengeite, diaboleite and phosgenite- implications for the analysis of cosmetic antiquity*, Mineralogical Magazine, 2003, **67**(1): p.103-111.
18. M. C. Gamberini, C. Baraldi, F. Palazzoli, E.Ribechini, P. Baraldi, *MicroRaman spectroscopic characterization of ancient cosmetics*, 2008, **47**(2): p.82-90.

19. E. V. Elslande, V. Guerineau, V. Thirioux, G. Richard, P. Richardin, O. Laprevote, G. Hussler, P. Walter, *Analysis of ancient Greco-Roman cosmetic materials using laser desorption ionization and electrospray ionization mass spectrometry*, Anal Bioanal Chem, 2008, **390**: p.1873-1879.
20. Ungar. T, Martinetto. P, Ribarik. G, Dooryhee. E, Walter. Ph, Anne.M, *Revealing the powdering methods of black makeup in Ancient Egypt by fitting microstructure based Fourier coefficients to the whole x-ray diffraction profiles of galena*, Journal of Applied Physics, 2002, **91**:(4) p.2455-2465.
21. M. Cotte, P. Dumas, G. Richard, R. Breniaux, Ph. Walters, *New insight on ancient cosmetic preparations by synchrotron-based infrared spectroscopy*, Analytica Chimica Acta, **2005**, 553: p.105-110.
22. M. Blanco, M. Alcala, J. Planells, R. Mulero, *Quality control of cosmetic mixtures by NIR*, Anal Bioanal Chem, 2007, **389**(5): p.1577-1583.
23. G. D. Kanias, *Instrumental neutron activation analysis of iron and zinc in compact cosmetic products*, Fres. Z. Anal. Chem, 1987, **327**: p. 351-354.
24. G. D. Kanias, *Determination of trace elements in eyeshadow face powder and rouge make-up cosmetics by neutron activation analysis*. J. Radioanalyt. Nucl. Chem, 1985, **89**: p.487-496.
25. P. C. Favaro, P. Bode, E. A. De Nadai Fernandes, *Trace elements in nail polish as a source of contamination of nail clippings when used in epidemiological studies*, J. Radioanalyt. Nucl. Chem, 2005, **264**: p.61-65.
26. A. Kawauchi, M. Ishida, I. Saitoh, *Measurement of titanium dioxide in cosmetic products with XRF spectrometry*, Spectroscopy Letters, 1996, **29**: p.345-366.
27. C. Roux, C. Lennard, *X-Ray Fluorescence in Forensic Science in Encyclopedia of Analytical Chemistry (Online)*, (Ed. R. A. Meyers) J. Wiley and Sons Ltd., **2006** ; 1-11

28. G. Misra, K. J. S. Sawhney, G. S. Lodha, V. K. Mittal, H. S. Sahota, *The Application of Energy-dispersive X-Ray Fluorescence Spectrometry (EDXRF) to Analysis of Cosmetic Evidence in Indian Nail Polishes*, Int. J. Radiat. Appl. Instrum. Part A, 1992, **43**: p.609-614.
29. A. Gordon, S. Coulson, *The Evidential Value of Cosmetic Smears in Forensic Casework, Journal of Forensic Science*, 2004, **49**: p.1244-1252.
30. K. Greenhough, *Forensic Analysis of Cosmetic Face Powders*, MSci Thesis, Michigan State Univ. **2007**.
31. W. H. Schmitt, *Chemistry & Technology of the Cosmetic and Toiletries Industry (2nd Ed.)*, Blackie Academic & Professional, London, **1996**.

Chapter 2: The Cosmetic Foundation Samples: Their appearance and Visible Spectra

2.1 Introduction

For cosmetic technicians, control of colour plays a vital role in producing quality face powders for consumers. Colourimetry, in the visible range (400nm-700nm) is employed to monitor colour, expressed in terms of red, green, yellow and blue values [1]. Currently, the US Food and Drug Administration (FDA) has approved the use of 64 colorants, inorganic or organic, dyes or pigments for use in cosmetic applications [2,3]. Foundation powder manufacturers, employ inorganic pigments in formulations to produce the variety of colours and shades available in the consumer market. Properties used to define the colour of cosmetics include, the hue, saturation or chroma and brightness. The hue defines the pure colour in terms of red, green, yellow or blue, and saturation is the amount of white that is mixed with the hue, providing a range of colour from 0-100%. A pure colour is considered to be fully saturated. Brightnes is a measure of the intensity of colour [4].

Visible spectroscopy is widely used in the analysis and identification of cosmetic products. Lipstick smears are often encountered as evidence in criminal forensic cases and the comparison of smears was reviewed by Ehara and Marumo using fluorescence spectrometry to discriminate between 174 lipstick samples [5]. Rodger et al. reported the UV-Vis analysis using resonance Raman spectroscopy to discriminate lipstick smears based on individual pigments present, as well as reviewing the techniques use for quality control applications [6].

Other UV-Vis studies in cosmetic analysis include the analysis of UV absorbent materials such as TiO_2. Jaroenwaoraluck et al. employed UV-Vis spectroscopy to study the differences and effectiveness of nanosized titanium dioxide as a sunscreen in cosmetics based on its UV absorption characteristics [7].

The amount of visible light reflected and absorbed is directly related to a material's colour [8] and Hoffman and Beussman reviewed reflectance spectroscopy in paint analysis, and the pigmentation required to give paint specific colours and demonstrated the use of visible reflectance spectroscopy to compare visually similar samples [9]. In a different field, visible spectroscopy is in widespread use for soil colour analysis and Rossel and Behrens use diffuse reflectance spectroscopy to identify soil samples based on absorptions associated with iron oxides present in minerals, such as goethite and hematite, in the visible region [10].

In this chapter, Visible Spectroscopy has been employed to characterize cosmetic foundation samples based on colour. This represents a preliminary analysis to introduce the cosmetic foundation samples that will be discussed throughout this thesis. Principal component analysis (PCA) has been applied to the spectral data giving separation of samples based on colour, indicating the range of samples examined.

2.2 Experimental

2.2.1 Sample Collection

Thirty-nine different loose and pressed powder foundation samples were purchased for analysis. These included 23 samples claimed to be mineral and 16 traditional-based formulations, in varying shades of colour, from 8 commercial manufacturers and suppliers in

the Australian market. Each sample was assigned a code comprising its type, 'M' or 'T' depending on whether it is marketed as a 'mineral' or 'traditional' face powder, a number, 1-8, identifying the manufacturer, and a second number indicating the product number in that set of manufacturers samples. The samples, with description and coding employed, are listed in Table 2.1 and 2.2.

All samples were fine, apparently homogenous powders. The pressed powders, were not as uniform as the loose, and exhibited a tendency to clump in their containers due to the presence of binders, that keep the powder in a compact form. The varying shades of colour, representative of the samples are displayed in Figure 2.1 and vary between manufacturers as well as within the same brand. The variation of colour from a single manufacturer, T3.1, T3.2 and T3.3, light, medium and dark tones, is evident in Figure 2.2.

Figure 2.1 Cosmetic Foundation samples M1.1, M6.4 and T8.2.

Table 2.1 Mineral-based foundation samples.

Number	Code	Manufacturer's Description	Foundation Type
1	M1.1	Translucent Fair	Loose Powder
2	M1.2	Translucent Medium	Loose Powder
3	M2.1	Ivory	Loose Powder
4	M2.2	Beige	Loose Powder
5	M2.3	Natural	Loose Powder
6	M2.4	Tan	Loose Powder
7	M3.1	Nude	Loose Powder
8	M3.2	Natural Fawn	Loose Powder
9	M3.3	Natural Tan	Loose Powder
10	M4.1	Natural Ivory	Loose Powder
11	M4.2	Natural Beige	Loose Powder
12	M4.3	Natural Honey	Loose Powder
13	M4.4	Natural Tan	Loose Powder
14	M5.1	Blushing Beige	Loose Powder
15	M5.2	Natural	Loose Powder
16	M5.3	Golden	Loose Powder
17	M6.1	Classic Ivory	Loose Powder
18	M6.2	Nude	Loose Powder
19	M6.3	Pure Beige	Loose Powder
20	M6.4	Tan	Loose Powder
21	M7.1	Soft Beige	Loose Powder
22	M7.2	True Nude	Loose Powder
23	M7.3	Natural Beige	Loose Powder

Table 2.2 Traditional foundation samples.

Number	Code	Manufacturer's Description	Foundation type
24	T6.1	Light	Loose Powder
25	T1.1	Creamy Natural	Pressed Powder
26	T1.2	Creamy Beige	Pressed Powder
27	T3.1	Medium	Loose Powder
28	T8.1	Ivory	Loose Powder
29	T8.2	Tan	Loose Powder
30	T2.1	Cream Beige	Pressed Powder
31	T2.2	Dark	Pressed Powder
32	T4.1	Outback Tan	Pressed Powder
33	T4.2	Outback Bisque	Pressed Powder
34	T1.3	Medium Translucent	Loose Powder
35	T6.2	Medium	Loose Powder
36	T2.3	Natural	Loose Powder
37	T3.2	Dark	Loose Powder
38	T3.3	Fair	Loose Powder
39	T4.3	Outback Beige	Pressed Powder

Figure 2.2 Cosmetic foundation samples of manufacturer T3.x showing colour shade varying from light to dark.

2.2.2 Sample Analysis

The reflectance spectra of the cosmetic powders were recorded using a portable Spectroradiometer (Model FieldSpec3, Analytical Spectral Devices Inc, Colorado, USA), providing a spectral range from 350nm to 2500nm at 1nm intervals and a spot size of 10mm. Measurements were recorded with a high intensity contact probe attachment (Analytical Spectral Devices Inc., Colorado, USA), designed for contact measurements with solid materials. The thickness of the samples was at least 0.5cm and was recorded against a non-reflective white background with a spectral resolution of 3nm. The instrument uses a modular silicon array detector and was calibrated using a Spectralon white panel, a polytetrafluoroethylene polymer resin compressed into a hard porous white material,

providing high diffuse reflectance over the UV-VIS-NIR region [11&12]. The wavelength range (400-800nm), covering the visible region, was used for data analysis. Extensive scatter and noise were apparent beyond these limits with this instrument.

2.2.3 Data Preprocessing

In visible spectroscopy, measurements were recorded using diffuse reflectance, and light scattering effects arise dependent on particle size and particle roughness. Generally, these effects are removed using preprocessing techniques, so that the spectra can be better interpreted in term of their chemical information [13]. Variations in data can occur between samples caused by sample particle size and will result in ineffective use of data analysis performed by multivariate techniques [14].

Normalization is a common technique for infra-red, UV-Vis absorption, fluorescence and reflectance spectroscopies to reduce the interference of scattering effects prior to data analysis. Normalizing involves setting each variable (an absorbance at each wavelength recorded) to constant area to give each variable an equal effect [15 &16].

The visible spectral data was preprocessed and examined with the aid of principal component analysis using MATLAB software (Ver. 7.10, Mathworks Inc., NSW, Australia) and the PLS toolbox (Eigenvector Research Inc., WA, USA).

2.3 Results and Discussion

2.3.1 Colour Classification

The 39 cosmetic foundation powders were initially classified subjectively into groups based on the colour shade of each sample. Each sample was categorized into one of 3 groups, light,

medium or dark, based on a visual comparison and manufacturer description. From Table 2.3, it is clear that there is a variety of shades across the samples and each manufacturer supplies a variety of foundation colours for consumers. Categorizing the foundations was undertaken to examine correlation between the observed colour and the results from visible spectral data.

Table 2.3 Colour classification of 39 cosmetic foundation samples, categorized into shades, Light, Medium or Dark.

Colour/ Shade	**Samples**
Light	M1.1, M2.1, M2.3, M3.1, M4.1, M4.2, M5.1, M6.1, M7.1, T6.1, T1.1, T1.2, T2.1, T3.3, T4.3, T8.1
Medium	M1.2, M2.2, M3.2, M4.3, M5.2, M6.2, M6.3, M7.2, T1.3, T2.3, T2.2, T3.1, T4.2, T6.2
Dark	M2.4, M3.3, M4.4, M5.3, M6.4, M7.3, T3.2, T4.1, T8.2

Raw spectral data were preprocessed, using the normalization function (norm-1) in the PLS Toolbox (Eigenvector Research Inc., WA, USA). Normalisation is conducted using the following equation

$$\tilde{\boldsymbol{x}}_{\boldsymbol{i}} = \boldsymbol{x}_{\boldsymbol{i}}.\boldsymbol{w}_{\boldsymbol{i}}^{-1} \qquad \text{(Equation 2.1)}$$

$\tilde{\boldsymbol{x}}_{\boldsymbol{i}}$ is the normalized form of sample *i* and w_i is the normalization weight for sample *i*.

The normalized weight, w_i is calculated by summing all variables for any given sample according to equation 2.2

$$\boldsymbol{w_i} = \sum_{j=1}^{J} |x_{i,j}| \qquad \text{(Equation 2.2)}$$

Normalisation gives the area equal to 1 under the curve where $x_{i,j}$ is the observed spectral values for sample i, j is the variable number (wavelength) and J is the total number of variables.

Visible reflectance values were transformed into absorbance,

$$\text{Absorbance, } \mathbf{X} = \log_{10}(1/\mathbf{R}) \qquad \text{(Equation 2.3)}$$

where **R** is the normalized visible reflectance data matrix for data analysis.

The visible spectra of foundation samples are presented in Figure 2.3 which shows (a) the visible reflectance raw data and (b) absorbance spectra after normalization. It is clear that normalization was successful in reducing scattering effects, and hence emphasizes the minor absorbance features of the samples. The samples exhibit absorbance bands in the blue and the green regions (400-570nm). The visible spectra appear similar and are not easily distinguishable.

Principal component analysis provides a means of summarizing such data whilst extracting maximum information, giving a better interpretation of the similarities and differences in spectral data based on the variance in absorbance of each sample [15].

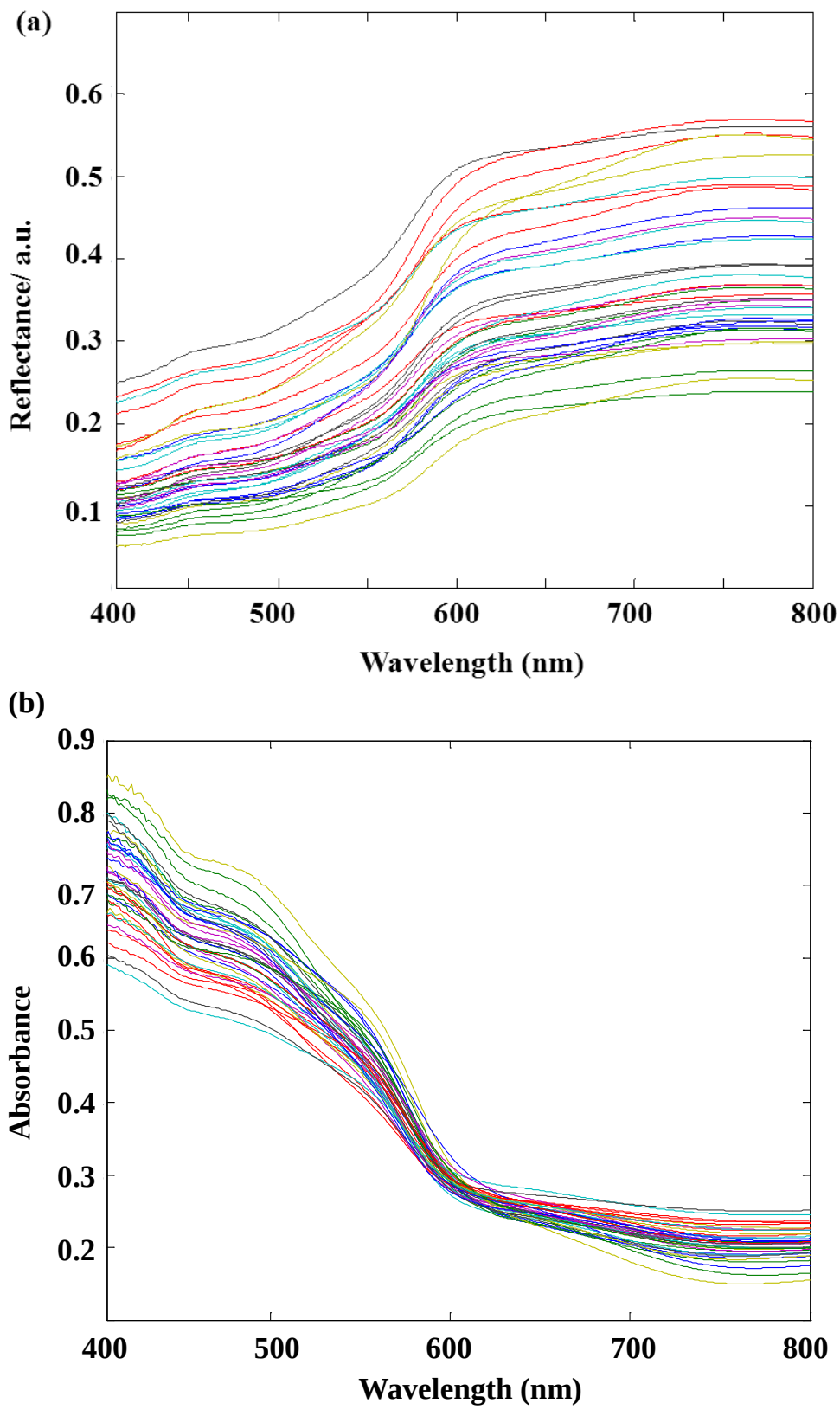

Figure 2.3 UV-Vis spectra of foundation powder samples, (a) non-processed raw data and (b) data after normalization and conversion to absorbance.

2.3.2 Principal Component Analysis

Principal component analysis (PCA) aims to reduce the dimensionality of multivariate data while revealing those variables that describe some inherent structure in the data and retaining as much of the data variation as possible [17,18]. The method generates a new set of variables, called principal components or scores, with each principal component being a linear combination of the original variables defined by the PC loadings. Principal component analysis finds the linear combination describing the largest variance, the first principal component, and then determines other linear combinations that have most of the remaining variance, giving further PC's, which are uncorrelated with the first principal component. Generally, a plot of the first two or three principal components provides sufficient information about the data to indicate any inherent pattern.

Principal component analysis transforms the absorbance data matrix $\boldsymbol{X}$, of dimensions I x J whose rows represent samples and columns represent variables (eg. an absorbance at each wavelength recorded), into a scores, **T**, and loadings, **P**, matrices, denoted by the equation,

$$\mathbf{X} = \mathbf{TP} \qquad \text{(Equation 2.4)}$$

T, the scores matrix, has as many rows as the original data matrix of dimension, I x J and **P**, the loadings matrix is of dimensions, J x J, which can be seen in Figure 2.4. The loadings express the magnitude (large or small) and manner (positive or negative) in which the original variables contribute to the principal components [17].

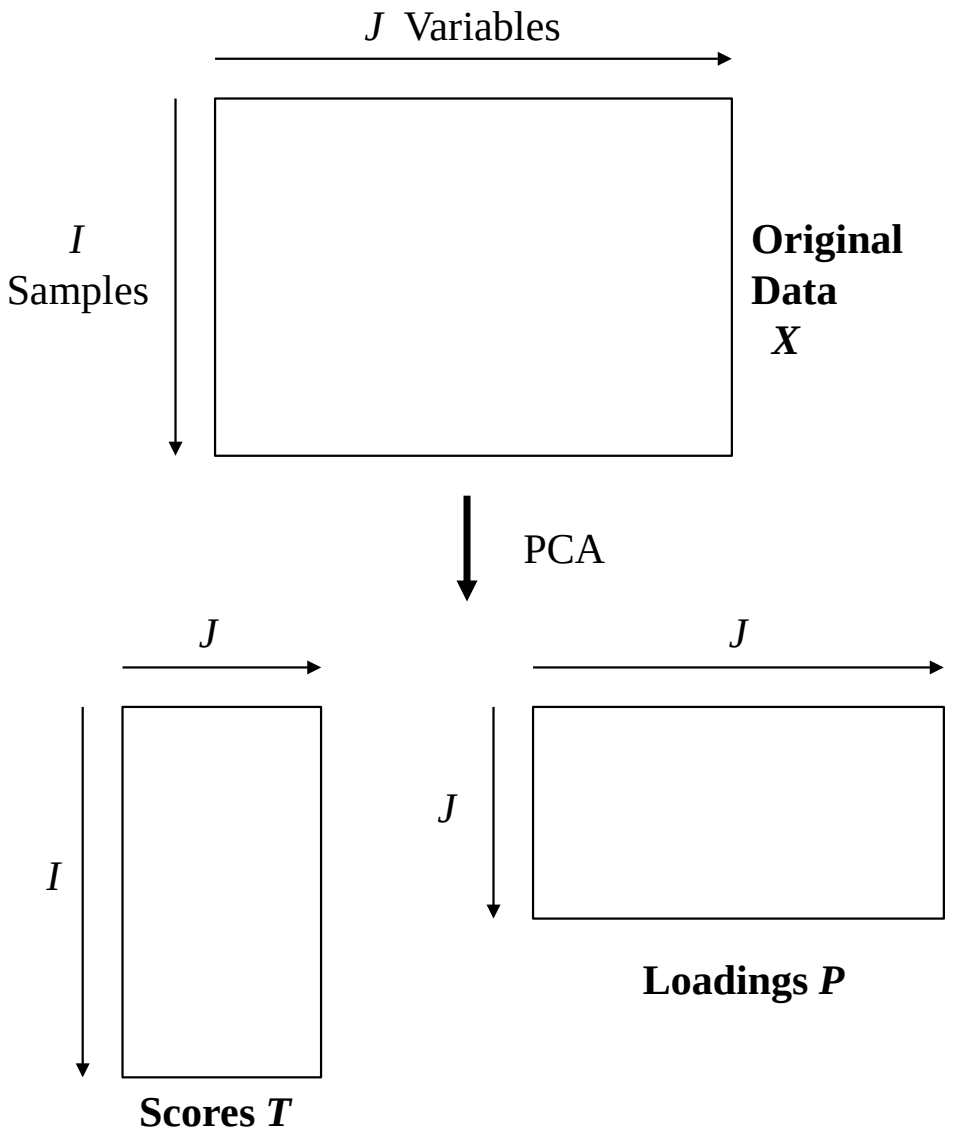

Figure 2.4 PCA method applied to original data matrix X, to produce, Scores T and Loading P matrices [19].

Principal component analysis was applied to the spectra and the result is summarized in Figure 2.5. Figure 2.5(a) displays a score plot of the 39 foundation powder samples projected on PC1 and PC2. The first two principal components account for 98% of the total variance contained in the spectral data. It is evident that samples are not grouping according to manufacturer and there is no distinct pattern in the data based on the foundation type, 'mineral' or 'traditional'. The samples are evenly distributed about the origin, confirming the

samples contain no visible outliers. Principal component analysis resolves prominent features in the visible spectral data and PC1 and PC2 can be interpreted in the loadings plot of Figure 2.5(b). The separation along the two principal components is defined by the wavelength absorption of the samples. Principal component 1 gives absorbance bands in the blue-green 400-500nm region, indicating reflectance in the orange-red visible region. Principal component 2 produced positive absorbance bands in the green-yellow 500-570nm region, indicating reflectance in the blue and red visible region. Based on the colour differences of the foundation samples, samples are grouping in accordance to the wavelength region of the absorbed colour. When a visual comparison of the colour of the samples is made with the scores plot (Figure 2.5(a)), it seems that samples that are light in colour are grouping along the positive region of the PC2 axis and those that have a darker colour shade have been projected along the PC1 axis. It can be assumed that samples of a lighter shade recorded absorbance in the green region and those darker in colour are exhibiting absorbance in the blue region. It can be assumed that the colour of foundation powders is due to the addition of yellow and red iron oxides, or a combination of both and light is absorbed depending on the iron oxide present. However, the type cannot be distinguished by qualitative visible spectroscopy.

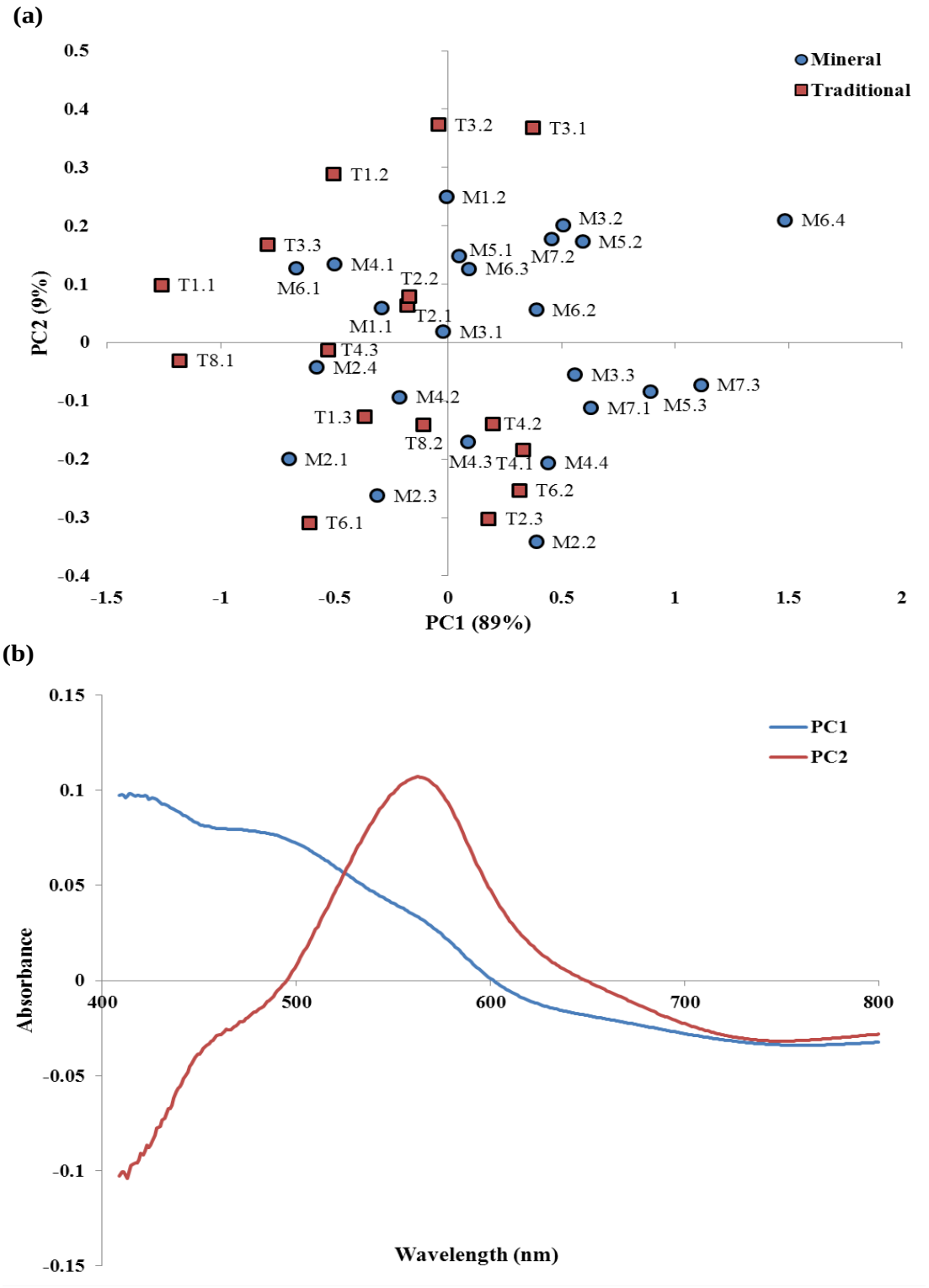

Figure 2.5 Scores plot (a) and the loadings plot (b) associated with PC1 and PC2 from principal component analysis of first derivative UV-Vis spectra of the 39 foundation samples.

2.3.3 Conclusion

The visible spectrum of foundation powders samples represents a preliminary analysis. Samples could not be grouped based on manufacturer or foundation type, but only by colour. The results indicate that the samples selected for this research are of a variety of differing colour and shades. Principal component analysis was successful in summarizing the data and resolving absorption features of the spectral data. The use of preprocessing was vital to the analysis, and normalization highlighted small difference in the spectral data that was not previously obvious. Visible spectroscopy was used to introduce the foundation sample set to this research. Further investigation of foundation powders was undertaken by XRF, XRD and IR spectroscopies for full chemical characterization and discrimination of samples. In the remaining chapters of the thesis, these analytical techniques will be discussed, with the aid of multivariate data analysis methods.

2.4 References

1. M. G. de Navarre, *The Chemistry and Manufacturer of Cosmetics*, Chapman & Hall, LTD., London, UK, **1941**.
2. H. Zollinger, Color Chemistry Syntheses, properties and application of organic dyes and pigments (3rd Ed.), Wiley-VCH, Zurich, Switzerland, **2003**.
3. T. Bombeli, Colorants for Cosmetic Products, Somerset Cosmetic Company, WA, USA- www.makingcosmetics.com- Date Accessed- 31/08/2012.
4. R. J. D. Tilley, *Colour and Optical Properties of Materials* (2nd Ed.), Wiley, Chichester, UK, **2010**.
5. Y. Ehara and Y. Marumo, Identification of lipstick smears by fluorescence observation and purge-and-trap gas chromatography, Forensic Science International, 1998, **96**:

p.1-10.

6. C. Rodger, V. Rutherford, D. Broughton, P. C. White W. E. Smith, *The in-situ analysis of lipsticks by surface enhanced resonance Raman scattering*, Analyst, 1998, **123**: p.1823-1826.
7. A. Jaroenworaluck, W. Sunsaneeyametha, N Kosachan, R. Stevens, *Characteristics of silica-coated TiO2 and its UV absorption for sunscreen cosmetic applications*, Surface and Interface Analysis, 2006, **38**: p.473-477.
8. H. Kaur, *Instrumental Methods of Chemical Analysis*, Pragati Prakashan, New Delhi, **2010**.
9. E. M. Hoffman and D. J. Beussman, *Paint Analysis Using Visible Reflectance Spectroscopy*, Journal of Chemical Education, 2007, **84**(11): p.1806-1808.
10. R. A. V. Rossel and T. Behrens, Using data mining to model and interpret soil diffuse reflectance spectra, Geoderma, 2010, **158**: p.46-54.
11. A.E. Stiegman, C. J. Bruegee A. W. Springsteen, *Ultraviolet stability and contamination analysis of Spectralon diffuse reflectance material*, Optical Engineering, 1993, **32**(4): p.799-804.
12. *A guide to reflectance coatings and materials*, Labsphere, North Sutton, USA- www.labshpere.com- Date accessed- 30/08/2012.
13. S. Sasic and Y. Ozaki, *Raman, Infrared and Near infrared Chemical Imaging*, Wiley, Hoboken, USA, **2010**
14. PLS Tool Box Manual (Ver. 6.5.2, Eigenvector Research Inc., WA, USA, 2012).
15. P. Gemperline, *Practical Guide to Chemometrics* (2nd Ed.), CRC Press, New York, **2006**.
16. MATLAB software user Manual (Ver. 7.13, Mathworks Inc., NSW, Australia, 2011).
17. M. Otto, *Chemometrics* (2nd Ed.), Wiley. VCH & Co., Weinheim, Germany, 2007.

18. C. Papachristodoulou, A. Oikonmou, K. Ioannides, C. Gravani, A study of ancient pottery by means of X-ray Fluorescence spectroscopy, multivariate statistics and mineralogical analysis, Analytica Chimica Acta, 2006, **573-574**: p.347-353.
19. R. G. Brereton, *Chemometrics for Pattern Recognition*, Wiley, Chichester, UK, **2009**.

Chapter 3: Elemental Analysis using X-ray Fluorescence

3.1 Introduction

X-ray Fluorescence is a rapid, qualitative and quantitative method for elemental analysis of, principally, solid or powder samples. It requires minimal sample preparation and samples are rarely destroyed or changed by exposure to X-rays. This is an important advantage for XRF analysis, as samples can be saved for future reference or other testing methods that are destructive [1] or when sample size is small. X-ray Fluorescence is based on the measurement of energy, or wavelengths, and intensities of X-rays emitted by a sample, when excited by a primary X-ray source [2].

The electrons of an atom are considered to be arranged in shells and when an absorbed X-ray photon has sufficient energy to displace an inner (usually K-shell) electron from the target atom, an unstable ion is produced. This leads to an electron from an outer shell dropping into the vacant position [3] resulting in the fluorescence radiations, Figure 3.1. If the vacancy is filled by an M electron then the X-ray produced is called a Kβ X-ray. If the vacancy is filled by an L electron then a Kα X-ray is produced. These emitted X-rays are characteristic of the atoms present in the sample, and elements are identified from the wavelengths or energies of this characteristic radiation [2].

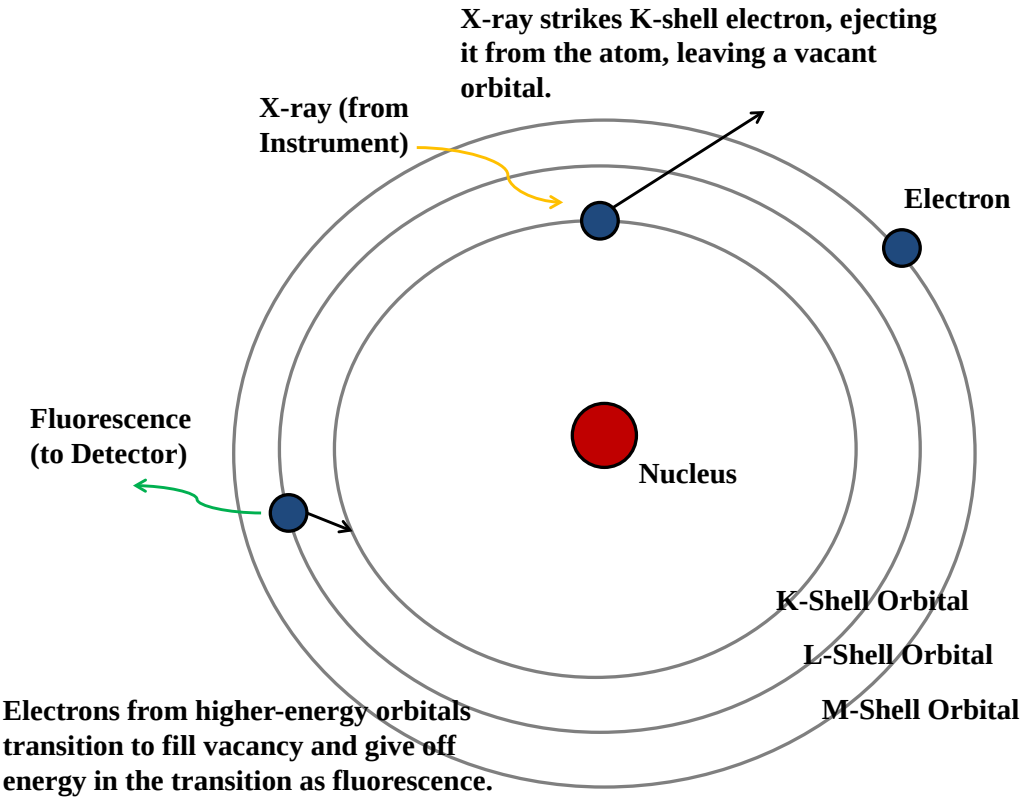

Figure 3.1 Electron shell transition to produce fluorescence radiation [4].

3.1.1 Wavelength-dispersive X-ray Fluorescence

A wavelength-dispersive XRF instrument, as shown in Figure 3.2, uses a primary X-ray source to excite the atoms of a sample. The resulting fluorescent radiation is collimated by a series of slits to an analysing crystal [1]. The crystal is mounted on a turntable which rotates through an angle θ. For each element being determined, an appropriate crystal is selected according to the Bragg Equation [2];

$$n\lambda = 2d \sin\theta \qquad \text{(Equation 3.1)}$$

where d is the inter-planar spacing in the atomic lattice of the crystal, λ is the X-ray wavelength, θ is the angle between the radiation and planes, and n is an integer representing the order of diffraction. Whenever the Bragg Equation is satisfied for a particular

wavelength, it is diffracted towards the detector [2]. The detector rotates through a 2θ angle to ensure it is in the correct position to receive any rays reflected from the crystal. The 2θ position of the detector corresponds to the diffracted characteristic line of the element being studied [3].

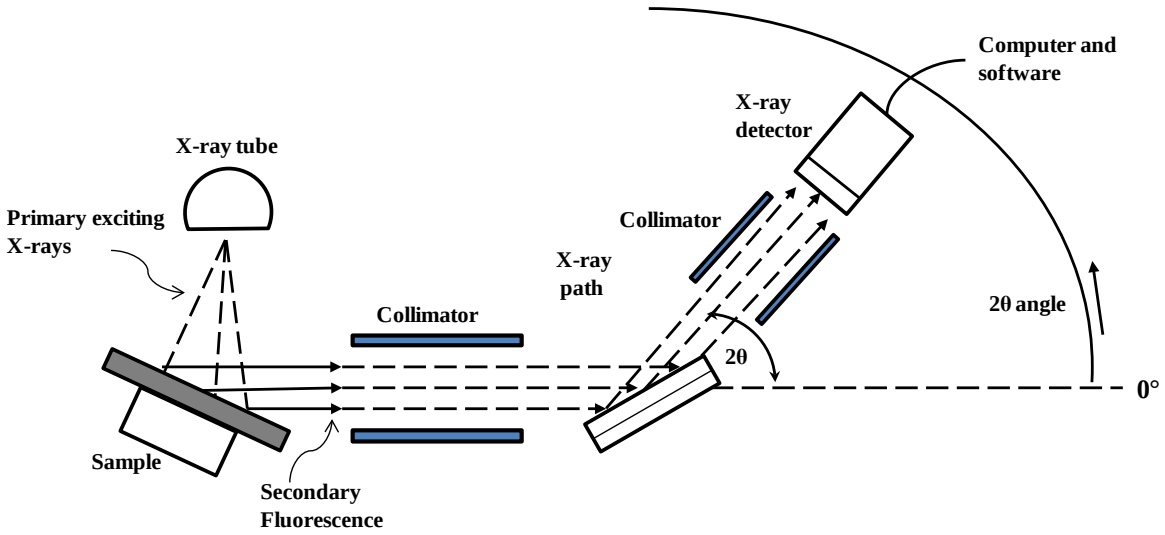

Figure 3.2 Schematic diagram WDXRF instrument [1].

3.1.2 Energy Dispersive X-ray Fluorescence

Energy Dispersive X-ray Fluorescence (EDXRF) is an alternative technique to the wavelength dispersive method. Figure 3.3 shows the instrumental features of an EDXRF spectrometer. Energy Dispersive X-ray Fluorescence uses a lithium-drifted silicon detector to determine characteristic X-rays based on their photon energies rather than on their wavelengths [2]. The Si-Li detector converts X-ray photons to a charge. Each time a pulse is produced, a number is generated that represents a channel, each channel representing a small range of energy. The data is interpreted through a multi-channel analyser and an entire energy spectrum is produced, consisting of a series of peaks (intensity versus energy). Peak height is determined

by the number of electrons per pulse and is directly proportional to the energy of the photon [5]. Each analyte line has a specific energy (keV), much like the 2θ to line values used to identify peaks in WDXRF.

Energy Dispersive X-ray Fluorescence methods are becoming increasingly popular and while instrumentation precision has improved, WDXRF is the preferred method for multi-elemental analysis. Energy Dispersive X-ray Fluorescence is a cheaper and more compact system because of the absence of an analysing crystal. Hence, qualitative analysis is more rapid and convenient than with wavelength dispersion. In comparison, the scanning WDXRF technique allows only one wavelength to enter the detector at a time, but this results in better elemental concentration detection limits than EDXRF and is thus the preferred method for quantitative analysis [1].

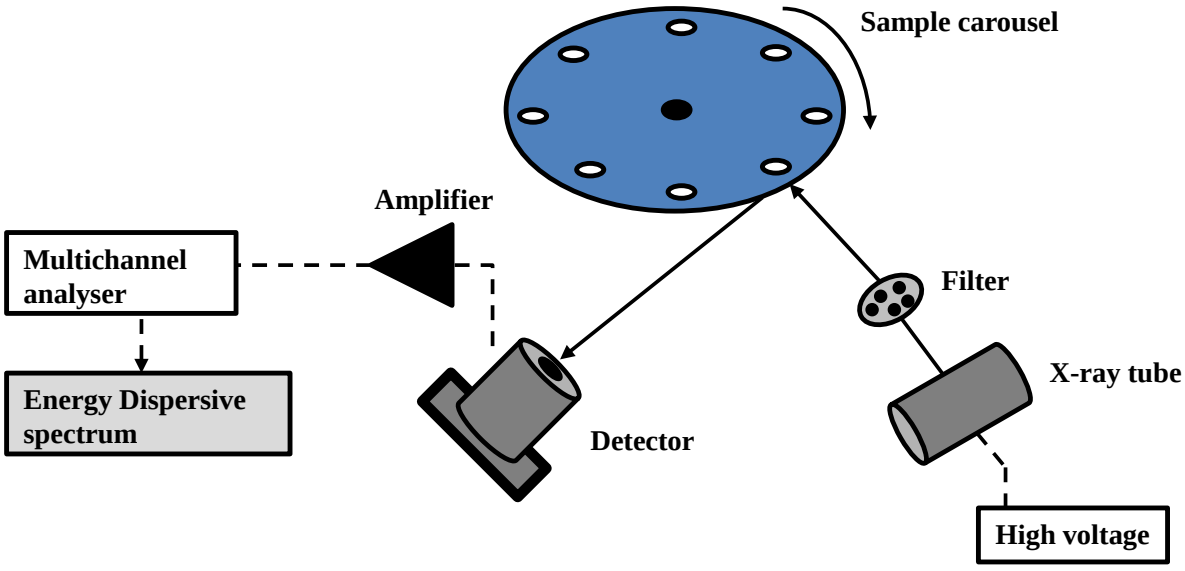

Figure 3.3 Sections of an EDXRF instrument [6].

In this study, wavelength-dispersive X-Ray Fluorescence (WDXRF) spectrometry has been employed for multi-elemental analysis of thirty-nine mineral and traditional ingredient

cosmetic powders (described in Chapter 2). Cosmetic foundation powders are comprised of various inorganic materials and XRF provides relative elemental concentrations. Powder samples are easily analysed by XRF with little sample preparation, making it an ideal method of elemental analysis.

3.2 Experimental

Thirty-nine different foundation samples were purchased for analysis. These included 23 mineral-based samples and 16 traditional-based formulations of loose and pressed powders, representing varying shades of colour, from 8 commercial manufacturers and suppliers in the Australian market. Each sample was assigned a code comprising its type, 'M' or 'T' depending on whether it is marketed as a mineral or traditional face powder, a number, 1- 8, identifying the manufacturer, and a second number indicating the sample number in that set of manufacturers samples. The samples, with description and coding employed, are listed in Table 2.1, Chapter 2.

3.2.1 Sample Analysis

Samples were prepared and presented to the XRF spectrometer as pressed pellets. A 2g portion of each sample was mixed with 8g of boric acid in a ceramic (ZrO) ring mill (Model 1A, Rocklabs Ltd., Auckland, N.Z.) and mixed thoroughly by grinding for 30 seconds before compacting at 300kPa into 40mm diameter discs.

Standard materials were examined to determine relative concentrations of elements present in ingredients of the type used in the production of the 39 foundation samples. Nine standards of readily available cosmetic grade raw materials were analysed, including titanium dioxide, zinc oxide, iron oxide and bismuth oxychloride (The Ponte Vedra Soap Shoppe Inc., Florida, USA). Other standards were prepared using magnesium oxide, silicon dioxide, aluminium oxide, calcium carbonate and dipotassium carbonate. In each case, standards were prepared

as pressed pellets using a 0.5g portion of each standard material and 9.5g of boric acid. The mixtures were ground in the ceramic mill for 30s to thoroughly mix prior to compacting into 40mm discs.

All samples and standards were examined using a wavelength dispersive XRF spectrometer (Model S4 Pioneer, Bruker AXS Gmbh, Karlsruhe, Germany). To cover the range of elements of interest, three dispersing crystals were employed, LiF200, PET, and OVO-55. Nine elements (magnesium, aluminium, silica, potassium, calcium, titanium, iron, zinc, bismuth) were selected for sample characterization, and the instrument operating details are summarised in Table 3.1. The concentration of each element was estimated by direct comparison of its background-corrected peak emission intensity with that from one of the appropriate standards, and then converted to percentage composition of the foundation sample. With the exception of magnesium, all elements' emission signals were recorded using two dispersing crystals and comparison of results obtained with different crystals indicated no significant differences in calculated concentrations.

Table 3.1 Instrumental conditions for WDXRF analysis of the cosmetic powders.

Crystal	2d Value	2θ Range	Rh Source voltage (kV)	Rh Source current (mA)	Detector	Collimator	Elements Monitored
LiF200	4.026	15-145°	50	81	Flow detector	0.46	Bi(Lα1), Zn(Kα1), Fe(Kα1),Ti(Kα1), Ca(Kα1), K(Kα1)
PET	8.7522	20-148°	27	150	Flow detector	0.46	Zn(Kα1),Fe(Kα1), Ti(Kα1),Ca(Kα1), K(Kα1),Bi(Lα1), Si(Kα1), Al(Kα1)
OVO-55	55.6	15-50°	27	150	Flow detector	0.46	Al(Kα1),Mg(Kα1)

3.3 Results and discussion

The elemental concentrations, as percentage by weight of sample, along with the mean, standard deviation and relative standard deviation, for the mineral and traditional foundation powders examined are presented in Table 3.2. From these results, the composition of the samples can be seen to vary quite considerably as reflected in the relative standard deviation (%) values.

Table 3.2 Results of the selected elemental analysis of the 39 cosmetic powders, with mean, standard deviation (STD) and relative standard deviation (RSD%).

Sample	Bi%	Zn %	Fe %	Ti %	Ca %	K %	Si %	Al %	Mg %
M1.1	0	1.47	3.71	1.63	1.05	1.11	21.1	4.88	15.77
M1.2	0	1.45	4.83	1.59	1.04	1.13	17.05	3.41	15.49
M2.1	0	0	4.1	0.41	0	5.41	20.64	29.75	1.93
M2.2	0	0	6.48	0.41	0	5.41	20.34	29.82	1.51
M2.3	0	0	5.74	0.42	0	5.44	20.79	30.73	1.55
M2.4	0	0	5.01	0.42	0	5.63	21.5	31.95	1.66
M3.1	12.41	11.89	3.75	0.46	0	2.87	12.98	20.48	0.07
M3.2	12.86	8.32	5.88	0.42	0	2.95	12.9	20.12	0.09
M3.3	12.25	7.41	9.7	0.46	0	2.69	11.18	17.55	0.08
M4.1	0	15.02	6.14	0.22	0	5.75	16.62	25.24	0.28
M4.2	0	14.99	7.16	0.23	0	5.74	17.41	26.79	0.32
M4.3	0	14.86	8.28	0.25	0	5.8	16.87	25.23	0.34
M4.4	0	13.9	10.78	0.24	0	5.45	16.82	24.97	0.47
M5.1	0	1.57	3.86	1.59	1.07	1.05	21.01	5.59	15.85
M5.2	0	1.51	6.29	1.63	1.06	1.08	20.62	5.53	15.92
M5.3	0	1.39	6.75	1.61	1.07	1.03	19.79	5.12	14.44
M6.1	5.57	15.86	3.62	9.04	0.03	1.93	8.11	9.54	0.76
M6.2	5.47	15.2	8.61	6.76	0	2.01	7.44	9.56	0.42
M6.3	5.25	14.77	8.23	7.31	0	1.93	7.66	10.13	0.4
M6.4	5.05	14.22	19.01	2.34	0	1.94	7.49	9.7	0.42
M7.1	0	0	8.58	0.92	0	6.76	20.47	34.3	0.25
M7.2	0	0	9.51	0.93	0	6.73	19.31	32.2	0.26
M7.3	0	0	14.34	0.61	0	6.43	19.61	33.57	0.3
T6.1	0	0	2.15	0.02	0.24	0.5	22.02	3.45	18.38
T1.1	0	2.79	2.09	0.77	0.18	0.11	20.45	2.81	18.34
T1.2	0	2.68	3.73	0.77	0.17	0.11	19.05	2.66	15.86
T3.1	0	0.93	2.38	1.87	0.42	0	22.95	0.62	22.39
T8.1	0	1.07	1.93	0	0.6	0	23.5	0.32	21.77
T8.2	0	0.76	3.32	2.84	10.99	0.03	11.62	2.75	8.9
T2.1	0	0	3.45	0.09	0.62	0.79	20.13	3.83	23.37
T2.2	0	0	3.49	0.07	0.71	0.81	19.6	3.75	23.17
T4.1	0	0.79	4.02	3.43	11.03	0.04	11.12	3.36	8.95
T4.2	0	0.82	1.8	2.48	11.07	0.02	12.63	2.83	10.76
T1.3	0	1.54	3.4	0.05	0.99	2.22	19.61	9.81	12.02
T6.2	0	0	3.07	0.03	0.27	0.51	24.58	3.8	22.28
T2.3	0	1.12	3.07	0.09	7.19	1.51	15	9.46	10.13
T3.2	0	0.85	5.41	2.06	0.29	0.06	24.14	0.91	24.31
T3.3	0	0.95	1.35	1.87	0.73	0.02	24.55	0.43	24.15
T4.3	0	0.83	2.16	2.14	11.67	0.04	13.71	2.95	11.14
Mean	1.51	4.33	5.57	1.50	1.60	2.39	17.49	12.82	9.35
STD	3.61	5.93	3.63	2.04	3.49	2.37	4.99	11.71	9.05
%RSD	239.05	136.90	65.14	136.07	217.51	99.44	28.54	91.39	96.78

3.3.1 Cluster analysis

Cluster analysis identifies groups within data by classifying objects with respect to their similarity. It aims to ensure similar objects are clustered together with minimal separation between objects in a cluster, while maximizing separation between different clusters [7]. However, it does not assume that an object belongs to only one group, but it may be part of two or even more. Cluster analysis usually uses a distance measure to assign objects to a particular cluster, grouping objects closest together in the pattern space to the same cluster. The most commonly referred to function for distance measure is the Euclidean distance, and for each variable and each cluster *g*, a mean is calculated over all samples in the cluster to give a centroid x_g. The Euclidean distance is defined by,

$$d^2_{ig} = (x_i - x_g) (x_i - x_g)^T \qquad \text{(Equation 3.2)}$$

where d^2_{ig} is the squared Euclidean distance between each sample *i* (represented by row vector $\mathbf{x}_i$) and the centroid of each cluster. The sample is assigned to the cluster with the lowest distance [8].

Hierarchial cluster analysis is a common method for partitioning object groups, graphically displayed in a tree-like dendrogram. The standard hierarchial clustering algorithms produce a set of cluster solutions, partitioning the objects into k=1,..., n clusters [9]. There are two methods for ordering objects hierarchially; the agglomerative method and the divisive method. The agglomerative method is more commonly used. In the first level of hierarchy, all n objects form a separate cluster, resulting in n clusters. In the next level the two closest clusters are merged, and so on until all objects are in one single cluster. Essentially, agglomerative clustering methods use distance measures to calculate a similarity or distance matrix between objects, resulting in a dendrogram. There are various agglomerative methods, to calculate the distance matrix of a set of objects.

The Ward's method uses the incremental within-cluster sum of squares as a result of joining two clusters denoted by r and s to calculate the distance measure d(r,s) defined by,

$$d(r,s) = \sqrt{\frac{2n_r n_s}{(n_r+n_s)}} \cdot \|\overline{x_r} - \overline{x_s}\|_2 \qquad \text{(Equation 3.3)}$$

Where $\bar{x}_r$ and $\bar{x}_s$ are the centroids of clusters r and s, n_r and n_s are the number of objects within each cluster and II II_2 is the Euclidean distance. The within cluster sum of squares is defined as the sum of squares of the distances between all objects in the cluster and the centroid of the cluster [10].

Hierarchial cluster analysis of the XRF data, using Ward's method, i.e. joining clusters to minimize within-cluster variance, produces the dendrogram illustrated in Figure 3.4. The dendrogram represents a significant reduction in dimensionality of the multi-elemental data describing the samples and distinct groups are evident. At the highest separation level there is clear distinction between the majority of mineral-type samples and the more traditional cosmetics, although mineral samples from manufacturer 1, M1.x, and manufacturer 5, M5.x, appear in the wrong group and cluster tightly with traditional types. At finer levels of separation, particularly with the mineral samples, there is good agreement between the cluster contents and individual manufacturers, M2.x, M3.x, M4.x, M6.x and M7.x all cluster in their own groups.

Although cluster analysis provides a clear illustration of the samples grouping according to elemental composition, the technique provides no information as to the relative significance on the role of each element in defining the nature of the observed clusters. A more informative picture and better interpretation can be achieved by employing principal components analysis, PCA [5, 9].

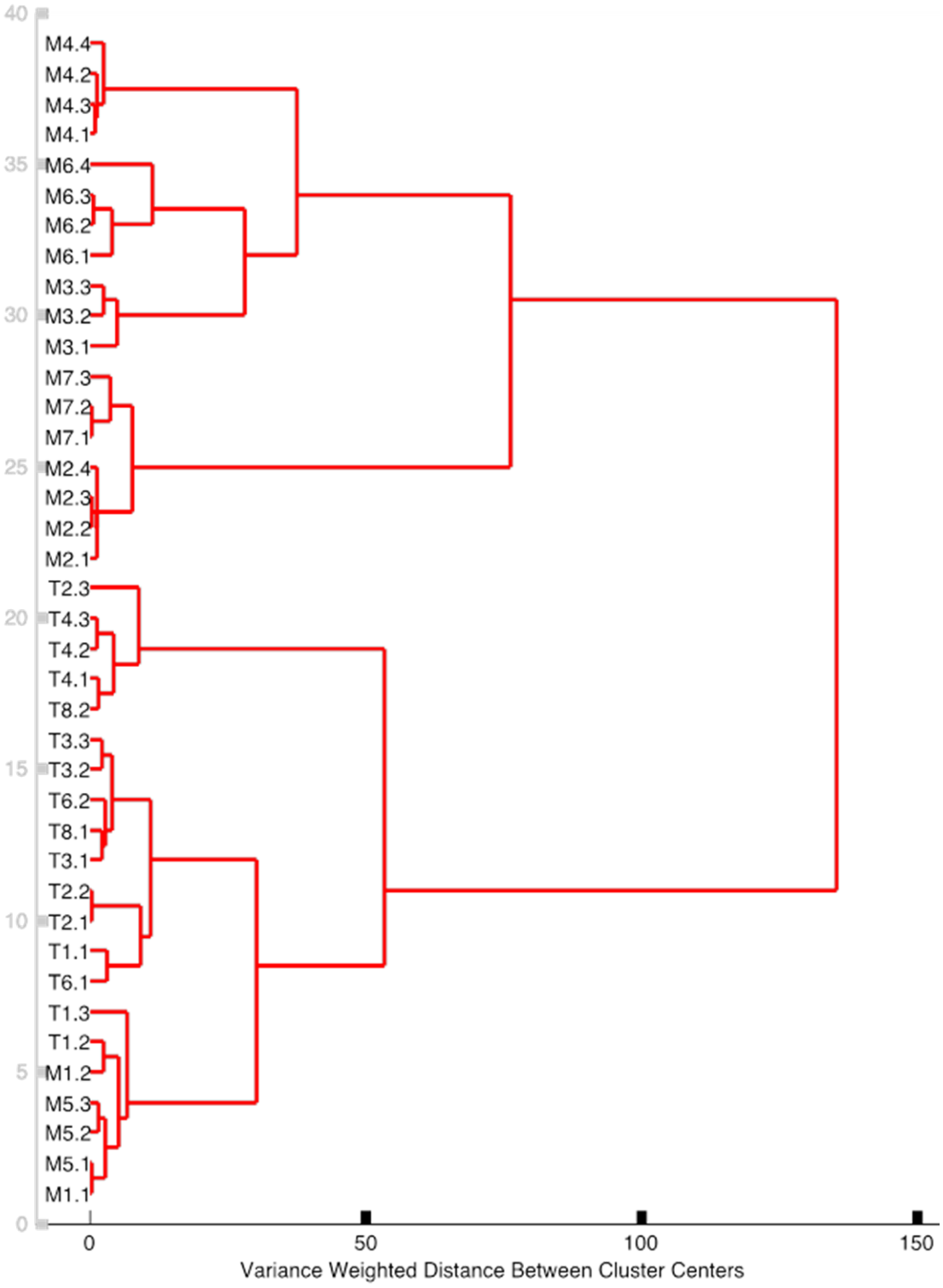

Figure 3.4 Dendrogram produced from cluster analysis, using Ward's method, of the elemental composition of the 39 foundation powders.

3.3.2 Principal Component Analysis

Principal component analysis was undertaken on the covariance data matrix of elemental concentrations, and the results are summarised in Figures 3.5 and 3.6. In Figure 3.5(a) a scores plot of the 39 samples projected on to PC1 and PC2 is shown. Together, these factors account for over 87% of the total variance contained in the analytical data. There is clear distinction between the traditional type of foundation powders and the majority of the mineral type, although once again samples M1.x and M5.x group with the traditional style of product. The separation is mainly along the axis defined by PC1 and, as seen in the factor loadings plot of Figure 3.5(b), this is defined largely by the relative concentrations of aluminium and magnesium.

Both elements are likely to be associated with clay minerals commonly used in cosmetic powders, including kaolin ($Al_2Si_2O_5(OH)_4$), used in foundation powders for its good covering power and adhesion as well as grease-resistance and perspiration-absorbent properties [12], mica ($KAl_2(AlSi_3O_{10})$), added to impart shine through the product [13], and talc ($Mg_3Si_4O_{10}(OH)_2$) employed for its ease of spreading over the skin. From examination of Figure 3.5 and Table 3.2 it is clear that the concentration of magnesium, and hence possibly talc, in a sample is a key factor in identifying a product as being of a mineral or traditional type of cosmetic. Talc is a common additive in traditional foundation formulations, but it is a known skin irritant and according to most manufacturer claims for mineral cosmetics, the new formulations should not contain additives that may be harmful to the skin [13].

Another easily identifiable difference between many samples is indicated by the concentration of calcium, with high amounts of calcium found in a number of traditional samples. This is illustrated in a plot of PC1 vs PC3, Figure 3.6. Like talc, calcium, as calcium carbonate or chalk, is an ingredient mainly used in traditional formulations. It is included in cosmetic

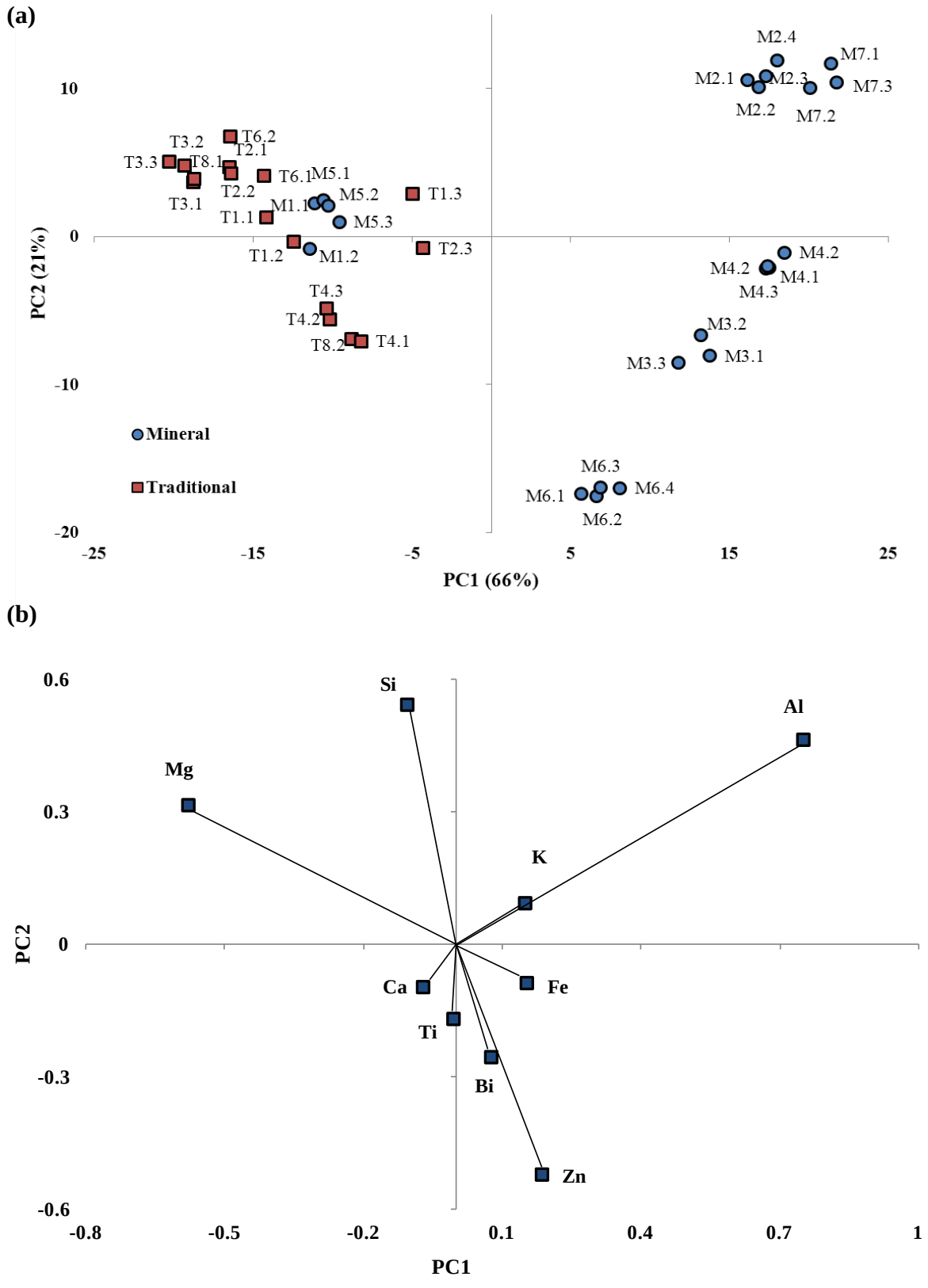

Figure 3.5 The scores plot (a) and the loadings plot (b) associated with PC1 and PC2 from principal components analysis of the elemental composition of the 39 foundation samples.

grade products for its covering power, absorption of perfume and ability to reduce the shine of talc [14]. Hence, it is used in conjunction with talc and is seen here in group T4.x, and samples T8.2 and T2.3.

Separation between manufacturers of mineral products is evident in Figure 3.5, with most samples falling into distinct groups according to manufacturer. This classification occurs mainly along the axis defined by PC2 which is strongly influenced by the relative concentration of clays (i.e. aluminium, magnesium, silica) and the heavier metals, zinc, bismuth and titanium, Figure 3.4(b). The clusters defined by M6.x and M3.x, both relatively high in zinc and bismuth, are particularly evident. Bismuth is associated with the additive bismuth oxychloride (BiOCl). This is a known skin irritant and it is surprising that it is incorporated into so-called 'chemical-free', mineral-based formulations. In Figure 3.7(a) the samples identified as belonging to the mineral-type, 18 in total excluding samples M1.x and M5.x, have been examined by PCA and the differences between manufacturers is clear, with the associated loadings plot of Figure 3.7(b) confirming the separation is due to relative concentrations of zinc, bismuth and aluminium in the samples.

Principal component analysis was applied to 21 foundation samples classified as traditional-based formulations. The scores and loadings plot associated with PC1 versus PC2 is shown in Figure 3.8. The main separation of samples is along the PC1 axis due to elemental concentrations of calcium, magnesium and silica. Samples T4.x and T8.2 are forming a cluster in the negative PC1 region due to the high calcium content present in these samples. Not all samples are clustering according to manufacturer type. Samples T8.x do not group together. Sample T8.2 contains a large amount of calcium, whereas sample T6.1 contains a very minimal amount. This was also found with samples T2.x, where sample T2.3 is not forming a cluster with T2.1 and T2.2. Sample T2.3 has varying amounts of calcium and aluminium in comparison to the other samples from the same manufacturer. Bismuth has had

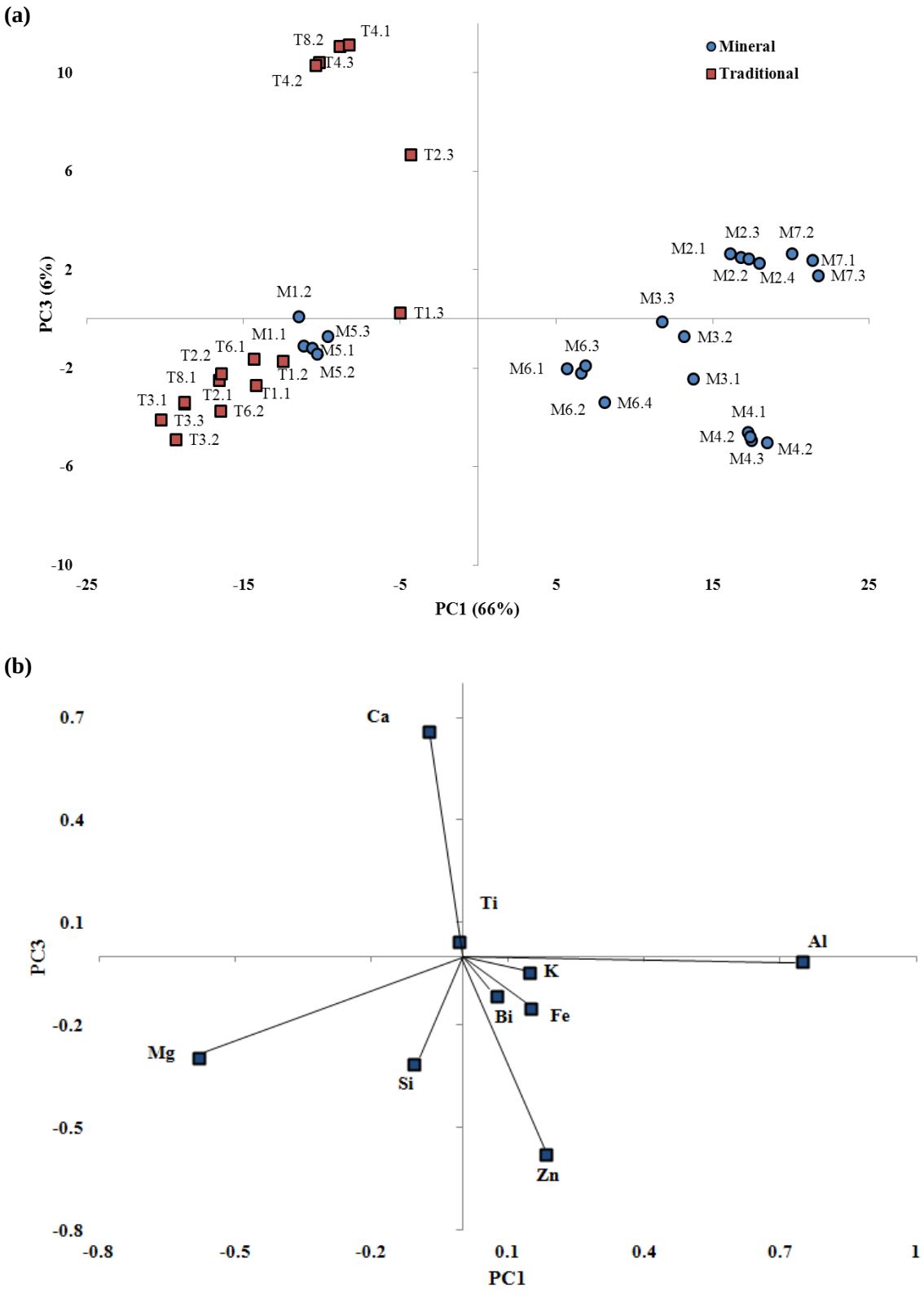

Figure 3.6 The scores plot (a) and the loadings plot (b) associated with PC1 and PC3 from principal components analysis of the elemental composition of the 39 foundation samples.

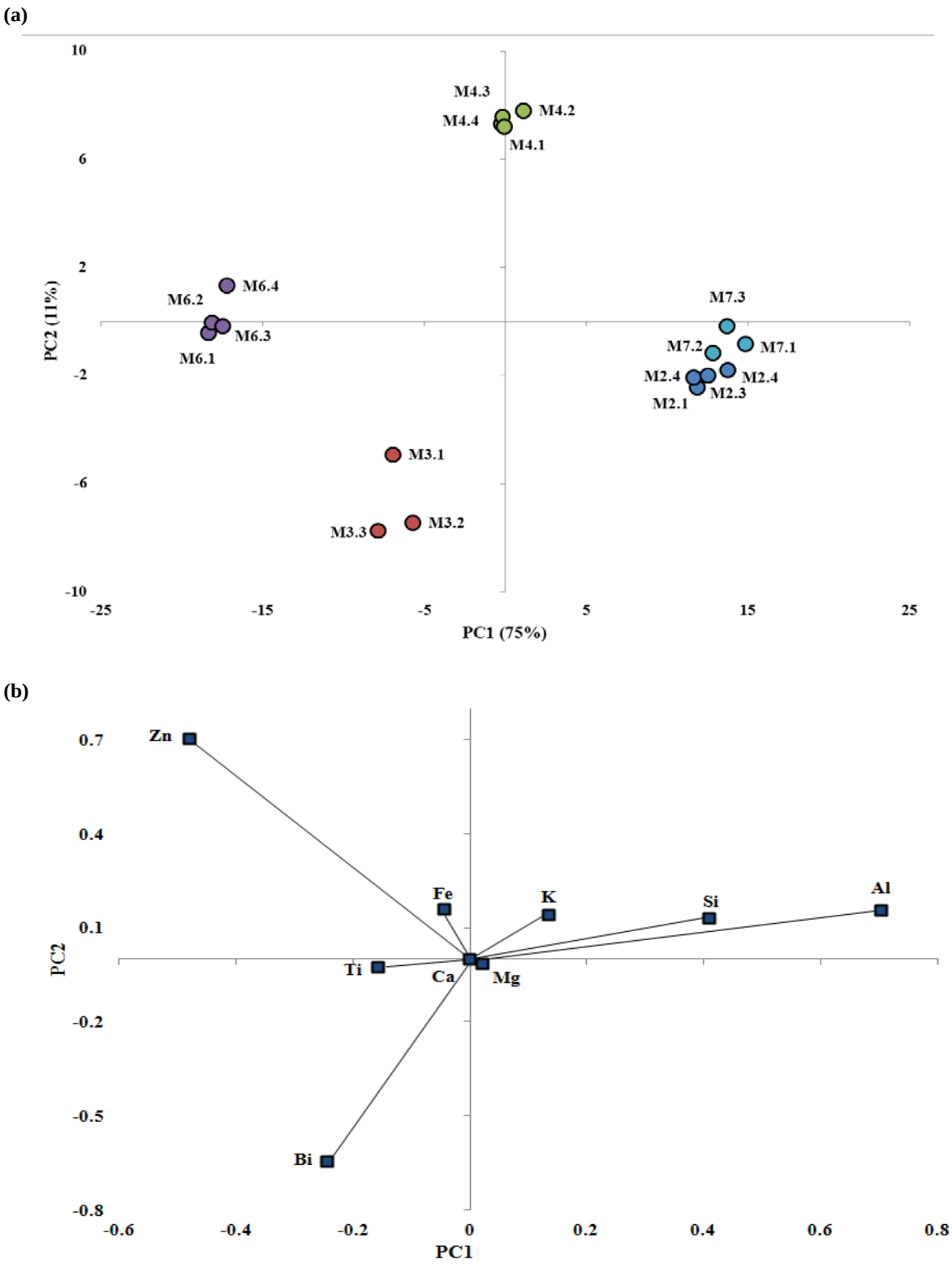

Figure 3.7 The scores plot (a) and the loadings plot (b) from principal component analysis of the elemental composition of the 18 foundation powers classified as mineral cosmetics.

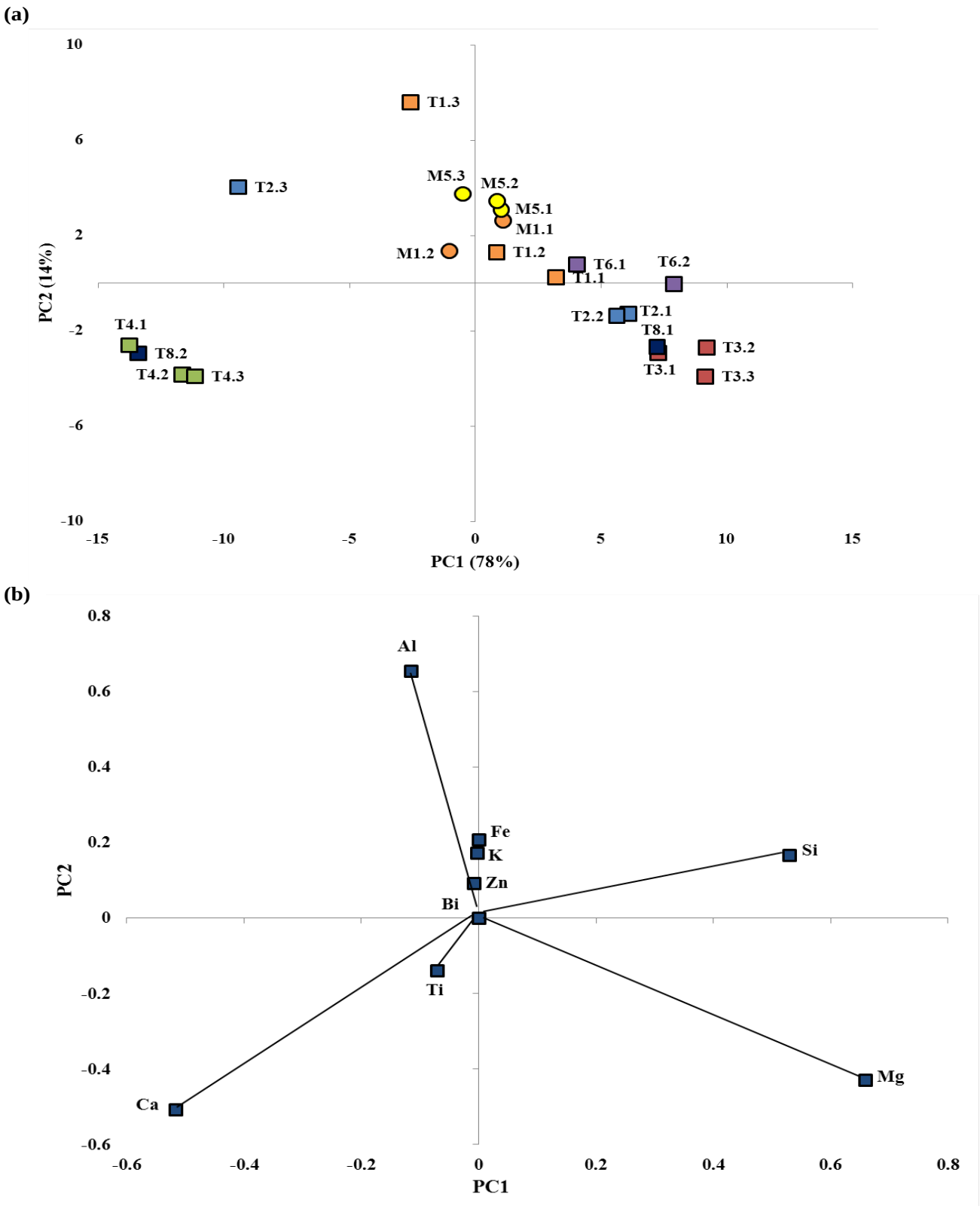

Figure 3.8 The scores plot (a) and loadings (b) from principal component analysis of elemental composition of the 21 foundation powders classified as traditional cosmetics.

no effect on the spread of samples in PC1 and PC2, as it is not present in any of the samples classified as traditional.

3.3.3 Discriminant Analysis

Discriminant analysis, also known as classification analysis, is a supervised pattern recognition technique in which samples are assigned to pre-determined groups according to multivariate data [7,9&15].

Discriminant analysis of cosmetic foundations was employed to classify formally samples into two groups; traditional or mineral formulations. Linear discriminant analysis was applied to the PC1 and PC2 scores of the relative elemental concentrations using XRF analysis. The results are plotted in Figure 3.9, in which there is a clear distinction and separation between the mineral-based and traditional formulations.

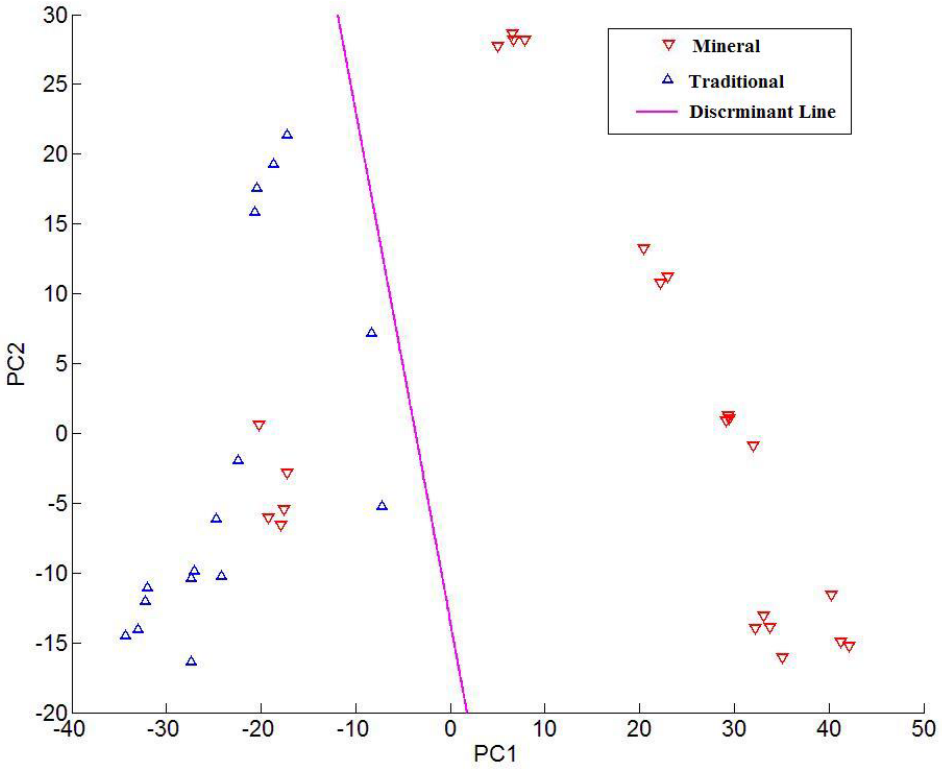

Figure 3.9 Linear Discriminant analysis using PC's scores obtained from XRF elemental concentrations of foundation samples.

However, 5 mineral-based formulations have been misclassified as traditional formulations with samples M1.x and M5.x grouped with traditional samples.

The results are best described in a confusion matrix, displayed in Table 3.3. The confusion matrix displays the errors made in the discriminant process, in which the known variables are placed into predicted groups. Of the 16 traditional-based formulations, all have been classified as traditional. However, of the 23 mineral-based formulations, 5 have been classified as traditional and 18 as mineral.

Table 3.3 Confusion Matrix of actual and predicted classification of Linear Discriminant analysis data using PC's scores obtained from XRF elemental concentrations of 39 foundation samples.

		Predicted	
		Traditional	**Mineral**
Actual	**Traditional**	16	0
	Mineral	5	18

3.3.4 Covariance and 2D Correlation

Cluster analysis, PCA and discriminant analysis were introduced in this chapter using discrete element, target, concentrations as variables. Whilst providing for efficient data analysis, much can be learned or confirmed by analysing the complete spectral profiles. The remainder of this chapter examines some techniques appropriate to full spectral analysis. These techniques are further developed in subsequent chapters.

Boxcar averaging using 3-point binning was employed to reduce and smooth data before spectral multivariate analysis. Covariance and correlation analysis was undertaken on XRF spectral data across all dispersing crystals. It is introduced in this chapter to highlight the

advantages of covariance and correlation techniques in identifying chemical information of samples in analytical methods. It was applied to XRF data, to aid in elemental analysis of cosmetic foundation samples as an alternative quantitative method to the use of internal standards. It is also valuable as an aid in identification of raw material components of cosmetic foundations using more than one spectral technique, for example XRF and XRD, which will be demonstrated in the next chapter.

Two-dimensional (2D) correlation spectroscopy seeks to highlight the similarity between variables, in this case, each elemental peak emission line. Spectral features with high correlation may arise from the same source, and hence a study of correlation can aid in interpreting data and provide insight into patterns within data.

Correlation, or interaction, between variables, x1 and x2, is given by their covariance, *Cov*.

$$Cov = \frac{\sum(x_{1i}-\bar{x}_1)(x_{2i}-\bar{x}_2)}{n-1} \qquad \text{(Equation 3.4)}$$

It can be represented as a simple rows cross-product of the, usually, mean-centered experimental matrix, **X**.

$$\mathbf{\Phi} = \mathbf{X}^{T} . \mathbf{X} \qquad \text{(Equation 3.5)}$$

Φ is the resulting matrix of *J* x *J* (*J* is the number of data points, spectral variables), **X** is the variable mean-centred experimental matrix of *i* x *j* (*i=1..I* is the number of samples) and T refers to the matrix transpose. In this study, each column of $\mathbf{X}^{T}$ corresponds to a mean-centred spectrum. Thus, **Φ** shows the correlation between the spectra according to the emission intensity changes.

The linear correlation coefficient, r_{jk}, between two variables j and k is defined by [7]:

$$r_{jk} = Cov / \sigma_j.\sigma_k \text{ , } -1 \leq 0 \leq +1 \qquad \text{(Equation 3.6)}$$

where σ_j and σ_k are the standard deviations associated with variables j and k respectively.

Generalized 2D correlation analysis gives a visual representation of the elemental compositional similarities and difference in the samples examined by XRF analysis. Two-dimensional correlation has proved useful for various kinds of spectroscopies such as NMR, IR, Raman, near-infrared and fluorescence spectroscopies [16]. The technique displays spectral data over two-dimensions, not only considering the specific individual spectra themselves but also the dynamics and changes associated with the spectral features across a set of samples [17]. The covariance matrix is sometimes referred to as a synchronous matrix that shows simultaneous spectral changes at any pair of spectral coordinates, eg. 2θ values or wavelength [18]. The 2D correlation maps will visually indicate correlated, positive and negative, and uncorrelated data features [17].

To examine all variable interactions, the XRF spectral data recorded using all dispersing crystals was combined to give an overall 'complete' spectrum of the elemental content present in foundation powders. The 2θ values of the LiF200, PET and OVO-55 crystal data were converted to wavelength using Braggs equation, $\lambda = 2d \sin\theta$, and 2d values from Table 3.1. The result was a single spectral matrix of 4398 wavelength values in the range 0.05 to 1.07nm for the 39 samples. Figure 3.10 shows the crystal overlay of the average of XRF spectra of the foundation samples analysed using the three diffracting crystals. Note that Rhodium is indicated as being present due to the Rhodium primary lamp source. Figure 3.11 shows the average of XRF data when the 3 dispersing crystals have been combined to create a completed spectra, displayed as a function of recorded data points, that are not related to 2θ. The spectral width of the emission peaks are more similar in the latter format, and this is used in subsequent data analysis.

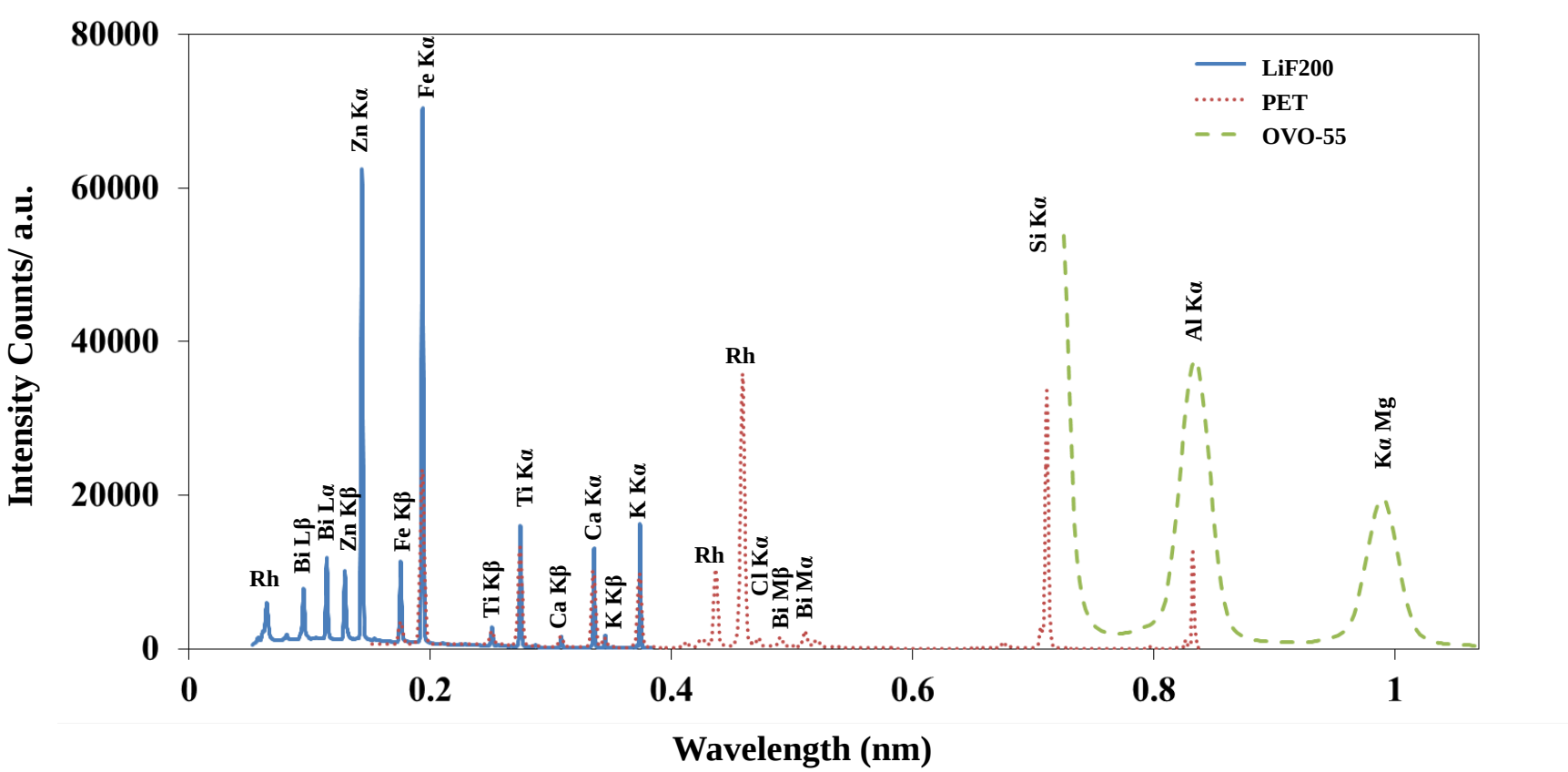

Figure 3.10 Plot of the average of the XRF spectra crystal overlay of LiF200, PET and OVO-55 dispersing crystal data, with α and β peak assignments.

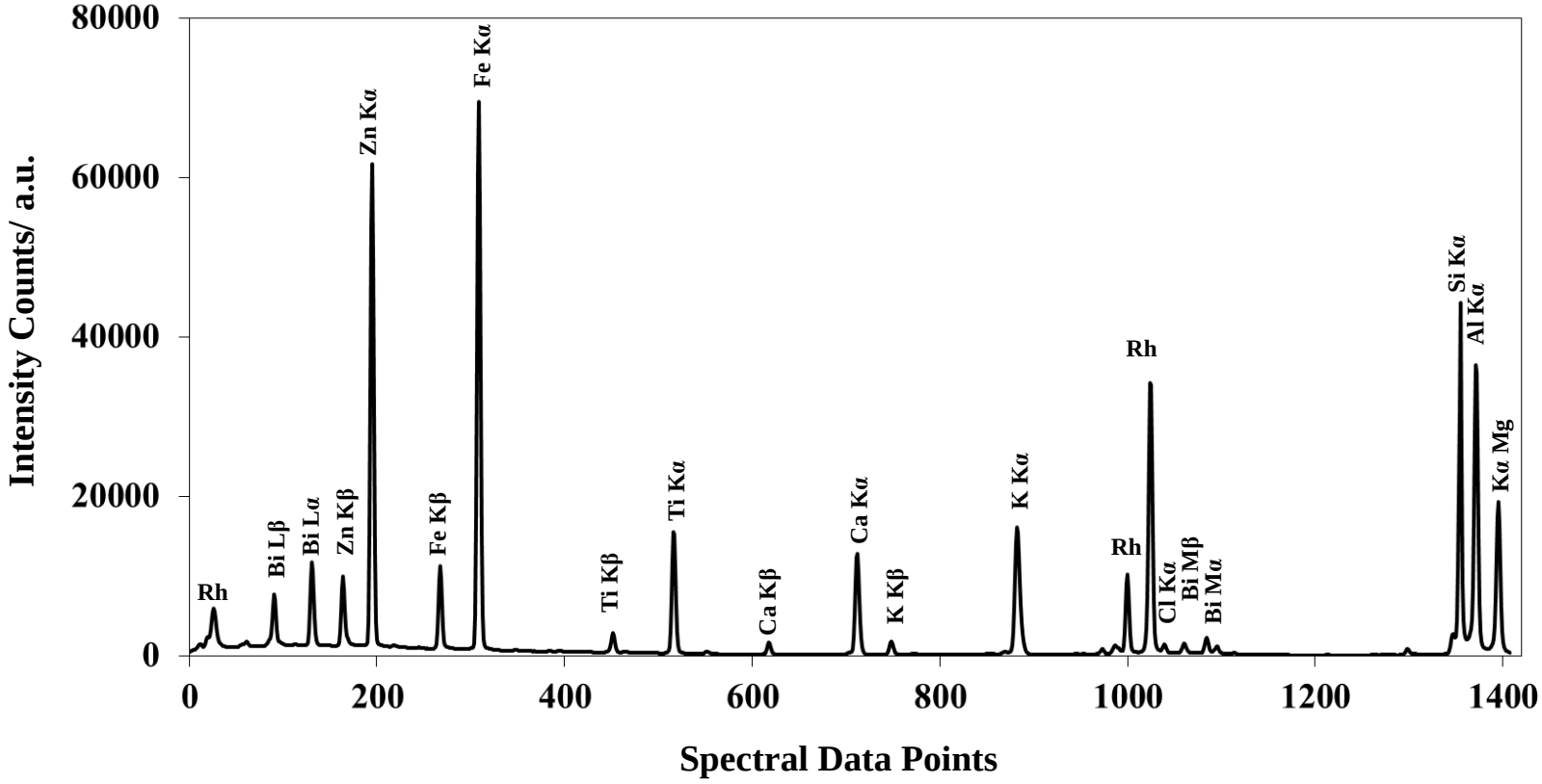

Figure 3.11 Plot of the average of XRF spectra of combined dispersing crystal data, displayed as data points (not related to 2θ), with α and β peak assignments.

Figure 3.12 shows the synchronous matrix, **Φ**, constructed from XRF data. The covariance plot gives a visual display of the positive (denoted by red) and negative (denoted by blue) correlations between elemental emission lines. A positive correlation indicates that elemental emission peak intensities are changing simultaneously. To aid with interpretation, correlation slices were produced for each element used in XRF analysis. Correlation slices of each element can be taken from the data at its particular Kα emission line across all samples. This is then cross-correlated with the entire XRF spectral data. As expected, each such slice has a high correlation between its α and β emission lines. In addition there is a strong positive correlation (0.99) between the Bi Lα and Cl Kα emission lines. This is probably due to the presence of bismuth oxychloride (BiOCl). There is also a significant positive correlation coefficient (0.98) between the Al Kα and K Kα emission lines, possibly due to the presence of mica, $KAl_2(AlSi_3O_{10})$. For each element analysed in this study, a vertical slice was taken from the correlation matrix (Φ) to help interpret the relevant information that may be difficult to see within the 2D synchronous plot. The 'slices' through **Φ** corresponding to bismuth and to aluminium are illustrated in Figure 3.13. The correlation coefficients between these elements and other peaks of significant covariance are labelled. For example, in Figure 3.13(b), the covariance slice for bismuth displays a large covariance value for the Zn Kα emission line, however, the correlation coefficient is 0.5, indicating poor correlation between bismuth and zinc. It should be noted that large covariance values do not imply a high correlation coefficient. Two-dimensional correlation maps source to highlight correlations between variables and can indicate potential relationships between variables. Its application in XRF elemental analysis is trivial, but is more useful when two sources of data are compared, and this is discussed in Chapter 4 when XRF data is shown to be useful in interpreting XRD patterns.

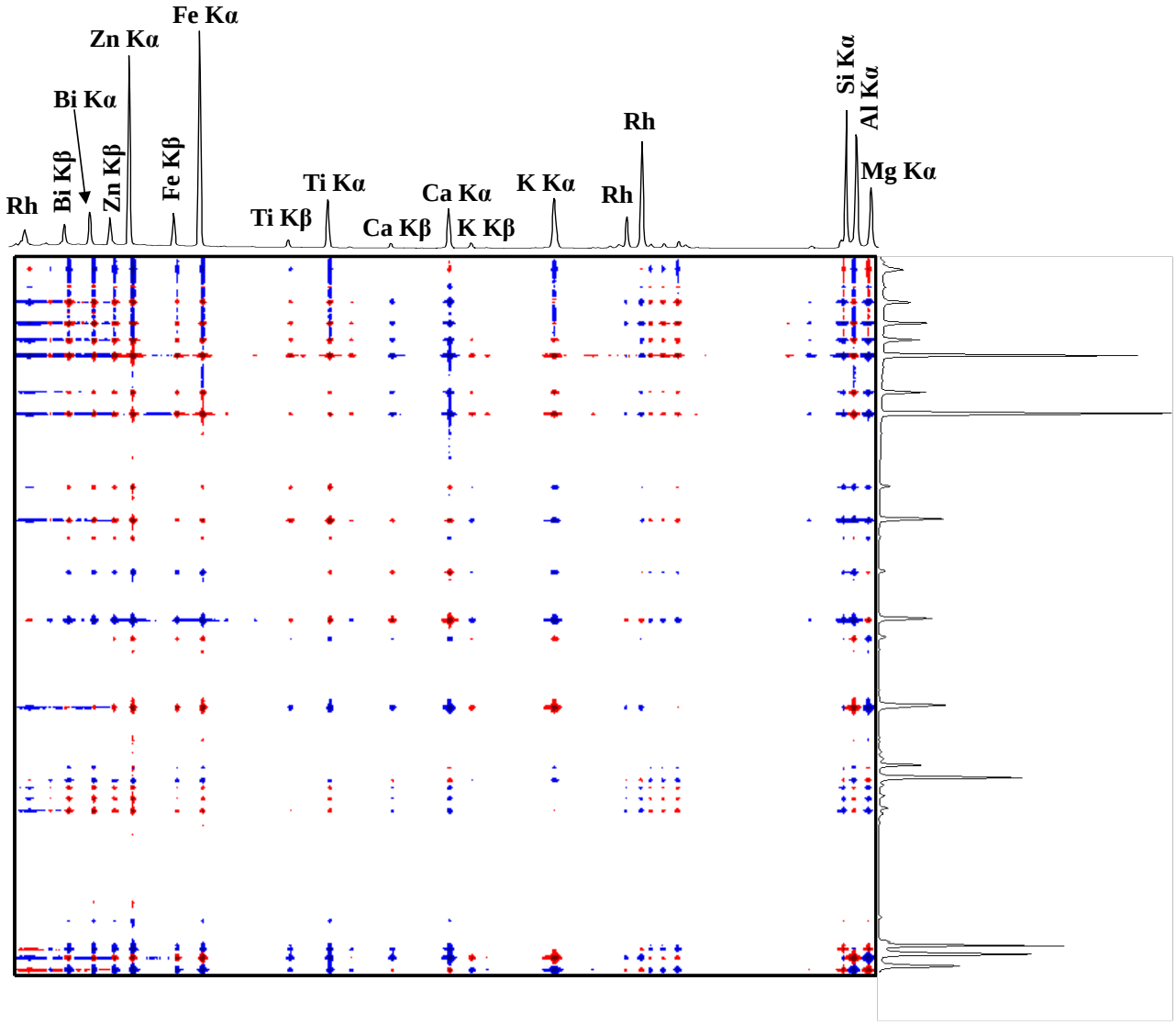

Figure 3.12 The synchronous matrix plot of XRF spectra. An average spectrum is presented along each axis to aid in identification correlating XRF elemental peaks. A positive correlation is represented in red and a negative correlation is represented by blue.

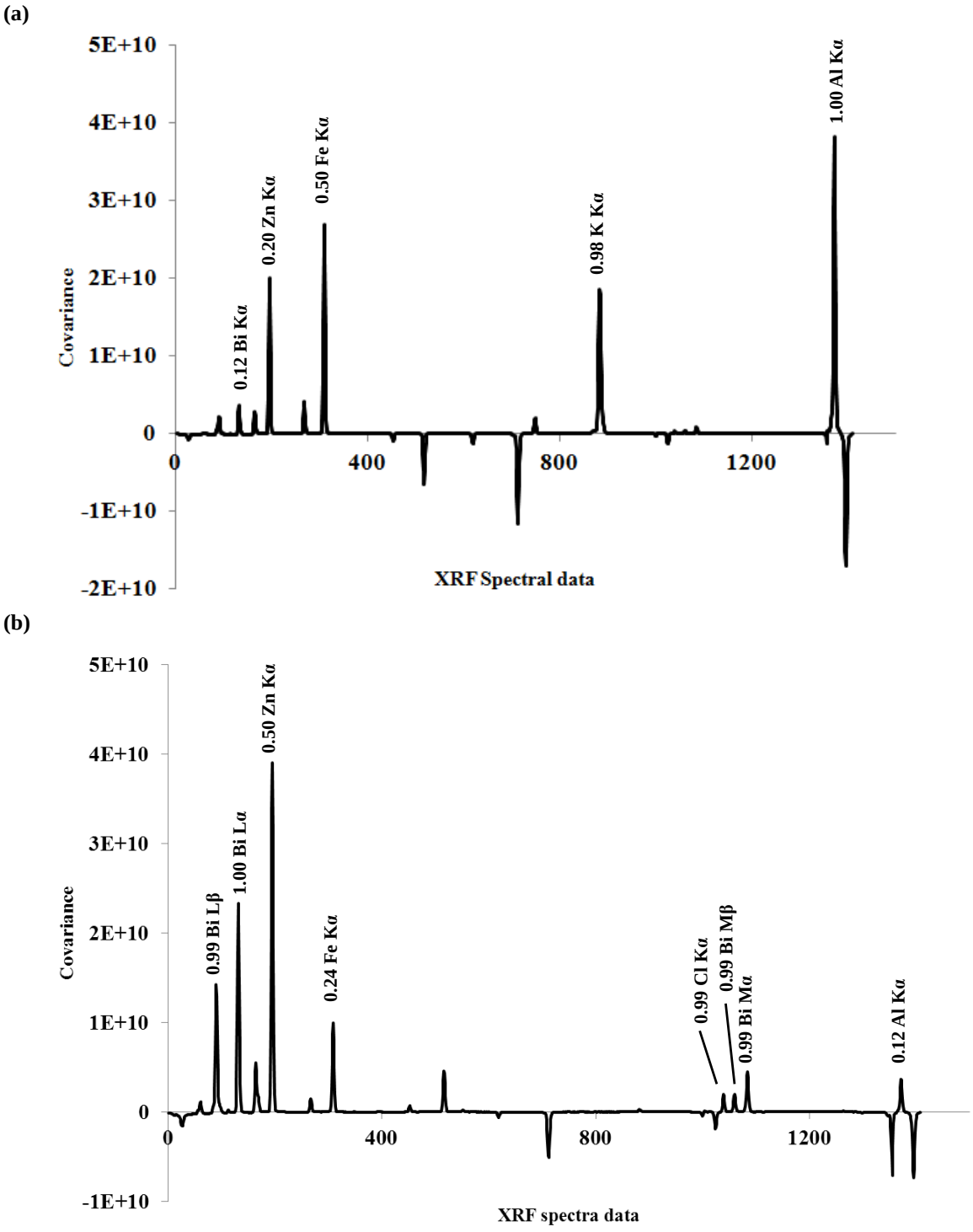

Figure 3.13 Elemental covariance slices of XRF spectral data for Al (a) and Bi (b) with correlation coefficients for corresponding β and α emission lines and correlation coefficients to other emission lines present.

3.3.5 Principal Component Analysis of Whole XRF Spectra

As well as performing PCA on the discrete elemental concentration data (sec.3.3.2), factor analysis was also applied to the matrix of full spectra, obtained as described in section 3.3.4. To ensure that scaling differences did not influence the PCA results, the XRF data were first standardized. For each variable (wavelength) the mean was subtracted and divided by its standard deviation, resulting in variables all having a standard deviation equal to one and a mean of zero [19].

Principal component analysis was undertaken on the standardized XRF spectral data for all foundation powder samples and the results are summarized in Figure 3.14. Principal component 1 and principal component 2 account for 53% of the total variance contained in the XRF data and, as before, there is a separation between the mineral-based and traditional-based foundation formulations. However, it is not as easily identified in comparison to the PCA results shown in Figure 3.5 using the relative target element concentrations. Once again samples M1.x and M5.x group with the traditional-based samples but unlike, results in Figure 3.5, samples M2.x are grouping more closely with the traditional samples. The main separation is along the PC1 axis, with mineral samples M2.x grouping to the left of the PC1 axis with the traditional samples. This is displayed in loadings plot of Figure 3.14(b) and shows that the separation is mainly due to magnesium and silica. A majority of the traditional samples group very closely in the positive PC1 region and it is difficult to see any clear separation between them. In the positive PC2 region, another group of traditional samples is clustered based on their high calcium content, samples T4.x, T2.3 and T8.2. These results were shown in the PCA of relative elemental concentrations.

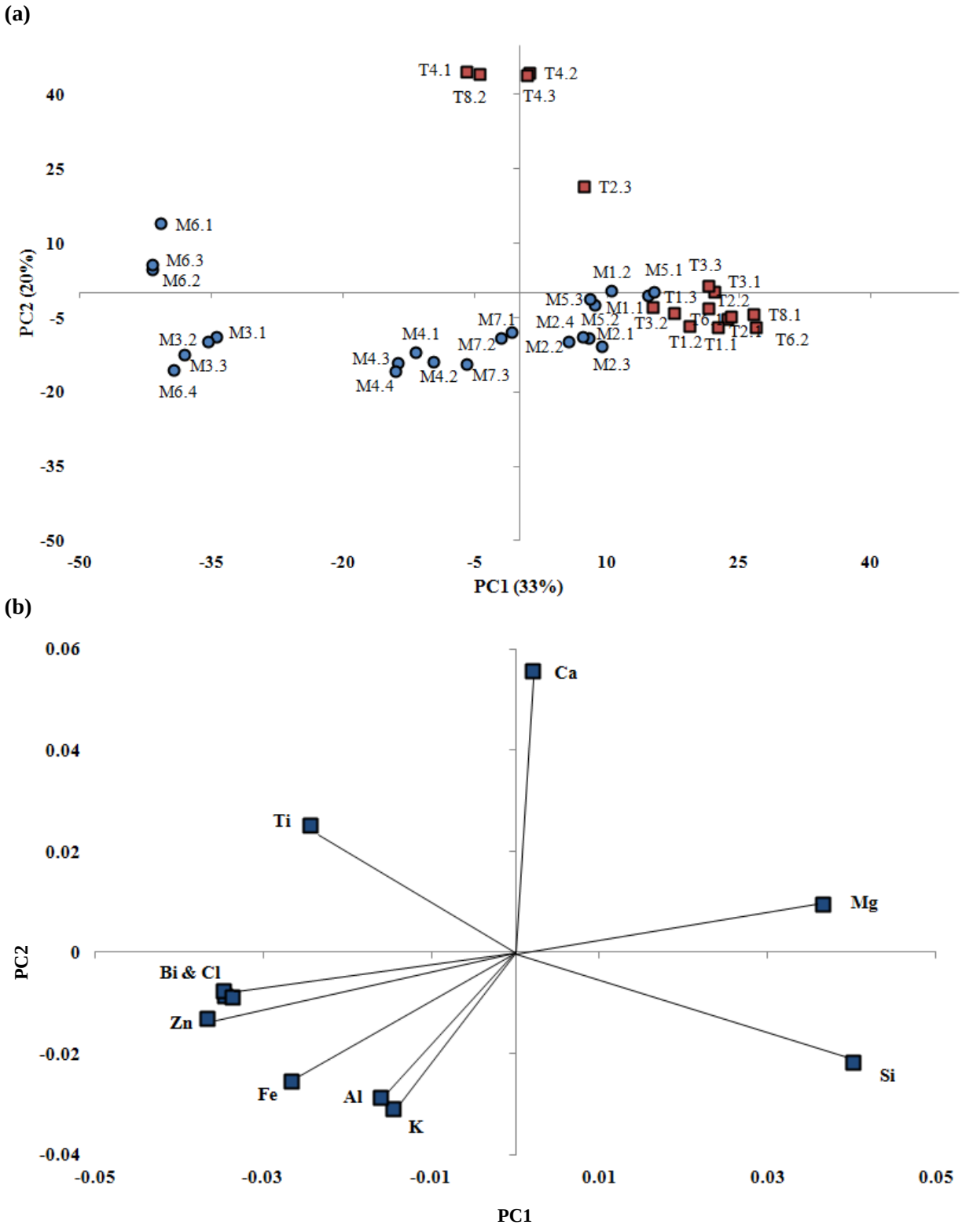

Figure 3.14 PCA of standardized XRF spectra, scores plot (a) and loadings plot associated with PC1 and PC2 of 39 foundation samples.

3.3.6 Simplisma

Simplisma (simple-to-use interactive self-modelling analysis) was applied to the XRF spectral data to seek to establish quantitative relationships between the XRF spectral data and the elemental concentrations, without the use of internal standards. Simplisma is introduced here, to demonstrate its use in resolving spectral mixture data, and is employed in later chapters using other characterization techniques. The simplisma method uses a so-called pure variable approach to resolve spectral mixtures into pure components. A pure variable is defined as a variable (e.g. an emission wavelength) that has contributions from only one of the components within the mixtures, i.e. a single element's emission with no overlap or interference from other species present in the sample [20]. The technique aims to estimate the pure component spectra and calculate the relative contribution of the pure components in the mixture spectra. As the pure variable intensities are directly proportional to the concentrations, they can be used to resolve spectra from the original data set [21]. However, for the pure variable approach to be successful in resolving a mixture data set, pure variables must be present. This is of the utmost importance, as if variables are not pure, results will not represent pure components but rather linear combinations of them [20]. In such cases, second derivative spectra can be used and have been proposed and are recommended for spectral data with highly overlapping components or baseline interferences [22].

The basis of the pure variable approach described by Windig et al., is graphically displayed in Figure 3.15 [21]. In Figure 3.15, vector **A** represents the pure variable for component A and vector **B** represents the pure variable for component B. Variables that are not pure will have contributions from component A and component B, and vectors that represent these non-pure variables will lie in between vectors **A** and **B**. The mean of all variables within data is used as a reference lying in the middle of all variables. The mean vector is represented by $\bar{\mu}$ in Figure 3.15. The first pure variable is defined as the variable vector that is furthest from the mean

vector and can be measured by the angle between the mean vector and the vector under consideration, denoted by γ [21].

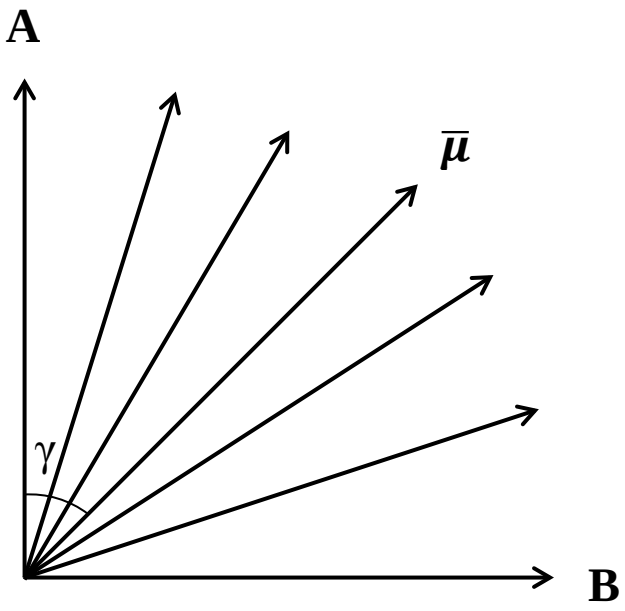

Figure 3.15 Graphical interpretation of the pure variable approach according to Windig et al. [21].

The angle, γ, is derived from the relation of the mean, $\bar{\boldsymbol{\mu}}$, standard deviation (deviation of a variable from the mean), **σ**, and the length, ***l***, of the vector of which the purity needs to be determined, from the following equation

$$l^2 = \bar{\mu}^2 + \sigma^2 \qquad \text{(Equation 3.7)}$$

This relation is visually interpreted in Figure 3.16, as a right angle triangle with sides σ, $\bar{\boldsymbol{\mu}}$ and ***l***. The angle γ represents the purity, by which the larger the angle, the higher the purity. Hence, purity is defined as the standard deviation divided by the mean, which is the tangent of angle γ.

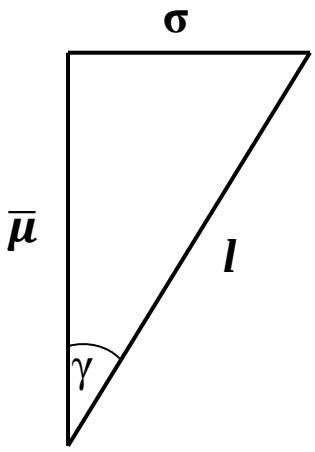

Figure 3.16 Vector representation by which the angle of purity, γ, is derived from the relation between the standard deviation, the length and the mean of the variable in which purity needs to be determined [21].

The pure variable approach seeks to identify pure variables as those exhibiting the maximum ratio of standard deviation to the mean of the data set [23]. The first pure variable identified will have the maximum ratio and once this is determined, the component with which it is associated is eliminated from the mixture. The second pure variable is the variable with the maximum ratio after elimination of the first pure variable.

The maximum ratio of standard deviation to the mean is referred to as the purity, and is given by

$$p_{ij=}\frac{\sigma_j}{\mu_j+\alpha} \qquad \text{(Equation 3.8)}$$

where p_{ij} is the purity of the variable *j* for the *i*th pure variable. μ_j and σ_j represent the mean and standard deviation of variable *j* and α is an offset for noise correction factor so that division by zero, or near zero, is not encountered. Typically, α is set to 1-3% of the largest variable value [24]. Once the first pure variable is determined the second is the one which is

the most independent of the first pure variable [25]. The offset is a constant value that reduces the effects of noise in the baseline [26].

Identification of the pure variables, from Eq. 3.8, provides the relative concentrations of each component in each sample mixture, and leads to resolution of the component spectra. This is undertaken as follows,

$$\mathbf{X} = \mathbf{C}.\mathbf{S} \qquad \text{(Equation 3.9)}$$

X is the original data row matrix (*I* x *J*), with **C** (*I* x *K*) matrix of contributions or 'concentrations' with k= 1...K representing the number of components present in the mixture. **S** is the (K x J) matrix with rows corresponding to the, K, pure component spectra. At this stage, **X** is recorded and known; however, **C** and **S** are not. An initial estimate of **C** is provided by the relative intensities of the sample at the pure variables determined in Eq. 3.8, and these are denoted by $\hat{\mathbf{C}}$.

The pure component spectra, $\hat{\mathbf{S}}$, can be estimated from Eq. 3.9 by least squares method using $\hat{\mathbf{C}}$ according to,

$$\hat{\mathbf{S}} = (\hat{\mathbf{C}}^{\mathbf{T}}.\hat{\mathbf{C}})^{-1}\,\hat{\mathbf{C}}^{\mathbf{T}}\mathbf{X} \qquad \text{(Equation 3.10)}$$

Spectra in $\hat{\mathbf{S}}$ are normalized to ensure that similar amounts of a component give spectra with similar total intensities, as given by Eq. 3.11 below:

$$w_i = \sum_{j=1}^{J} \left|\hat{s}_{i,j}\right| \qquad \text{(Equation 3.11)}$$

and $\hat{\mathbf{S}}$ is normalized to **S**,

$$\mathbf{S} = \boldsymbol{w}^{-1}\,\hat{\mathbf{S}} \qquad \text{(Equation 3.12)}$$

The final step is to re-calculate the contributions to **S** from the components according to the following least squares estimate:

$$\mathbf{C}^{T} = (\mathbf{S}.\mathbf{S}^{T})^{-1}\,\mathbf{S}\mathbf{X}^{T} \qquad \text{(Equation 3.13)}$$

Simplisma was applied to 18 XRF spectra obtained with a LiF200 dispersing crystal. The 18 true mineral foundations were chosen, which excluded samples M1.x and M5.x. The spectral data were arranged in the matrix **X**, (18 x 1586), (I x J) where I is the number of spectra and J is the number of variables (2 theta angles). Calculations were carried out in MATLAB using a program developed in-house, based on the algorithm described by Windig [27]. From previous XRF quantitative analysis, 5 major elemental components should be resolved from the LiF200 data. Figure 3.17 shows the successive purity spectra for each of the pure variables identified using the simplisma approach. The plot of the purity spectrum is the purity value, Pij, at each variable (j=1..J) from equation 3.7 [28]. Each plot, (a) to (e) represents the individual pure variables ranked from 1(a) to 5 (e) based on standard deviation. The variable with the largest standard deviation is the first pure variable and so forth. The simplisma function, using an offset (α) value of 3%, determined (a) as the first pure component. The green markers on each plot indicate the maximum ratio peak corresponding to the pure variable. As each pure variable is identified, it is eliminated from the purity spectrum [24]. In plot (b) the peak identified as the first pure variable is no longer present in the second pure variable purity spectrum. To identify the components present in the XRF spectra, simplisma calculates the resolved spectrum of each pure variable identified.

Figure 3.18 displays the resulting resolved spectra from the 18 mineral sample data matrix obtained using the LiF200 crystal data. The 5 resolved spectra, correspond to pure variables identified at 86.3°, 33.17°, 41.81°, 57.53° and 136.67° 2θ angles. From prior knowledge, these pure variables can be equated with Ti, Bi, Zn, Fe and K respectively. All variables are

true pure variables as each resolved spectrum is representative of an elemental component that has no contributions from any of the other pure components. Each resolved spectrum represents a Kα elemental line and its corresponding Kβ elemental peak.

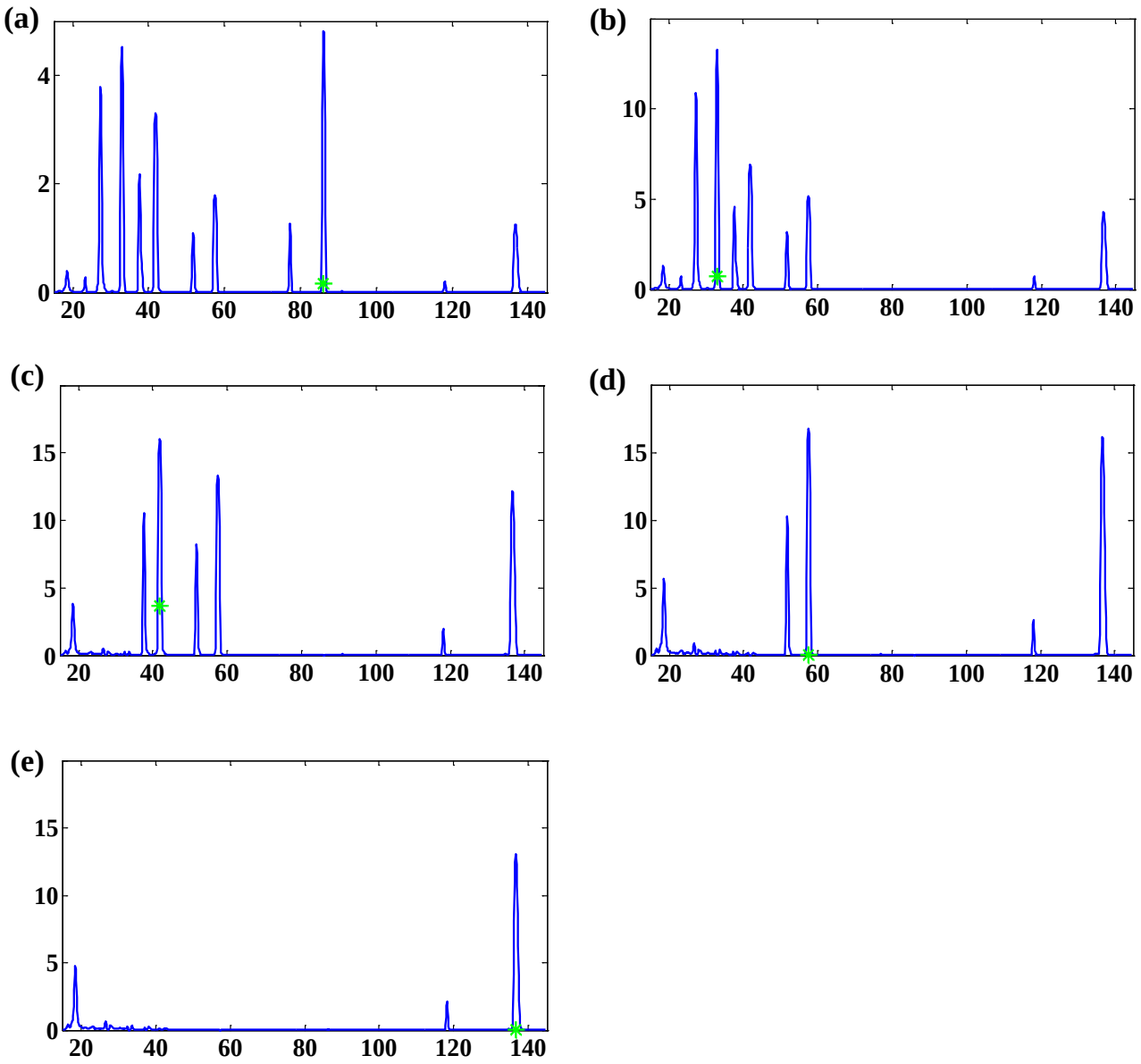

Figure 3.17 The successive series of purity spectra (a)-(e) resulting from simplisma function with the LiF200 crystal XRF spectra of true mineral foundation samples.

Figure 3.19 corresponds to the contribution or 'concentration' profiles of the pure variables calculated using simplisma. In comparison, Figure 3.19 also shows the relative concentrations of the major components as determined from quantitative analysis (Table 3.2). It is clear that the relative elemental concentrations of each sample, match the contribution profiles of the pure variables. This serves to validate the simplisma approach as an appropriate technique for curve resolution of XRF data sets.

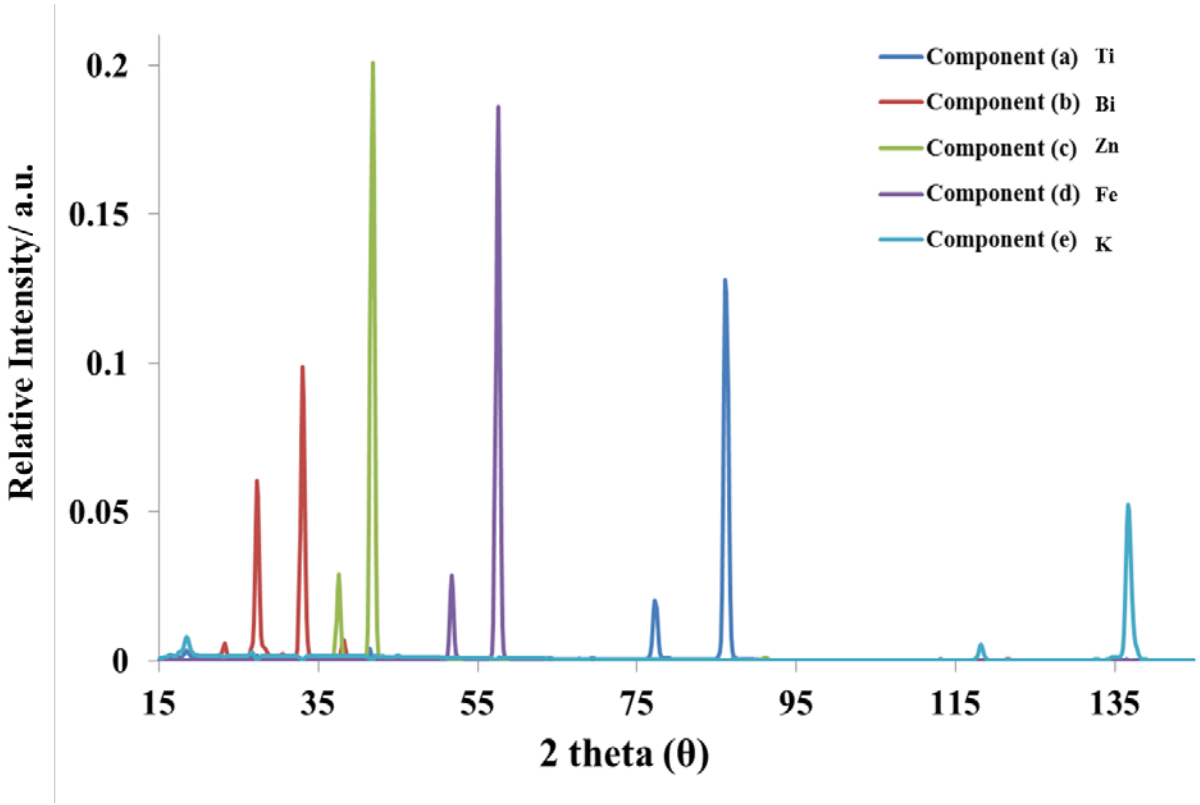

Figure 3.18 Resolved spectra of the LiF200 XRF data set, components (a)-(e), corresponding to the purity spectra shown in Figure 3.17.

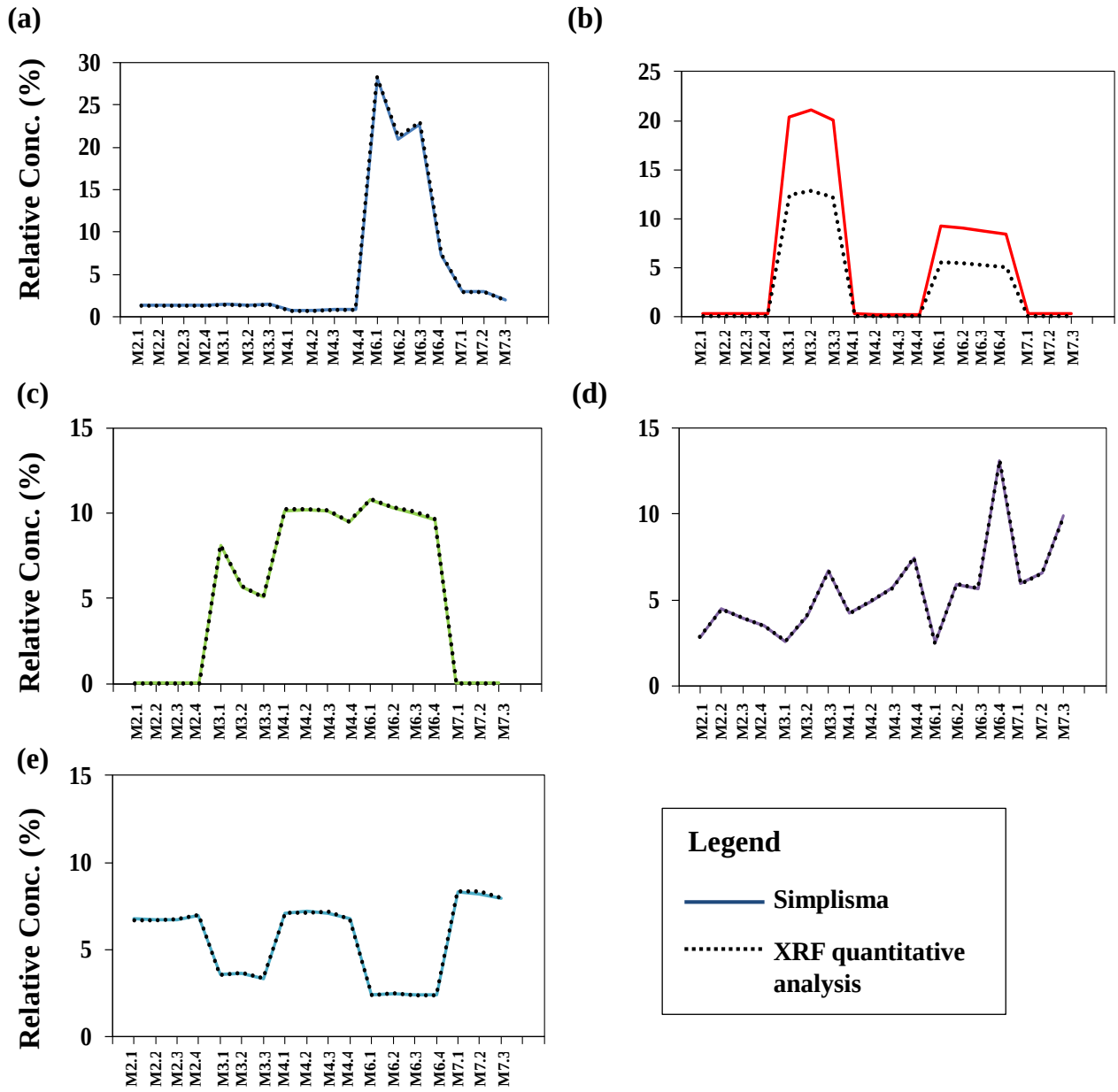

Figure 3.19 shows the 'concentration' or contribution profiles of the resolved Simplisma spectra from Figure 3.16 components (a) Ti (b) Bi (c) Zn (d) Fe and (e) K with the concentration profiles from quantitative analysis (Table 3.2) shown for comparison.

3.4 Conclusion

X-ray Fluorescence is an effective, efficient and rapid method of elemental analysis of cosmetic powder formulations. Quantitative measurements were obtained for aluminium, bismuth, calcium, iron, potassium, magnesium, silica, titanium and zinc. Using cluster analysis, discriminant analysis and principal components analysis the samples could be clearly identified as being of traditional or mineral formulation, and in the case of the mineral samples specific manufacturers could be distinguished. Of the samples examined, samples from two suppliers marketed as mineral-based were determined as being more appropriately described as traditional formulations.

Principal component analysis of the elemental concentration data could distinguish and discriminate between modern mineral foundation powders and the more traditional formulations, according to the magnesium and calcium concentrations in the samples (probably representative of talc and chalk respectively). In addition we could also distinguish between manufacturers of mineral samples according to levels of pigmentation, bismuth, and clays as indicated by aluminium content. This affords the opportunity to employ the methodology in forensic science for the identification of cosmetic powder that could be easily transferred to, and between, fabrics in a potential crime scene.

The major difference between the mineral and traditional foundation powders examined was that all traditional based samples contained varying amounts of talc and calcium carbonate. However, a small number of mineral-based samples (from two manufacturers) also appeared to contain these ingredients. This is of concern as these products should not contain any potential skin irritants and talc should not be used in their production. The presence of bismuth oxychloride in a significant number of the mineral samples from two suppliers could also be of concern.

Since mineral cosmetics command a premium price, due to them being marketed as 'chemical free' and not containing irritants, it is important that consumers have recourse to independent analytical data.

Principal component analysis and linear discriminant analysis, proved effective in highlighting and separating foundation samples according to type and the elemental content within each sample.

Generalized 2D correlation was effective in highlighting the positively and negatively correlated elemental emission lines within XRF data. It gave an insight into the relationship between the elemental content of the raw materials within foundation powders.

Simplisma can be utilized to decompose XRF mixture spectra for variable selection. It is ideal for XRF spectra as peak intensities are clean, with no overlap of peaks and with little background noise.

Elemental analysis of cosmetic foundation powders provided significant information into the ingredients used in their production. However, for full identification and characterization of these samples, further analysis is required. The next chapter will look at the mineral phases present using X-ray Diffraction analysis. This will give a better understanding of the raw materials used. The knowledge determined through XRF analysis will aid in the XRD interpretation of results and chemometric data analysis techniques will be applied to XRD data in conjunction with XRF data to further characterize foundation powder samples.

3.5 References

1. M. S. Shackely, *X-ray Fluorescence (XRF) in Geoarchaeology*, Springer Science+Business Media, LLC, New York, USA, **2011**.

2. C. Whiston, *X-ray Methods*, John Wiley & Sons, London, UK, **1987**.

3. G. R. Lachance and F. Claisse, *Quantitative XRF Analysis Theory and Applications*, John Wiley & Sons, England, **1995**.

4. http://www.thefabricator.com/article/metalsmaterials/whats-that-materialr, Date Accessed- 01/06/2012.

5. G.R. Chatwal and S.K. Anand, *Spectroscopy (2nd Ed.)*, Himalaya Publishing House, New Delhi, India, **2009**.

6. F. Rouessac and A. Rouessac, *Chemical Analysis, Modern Instrumentation Methods and Techniques (2nd Ed)*, John Wiley & Sons, Chichester, England, **2007**.

7. M. J. Adams, *Chemometrics in Analytical Spectroscopy (2nd Ed.)*, Royal Society of Chemistry, Cambridge, UK, **2004.**

8. R. G. Brereton, *Chemometrics for Pattern Recognition*, Wiley, UK, **2009**.

9. K. Varmuza and P. Filzmoser, *Introduction to Multivariate Statistical Analysis in Chemometrics*, CRC Press, **2009**.

10. MATLAB software (Ver. 7.10, Mathworks Inc., NSW, Australia) and the PLS-Toolbox (Eigenvector Research Inc., WA, USA).

11. M. Otto, *Chemometrics (2nd Ed.)*, Wiley. VCH & Co., Germany, **2007**.

12. H. Butler, W. A. Poucher, *Poucher's perfumes, cosmetics and Soaps (9th Ed.)*, Kluwer Acadmic Publishers, Boston, **2000**.

13. M. S. Balsam, E. Saggarin, *Cosmetic, Science and Technology Volume 1 (2nd Ed.)*, Wiley-Interscience, New York. **1972**.

14. J. E. Kogel, N. C. Trivedi, J. M. Barker, S. T. Krukowski, *Industrial Minerals and Rocks, (7th Ed.),* Soc. Mining, Metallurgy and Exploration, Colorado, USA, **2006**,

15. V. Pawlowsky-Glahn, A. Buccianti, *Compositional Data Analysis*, Wiley, West Sussex, **2011**.

16. S. Sasic, A. Musyznski, Y. Ozaki, *A New Possibility of the Generalized Two-Dimensional Correlation Spectroscopy. 1. Sample−Sample Correlation Spectroscopy*, 2000, **104**(27): p.6380-6387.

17. G. M. Kirwan, S. Clark, N. W. Barnett, J. O. Niere, M. J. Adams, *Generalised 2D-correlation NMR analysis of a wine fermentation*, Analytica. Chimica. Acta., 2008, **629**(1-2): p.128-135.

18. I. Noda and Y. Ozaki, *Two-Dimensional Correlation Applications in Vibrational and Optical Spectroscopy*, John Wiley & Sons, Chichester, England, **2004**.

19. T. Naes, T. Isaksson, T. Fearn, T. Davies, *A user friendly guide to Multivariate Calibration & Classification*, NIR Publications, Chichester, UK, **2002.**

20. B. M. Wise, J. M. Shaver, N. B. Gallagher, W. Windig, R. Bro, R. S. Koch, *Chemometrics tutorial for PLS_Toolbox and Solo*, Eigenvector Research Inc., Wenatchee USA, **2006**.

21. W. Windig, D. E. Margevich, W. P. McKenna, *A novel tool for two-dimensional correlation spectroscopy*, Chemometric and Intelligent Laboratory Systems, 1995, **28**: p.109-128.

22. W. Windig, B. Antalek, J. L. Lippert, Y. Batonneau, C. Bremard, *Combined Use of Conventional and Second-Derivative Data in SIMPLIMA Self-Modeling Mixture Analysis Approach*, Anal. Chem., 2002, **74**: p.1371-1379.

23. W. Windig and C. E. Heckler, *Self-modeling mixture analysis of categorized pyrolysis mass spectral data with the SIMPLISMA approach*, Chemometric and Intelligent Laboratory Systems, 1992, **14**: p. 195-207.

24. W. Windig, D. A. Stephenson, *Self-Modeling Mixture Analysis of Second-Derivative Near-Infrared Spectral Data Using the Simplisma Approach*, Anal. Chem., 1992, **64**: p.2735-2742.

25. W. Windig and J. Guilment, *Interactive Self-Modeling Mixture Analysis*, Analytical Chemistry, 1991, 63:p.1425-1432.

26. Y. Batonneau, J. Laureyns, J. Merlins, C. Bremard, *Self-modeling mixture analysis of Raman microspectrometric investigations of dust emitted by lead and zinc smelters*, Analytica Chimica Acta, 2001, **446**: p.23-27.

27. W. Windig, *Spectral data files for self-modeling curve resolution with examples using the Simplisma approach*, Chemometric and Intelligent Laboratory Systems, 1997, **36**: p.3-16.

28. A. Bogomolov, M. Hachey, *Application of SIMPLISMA purity function for variable selection in multivariate regression analysis: A case study of protein secondary structure determination from infrared*, Chemometric and Intelligent Laboratory Systems, 2007 **88**: p. 132-142.

Chapter 4: X-ray Diffraction

4.1 Introduction

The main application of X-ray Diffraction (XRD) is the elucidation and identification of the crystal structure of materials [1]. XRD measures the position (in terms of diffraction angle) and intensity of a monochromatic X-ray beam diffracted by a crystalline solid.

Crystals consist of regular three dimensional array of atoms, ions and molecules. The smallest repeating unit is referred to as the unit cell, each with 3 sides (a, b & c) and 3 angles (α, β & γ). Planes are the repeating array of atoms within the crystal, each plane is identical to the next. The repeat distance (d) between each plane is called the interplanar spacing which contains all atoms in the structure [2]. Crystals have the ability to reflect an X-ray beam when the Bragg equation is satisfied [2]

$$2d \sin\theta = n\lambda \qquad \text{(Equation 4.1)}$$

The Bragg equation was developed by W.L Bragg in 1912 and gives the relationship between the diffraction angle θ, crystal plane dimensions, d, the wavelength of incident radiation, λ, and n is an integer specifying the order of reflection [2]. The Bragg equation can only be obeyed for a particular family of planes and it is unlikely that a particular plane will be at the correct angle to satisfy the Bragg equation. The crystals must be rotated until they are positioned at the right angle or powdered to produce millions of small crystals with planes in all possible directions, making it easier to satisfy the Bragg law. Figure 4.1 shows a beam of X-rays incident on the surface of a crystal sample at an angle θ. A, B and C represent the family of planes of regular arrays of atoms within a crystal with d spacings between them. 1,

1a, 2, 2a and 3 represent the incident rays and 1', 1a', 2', 2a' and 3' the corresponding scattered rays from striking a crystal. The diffraction angle is always represented as 2θ, which is the angle between the diffracted and transmitted X-ray beam [3].

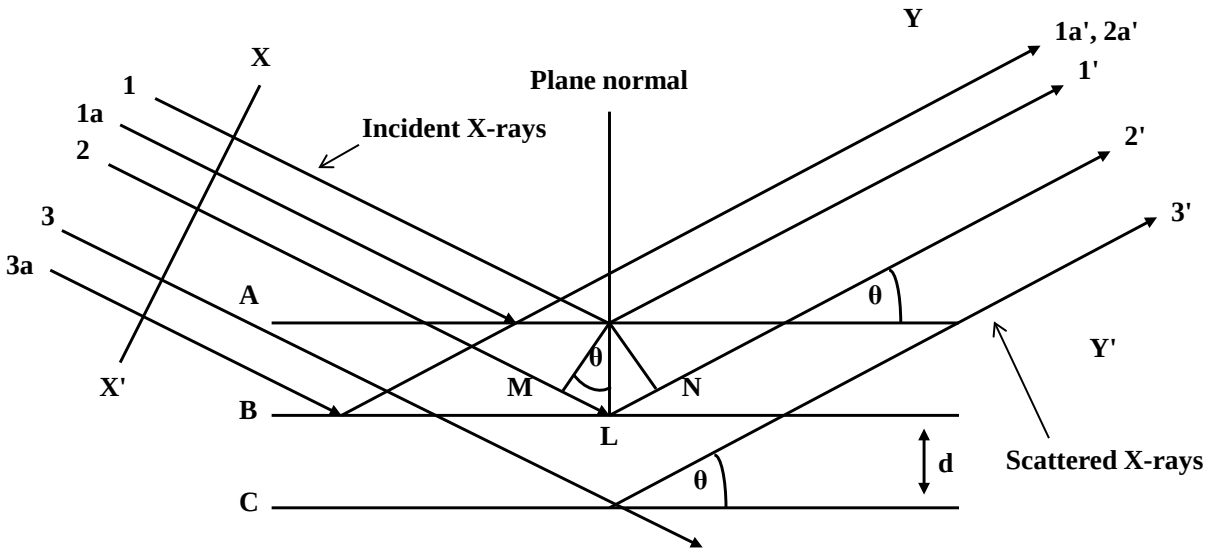

Figure 4.1 Diffraction of X-rays by a crystalline substance according to the Bragg equation [3].

4.1.2 Powder X-ray Diffraction

The ideal powder sample consists of a large number of small crystals with random orientation [4]. Powder diffraction uses a monochromatic beam of X-rays directed at the powdered sample and a diffracted ray is observed when the Bragg law is satisfied. The diffracted rays are reflected to the detector, situated on a table that rotates through 2θ degrees, to ensure that the detector is always in the correct position to attain all possible diffraction directions of the lattice [2].

Every crystalline substance has a unique X-ray powder pattern with diffraction line position dependent upon the unit cell size, and line intensity dependent on the type of atoms present and their arrangement within the crystal. In 1936, Hanawalt devised a system of classifying

powder patterns so that unknown patterns could be identified [2]. This method used the d values (interplanar spacings) and relative intensities to identify unknowns [2]. Today, component identification is still undertaken using Hanawalt's method, based on a search/matching technique using Powder Diffraction Files (PDF) produced by the Joint committee on Powder Diffraction Standards (JCPDS) [5]. PDF's consist of a collection of single phase reference patterns that are compared against the unknown diffraction pattern to find potential matches [6]. If the unknown powder diffraction is of a single phase, identification can be simple, however, when the diffraction pattern is a mixture of two or more phases, identification becomes more difficult. Hanawalt developed the method of utilizing the three strongest lines in the diffraction pattern (d_1, d_2, d_3) to search the PDF database, in order of their decreasing peak intensities. When an appropriate match of d-spacings and relative intensities of a standard PDF is found, identification is considered complete [7]. Quantitative XRD analysis utilizes this approach measuring the phase or phases of an unknown sample and estimating relative proportions of different phases in multiphase samples by comparing peak positions and intensities to JCPDS standards [2].

There are various methods currently used for quantitative analysis of diffraction patterns based on peak intensities, such as the reference intensity ratio (RIR) method. The RIR method scales all diffraction data to the diffraction pattern of standard reference materials [8]. The unknown sample diffraction pattern is ratioed to the standard reference and set to a constant. Ratios to the standard reference and measure of peak areas are used to determine the concentration of phases in the unknown sample. The RIR method has previously been exploited for quantitative analysis of unknown geological samples with the use of XRF and XRD [9]. The Bruker corporation, have developed a method of combining XRF and XRD for quantitative analysis of unknown geological samples. Using the DIFFRAC plus EVA software, a search-match algorithm is applied to XRD data, and semi-quantitative analysis

determined by the reference-intensity-ratio (RIR) for the XRD and XRF data simultaneously. Crude elemental concentrations (present or absent) obtained through XRF are used to confirm the presence or absence of minerals in geological samples and highlight the correctness of the XRD phase identification results [9].

Powder XRD is employed in this chapter to investigate structural information relating to the crystalline content (mineral and inorganic components) of the foundation cosmetic samples. Analysis of cosmetics using XRD has received little attention in the scientific press but because the ingredients used in foundations are highly crystalline, it is an ideal method for identification. Here, the technique is employed with multivariate data analysis, including generalized 2D correlation, Principal Component Analysis (PCA) and Simplisma to aid in diffraction pattern interpretation.

XRD is considered an accurate analytical method for determining the presence of mineral and clay phases in samples. When the sample chemistry and/or origin are unknown, ambiguous results can be obtained and phase identification can be difficult [9]. Elemental concentrations obtained by XRF analysis (from Chapter 3: X-Ray Fluorescence) can be correlated with XRD data to further aid in peak identification. Generalized 2D correlation analysis was used to represent the magnitude of correlation between the two analysis techniques based on changes in component intensities. In this study, XRF and XRD were used as complementary methods in investigating the raw material composition and quantitative analysis of cosmetic foundation powders.

Generalized 2D correlation has been widely used across various techniques, such as NMR, IR, Raman, near-infrared and fluorescence spectroscopies [10]. In this study, the use of generalized 2D correlation aims to establish a relationship between different spectroscopic techniques, in this case, XRF and XRD. However, in the case of comparing two different

spectroscopies, 2D correlation has been studied to establish relations between near-IR and near-IR-FT (Fourier transform) Raman spectroscopy. According to Windig et al., the so-called correlation maps can be quite complex and he proposed to resolve original 2D maps into sub-2D maps for a simper interpretation [11].

Difficulties can occur with XRD. The major problems encountered during the experiments, described here are due to the multiplicity of lines in diffraction patterns arising from the numerous components present in samples. In addition, poorly defined diffraction patterns, where components cannot be easily identified are problematic [12].

4.2 Experimental

As with the XRF studies (Chapter 3), thirty-nine different foundation samples were analysed. These included 23 labelled as being mineral-based samples and 16 traditional-based formulations of loose and pressed powders, representing varying shades of colour, from 8 commercial manufacturers and suppliers in the Australian market. As before, each sample was assigned a code comprising its type, 'M' or 'T' depending on whether it is marketed as a mineral or traditional face powder, a number, 1- 8, identifying the manufacturer, and a second number indicating the sample number in that set of manufacturers samples. The samples, with description and coding employed, are listed in Table 1 (Chapter 2: The Cosmetic Foundation Samples: Their appearance and Visible Spectra).

4.2.1 Raw Component Analysis

Cosmetic foundations contain a variety of raw materials, each possessing their own properties and desired characteristics that contribute to the final formulation product. As the mixture of

materials is complex, cosmetic grade raw materials were examined independently to aid in the characterization of cosmetic foundation samples by XRD.

Raw materials were purchased from various cosmetic suppliers to ensure they were of cosmetic grade. Of these cosmetic suppliers, two were Australian-owned, All Colour Supplies Pty. Ltd. and Big Tree Supplies, Brisbane Queensland and the remaining materials were obtained from The Ponte Vedra Soap Shoppe Inc, Florida USA. Talc and kaolin certified standards were purchased from Graham B. Jackson Pty. Ltd., Dandenong Victoria. There was a wide variety of cosmetic grade ingredients, differing in particle size, colour and chemical properties to produce specific functions of cosmetic products. Other materials (all A.R Grade) were readily avaliable from a range of manufacturers. Various forms of each material were obtained and are described in Table 4.1 and 4.2.

Table 4.1 Cosmetic grade iron oxides purchased for analysis of foundation powder samples. (PVSS)- Ponte Vedra Soap Shoppe, (ACS)- All Colour Supplies.

Iron Oxide/ Description	**Supplier**	**CAS number(s)**
Sienna Brown Iron Oxide	PVSS	1309-37-1, 1317-61-9, 51274-00-1
Medium Brown Iron Oxide	PVSS	1309-37-1, 1317-61-9, 51274-00-1
Deep Red Iron Oxide	PVSS	1309-37-1
Ochre Brown Iron Oxide	PVSS	1332-37-2
Orange Iron Oxide	PVSS	51274-001, 1332-37-1
Brown Iron Oxide	PVSS	12227-89-3, 1332-37-2, 51274-00-1
Oxide- Brown	ACS	12227-98-3
Oxide- Red	ACS	1332-37-2
Oxide- Yellow	ACS	51274-00-1

Table 4.2 Cosmetic grade raw materials purchased for analysis of cosmetic foundation powders. (PVSS)- Ponte Vedra Soap Shoppe, (GBJ) Graham B. Jackson.

Raw Material/ Description	**Supplier**	**CAS number(s)**
Titanium Dioxide (Rutile)	PVSS	13463-67-7
Titanium Dioxide (Micronized- 15nm particle size)	PVSS	13463-67-7
Zinc Oxide (Low-Micron- 0.12 microns particle size)	PVSS	1314-13-2
Mica (Pearl Flake)- blended with titanium dioxide	PVSS	1200-26-2 13463-67-7
Sericite Mica	PVSS	1200-1-26-1
Magnesium Stearate	PVSS	557-04-0
Bismuth Oxychloride	PVSS	7787-59-9
Talc- DC60131	GBJ	14807-96-6
Talc- DC60132	GBJ	14807-96-6
Kaolin- DC60122	GBJ	1332-58-7
Kaolin- DC60123	GBJ	332-58-7
Zinc Oxide	Ajax	1314-13-2
Kaolin	CNAC	1332-58-7
Titanium Dioxide	Austiox	13463-67-7

Each cosmetic material has specifications on the grade and quality required to be incorporated into cosmetic products.

4.2.2 Sample Analysis

All cosmetic foundation samples and raw materials were analysed using a powder XRD diffractometer (Model Bruker D8 Advance, Bruker AXS Gmbh, Karlsruhe, Germany) with Cu Kα (λ= 1.5406 Å) radiation at 40kV and 35mA. Minimal sample preparation was required for analysis. Samples were packed into sample holders and placed into the instrument. Foundation powders were scanned over a 2θ range from 3-50°. Data was collected in raw file form (.raw) and converted to UXD file format using the File Exchange Program XCH (Ver. 5.0.10, 2004, Bruker AXS, Socabim, Karlsruhe, Germany) before data analysis. Each diffraction pattern consisted of 2351 data points in which intensity was recorded every 0.02°.

4.2.3 Data Processing

To identify the components present in cosmetic foundation samples, Bruker Diffrac plus 2005 Evaluation (EVA) software (Ver. 11.0, Bruker AXS Gmbh, Karlsruhe, Germany) was employed to perform a search/match analysis by comparing sample patterns to reference patterns from a ICDD Powder Diffraction Files (PDF) database. For the search/match method to obtain greater accuracy, pre-treatment of foundation sample scans was required. Background subtraction was undertaken to "flatten" diffraction patterns and to define the level of noise, allowing the search algorithm to identify which part of the diffraction pattern is significant signal, and which part is noise [13]. The algorithm uses Euclidean distances to match reference diffraction patterns to unknowns, based on diffraction angles and peak intensities. Background subtraction is vital for the search algorithm to successfully match patterns as it eliminates the background noise under the diffraction pattern that the algorithm would otherwise consider as diffraction peaks.

The search is conducted based on user-selected criteria. As the foundation samples are multi-

phases mixtures, the components present may have only a few or many diffraction lines in the same 2θ range. The search criteria aim to give the user a greater chance of identification by searching based on the complexity or the simplicity of their sample patterns. Typical criteria are: (a) favour simple patterns (patterns sharing few lines), (b) favour complex patterns (patterns sharing many lines) and (c) neutral (giving equal chances to all patterns that may be present) [13]. For the analysis of cosmetic foundation samples, the "favour simple patterns" was found to give the best matches to known cosmetic grade ingredients.

4.3 Results and Discussion

Alignment of XRD data was required before data analysis. A shift array function using MATLAB was used to correct alignment for samples that exhibited visible peak shifts and the data were circularly shifted, left or right, by $<\pm 10$ readings. A negative shift size value indicates the sample data arrays were shifted to the left [14]. Once aligned visually, 5-point binning was employed to smooth data and reduce the number of variables considered.

4.3.1 Comparison of Diffraction patterns using EVA

The DIFFRAC search and match method was carried out for all foundation powder samples. The resulting PDF's matched for each sample are presented in Tables 4.3 and 4.4 for mineral foundations and traditional samples, respectively. In general, the search and match procedure returned results that were expected, however many results did not comply with known compounds found in foundation formulas and many 'hits' could be disregarded. Talc was matched with all traditional-based samples, and as expected matched with samples M1.x and M5.x which have been classified with traditional samples. The search produced duplicate patterns of Talc-2M, different diffraction patterns corresponding to the same chemical phase

for matches to diffraction patterns of samples. The EVA search matched potassium magnesium aluminium silicate hydroxide to the diffraction pattern of sample M1.1. This is an unlikely component, as the other samples from the same manufacturer, matched results of Talc-2M and it could be assumed that the manufacturer would use similar raw materials across all their products. This indicates that component phase matches were not always of cosmetic grade.

The diffraction patterns of the mineral-based samples matched well with differing diffraction patterns and forms of muscovite. Muscovite is a common form of mica and is similar to sericite mica, the form often used in cosmetic production. Sericite mica was not found in the EVA PDF database and the closest match was found to be muscovite. As expected, bismuth oxychloride was easily identified in samples M3.x and M6.x in the form of synthetic bismoclite. The search matched diffraction patterns of zinc oxide, titanium dioxide and calcium carbonate to sample diffraction pattern in the forms of, zincite, anatase/rutile and calcite, respectively. These results were compared to the relative elemental concentrations of zinc, titanium and calcium obtained by XRF analysis. For zinc oxide, EVA matched zincite to samples M3.x, M4.x and M6.x. This agreed with elemental concentration profiles produced from XRF. However, XRF found zinc to be in samples M1.x and T1.x, although in smaller concentrations, and the EVA search was unable to match zinc oxide to their diffraction patterns. This was also the case with titanium dioxide. Samples M3.x, M4.x and M6.x were matched with either anatase or rutile, but EVA failed to match sample T8.2 which also contained titanium according to XRF results. Calcite ($CaCO_3$) was found to be present in samples T4.x but according to XRF results, samples T8.2 is high in calcium and T2.3 contained smaller amounts of calcium. Individual, expected, components, such as kaolin and iron oxides, were then searched, to find the best fit. Kaolin was matched to various traditional

Table 4.3 EVA search matches for foundation samples classified as mineral-based formulation

Component Name/ Sample	**M2.1**	**M2.2**	**M2.3**	**M2.4**	**M3.1**	**M3.2**	**M3.3**	**M4.1**	**M4.2**	**M4.3**	**M4.4**	**M6.1**	**M6.2**	**M6.3**	**M6.4**	**M7.1**	**M7.2**	**M7.3**
Muscovite-2M1 $(K_2(SiAl)O_{10}(OH,F)_2$		×	×	×	×	×	×	×	×	×	×	×	×	×	×	×	×	×
Muscovite $H_2KAl_3(SiO_4)_3$	×																	
Kaolinite $(Al_2(Si2O_5)(OH)_{4)}$	×		×	×														
Kaolinite 1A $(Al_2(Si_2O_5)(OH)_4)$		×						×		×	×							
Bismoclite (BiOCl)					×	×	×					×	×	×	×			
Zincite (ZnO)					×	×	×	×	×	×	×	×	×	×	×			
Zinc Hydroxide $(Zn(OH)_2)$							×											
Anatase (TiO_2)												×	×	×	×			

Table 4.4 EVA search matches for foundations classified as traditional-based formulas.

Component Name/ Sample	**M1.1**	**M1.2**	**M5.1**	**M5.2**	**M5.3**	**T6.1**	**T1.1**	**T1.2**	**T3.1**	**T8.1**	**T8.2**	**T2.1**	**T2.2**	**T4.1**	**T4.2**	**T1.3**	**T6.2**	**T2.3**	**T3.2**	**T3.3**	**T4.3**
Talc-2M (Mg3Si4O10(OH)2		×	×	×	×	×	×	×	×	×	×	×	×	×	×	×	×	×	×	×	×
Muscovite $H_2KAl_3(SiO_4)_3$						×											×				
Muscovite 3T Si-rich													×					×			
Kaolinite $(Al_2(Si2O_5)(OH)_{4)}$										×	×										
Kaolinite 1A $(Al_2(Si_2O_5)(OH)_4)$							×	×						×	×	×					×
Potassium Magnesium Aluminium Silicate	×																				
Hydrogen Aluminium Silicate						×															
Calcite ($CaCO_3$)														×	×						×
Rutile (TiO_2)							×		×		×					×			×	×	
Anatase (TiO_2)														×							×

and mineral-based samples in differing diffraction patterns of kaolinite. Iron oxides could not be matched in the diffraction patterns of foundation samples. This was unfortunate but expected because of the fluorescence of iron by the Cu Kα radiation [2]. Overall, many cosmetic grade ingredients used for foundation powders were not found in the EVA database, leaving unidentified peaks in the data. X-ray Fluorescence provided prior knowledge to the expected components present in samples and aided in the EVA search by limiting the results produced. The EVA search/match method, was useful in providing some information regarding the phase analysis of cosmetic foundation powders and could be used as a preliminary analysis. However, it did not provide a full characterization of foundation samples and the use of cosmetic raw material diffraction pattern data was considered to be a more appropriate method of component identification. There is difficulty in identifying components of multi-phase mixtures due to overlapping peaks and phases that appear in low concentrations as only few of their diffraction peaks will be seen. This problem was encountered for both peak identification methods. To help with overlapping peaks and to validate whether particular components are present or not, 2D Generalized correlation was employed with elemental concentrations obtained through XRF analysis. The simplisma method was also applied to XRD data to resolve sample 'mixtures' and reduce the problem of overlapping peaks.

4.3.2 Comparison of Diffraction patterns using cosmetic raw materials

The diffraction patterns of the 39 cosmetic foundation samples analysed by XRD varied greatly. Differences in diffraction patterns were found between the mineral and traditional foundation types, as well as by manufacturer. The diffraction patterns of M3.3, M4.4 and T4 are shown in Figure 4.2 and give an example of the differences in diffraction patterns between mineral and traditional formulas and those samples that contain bismuth. Diffraction peaks

appear at differing 2θ angles and there are defined differences in the peak intensities of each type of sample. Further investigation was required to interpret the diffraction patterns and understand the differences between patterns and the analysis of cosmetic raw materials was employed to aid interpretation.

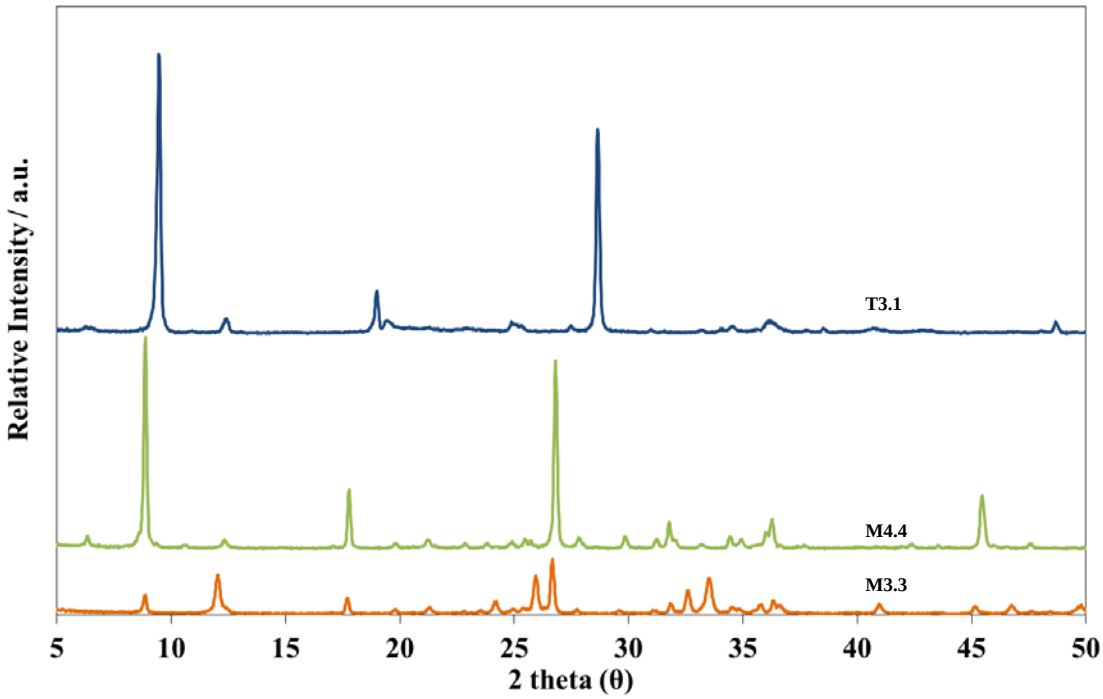

Figure 4.2 Diffraction patterns produced through XRD analysis of samples M3.3, M4.4 and T3.1.

Reference Materials

To aid in peak identification of foundation powder diffraction patterns, the diffraction patterns of common raw materials were recorded, Figure 4.3. Those can be compared to those from foundation samples and most of the sample peaks can be identified. The raw material diffraction patterns can be used to determine the differences in the diffraction patterns displayed in Figure 4.2. The noticeable difference between the diffraction pattern of T3.1 and samples M3.3 and T4.4 is the presence of talc in the traditional sample diffraction pattern. It seems that talc is the dominant ingredient in this sample type. The other raw material visibly present is kaolin, with diffraction peaks at 2θ angles 12.3° and 24.8°. The talc peaks are so

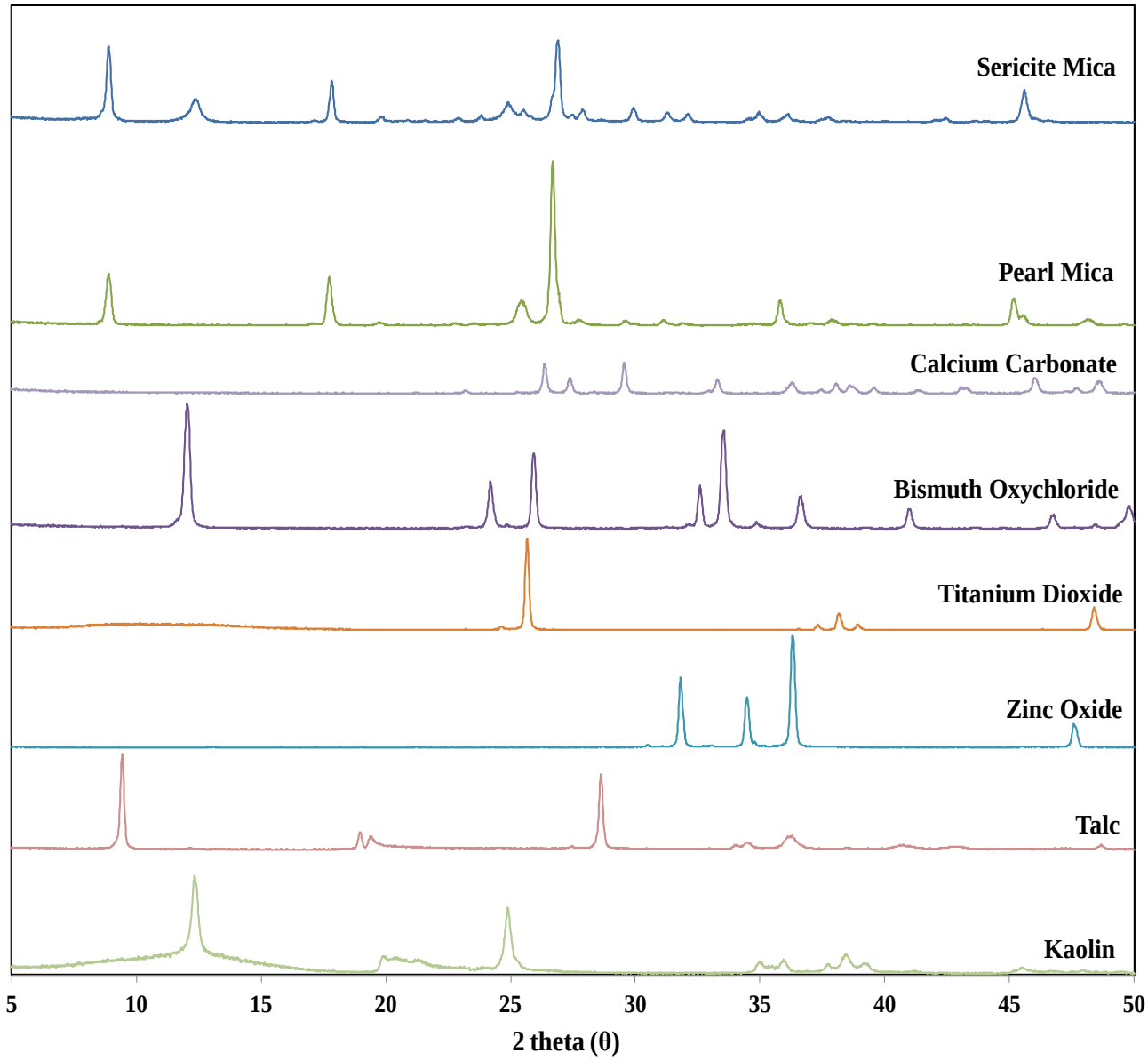

Figure 4.3 Cosmetic grade raw material diffraction patterns analysed by XRD.

intense, that no other diffraction peaks are visible in comparison.

Sample M4.4, does not contain talc but instead mica peaks at 2θ angles 8.9°, 17.8°, 26.7° and 45.6°. From the relative elemental concentrations produced from XRF analysis, sample M3.3 is known to contain bismuth and this is evident in the diffraction pattern as diffraction peaks match those of bismuth oxychloride at 2θ angles 12.02°, 24.16°, 25.9°, 32.5° and 33.5°. Mica

peaks are also visible in M3.3, however, the peak intensities are much lower in comparison to the diffraction peaks identified in M4.4.

The information gained by comparing the raw material XRD patterns with the sample XRD patterns was used essentially as a database for peak assignment as the EVA software did not produce accurate 'hits' for cosmetic grade ingredients.

Based on the peak intensities found through XRD analysis of raw materials and of the samples, the most prominent components found in samples were mica and talc. These were the most easily identifiable components by eye. Bismuth oxychloride and kaolin were also clearly observed in samples. However, ingredients such as titanium dioxide, zinc oxide and calcium carbonate produced XRD patterns with lower intensity peaks in comparison to other ingredients and were often lost in the diffraction patterns.

The diffraction patterns of yellow, red and brown iron oxides are displayed in Figure 4.4. The intensities obtained by XRD are significantly lower than the other raw materials. There is clear difference in the diffraction patterns of the iron oxides, and one would assume that the type of iron oxide used in each foundation sample would be easily determined; however this is not the case. Significant problems occurred due to the inability to measure iron with the use of a Cu Kα source. If a copper source is used to analyse iron, fluorescent radiation is emitted, resulting in iron diffraction peaks being reduced in intensity and not properly measured. Generally, Co Kα radiation can be used for samples containing iron, to overcome the problem of fluorescence. However, a Co Kα radiation source was not readily available for these experiments.

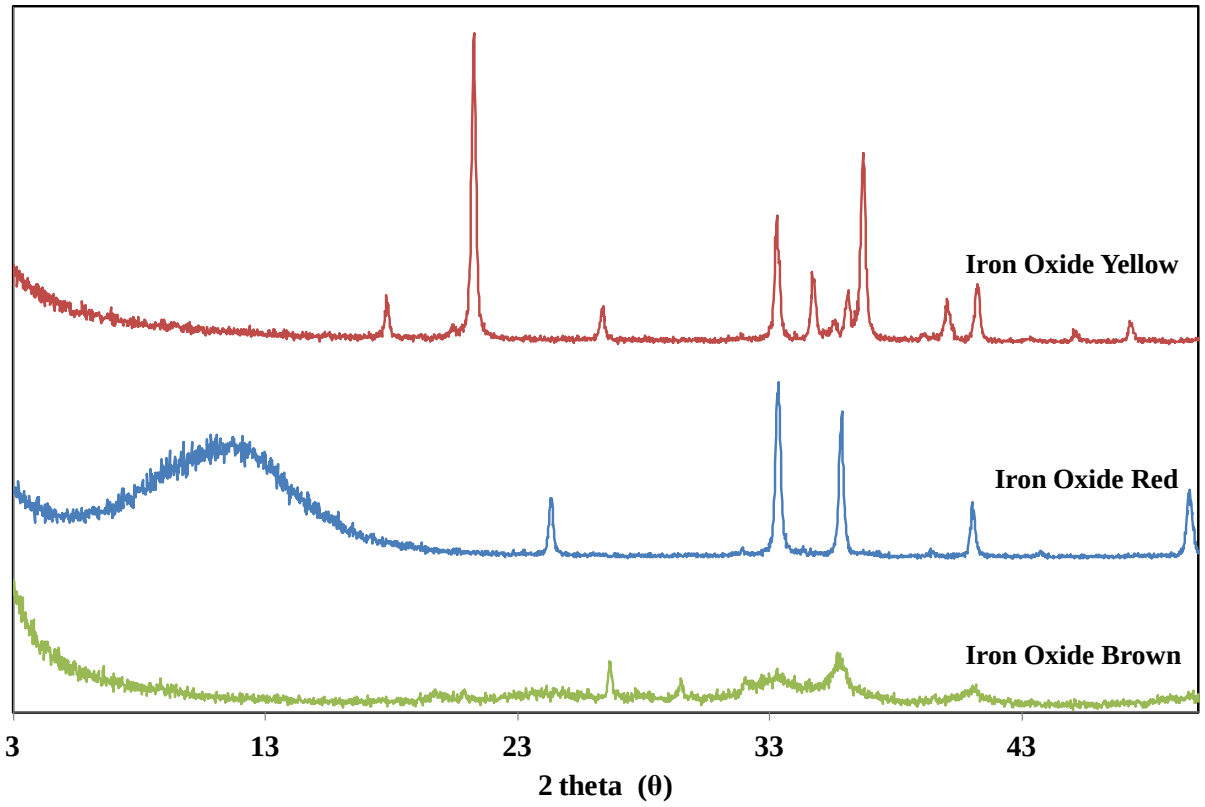

Figure 4.4 Diffraction patterns of various iron oxides used in cosmetic foundation production; yellow iron oxide (hydrated ferrous oxide- $Fe(OH_3)$), red iron oxide (ferric oxide- Fe_2O_3) and brown iron oxide (combination of both yellow and red iron oxides).

Due to the complex nature of the samples, extensive overlapping of component peaks is observed in their diffraction patterns, and not all peaks could be identified by eye.

4.3.3 Principal Component Analysis

Principal component analysis was applied to the, 39 (samples) x 783 (2 theta angle range) aligned and binned matrix produced by XRD analysis. The first two principal components account for 89% of the total variance in the dataset. A score plot of the first two PCs and loadings vectors of the cosmetic foundation powder samples is shown in Figure 4.5. There is a distinct split between the mineral and traditional samples; with all but 5 mineral samples

separated along the positive PC1 axis and all traditional samples distributed across the negative PC1 axis.

Once again samples M1.1, M1.2, M5.1, M5.2 and M5.3 are clearly aligned with the traditional foundation class. The diffraction patterns of cosmetic grade raw materials, previously discussed were used to assign peaks in the loadings plots. The loadings plot, Figure 4.5(b), show the components present in and describes the spread of the foundation samples in the PC scores. Results indicate that the main components responsible for the spread along the PC1 axis are talc (negative weighting) and mica (positive weighting). Samples M4.x are separated to the far right of the PC1 axis, indicating that they may contain larger amounts of mica than samples M7.x and M2.x. The traditional samples contain relatively the same components, whereas the mineral samples are clearly separated into two distinct groups along the PC2 axis. The separation of samples M3.x and M6.x from the other mineral-based formulations, are grouping in the negative region of the PC2 axis which is defined by the presence of bismuth oxychloride in these samples (c.f. Table 3.2). Ingredients such as, titanium dioxide and zinc oxide seem to have little effect on the variance reflected on PC1 and PC2. The effect of zinc oxide is better illustrated in PC1 and PC3, shown in scores and loadings plot of Figure 4.6. The separation of mineral manufacturer type is more evident in PC1 vs PC3 than in comparison to PC1 vs PC2 from Figure 4.5(a). PC1 vs PC3 shows the separation of samples M4.x with M2.x and M7.x along the PC3 axis due to zinc oxide. There is also an identifiable difference and separation of the traditional-based formulas and the mineral foundations classified as traditional along the PC3 axis. Samples M5.1, T4.x and T2.3 are grouping separately from the other traditional-based samples due to their high content of calcium carbonate (c.f. calcium concentrations in Table 3.2).

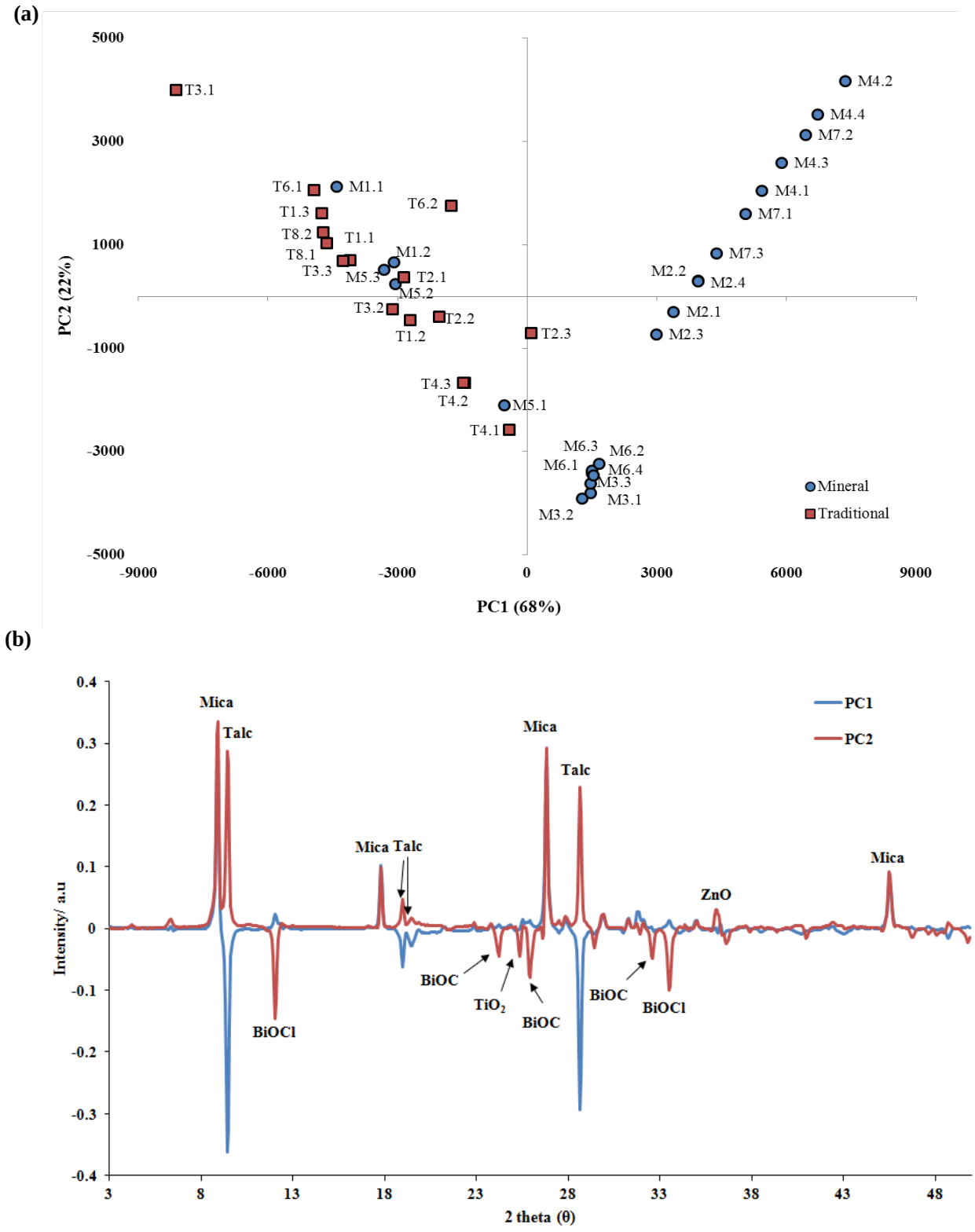

Figure 4.5 The scores plot (a) and the loadings plot (b) associated with PC1 and PC2 from principal components analysis of phase data obtained through XRD analysis of the 39 foundation samples.

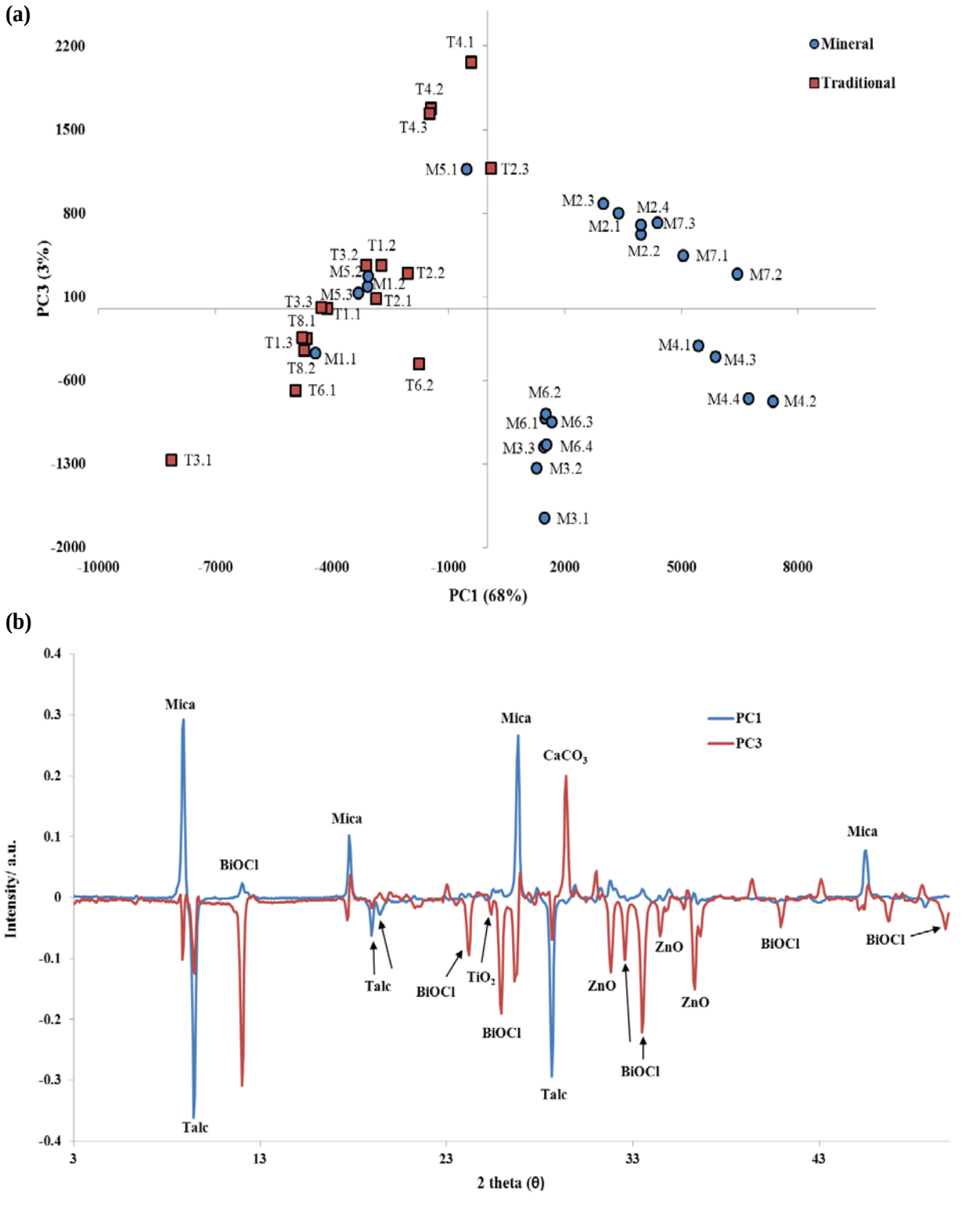

Figure 4.6 The scores plot (a) and the loadings plot (b) associated with PC1 and PC3 from principal components analysis of phase data obtained through XRD analysis of the 39 foundation samples.

In Figure 4.7(a) the samples identified as belonging to the mineral-type have been examined by PCA and the differences between manufacturers is clear, with the associated loadings plot of Figure 4.7(b) confirming the separation is due to the presence of bismuth oxychloride, zinc oxide, kaolin and mica in the samples. Kaolin has separated samples M2.x along the negative region of PC2.

The PCA results of XRD data, complement and agree with the results of the PCA applied to relative elemental concentrations produced through XRF analysis. Samples group similarly based on the components present in each sample. However, PCA results for XRD data show samples M2.x and M7.x grouping separately. This separation is due to the differences in the amount of kaolin present between samples. XRF analysis could not distinguish between these differences regarding the amount of kaolin, as XRF could not confirm the concentration of kaolin from elemental analysis.

Similarly, PCA has been employed for samples classified as traditional-based formulas and the scores and loadings plot is shown in Figure 4.8. Separation of samples has occurred along the PC1 axis due to calcium carbonate and talc. Samples T4.x and M5.1 have grouped in the negative PC1 region due to their calcium carbonate content. Sample T6.2 is not clustering with any of samples. The loadings plot indicates that this sample has higher mica content in comparison to the other foundation samples.

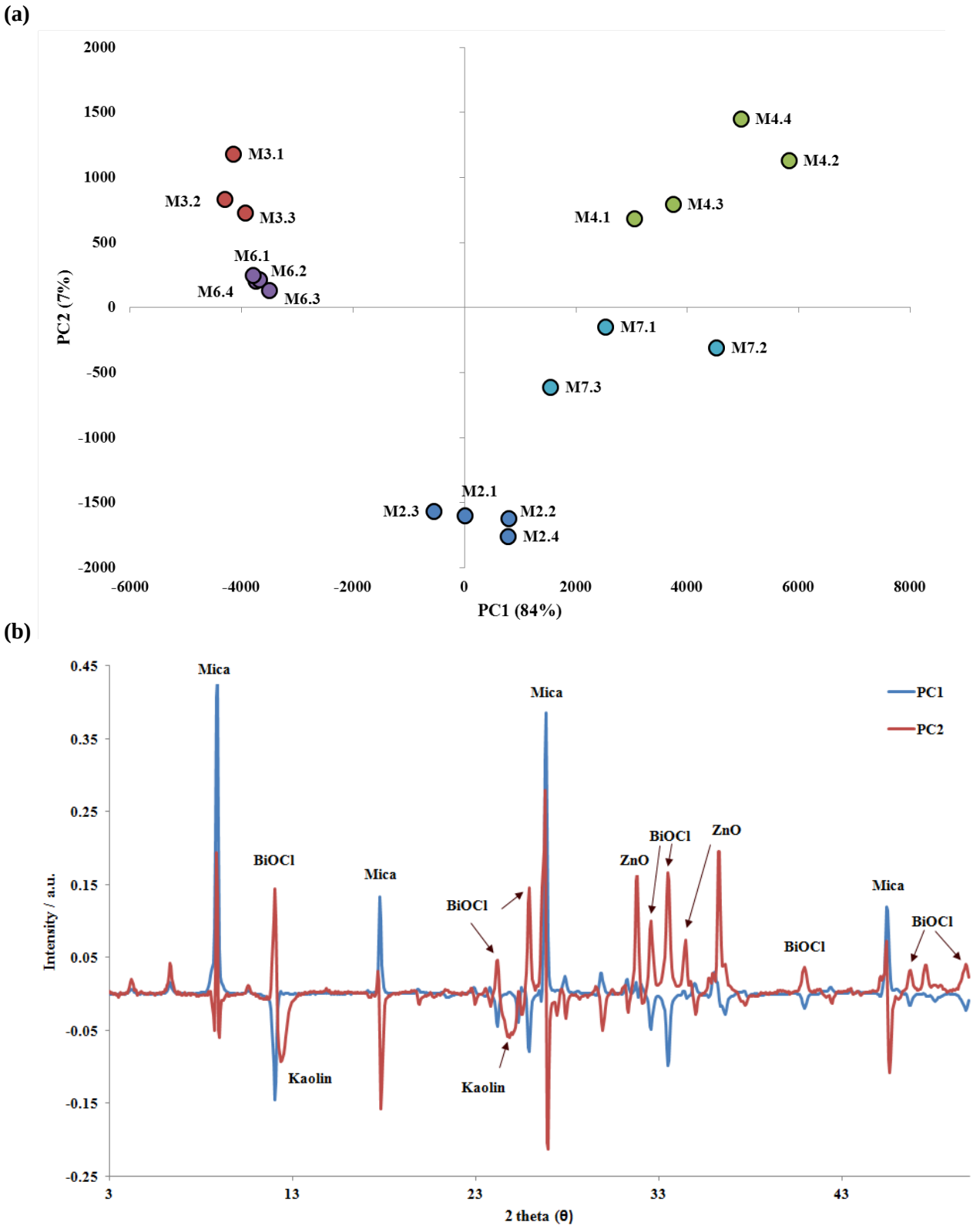

Figure 4.7 The scores plot (a) and the loadings plot (b) associated with PC1 and PC2 from principal components analysis of phase data obtained through XRD analysis of the 18 mineral based foundation samples

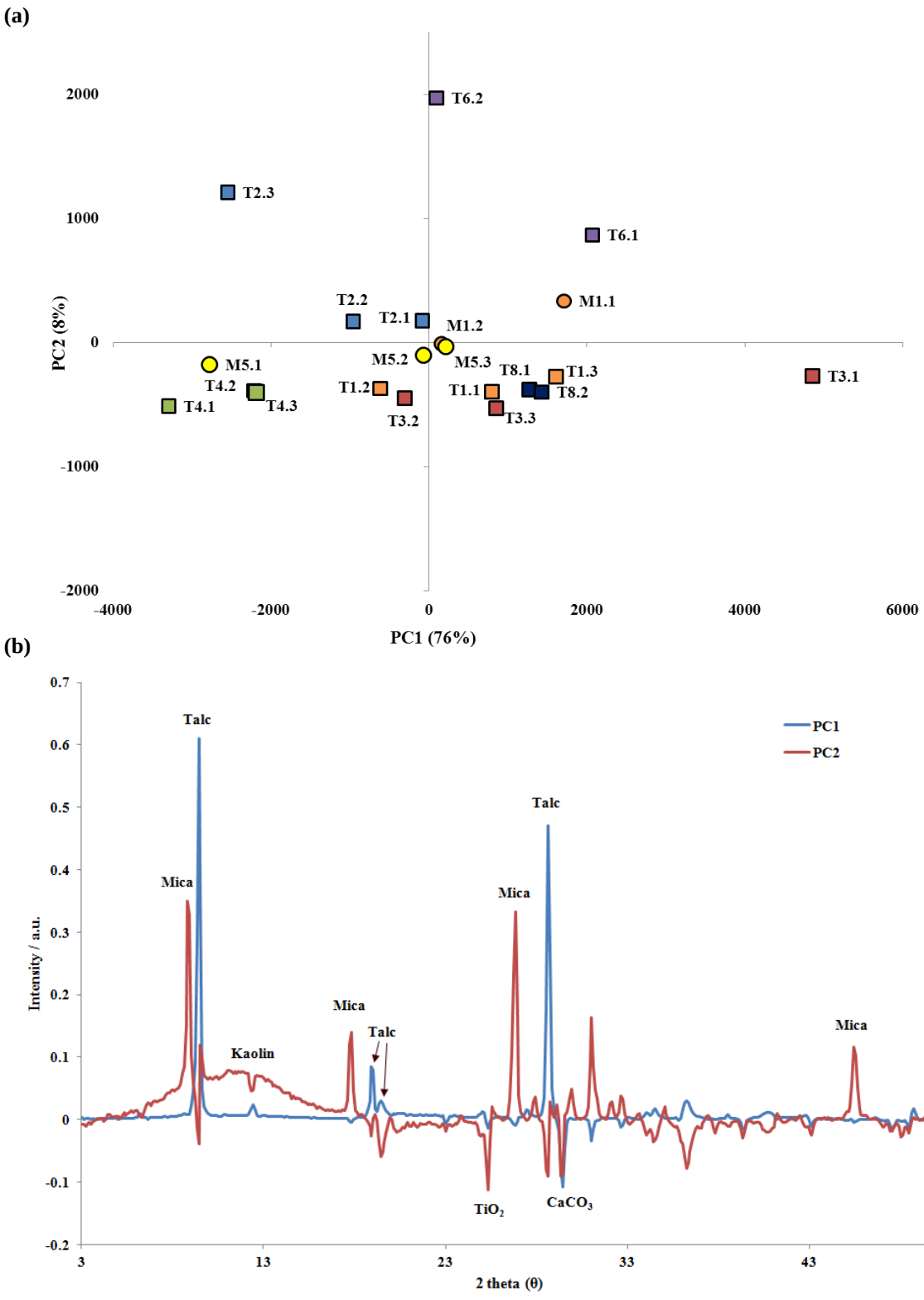

Figure 4.8 The scores plot (a) and the loadings plot (b) associated with PC1 and PC2 from principal components analysis of phase data obtained through XRD analysis of the 23 traditional-based foundation sample.

4.3.4 Covariance and Correlation

To further aid in XRD interpretation, and identification of components in diffraction patterns, XRF elemental data was correlated with XRD data. This was done to highlight visually any relationship between relative elemental concentrations and the phase analysis of materials in samples. As there are unidentified peaks in the recorded sample diffraction patterns, it is possible that XRF elemental lines will correlate with diffraction peaks and hence help identify the component producing that diffraction peak. This method uses the correlation coefficient to estimate the degree of similarity between variables, in this case, XRF spectra as being indicative of elemental concentrations and XRD peak intensities as indicating phase composition. The theory of covariance and correlation was previously mentioned in Chapter 3: X-Ray Fluorescence.

A 2D covariance matrix using both data sets for all samples was constructed to produce,

$$\mathbf{\Phi} = \mathbf{XRD}^{T}.\mathbf{XRF} \qquad \text{(Equation 4.2)}$$

where **XRD** and **XRF** are the mean-centred data matrices obtained from diffraction data (39x 469) and XRF spectra (39 x 942) respectively. Figure 4.9 shows a 2D covariance contour map of XRD vs. XRF, in which only positive correlations are displayed. The red colour indicates a positive correlation of XRF α or β elemental emission lines with diffraction peaks of the XRD data. Although it is visibly clear that there are numerous positive correlations between the XRF and XRD, the 2D covariance map can be difficult to interpret by eye and 2D correlation slicing was employed to aid in the interpretation of the 2D map.

A correlation slice of each element was taken from the XRF data at its particular Kα emission line across all samples. This was then cross-correlated with the entire XRD data set to determine correlation coefficients of elemental emission lines correlated with the diffraction peaks. The correlation method worked more successfully with the mineral components such

as bismuth oxychloride, zinc oxide, titanium dioxide and mica. The mineral-based formulations use fewer ingredients in their production than in comparison to the traditional-based formulations. The mineral samples seem to contain similar components between manufacturers, differing in the ratios in the amounts in which each ingredient is used. The heavy metals associated with bismuth oxychloride, zinc oxide and titanium oxide materials are less likely to differ worldwide. The traditional samples seem to use a wider variety of ingredients and the form of talcs and kaolin employed can differ between manufacturers, making their classification and characterization more difficult. Kaolin ($Al_2Si_2O_5(OH)_{4)}$ could not be represented by one single element in XRF analysis as its chemical formula consists of aluminium and silica and these elements are also present in mica and talc. Thus aluminium and silica produce poor correlation coefficients values between XRF intensities and XRD diffraction pattern data. Bismuth oxychloride, zinc oxide, titanium dioxide and mica returned correlation coefficients values close to 1. This was not unexpected as the bismuth, zinc, titanium and potassium XRF emission lines best represent the mineral phases present. The correlation coefficients for mineral-based samples, of bismuth oxychloride, titanium dioxide and zinc oxide are shown in Figure 4.10 projected on the covariance slice of each component. We can see that the 2θ peak positions that have highly correlated data, match with the diffraction peaks of the raw materials XRD patterns. Titanium dioxide was not as prominent in the covariance slices but this may be due to the peak intensities of its diffraction peaks in comparison to other components. If we refer back to the relative elemental concentration of titanium in the samples, they are lower in comparison to the relative elemental concentrations of bismuth and zinc. Iron oxides did not produce a high correlation with the Fe Kα emission line, even though XRF analysis determined large amounts of iron are present in samples. This could be due to the poor diffraction patterns produced from XRD analysis and the many phases containing iron. The correlation of silica produced correlation coefficient values of

around 0.3 with the XRD data. Silica is present in talc, mica and kaolin. It is difficult to assign a relationship with one particular component or their diffraction peaks. This was an expected outcome. Aluminium matched consistently with most of the diffraction peaks of mica, with correlation coefficients ranging from 0.88 to 0.91. However, aluminium is also present in kaolin so it cannot be assumed that all these peaks are mica. Talc is a hydrated magnesium silicate, and it was assumed that the diffraction peaks of talc within sample mixtures would have a very high correlation with the Mg Kα emission line.

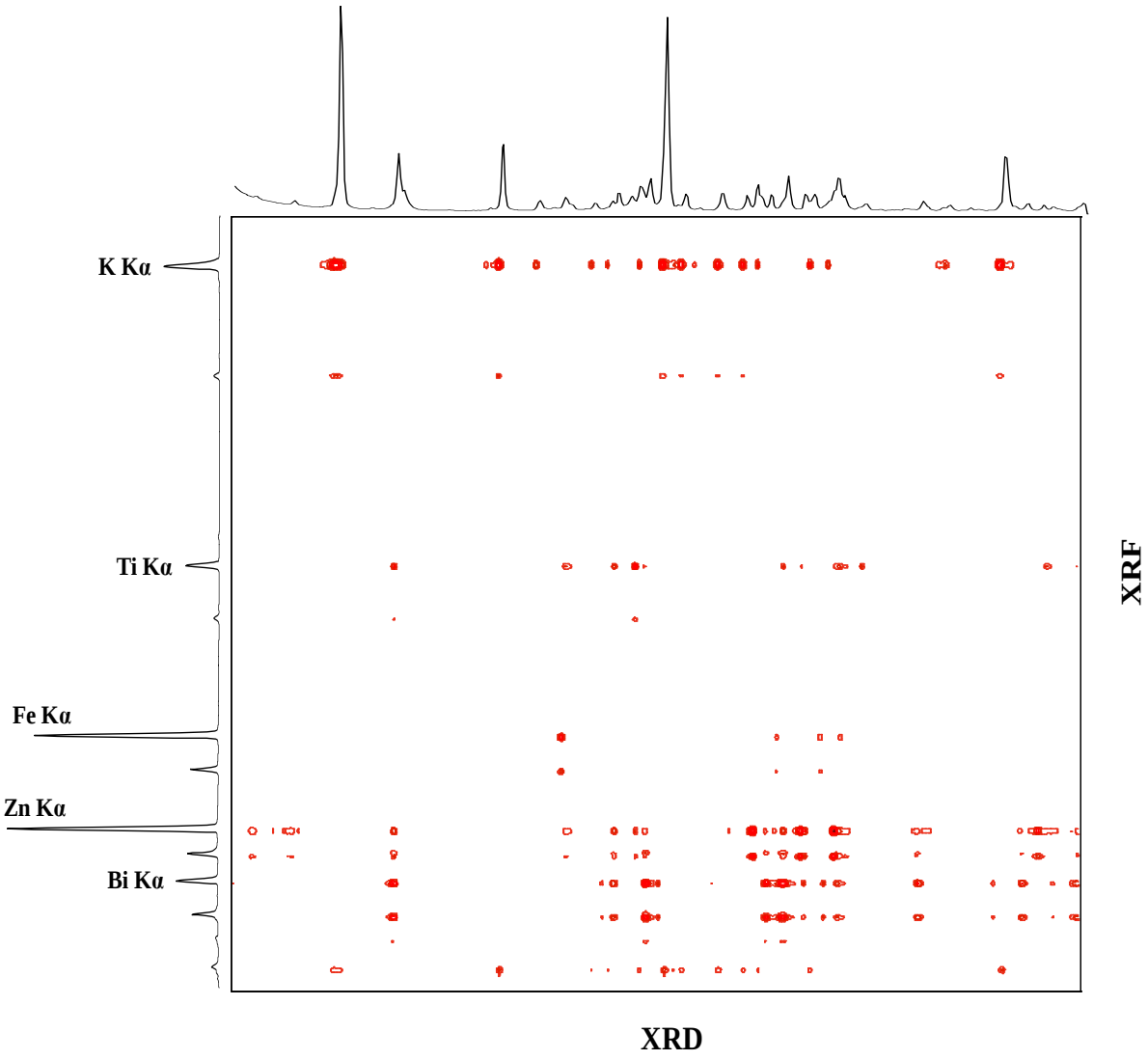

Figure 4.9 The covariance contour plot of XRD vs. XRF. An average spectrum of each technique is presented along each axis to aid in identification, showing the positive correlation of XRF elemental emission lines with XRD diffraction peaks.

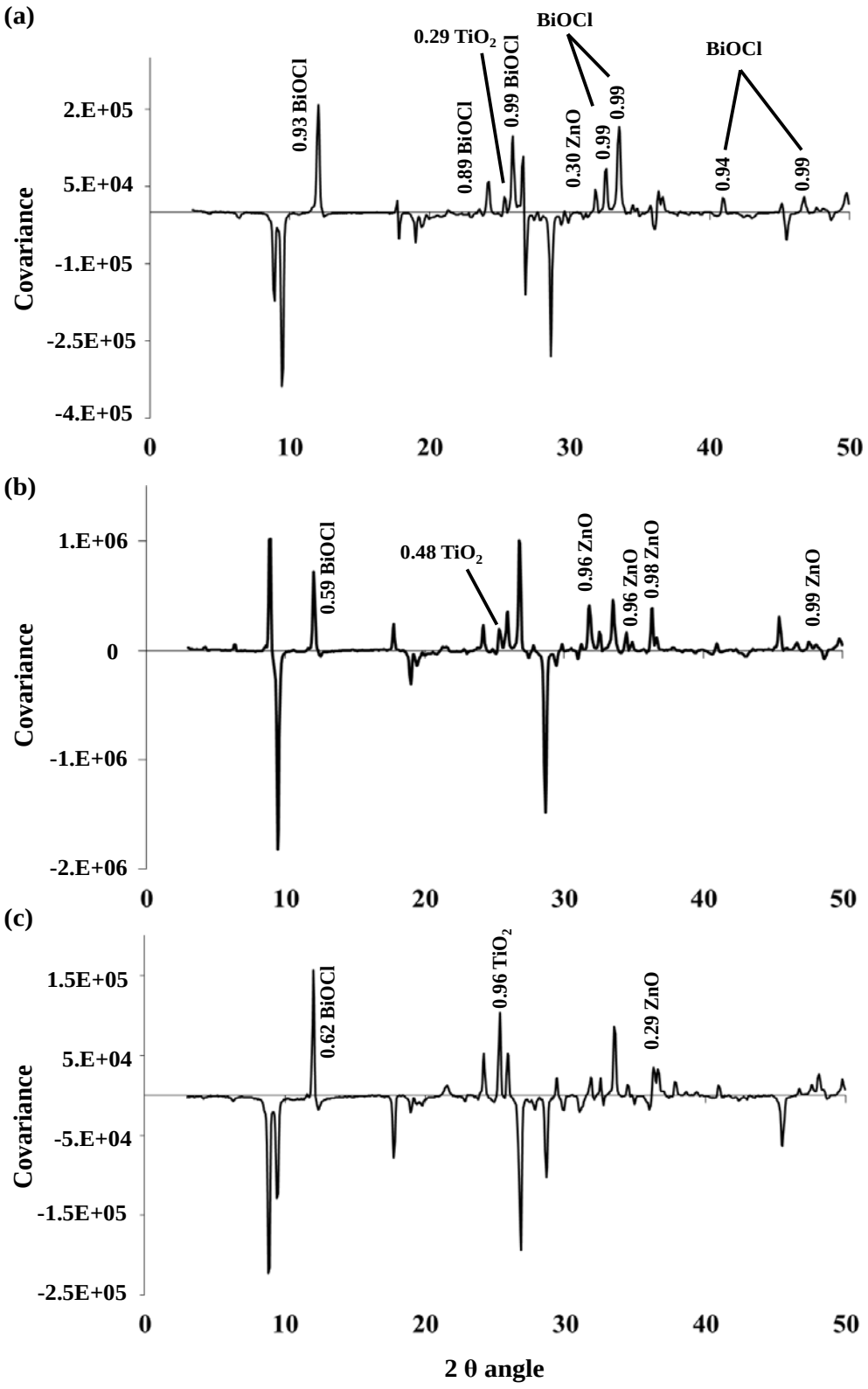

Figure 4.10 Covariance slices obtained from correlation of XRF and XRD data. The correlation coefficients projected on the covariance slices of BiOCl, ZnO and TiO_2 are displayed.

Correlation coefficient values of around 0.8 were calculated, which were lower than expected. This may be due to the high levels of talc present in the traditional samples, causing high peak intensities of talc in the XRD diffraction patterns. The peak intensities of talc are so high, meaning the peak intensities of the other components are very small in comparison, change between samples is insignificant and therefore, correlation of peaks with changing elemental concentration does not occur.

In summary, 2D generalized correlation of XRF elemental data and XRD phases data was successful in finding relationships between the two techniques. XRF data was able to provide a link between the elemental information and the phase components that were present in powder foundation samples and XRF elemental data can aid in peak identification of foundation sample diffraction patterns. However, its use is limited and is only successful for components that may have a single element that can be represented by a crystal phase. It was not successful with all components present in cosmetic foundations, because they consist of a mixture of crystalline substances, and not all could be identified using 2D correlation.

4.3.5 Simplisma analysis of XRD data

Simplisma was applied to the XRD data to attempt resolve the mixture of phases found in cosmetic powders. It was used to examine and differentiate between diffraction peaks broadened due to overlapping component peaks. Simplisma was discussed in Chapter 3: X-Ray Fluorescence and the same technique was applied to XRD data. Because the samples consist of a complex mixture of mineral and clay materials, the simplisma approach, seems like an appropriate method to aid in XRD interpretation. It has the ability to separate components from spectral mixtures, or in this case, diffraction pattern mixtures, using the pure variable approach (refer to Chapter 3: X-Ray Fluorescence). It is useful for XRD,

because as each pure variable is calculated it is eliminated from the data set, and therefore cannot influence the calculation of the next pure variable and its contributions. The aim in using this method was to determine whether the pure variables in the XRD data can be successfully resolved, overcoming the issue of overlapping diffraction peaks.

X-ray Diffraction data was separated into two groups of 18 mineral foundations (which excluded samples M1.x and M5.x) and 21 traditional foundations (which included samples M1.x and M5.x). This was done to aid in a better separation of components using simplisma as the groups contained differing ingredients. A program (purespec.m) was created in-house from the algorithm described in Windig's et al. paper (refer to Chapter 3) in MATLAB to perform the simplisma function and produce the pure spectra and their 'concentration' contributions. The program calculated the purity of each component based on the highest standard deviation and gave the 2θ angle position of the diffraction peak. Once a component is identified, it is eliminated from the dataset. Based on the knowledge gained from the XRD analysis of cosmetic raw materials, the diffraction peaks could be matched to the known ingredients in the samples. A 18 x 496 matrix, with XRD data of mineral-based samples only, in rows was applied to the purespec.m function with an offset, α, value of 3%. The simplisma function determined 6 components to be present in the mineral foundation samples. One of the forms of mica was determined as the first pure component, as it is a major ingredient in the mineral-based foundations. Due to the slight difference in the diffraction peaks of the sericite and pearl mica diffraction patterns simplisma has separated the two forms of mica. Bismuth oxychloride had a high variance value due to samples M3.x and M6.x being the only samples to contain traces of bismuth oxychloride and is identified as a component. Iron oxides were not found as pure components. As mentioned before, this is due to the fluorescence of iron in XRD analysis.

To have a better understanding of the pure components, the resolved pure spectra need to be investigated. Figure 4.11 shows the resolved spectra calculated by simplisma and the corresponding diffraction patterns of the raw components best matching each spectrum. Not all the resolved spectra match well to those of the raw materials analysed previously, Figure 4.3. Some of the resolved spectra seem to be linear combinations of components, rather than pure components. The resolved spectra resemble mixtures of diffraction patterns of known materials, which could be caused by overlapping peaks. But pure components will be assigned based on the standard deviation values and the corresponding 2θ angle peak position produced by Simplisma. Pure component 1 matched the diffraction peaks of sericite mica more closely than pearl mica. Sericite mica diffraction pattern has a peak at 12.32° that was not present in the resolved spectra (Figure 4.11(a)). X-ray Diffraction analysis of kaolin determined similarly a diffraction peak at 12.42°. We can assume due to peak overlap, it was not resolved for sericite and as the peak intensity is greater for kaolin, it would be resolved with that component. The second pure component was determined as bismuth oxychloride and the resolved spectra reflect the original XRD pattern of bismuth oxychloride. The resolved spectra for component 6, shows the major diffraction peaks for zinc oxide, however the relative contributions do not agree with those found from the simplisma application to XRF data studied in Chapter 3. The relative contributions of each pure component is shown in Figure 4.12. The ‘concentration’ contributions do not seem correct because the spectra that are resolved are not the ‘pure’ spectra of the components present. This may be due to the overlapping of component diffraction peaks. To explain why peak overlap is causing incorrect ‘concentration’ contributions we will look at bismuth oxychloride. The resolved spectra Figure 4.11(b) resembles that of the original bismuth oxychloride XRD pattern. We know from the XRF elemental analysis results from the previous chapter, that only samples M3.x and M6.x contain traces of bismuth. However, this is not represented in the bismuth

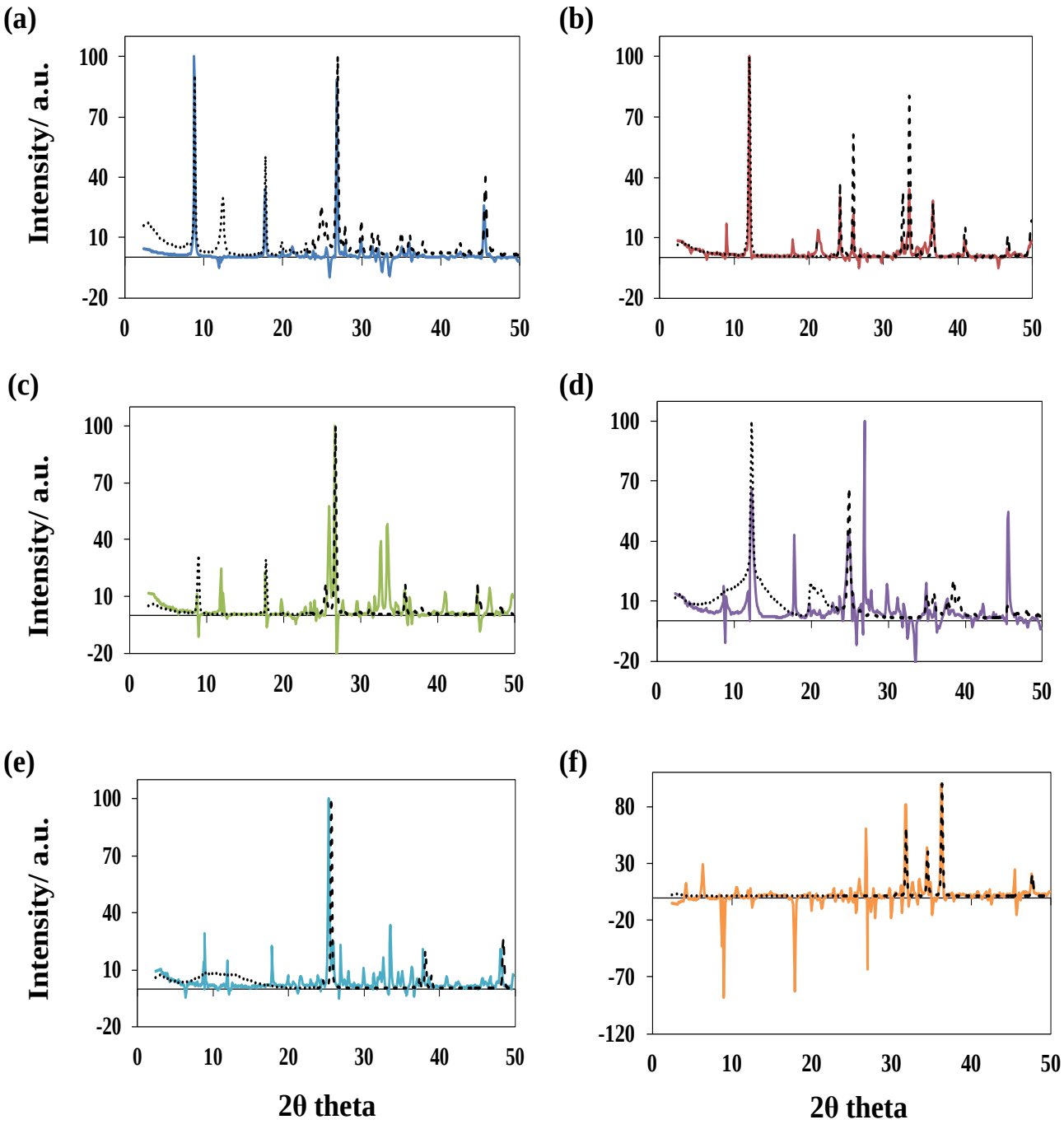

Figure 4.11 Resolved spectra from Simplisma analysis of XRD data from mineral samples, components with the 'real' diffraction pattern of each component (dotted lines),(a) Sericite mica (b) Bismuth oxychloride (c) Pearl mica (d) Kaolin (e) TiO_2 & (f) ZnO.

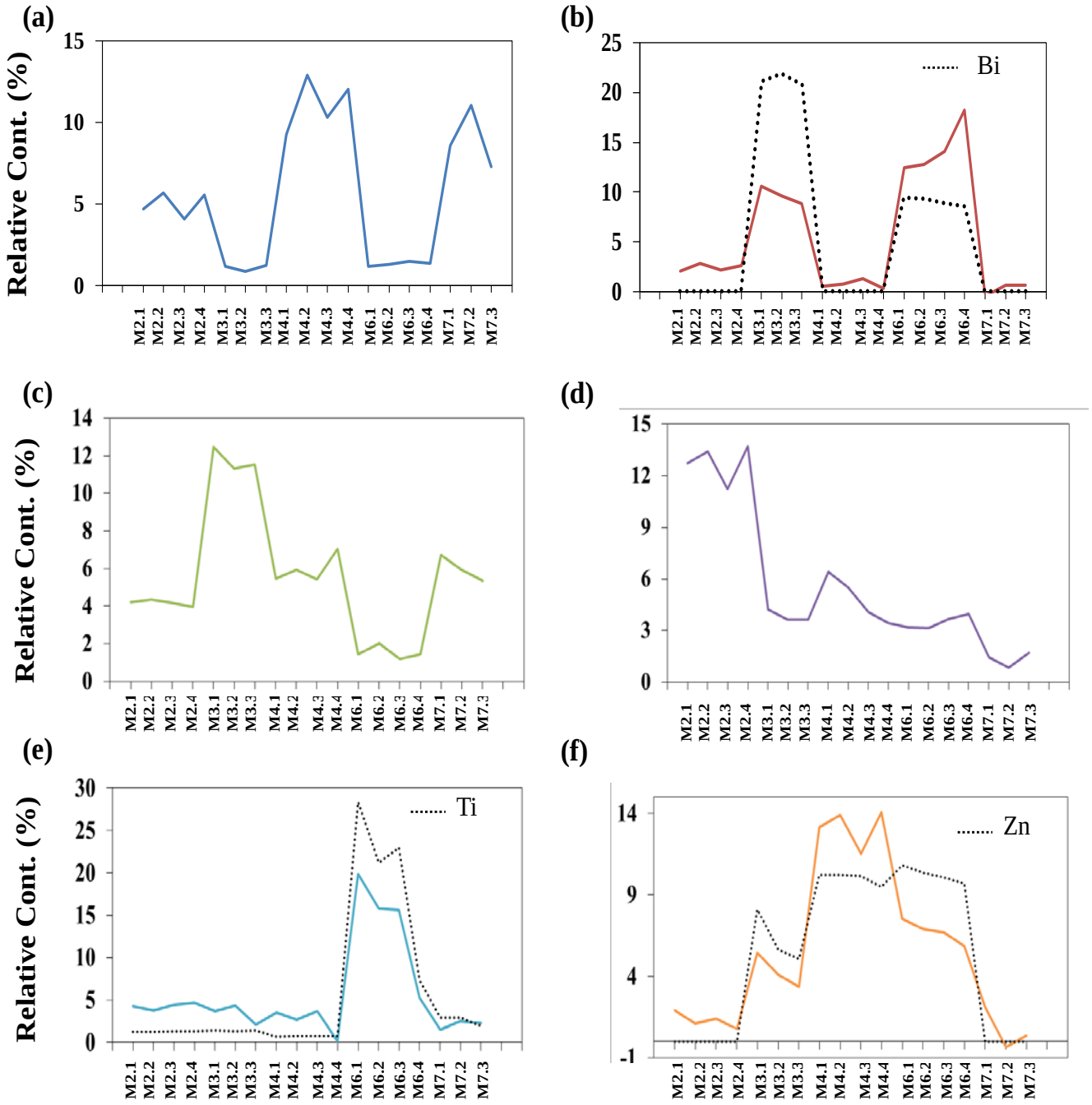

Figure 4.12 Relative contribution profiles of the Simplisma resolved spectra from Figure 4.11 Components (a)-(f) with true concentration profiles of Bi, Ti and Zn (dotted lines) from Table 3.2 for comparison.

oxychloride contribution profile. The contribution profile indicates that all mineral samples but one, have bismuth oxychloride contributions. To understand why this is occurring we must look at the diffraction pattern of the mineral foundation samples. Figure 4.13 shows the overlap of a bismuth oxychloride diffraction peak with a kaolin diffraction peak. The simplisma method estimates the concentration contributions based on the peak intensities. Figure 4.13 clearly shows a distinction between samples that contain bismuth oxychloride as the peak intensity at that 2θ position is not equal to zero. Other components such as zinc oxide, also incur this problem. Zinc oxide has overlapping diffraction peaks with bismuth oxychloride in the 30° 2θ angle region.

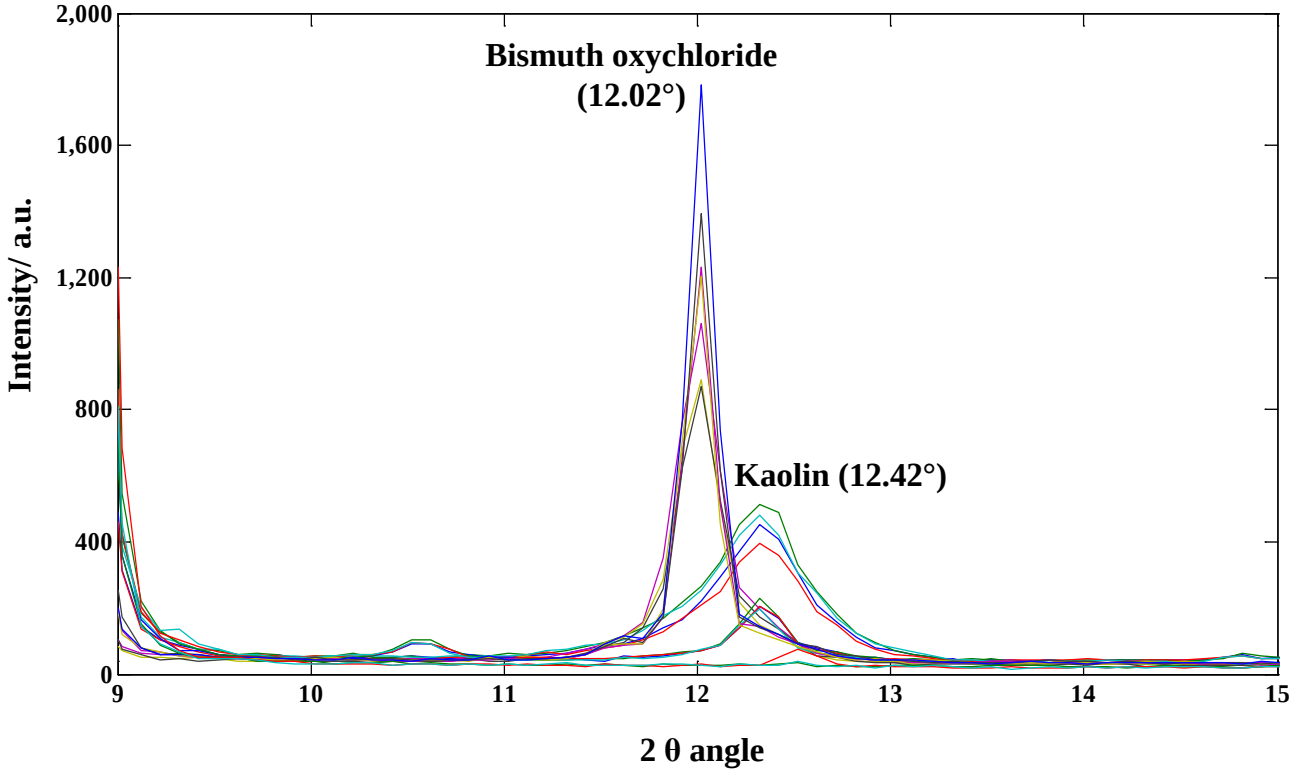

Figure 4.13 Overlap of bismuth oxychloride and kaolin diffraction peaks.

The 21 x496 XRD matrix of traditional sample data was also examined. Simplisma identified pure components with diffraction peak positions that did not match diffraction patterns of the cosmetic raw materials analysed previously. The EVA database was searched to find any appropriate peak matches for the diffraction peaks at 29.42°, 31.02° and 32.62° and the results indicate the presence of an iron oxide, aluminium trioxide and calcium carbonate respectively. These matched mineral phases have similar chemical structures of materials found in cosmetic foundations and were expected hits. Iron oxides are present in the samples, and looking back at the raw material XRD patterns, it was found that the cosmetic grade brown iron oxide had a diffraction peak at 29.42°. Calcium carbonate is a known ingredient in the traditional foundation formulas but may be found in a differing chemical form than the one analysed in this study.

The resolved 'pure' spectra for the traditional sample data are displayed in Figure 4.14 and the corresponding contribution profiles in Figure 4.15. The simplisma application to traditional samples does not seem as successful in resolving XRD mixture data as with the mineral samples. Not all resolved spectra were related to the diffraction patterns of raw materials shown in Figure 4.3. The first pure component gave resolved spectra which matched with the diffraction peaks of the talc diffraction pattern. It was assumed that the magnesium concentration found through XRF analysis would be representative of the concentration of talc in samples. Comparing the relative magnesium concentration (from XRF results Table 3.2) with the concentration contribution of talc (Figure 4.15(a)) the results do not correlate. Magnesium stearates can be incorporated into traditional foundation formulas as a binder or for water proofing properties [15]. It is more likely to be present in traditional samples that are in pressed powder form. It can be assumed that magnesium stearate may be present in samples and may contribute to the magnesium concentration that was determined by XRF analysis. Magnesium stearate from a cosmetic supplier was analysed by XRD. The

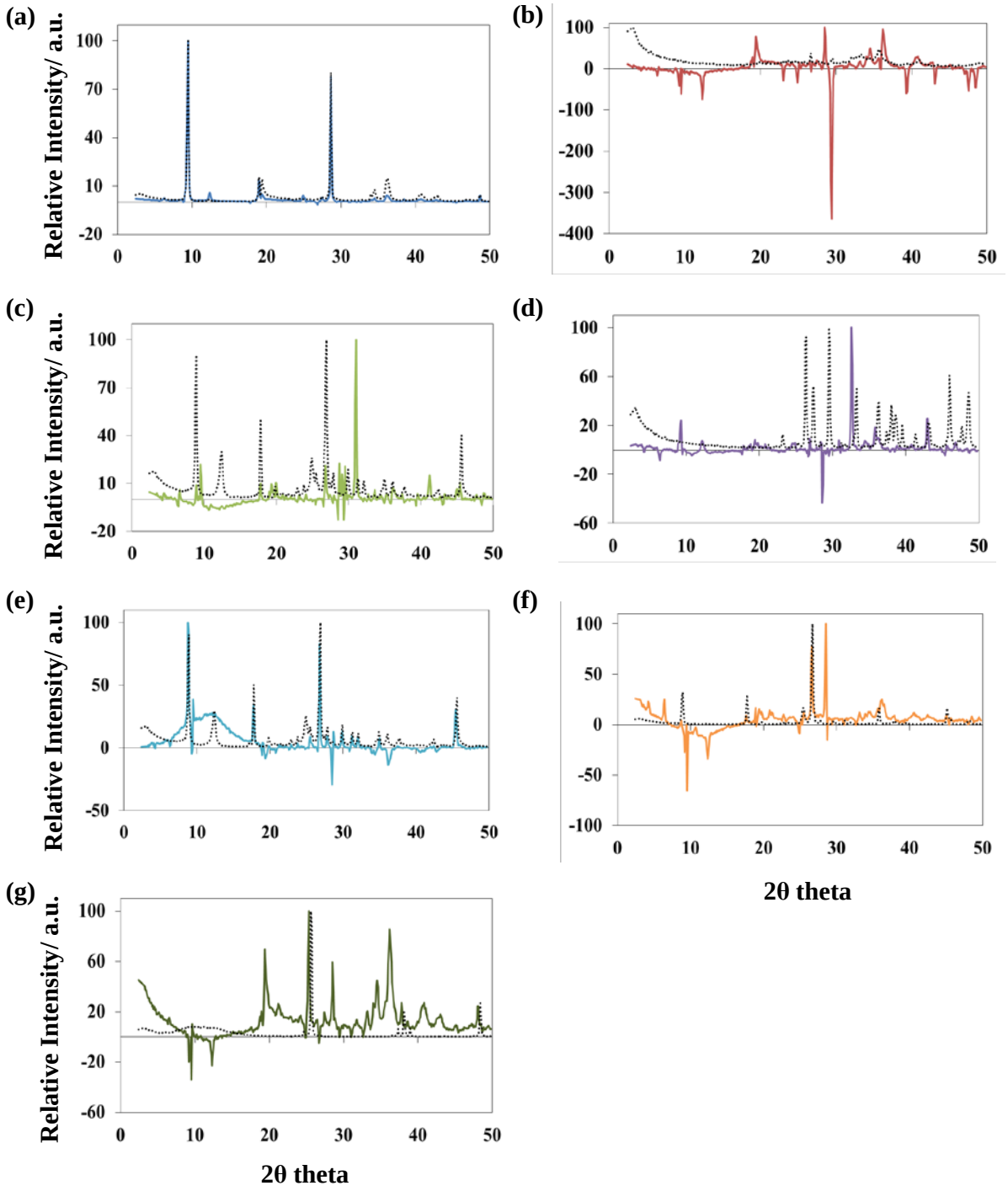

Figure 4.14 Resolved spectra from Simplisma analysis of XRD data from traditional samples, components, with the 'real' diffraction pattern of each component (dotted lines). (a) Talc (b) Brown Iron Oxide (c) Sericite mica (d) Calcium carbonate (e) Sericite mica (f) Pearl mica & (g) TiO_2,

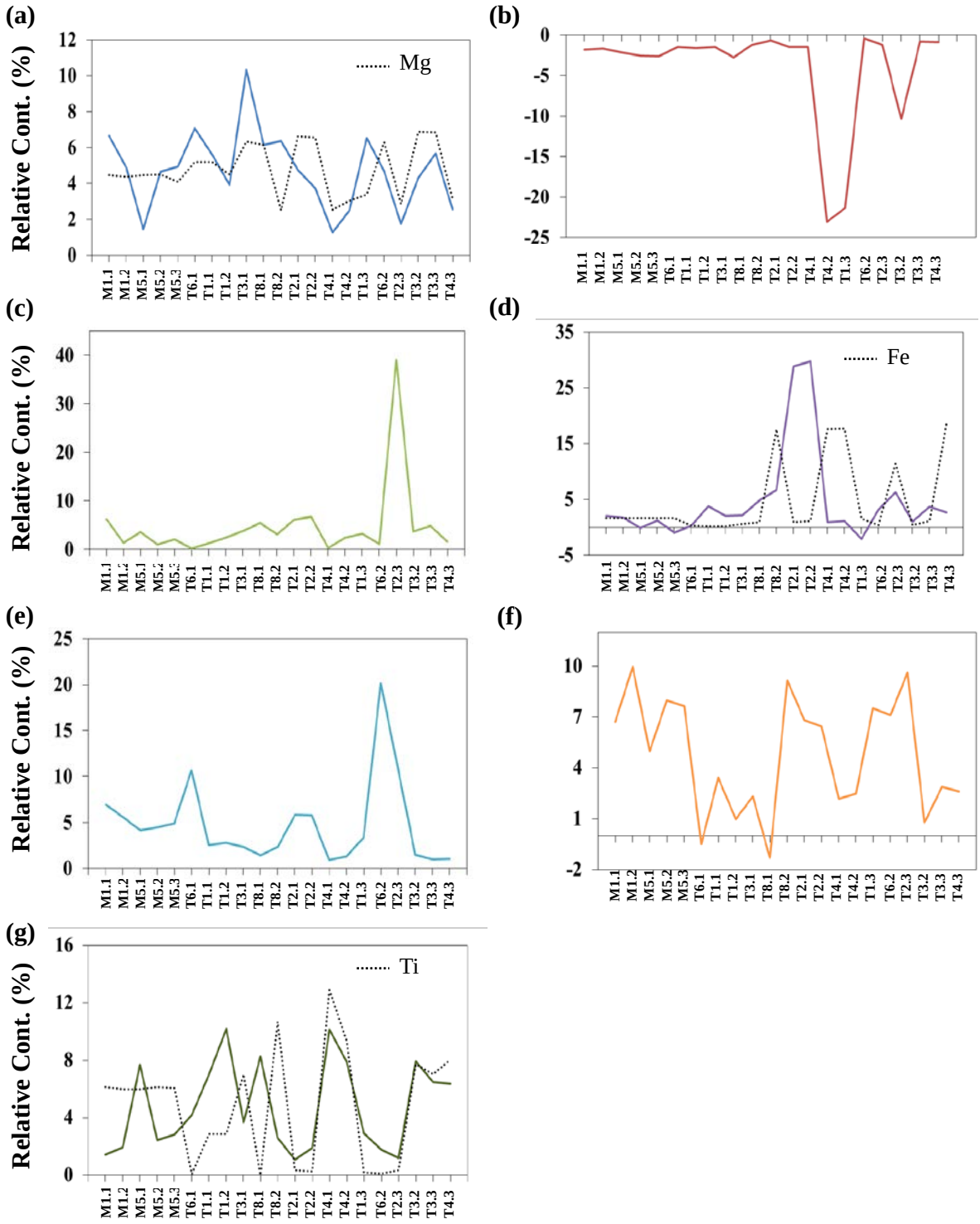

Figure 4.15 Relative contribution of the Simplisma resolved spectra from Figure 4.14. Components (a)-(g) with true concentration profiles of Mg, Fe, Ca & Ti.

diffraction pattern was quite simple and was found to have a major diffraction peak at 21.3°. However, this peak was not clearly visible in the sample diffraction patterns, due to overlap and poor peak intensity, and could not be determined by XRD analysis. It is anticipated that infrared analysis will determine whether magnesium stearate is present in foundation samples.

4.3.6 Simplisma using Combined XRF and XRD data

Resolving the XRD patterns can be assisted and improved by using known XRF data. The correlation matrix of two different spectroscopies applied to the same samples provides a useful interpretation tool to establish relationships between two spectroscopies [11]. The correlation matrix describing the relationship between the XRF and XRD data is given by,

$$\mathbf{\Phi} = \mathbf{XRD}^{T}.\mathbf{XRF} \qquad \text{(Equation 4.2)}$$

where XRD and XRF are the mean-centred data matrices obtained from diffraction data (39 x 469) and XRF spectra (39 x 942) respectively.

XRF LiF200 crystal data were used in conjunction with XRD data, to help with identification of the resolved spectra produced using the simplisma approach. The method produced resolved spectra and concentration profiles for both the XRF and XRD data. An 18 x 942 XRF matrix and 18 x 469 XRD matrix were examined using an in-house program created from the algorithm described in Windig's et al. paper [11], copurespec.m with 5 components and an offset, α, value of 3%. The procedure is an extension of the single matrix simplisma program discussed above (Chapter 3). The cross-product data matrix is analysed to produce a purity matrix, as defined by Eq. 3.8 that results in sets of pure variables for both XRF and XRD. Variables considered to have high co-purity may be assumed to describe the same component. As before, relative intensities of the pure variables are considered as reflecting relative contributions of each component and are used to calculate estimated pure component

spectra (Eq. 3.10) and subsequently relative concentrations (Eq. 3.13).

The program was restricted to 5 components as the XRF LiF200 data used contained only 5 elements and including more than 5 components would have no effect on the copurespec function. Figure 4.16 displays resolved spectra for XRF using LiF200 crystal data and corresponds to pure variables identified at 33.17°, 136.67°, 86.3°, 41.81° and 57.53° 2θ angles. From prior knowledge, these pure variables can be equated with bismuth, potassium, titanium, zinc and iron respectively. All pure variables are true pure variables as each resolved spectrum is representative of an elemental component that has no contributions from any other pure component. Each resolved spectrum represents a Kα elemental line and its corresponding Kβ elemental peak. As XRF data has resolved pure component, it is assumed there will be a correlation between resolved spectra of XRD data and XRF results will aid in the interpretation.

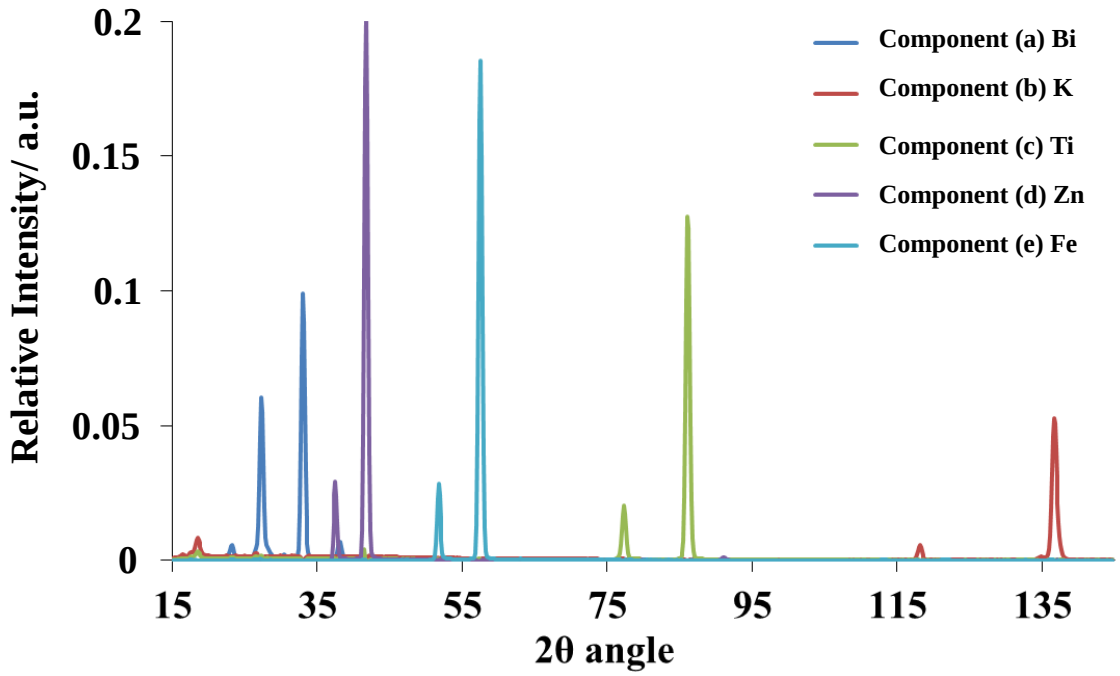

Figure 4.16 Resolved XRF spectra from Simplisma using combined XRF and XRD data, components (a)-(e).

The resolved spectra of XRD data by copurespec method are displayed in Figure 4.17. Resolved diffraction patterns were investigated using the raw material diffraction data that corresponds to the pure components resolved by XRF data. For example, in Figure 4.16, bismuth was the first pure component resolved, therefore it is assumed that the first component to be resolved in Figure 4.17(a) will resemble bismuth oxychloride. Not all components were completely resolved and resembled combinations of more than one pure component. Components (a) (b) and (c) were relatively similar to diffraction patterns of bismuth oxychloride, mica and titanium dioxide.

The concentration profiles of the XRF and XRD techniques were converted to relative concentrations (%) and are displayed in Figure 4.18 showing a comparison of results for each method. Results are not as accurate as those produced through quantitative XRF analysis but give a rough indication the proportions of each element present in the mineral-based samples. The concentration profiles produced using the copurespec function show which samples contain significant amounts of bismuth, iron, titanium and zinc and comply with relative concentrations previously determined in Chapter 3.

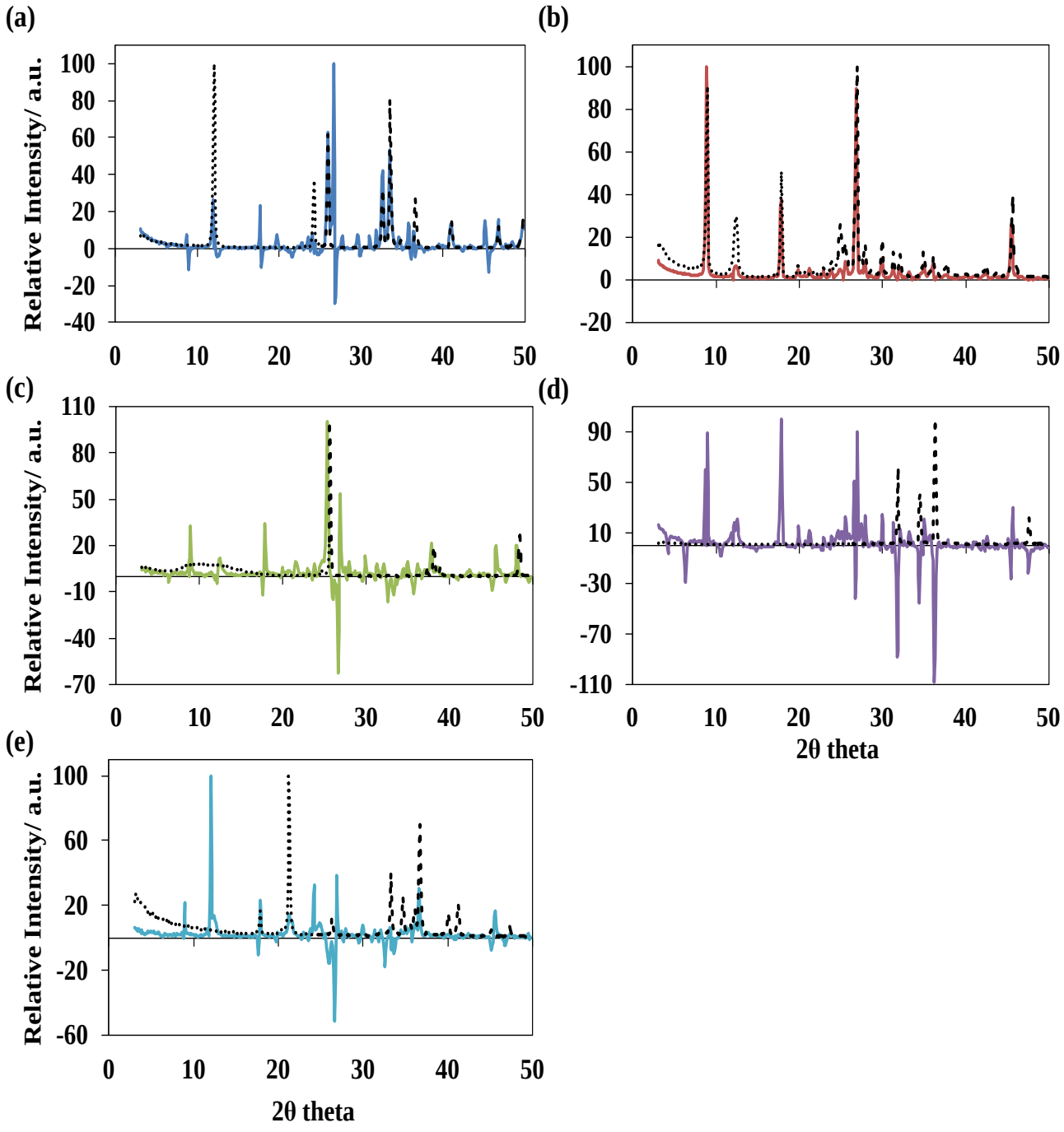

Figure 4.17 Resolved spectra of XRD from Simplisma using combined XRF and XRD data with 'real' diffraction pattern of each component (dotted lines), components (a) Bismuth Oxychloride (b) Mica (c)Titanium Dioxide (d) Zinc Oxide & (e) Iron Oxide.

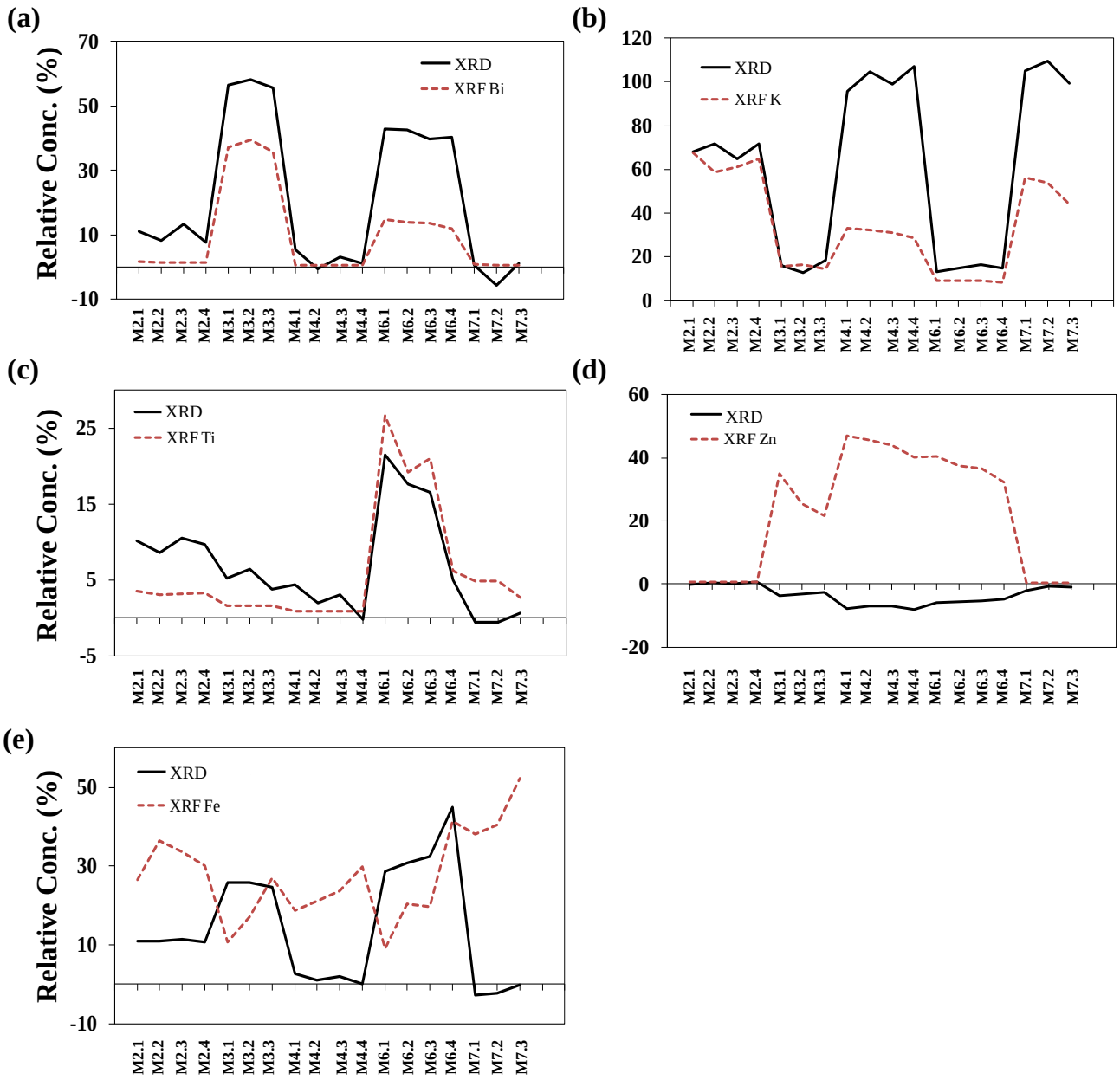

Figure 4.18 Relative concentrations (%) profiles of XRD data and elemental XRF data, resolved by SIMPLISMA method.

The application of the copurespec function to mineral sample XRD data produced concentration profiles with some negative values. This indicates that peak intensities in the diffraction patterns of the components within the samples did not correspond with the peak intensities of the elemental emission lines produced from XRF analysis. For example, the diffraction peaks for zinc oxide are not as clearly visible in the diffraction patterns of samples

than in comparison to the XRF emission line. This does not mean that zinc oxide is not present, just that another approach may be more successful in resolving components from the XRD data. A non-negative constraint method might be a better approach to compensate for the components present with lower diffraction peak intensities.

4.3.7 Multivariate Curve Resolution Alternating Least Squares

Multivariate Curve Resolution Alternating Least Squares (MCR-ALS) has become an increasingly popular method used to decompose data matrices of mixtures into spectra components and concentration profiles [16]. The multivariate curve resolution process utilizes constrained alternating least squares optimization to extract the pure component spectra and concentration profiles associated with the number of components, of the data matrix, **X**, according to the following equation

$$\mathbf{X} = \mathbf{C}\mathbf{S}^{T} + \mathbf{E} \qquad \text{(Equation 4.3)}$$

where **E** is the residual matrix containing the variance, **S** are the pure component spectra ($\mathbf{S}^{T}$ is the transpose) and **C** are the concentration profiles associated with the resolved components. It is possible to obtain the existence of each component as well as an initial estimate of the concentration profiles using either simplisma or evolving factor analysis [17]. The number of components and initial concentrations are used by the alternating squares optimization, to produce a new estimate of the spectra matrix **S** and then of the concentration profiles **C** using:

$$\mathbf{S}^{T} = \mathbf{C}^{+T}\,\mathbf{X}_{est} \qquad \text{(Equation 4.4)}$$

$$\mathbf{C} = \mathbf{X}_{est}\,\mathbf{S}^{+} \qquad \text{(Equation 4.5)}$$

where $\mathbf{C}^{+} = \mathbf{C}(\mathbf{C}^{T}\mathbf{C})^{-1}$ and $\mathbf{S}^{+} = \mathbf{S}(\mathbf{S}^{T}\mathbf{S})^{-1}$ are the pseudoinverses of the matrices **C** and **S** respectively [18]. $\mathbf{X}_{est}$ is a PCA noise filtered estimate of **X** and is generally used to improve

the stability of the pseudoinverse calculations [18]. As mentioned previously, the selection of the correct number of components is important. Too few components will cause small-variance components to be undetectable. An estimation of the number of components can be obtained through chemometric analysis using methods such as PCA.

The MCR-ALS method has been shown in near-infrared and UV spectrphotometric studies to provide improved resolution and enable quantitative analysis of complex mixtures. Azzouz and Tauler reported the use of MCR-ALS to resolve and aid in quantification of analytes in pharmaceutical and agricultural samples [19].

Multivariate Curve Resolution Alternating Least Squares was applied to XRD data of the true mineral-based formulations for quantitative determination of components present in the mixtures using the mcr function in the PLS tool-box. MCR-ALS was conducted using six components. The six components represented the possible raw materials expected in the mineral-based formulas and the number was consistent with the number of components resolved using simplisma. The MCR function produced a scores matrix of 469 x 6 of the resolved component spectra and a loadings matrix of 18 x 6 corresponding to the concentration profiles of the resolved components. The resolved spectra and concentration profiles determined by MCR-ALS using 6 components are displayed as relative concentrations (%) in Figure 4.19 and Figure 4.20 respectively. Resolved diffraction patterns were investigated using the raw material diffraction data to identify the components resolved by the MCR-ALS method. Components 1-4 were not completely resolved and the resolved spectra resembled combinations of more than one raw material. This would have occurred due to the misalignment of diffraction peaks between samples or because the raw material present was not one that was used as a reference in this research. Diffraction peaks of the resolved spectra were compared with diffraction peaks of the raw materials by matching the 2θ angle values. Component 5 resembles the diffraction pattern of bismuth oxychloride and

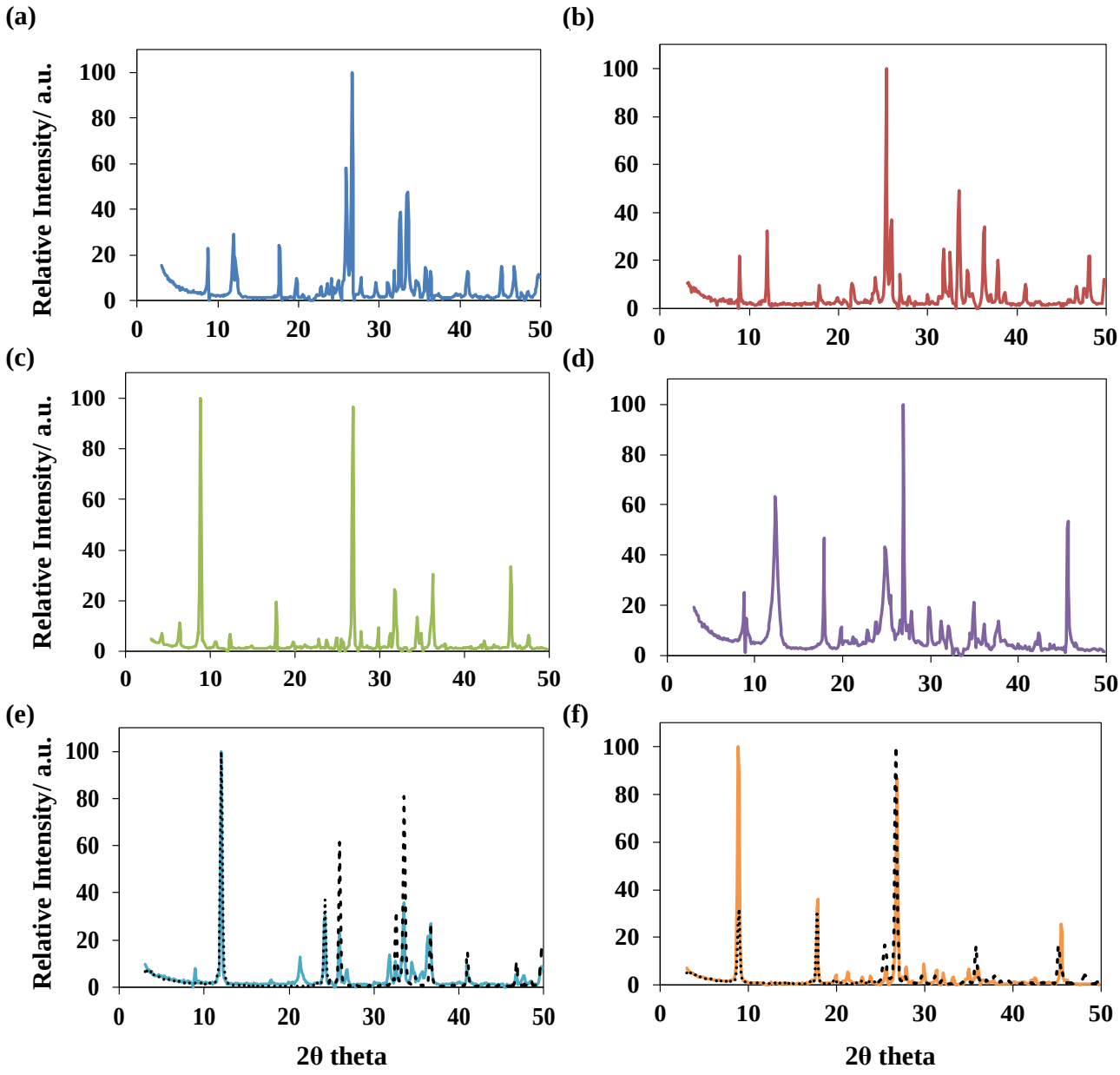

Figure 4.19 Resolved spectra of the 6 components determined by MCR-ALS of (a) Component 1 (b) Component 2 (c) Component 3 (d) Component 4 (e) Component 5 & (f) Component 6.

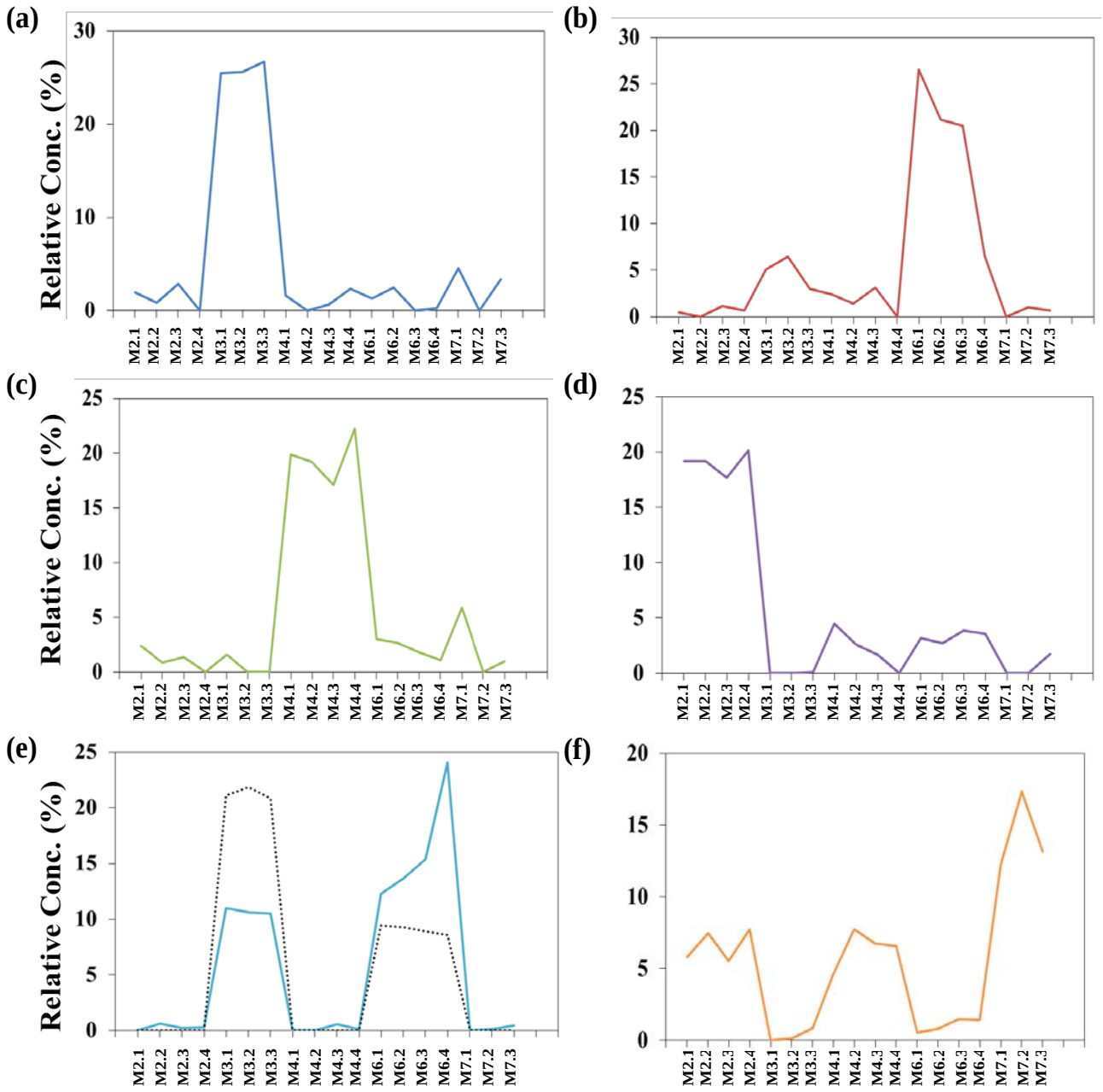

Figure 4.20 Concentration profiles of the 6 components determined by MCR-ALS of (a) Component 1 (b) Component 2 (c) Component 3 (d) Component 4 (e) Component 5 & (f) Component 6, displayed as relative concentrations (%).

the concentration profile is consistent with relative concentrations of bismuth produced through XRF analysis (refer to Table 3.2). The resolved spectrum for component 6 resembles the diffraction pattern of pearl mica. However, the concentration profile cannot be directly linked to one particular element

analysed through XRF, as it contains varying amounts of potassium, aluminium and silica.

Pure component data was applied to MCR-ALS method with mineral-based sample data to see whether raw material data would aid in resolving component mixtures. MCR-ALS method was applied to the 469 x 18 XRD data matrix of mineral-based formulation and a 469 x 6 XRD data matrix of raw material data. The raw materials selected for MCR-ALS were kaolin, titanium dioxide, zinc oxide, bismuth oxychloride, pearl mica and sericite mica. A scores matrix of 469 x 6 of the resolved spectra and a loadings matrix of 18 x 6 corresponding to the concentration profiles of the resolved components were produced. The resolved spectra and concentration profiles for each raw material component are displayed in Figure 4.21 and Figure 4.22 respectively.

Bismuth oxychloride, pearl mica and sericite mica were successfully resolved and resemble the diffraction patterns of these components. However, the remaining components have not produced resolved spectra true to the diffraction patterns of kaolin, titanium dioxide and zinc oxide and resemble mixture of various raw components. The concentration profile of bismuth oxychoride is consistent with the relative concentrations of bismuth determined through XRF. The concentration profiles of pearl mica and sericite mica cannot be directly compared to the relative concentrations examined by XRF. Virtual data is produced that does not match the raw materials. This virtual data finds the best fit with the XRD mineral sample data, and hence changes the concentration profiles.

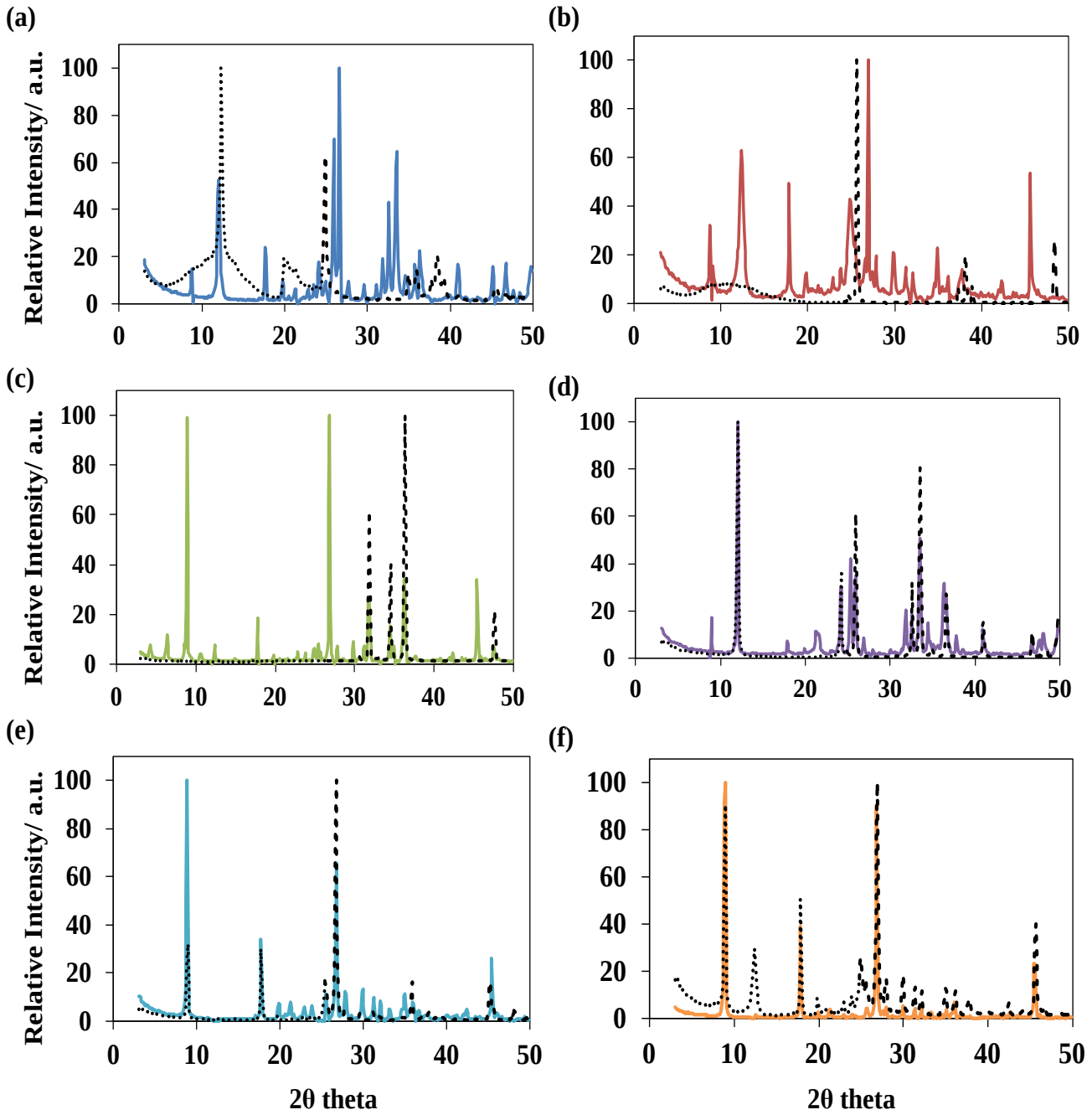

Figure 4.21 Resolved spectra of the 6 components determined by MCR-ALS of (a) Kaolin (b) TiO_2 (c) ZnO (d) BiOCl (e) Pearl Mica & (f) Sericite Mica.

To show how the diffraction patterns of the pure components fitted with the diffraction patterns of the mineral-based samples, the MCR-ALS scores matrix was multiplied by the MCR-ALS loadings matrix to produce a virtual data matrix. The original sample data, the virtual data and the subsequent difference or error between the two are plotted and displayed in Figure 4.23 for (a) sample M2.1 and (b) sample M6.4. The error is minimal because the virtual data has been produced from the pure components, creating resolved spectra for components that do not exist, therefore the fit is good. However, the virtual data does not match the diffraction patterns of the raw materials so the fit is not correct. MCR-ALS was essentially used to make a comparison between results determined by simplisma, to see how it would resolve components from XRD data. But like simplisma, not all components could be successfully resolved.

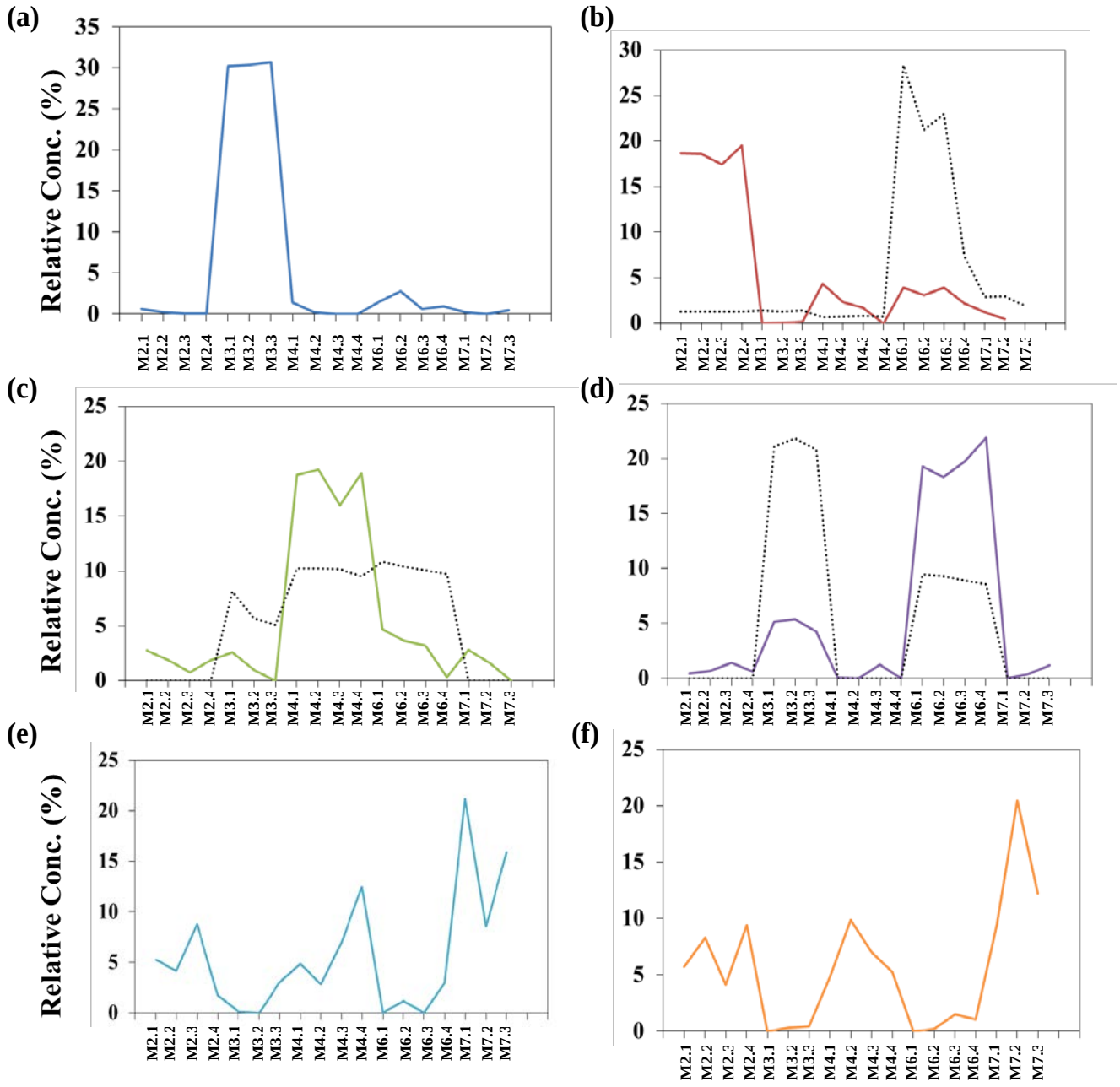

Figure 4.22 Concentration profiles of the 6 components determined by MCR-ALS of (a) Kaolin (b) TiO_2 (c) ZnO (d) BiOCl (e) Pearl Mica & (f) Sericite Mica, displayed as relative concentrations (%).

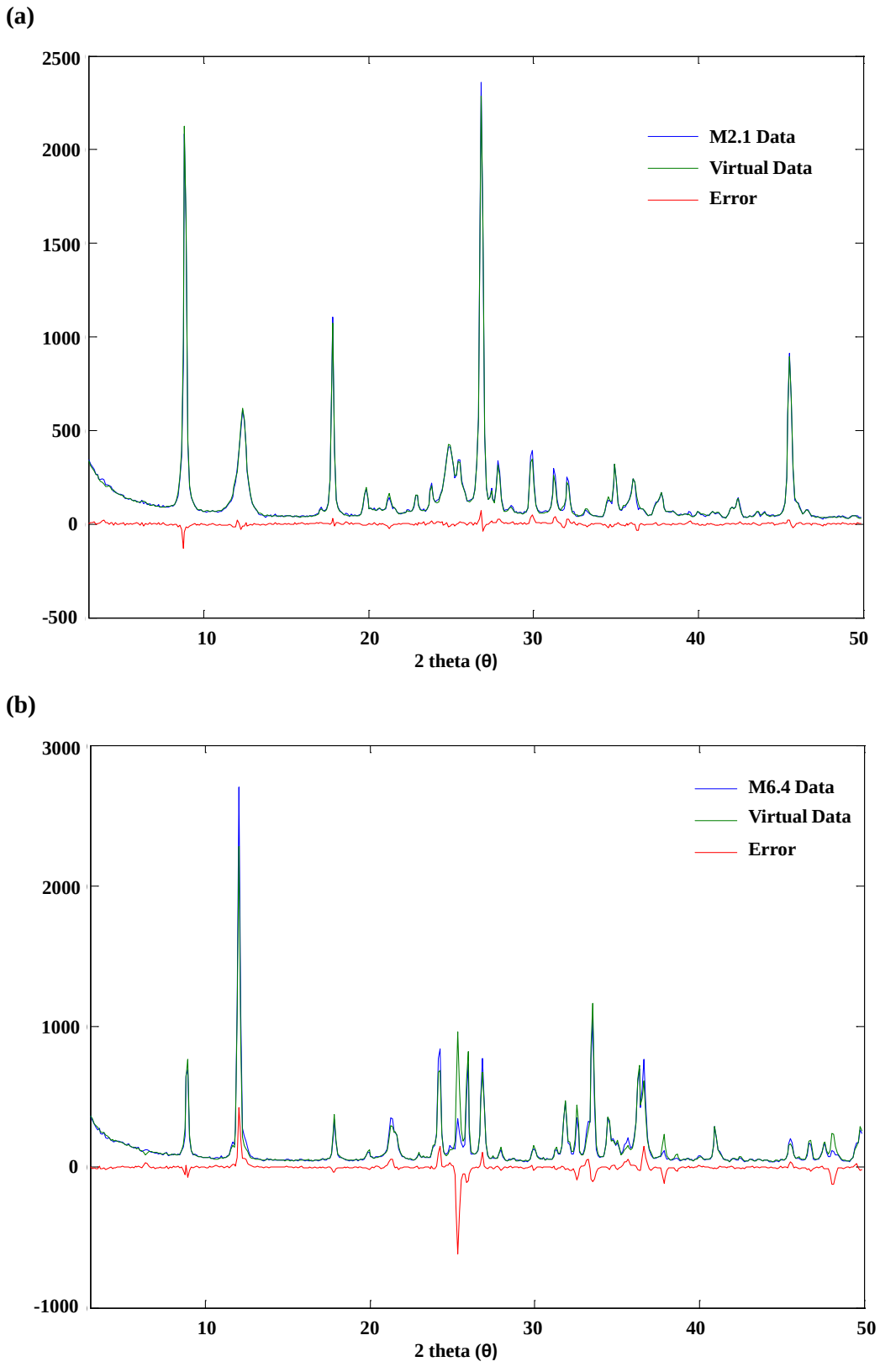

Figure 4.23 MCR-ALS applied to XRD data for samples (a) M2.1 and (b) M6.4 showing the error between the virtual data and the original data for each sample.

4.3.8 Non-negative Least-Squares Constraint

The least-squares method with nonnegative constraint is often applied to curve resolution problems. Least-squares methods provide a model to describe the large number of observations by estimating parameters in experimental data. For experimental data matrix, $\boldsymbol{x_{meas}}$, let the unknown parameters be denoted by the vector $\boldsymbol{x_{std}}$, where $\boldsymbol{x_{std}} = (\boldsymbol{x_{std1}},\ldots,\boldsymbol{x_{stdn}})$, and the set of observed values is given by **C**. The aim is to reconstruct vector $\boldsymbol{x_{std}}$ so that it best describes the observed values [20]. Experimental parameters represent quantities that are only expressed as non-negative values, eg. concentrations, peak intensities, therefore, the model must include non-negative constraints, where it is subject to $\boldsymbol{C} \geq 0$, proposed by the following equation [14]:

$$\|\boldsymbol{x_{std}}.\boldsymbol{C} - \boldsymbol{x_{meas}}\|^2 = min, \boldsymbol{C} \geq 0 \qquad \text{(Equation 4.6)}$$

where $\boldsymbol{C}$ are the concentration profiles for each of the raw material standards denote by $\boldsymbol{x_{std}}$.

Non-negative least-squares (NNLS) was applied to XRD data using an in-house program, matrixlsqnonneg.m, for mineral and traditional foundation samples using all 12 pure components. Tables 4.5 and 4.6 show the concentration profiles obtained through non-negative least-squares method of each of the raw materials present in the mineral and traditional-based formulations. As expected, the mineral-based samples contained predominately mica, differing in the pearl and sericite mica, differing in amounts between manufacturers and samples from the same manufacturer.

This method was more successful in producing concentration profiles consistent with XRF results than MCR-ALS. Bismuth oxychloride was found to be present in samples M3.x and M6.x, zinc oxide in samples M3.x, M4.x and M6.x and titanium dioxide in samples M6.x, however, titanium dioxide produced by NNLS were significantly lower than XRF results. A discrepancy produced by NNLS was the relative concentrations of calcium carbonate found in

samples M3.x and to a lesser extent samples M6.x. X-ray Fluorescence analysis found no traces of calcium within these formulations. Small amounts of kaolin were determined in samples M2.3, M3.x and M6.1 but EVA search matches and PCA of XRD indicate that kaolin was only present in samples M2.x and M4.x.

The presence of a stearate was an unexpected ingredient. Non-negative least squares determined significant relative concentrations of magnesium stearate in samples M6.x and small traces in samples M.2.1, M2.3 and M3.x. Magnesium stearate and zinc stearate have similar diffraction patterns. Patterns consist of peaks at 3°, 6°, 21.3° and 37.8° 2θ angles [21&22]. Diffraction patterns of M2.x and M3.x had no visible diffraction peaks of stearate, while M6.x displayed peaks at 2.13° but no others. X-ray Fluorescence results found very small amounts of magnesium to present in these samples. Zinc was determined in samples M3.x and M6.x but not in sample M2.x. X-ray Fluorescence and X-ray Diffraction analysis produced insufficient evidence of the presence of stearate. Further investigation would be required, eg. IR spectroscopy, to determine whether magnesium stearate or zinc stearate has been included in these formulations.

Non-negative least squares of the traditional samples show a wider variety in the raw materials used for in their production when compared with the mineral samples. As anticipated, the traditional-based formulations contained smaller amounts of pearl and sericite mica than the mineral-based samples with very large amounts of talc. Talc was found to be present in samples in differing forms across all traditional formulations. Non-negative least squares method calculated two forms of kaolin to be present in samples M5.1, T6.1, T1.1, T1.2, T6.2 and T4.3. The diffraction pattern of M5.1 show no evidence that kaolin is present in this sample but the value produced by NNLS is significantly large. EVA search/match results indicate kaolin to be incorporated into samples M1.x and M4.x. However, NNLS results determined the concentration in samples T1.3 to be zero. The presence of kaolin in

Table 4.5 Relative concentrations (%) calculated using nonnegative least-squares method applied to XRD data of mineral foundation samples.

Sample/ Component	Pearl Mica	Sericite Mica	BiOCl	$CaCO_3$	TiO_2	ZnO	Talc 1	Kaolin 2	Kaolin 3	Magnesium Stearate	Kaolin
M2.1	4.37	93.24	0.43	0	0	0	0	0	0	1.91	0
M2.2	2.92	97.05	0.02	0	0	0	0	0	0	0	0
M2.3	4.61	85.91	1.01	0	0	0.59	0	0	0	6.50	1.28
M2.4	1.53	98.47	0	0	0	0	0	0	0	0	0
M3.1	27.09	0.00	41.08	7.41	0.29	11.94	0.22	1.78	4.64	4.83	0
M3.2	23.82	0.00	43.38	9.67	0.66	9.33	0.19	0.14	5.58	7.23	0
M3.3	29.42	0.00	40.83	7.99	0	7.44	0.08	6.16	1.08	7.00	0
M4.1	15.41	74.62	0	0	0	9.97	0	0	0	0	0
M4.2	13.89	80.24	0	0	0	5.87	0	0	0	0	0
M4.3	13.39	78.39	0	0	0	8.23	0	0	0	0	0
M4.4	18.78	75.08	0	0	0	6.14	0	0	0	0	0
M6.1	6.68	23.58	35.04	1.65	1.69	15.96	0.50	3.07	0	11.83	0
M6.2	5.48	24.34	35.15	3.04	1.47	14.69	0.14	0.14	0	15.42	0
M6.3	4.56	30.03	35.32	1.14	0.71	14.10	0	0	0	13.10	0
M6.4	3.63	25.45	41.69	1.09	0	12.83	0	0	0	14.86	0
M7.1	19.62	80.38	0	0	0	0	0	0	0	0	0
M7.2	12.83	87.17	0	0	0	0	0	0	0	0	0
M7.3	16.92	83.08	0	0	0	0	0	0	0	0	0

samples T6.x is consistent with interpretation their diffraction patterns. The relative concentrations of calcium carbonate were found to be significantly high in samples T4.x and T2.3. X-ray Fluorescence results determined these samples have a high calcium content, along with sample T8.2, while the NNLS method produced an insignificant amount of calcium carbonate. Sample M5.1 produced a relatively high concentration of calcium carbonate. Although, XRF analysis determined traces of calcium in this sample the result is not consistent as XRF found similar concentrations in samples M5.2 and M5.3 which is not reflected in NNLS results. Results for components with relatively low concentrations are inconsistent. For example, the method determined traces of zinc oxide in sample M5.1 but not in the other samples from this manufacturer. Whereas, results for XRF show concentrations of zinc in all M5.x samples. This may be due to peak alignment issues within the sample diffraction patterns, causing misinterpretation of the data with the raw material diffraction patterns. Results indicate that the NNLS method is not an accurate measure for determining concentration profiles, but can provide an estimate of the components present and the quantities that may be present in samples.

The concentration profile matrix produced by NNLS was multiplied by the original pure component matrix to produce a virtual mixture data matrix. The virtual data was compared with the original sample data, and the error between them calculated. Figure 4.24 displays the virtual data fit to the original sample data and the error for (a) M2.1 and (b) M4.3. Figure 4.24(a) shows a good fit between the virtual data and the original data for sample M2.1. The error is minimal and the main differences are those between the relative peak intensities of the components present. The split of peaks that occurs in the error is due to the misalignment of certain diffraction peaks within the XRD sample data. The error between the virtual data determined by NNLS and the original XRD data was more realistic than the error predicted by MCR-ALS. Even though the virtual data does not give an ideal fit to original data for each sample, it does confirm which raw materials are present and which are not. It also indicates

Table 4.6 Relative concentrations (%) calculated using nonnegative least-squares method applied to XRD data of traditional foundation samples.

Sample/ Component	Kaolin 1	Pearl Mica	Sericite Mica	BiOCl	CaCO3	Talc 2	TiO_2	ZnO	Talc 1	Kaolin 4	Magnesium Stearate
M1.1	0	5.38	8.16	0	0	61.48	0	0	24.98	0	0
M1.2	0	5.84	10.00	0	2.06	68.46	0	0	10.70	0	2.74
M5.1	0	4.95	5.00	1.57	13.39	25.63	1.35	5.30	9.31	14.18	19.32
M5.2	0	6.24	3.61	0	4.24	63.54	1.35	0	17.17	0	3.57
M5.3	0	6.71	2.48	0	4.41	58.78	0.92	0	22.59	0	3.79
T6.1	13.44	1.03	048	0	0	52.41	3.92	0	28.60	0	0
T1.1	0.54	0	1.80	0	0	64.84	0.45	0	15.76	8.22	7.64
T1.2	0	0	0	0	3.39	48.46	0	2.42	13.46	13.79	15.72
T3.1	0	0	0	0	0	68.47	0	0	31.53	0	0
T8.1	0	0	0	0	14.32	68.18	0	1.42	25.39	0	2.00
T8.2	0	5.84	0	0	1.35	80.49	0	0	11.13	0	1.15
T2.1	0	3.21	13.69	2.81	1.80	66.40	0	0	10.34	0	1.16
T2.2	0	5.81	12.45	4.26	3.80	56.19	0	0	9.53	0	7.92
T4.1	0.26	2.66	0	0	31.47	24.27	1.97	0	8.88	23.09	7.38
T4.2	3.58	2.78	0	0	25.39	35.54	1.60	0	22.55	6.34	2.21
T1.3	0	2.75	1.81	0	0	72.76	0	0	22.67	0	0
T6.2	12.25	5.28	25.60	0	0	40.32	3.71	0	12.74	0	0
T2.3	0	12.07	30.37	0	14.35	24.46	0	0	11.13	0	7.57
T3.2	0	0.95	0	0	4.87	60.17	0	2.57	21.10	0	8.91
T3.3	0	0	0	0	2.31	78.53	0	0	15.08	0	2.11
T4.3	7.15	2.96	0	0	22.67	44.62	1.42	0	18.97	2.21	0

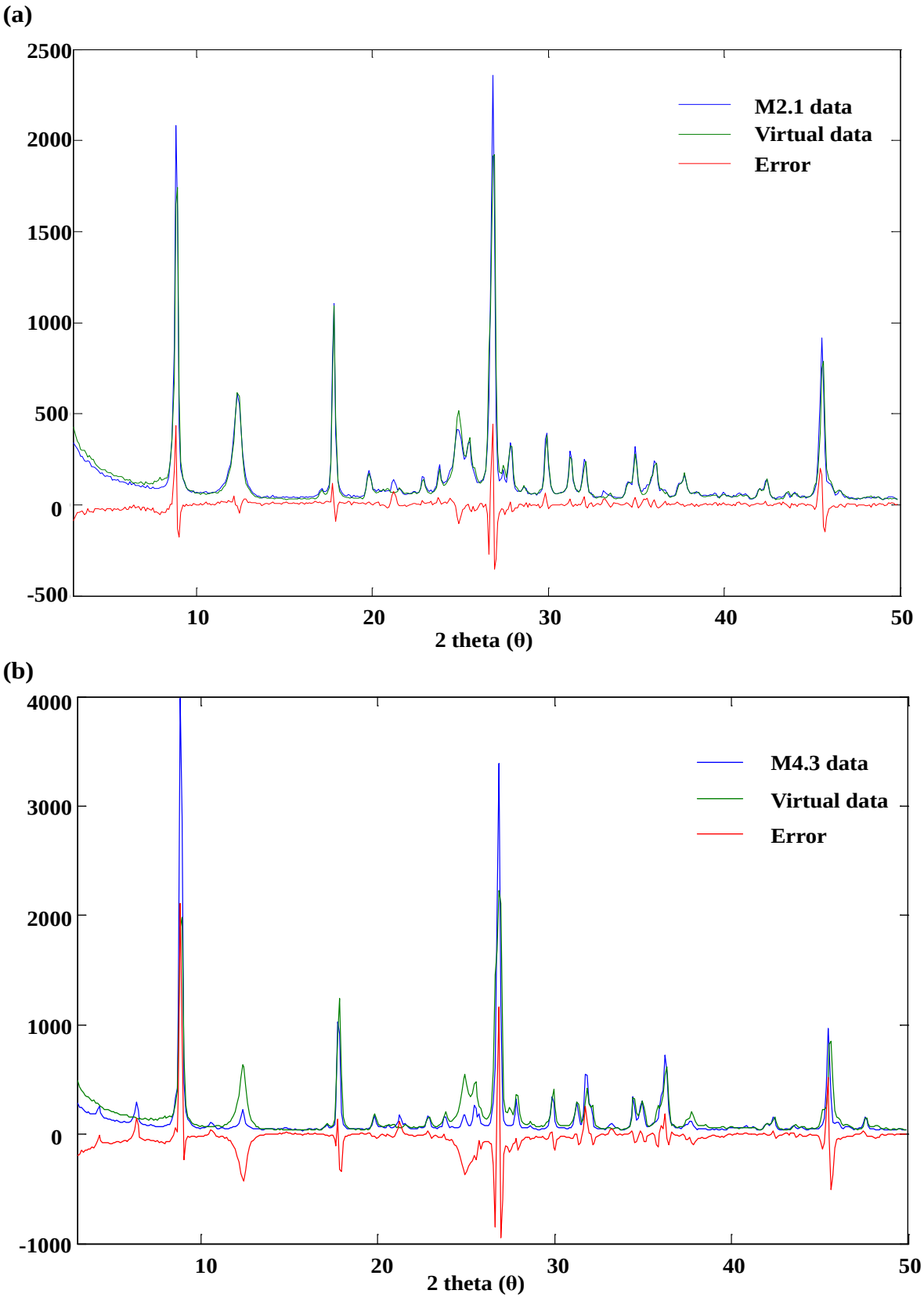

Figure 4.24 Nonnegative least-squares applied to (a) M2.1 and (b) M4.3 showing error between the virtual data and original data for each sample.

that raw materials appear in these samples may not be in the same form as analysed in this research. This is shown in Figure 4.24(b), sample M4.3 where two diffraction peaks at 2θ angles 4.25° and 6.35° do not match diffraction peaks from the virtual data. The diffraction patterns of these peaks are not those of the raw materials analysed by XRD. Sample M2.1 is a better fit with the virtual data than sample M4.3 and materials used are likely to be similar to those of the reference raw materials. There is a larger discrepancy in the error between the virtual data and the original data for M4.3, indicating that the components used are less like the reference components. The differences in the error between samples M2.1 and M4.3 show the variety of raw materials that are used in the mineral foundation formulations and that differing forms of these materials are used depending on the manufacturer.

Figure 4.25 shows the virtual data fit with traditional samples. Results differed from the mineral-based samples. Figure 4.25 (a) displays the virtual data fit with sample T3.3. The error is minimal and the fit quite good, with peak intensity differences between the original and the virtual data. In comparison, sample T2.3 shown in Figure 4.25 (b), has a 'bad' fit with the virtual data, with a significantly larger error. Diffraction peaks at 2θ angles 6.24°, 12.44° and 25.14° appear in the virtual data but not in the original. These diffraction angles match peaks in the diffraction pattern of Talc 1. This indicates that this particular form of talc is not used as an ingredient in sample T2.3. There are components in the original data which do not match the raw materials used in analysis. The major peaks occur at 2θ angles 19.94°, 29.54°, 31.04°, 32.64° and 41.24°. This indicates that other raw materials have been used in the production of sample T2.3 or the materials are in a differing form than and are unlike the reference raw materials. The relative concentrations of traditional-based samples obtained by NNLS from Table 4.6 show a wide variety of raw materials that can be included in formulations. The raw materials used may differ worldwide and between manufacturers. Due to the wider variety of ingredients, the traditional samples are more difficult to characterize than the mineral samples.

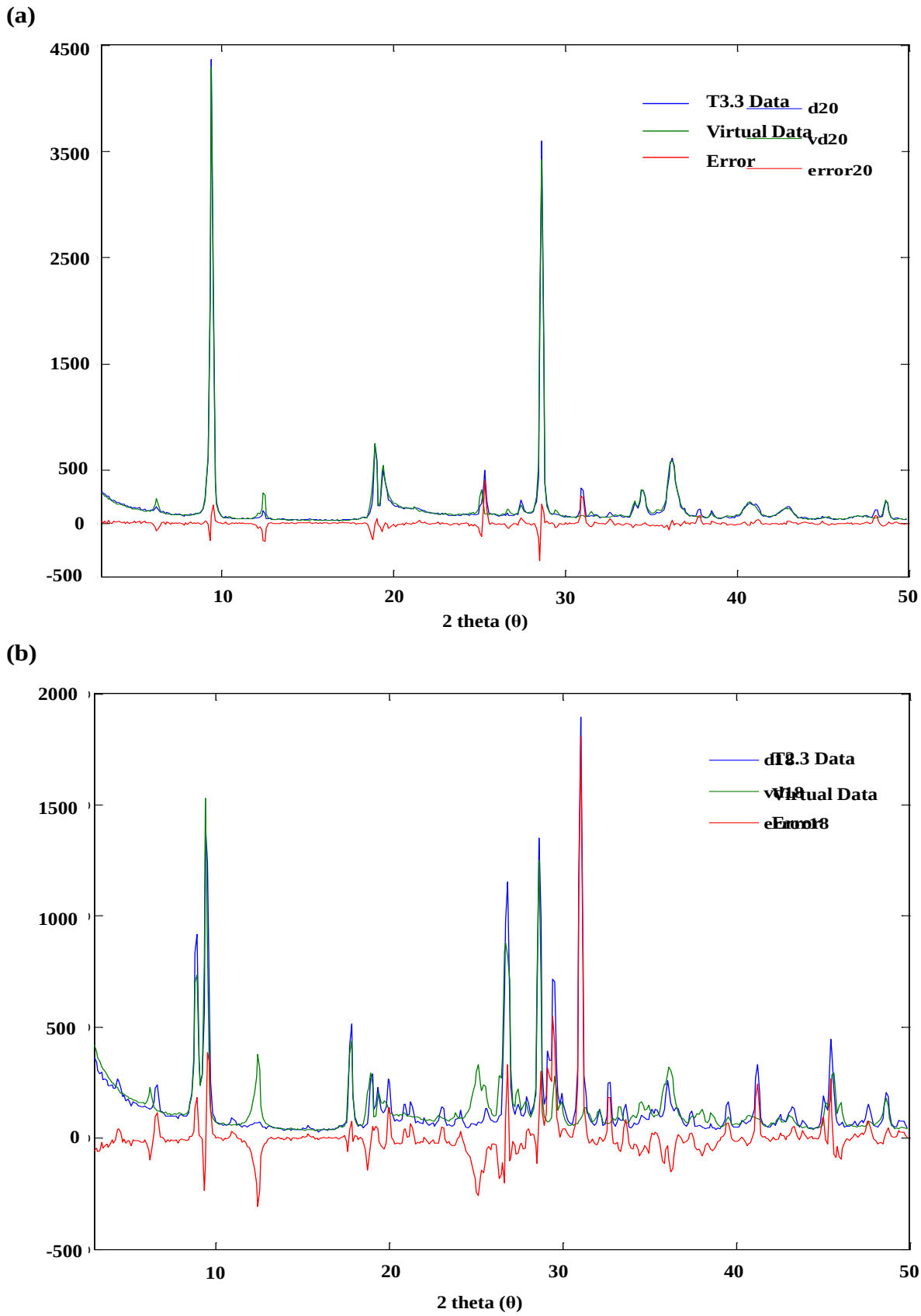

Figure 4.25 Nonnegative least-squares applied to (a) T3.3 and (b) T2.3 showing error between the virtual data and original data for each sample.

4.4 Conclusion

X-ray Diffraction analysis was effective in providing an overview of the mineral and clay phases used for cosmetic foundation production. Analysis of cosmetic grade raw materials was useful in peak identification, but not all diffraction peaks could be determined by eye. Results obtained using an available commercial database provided a preliminary analysis, however, it did not provide a full characterisation, as many of the matches were not cosmetic grade and did not comply with XRF results.

X-ray Diffraction analysis enabled identification of kaolin in diffraction patterns of samples. This was achieved through XRD analysis of cosmetic raw materials and through EVA search/match. Kaolin could not be identified through XRF analysis as there was no sole element that could be represented by kaolin. The aim of applying 2D correlation to two differing analysis techniques was to highlight its ability to provide a relationship between the elemental concentration and the structural phases found in samples. Two-dimensional correlation of XRD with XRF data proved successful in producing positive correlations between the elemental emission lines and the diffraction patterns of cosmetic raw materials. This method helped to validate peak identification of foundation samples that had been determined when comparing diffraction patterns of raw materials, and identifying peaks that could not be identified in this process. Correlation coefficients for traditional samples were not as high as those produced from the mineral sample data set. Due to the complexity of the chemical formulas of the raw materials, elemental analysis cannot solely be used for XRD peak identification. Only components, such as bismuth oxychloride, titanium dioxide, zinc oxide and to an extent mica could be identified by correlation with XRF.

Simplisma was not as successful in deconvoluting diffraction patterns of components found in traditional samples. The major problem in using simplisma on this data set was the large intensity peaks produced by the presence of talc. This inhibited other known components

from being resolved from the data. Simplisma was better suited to the mineral-based formulations. However, concentration contributions determined did not always match those produced from XRF data. A possible reason is due to the complex nature of the samples and overlap of diffraction peaks of materials that are present. Peak overlap resulted in incorrect calculation of concentration contributions. This problem may have also affected the results of 2D correlation. Base line correction techniques or data smoothing may help aid the problems caused by peak overlap.

X-ray Diffraction analysis of iron oxide was unsuccessful. Iron oxide identification in samples proved difficult and was not a relevant factor in any of the chemometric analysis tools used on this chapter.

Simplisma indicated the presence of two forms of mica; sericite and pearl mica. Other methods, such as infra-red spectroscopies need to be employed, to help with identification of iron oxides and differing component phases of materials such as mica with the aid of PCA, 2D correlation and simplisma.

Multivariate curve resolution did not provide accurate concentration profiles for the components present in the mineral-based samples. The virtual data produced did not resemble the raw materials present and the fit it provided to the original data matched well because the resolved spectra was created from the original data.

Nonnegative least-squares provided an insight into the quantities of each component that was present in the mineral and traditional-based formulas. Not all results were consistent with relative elemental concentrations determined through XRF, but patterns between the two data sets did arise and NNLS was able to provide information on the differing forms component phases, such as kaolin, mica and talc that could not be represented by a single element in XRF. The comparison of the virtual data produced by NNLS with the original XRD data was able to provide information on which raw materials were present and which were not in each sample. Some samples had a better fit with the virtual data than others, which indicates that

manufacturers are using differing forms of ingredients and some were not the same as the reference materials used in analysis. Infrared spectroscopies may provide a better insight into the forms of raw materials present in the cosmetic foundation samples.

4.5 References

1. Y. Leng, *Materials characterization introduction to microscopic and spectroscopic methods*, John Wiley & Sons Inc., Hoboken, Singapore, **2008**.
2. C. Whiston, *X-ray Methods (1st Ed.)*, John Wiley & Sons, London, UK, **1987**.
3. Y. Waseda, E. Matsubara, K. Shinoda, *X-Ray Diffraction Crystallography Introduction, Examples and Solved Problems*, Springer-Verlag, Heidelberg, Germany, **2011**.
4. B. Warren, *X-ray Diffraction*, Dover Publications, New York, USA, **1990**.
5. D. K. Smith and R. Jenkins, ICDD and the Powder Diffraction File Past, Present and Future, published by the International Centre for Diffraction Data, **1996**
6. Moore. D, R. Reynolds. *X-ray Diffraction and Identification and Analysis of Clay Minerals (2nd Ed.)*, Oxford University Press, New York, USA, **2007**.
7. J. D. Hanawalt, Prof. Emeritus, *Manual Search/Match Methods for Powder Diffraction in 1986*, Powder Diffraction, 1986, **1**(1): p. 7-13.
8. Semi-Quantitative Analysis by XRD, H&M Analytical Services Inc., NJ, USA, **2002**.
9. Bruker Lab report XRD58, Quantitative Analysis of Geological Samples: Combined XRD-XRF Analysis, Karlsruhe, Germany, **2010**.
10. S.Slobodan, A.Muszynski and Y. Ozaki, *A New Possibility of the Generalized Two-Dimensional Correlation Spectrosctopy. 1. Sample-Sample Correlation Spectroscopy*, J. Phys. Chem. A, 2000, **104**: p.6380-6387
11. W. Windig, D. E. Margevich, W. P. McKenna, *A novel tool for two-dimensional correlation spectroscopy*, Chemometrics and Intelligent Laboratory Systems, 1995,

28: p.109-128.

12. G.W. Brindley. Identification of clay minerals by XRD analysis- http://www.clays.org/journal/archive/volume%201/1-1-119.pdf
13. Diffrac plus EVA Search/Match User Manual, Bruker AXS Gmbh, Karlsruhe, Germany, **2005**.
14. MATLAB software (Ver. 7.10, Mathworks Inc., NSW, Australia) and the PLS-Toolbox (Eigenvector Research Inc., WA, USA).
15. Balsam, S., Gershon, Rieger and Strianse, *Cosmetics: Science and Technology. Vol. 1*, John Wiley & Sons Inc, **1972**.
16. J. Jaumot, R. Gargallo, A. Juan, R. Tauler, *A graphical user-friendly interface for MCR-ALS: a new tool for multivariate curve resolution in MATLAB*, Chemometrics and intelligent laboratory systems, 2005, 76: p.101-110.
17. R. Tauler and B. Kowalski, *Multivariate Curve Resolution Applied to Spectral Data from Multiple Runs of an Industrial Process*, Anal. Chem, 1993, **65**: p2040-2047.
18. B. M. Wise, J. M. Shaver, N. B. Gallagher, W. Windig, R. Bro, R. S. Koch, *Chemometrics tutorial for PLS_Toolbox and Solo*, Eigenvector Research Inc., Wenatchee USA, 2006.
19. T. Azzouz and R. Tauler, *Application of multivariate curve resolution alternating least squares (MCR-ALS) to the quantitative analysis of pharmaceutical and agricultural samples*, Talanta, 2008, 74: p.1201-1210.
20. D.Chen and R. J. Plemmons, *Nonnegativity Constraints in Numerical Analysis*, Wake-Forest University, Winston-Salem, USA. Date Accessed- 22/03/13.
21. R.D. Vold and G. S.Hattiangdi, *Characterization of Heavy Metal Soaps by X-Ray Diffraction*, Industrial and Engineering Chemistry, 1949, **41**(10): p.2311-2321.

22. V. Swaminathan and D. O. Kildsig, *An Examination of the Moisture Sorption Charcateristics of Commercial Magnesium Stearate,* AAPS PharmSciTech, 2001, **2**(4): p.73-79.

Chapter 5: Analysis of Cosmetic Foundations using Infrared Spectroscopies

5.1 Introduction

Fourier Transform Infrared spectroscopies in the mid (400-4000 cm^{-1}) and near-infrared regions (4000-10000 cm^{-1}) have proved successful techniques for identifying mineral compositions. While absorption methods can be used for mineral characterization, reflectance methods are commonly employed for such studies [1]. Diffuse reflectance FT-IR is highly effective in retrieving information concerning the mineral composition and structure of cosmetic foundation powders. It is a fast, non-destructive means of measurement with simple sample preparation compared with the preparation of KBr discs [2] used in transmission/absorption studies. Diffuse reflectance is defined by the IR radiation emerging from a powdered sample after it has undergone absorption, refraction, reflection and scattering in a majority of the material [3]. Diffuse reflectance is dependent upon the particle size and surface morphology of powdered sample materials, which can be altered and controlled during sample preparation. The recorded DRIFT spectrum results from the scattering of the irradiated powdered sample, a combination of diffuse and specular reflectance. Specular reflectance contains little spectral information and is a reflection from the front surfaces of the sample being analysed. It can lead to distortions in the DRIFT spectra but can be minimized by correct sample preparation [2].

The characterization of cosmetics powders using diffuse reflectance techniques has not previously been reported. However, mid-infrared and near-infrared diffuse reflectance

spectroscopy has been widely used for the characterization of mineral components in, for example, soils. Nguyen et al. applied DRIFT spectroscopy for mineral characterization of soils to highlight the advantages the technique provided over the use of pressed KBr discs in the mid-infrared region. It was reported that the degree of scattering as well as total absorption in intense spectral regions and the sloping base-lines caused by pressed discs, do not appear in DRIFT spectra. However, distortion of strong bands can occur, but can be inhibited with sample grinding and a degree of dilution with KBr powder [3&4]. McCarty employed diffuse reflectance in the mid and near-infrared regions to obtain information of the organic and inorganic components present to quantify organic and inorganic matter relating to carbon in 273 soil samples [5].

In this study, diffuse reflectance across the mid-infrared (MIR) and near-infrared (NIR) regions is used to obtain complementary characteristic spectra in both regions, providing a more complete means of analysis. The MIR region can provide structural information relating to fundamental vibrations, while the NIR region provides complex structural information due to weaker and broader vibration overtones and combination bands [5] due to the presence of O-H, C-H, C-O and N-H bands [6]. Principal component analysis has been applied to spectral data to investigate trends in material composition of samples between manufacturers. Two-dimensional correlation is shown to be a useful tool for the analysis and interpretation of spectroscopic data.

5.2 Experimental

As with previous studies, thirty-nine foundation samples were analysed, 23 mineral-based samples and 16 traditional-based formulations. The samples, with description and coding employed, are listed in Table 2.1 (Chapter 2). Known raw materials of cosmetic foundation

were also analysed. The raw materials, with description and supplier details are listed in Table 4.1 and Table 4.2 (Chapter 4).

5.2.1 Sample Analysis

All samples and raw materials were analysed using a FT-IR Spectrometer (Model Spectrum 100, Perkin-Elmer, Shelton, USA) with a DRIFTS attachment (Specac Limited, Slough, UK). Approximately 2mg of sample were mixed with approximately 200mg of KBr and thoroughly ground. The stainless steel holders were filled with the sample and KBr mixture and the surface flattened with a spatula. Diffuse reflectance spectra were measured over the 400-4000 cm^{-1} mid-infrared region at 2 cm^{-1} intervals. For each sample and raw material 16 scans were averaged at a spectral resolution of $8cm^{-1}$.

For the near-infrared region, all samples and raw materials were analysed without KBr. The stainless steel sample holders were filled with the samples and surface flattened with a spatula. Diffuse reflectance was measured in the near-infrared region, 4000-8000 cm^{-1} at $2cm^{-1}$ intervals. For each material 128 scans were recorded at a resolution of $16cm^{-1}$.

5.2.2 Data Processing

Vibrational spectroscopy techniques generate large amount of data and appropriate multivariate statistical methods are employed for data interpretation [7]. All raw reflectance data were converted to absorbance ($\log_{10}(1/R)$). Principal component analysis and 2D correlation were used to interpret and identify components in FT-IR data. Principal component analysis reduces the dimensionality of multivariate data by generating a new set of variables called principal components. Each component is characterized by its loadings and scores. Loadings plot are calculated for each PC and indicate which variables (reflectance at each wavenumber) contribute to the variance explained by each PC [7]. However, spectral

pre-processing was required before chemometric analysis to reduce light scattering, base-line drift and random noise that can affect the interpretation of the results. Light is reflected and transmitted when the refractive index changes, as occurs when the light meets a particle in a powder [8]. The amount of scatter is dependent on the physical nature of the sample particles, and spectral path length is largely dependent on sample particle size [9]. Variations within spectra can be due to how densely samples are packed, as well as how finely each sample is ground. Various scatter correction techniques were trialled, such as Savitzky-Golay [10] and Multipicative Scatter Correction (MSC) [11], but Standard Normal Variate (SNV) transformation gave the best results here for chemometric analysis. Standard normal variate centres and scales individual spectra. According to Barnes et al., SNV at each wavelength removes variation on an individual sample by the use of the following equation, where x_{ij} represents each spectrum at the *j*th wavelength for the *i*th sample:

$$X_{ij,SNV} = \frac{(x_{ij} - \bar{x}_i)}{\sqrt{\frac{\sum_{i=1}^{j}(x_{ij} - \bar{x})^2}{j-1}}} \qquad \text{(Equation 5.1)}$$

and where $\bar{x}_i$ is the mean response value for spectrum *i* and *j* is the number of variables (absorbance at each wavelength) in the spectrum [12]. So, SNV mean-centres each spectrum and scales each spectrum by its standard deviation.

5.3 Results and Discussion

All reference material and sample spectra were subjected to SNV pre-processing using MATLAB. Once scatter corrected, a 3-point binning was employed to smooth data and reduce the number of variables considered.

5.3.1 Spectral Analysis of Reference Materials in the Mid-Infrared Region

Diffuse reflectance infrared fourier transform spectra in the mid-infrared region of mineral components found in cosmetic foundation powders are presented in Figures 5.1 and 5.2.

The DRIFT spectrum of kaolin (see Figure 5.1(a)) contains stretching vibrations for two types of hydroxyl groups, outer hydroxyl and inner surface hydroxyl groups. Four distinct bands can be observed at 3698, 3672, 3655 and 3622 cm^{-1}. The three higher frequency bands are assigned to the outer hydroxyls and the bands near 3622 cm-1 the inner surface hydroxyl [13]. The spectra of clay minerals display Si-O stretching and bending in the 1300-400 cm^{-1} region, however, the shape and the positions of the bands are dependent on the layering of the silicate structure. Kaolin exhibits several strong bands due to Si-O stretching vibrations in the 1120-1000 cm^{-1} region characteristic of its 1:1 layer structure, in which Al(III) and Si(IV) lie in the octahedral and tetrahedral positions, respectively [14]. The Al-OH bending vibrations in kaolin occur near 937 and 915 cm^{-1} and arise from inner and surface hydroxyl groups [15]. Further bands can be seen in the 800 and 470-420 cm^{-1} region [3].

The MIR spectra for pearl and sericite mica are fairly similar. The significant differences are the OH group bands characteristic of micas near 3654, 3653 and 3635 cm^{-1} observed only in the in the sericite mica IR spectrum. Both exhibit Al-OH bands from 930 cm^{-1} and 915 cm^{-1} [21]. Since pearl mica is blended with titanium dioxide (see Table 4.2) it exhibits differences in spectral features in the region near 700 cm^{-1} in comparison to sericite mica and displays similarities to the MIR spectra of titanium dioxide displayed in Figure 5.2(a).

Carbonates absorb in regions near 1450, 880 and 700 cm^{-1} due to the C=O vibrations. The band near 1450 cm^{-1} is a characteristic feature of the calcite form of $CaCO_3$ [16] and can be seen in the diffuse reflectance spectrum displayed Figure 5.1 (b). Talc exhibits OH stretching, of the Mg_3OH group at 3676 cm^{-1} [17]. Lattice vibrations of the Mg-OH in talc are observed

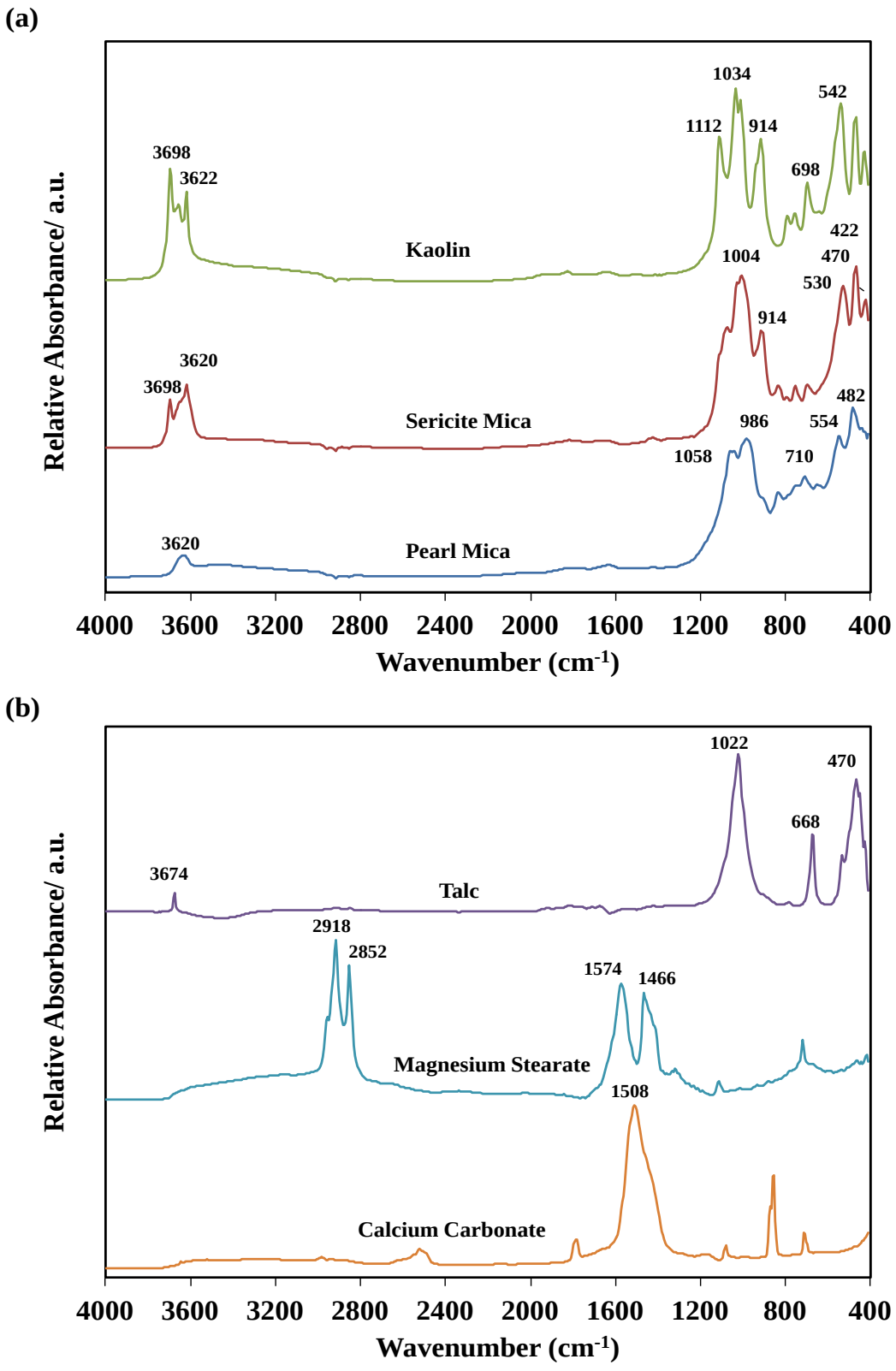

Figure 5.1 DRIFT spectra of mineral components used in production of cosmetic foundation powders in the mid-infrared region.

near 670 and 464 cm^{-1} [18]. The diffuse reflectance spectrum of magnesium stearate exhibits some of the features typical of stearic acid. The symmetric and asymmetric CH_2 stretching bands can be observed near 2900 cm^{-1} and a C=O stretching vibration near 1570 cm^{-1} [19&20]. A CH_2 scissoring vibration appears near 1466 cm^{-1}.

The diffuse reflectance spectra of zinc oxide and titanium dioxide shown in Figure 5.2(a) are relatively simple. Little chemical information can be found from the MIR spectra. The MIR spectrum of bismuth oxychloride displays a sharp peak at 536 cm^{-1}.

The reflectance spectra for iron oxides are displayed in Figure 5.2(b). There are similar characteristic features in each of the spectra with bands observed in the 900 to 400 cm^{-1} region. Fourier Transform Infrared study of iron oxides is well established. Characteristic absorption bands that are observed are due to OH stretching and Fe-O lattice vibrations [22]. The MIR spectra of orange iron oxide contains absorption bands characteristic of goethite. Bands are observed near 3150, 890 and 795 cm_{-1}, due to Fe-OH stretching, while Fe-O vibrations are observed at a lower wavenumber, near 600 cm^{-1} [23]. The MIR spectra of deep red, medium brown and dark brown iron oxides exhibit a broad absorption near 620 cm^{-1}, characteristic of the spectra of hematite due to OH stretching vibrations [24].

In comparison, the spectra of ochre shows absorption bands characteristic of maghemite, in which bands are observed near 680, 650 and 554 cm^{-1} due to Fe-O vibrations [25].

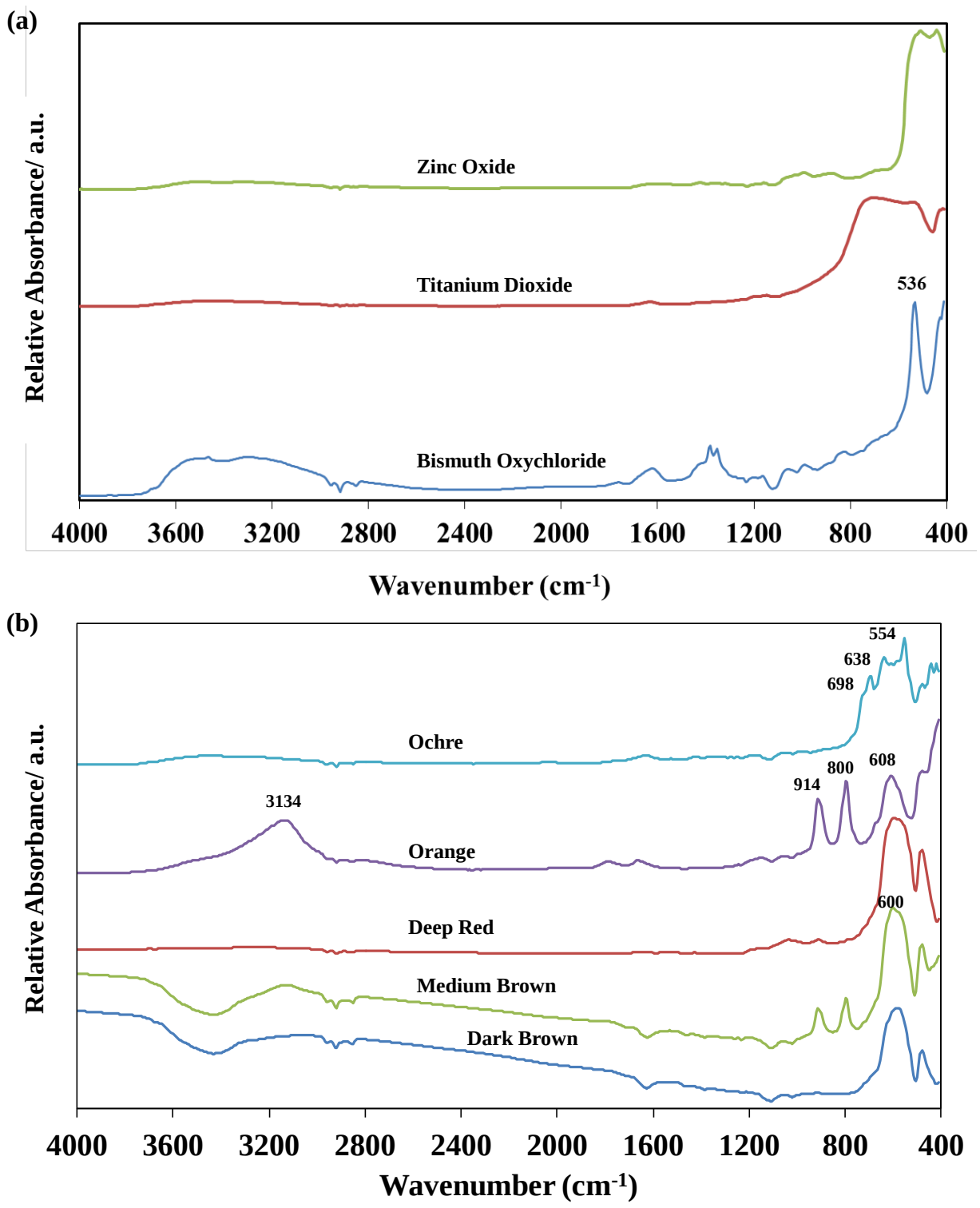

Figure 5.2 DRIFT spectra of cosmetic metal and iron oxides used in foundation powder production in the mid-infrared region.

5.3.2 Comparison of Spectral Data in the mid-infrared region using reference materials

The DRIFT spectra of traditional and mineral-based foundation powders in the mid-infrared region (400-4000 cm^{-1}) are presented in Figure 5.3 and 5.5 respectively. There are visible differences between the mineral and traditional foundation types, as well as by manufacturer. The spectra of traditional foundation samples (Figure 5.3) contain absorbance bands characteristic of talc at 3674, 1022, 670 and 460 cm^{-1}. Bands appear in all traditional-based samples at 2918 and 2852 cm^{-1} that resemble the CH_2 stretching bands of magnesium or zinc stearate. However, not all samples exhibit stearate C=O stretching vibration near 1570 cm^{-1} and the CH_2 scissoring vibration near 1466 cm^{-1}. A strong, broad band observed near 1466 cm^{-1} is representative of calcium carbonate. A closer investigation is required to distinguish these differences between samples. The major spectral differences between traditional-based samples are displayed in Figure 5.4.

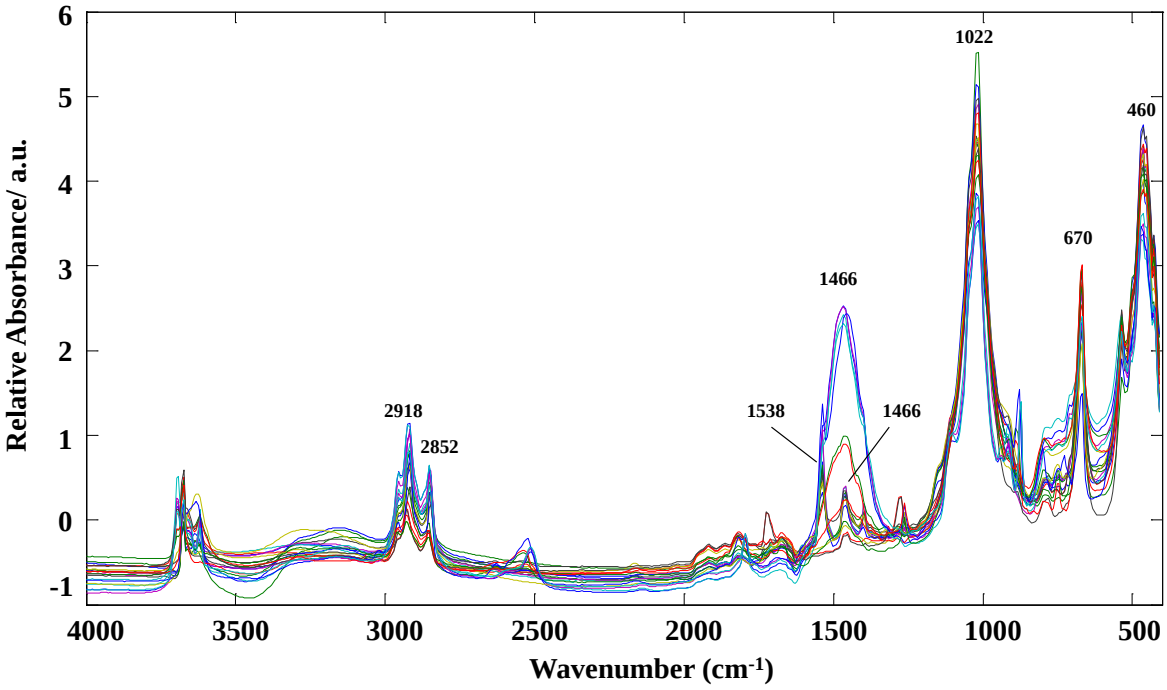

Figure 5.3 FTIR spectra of the 21 traditional-based foundation formulations recorded in the mid-infrared region.

Calcium carbonate, distinguished by a broad band near 1466 cm^{-1} was found to be present in the MIR spectra of T2.3, T4.x and T8.2 and is displayed in Figure 5.4(a). This finding was consistent with XRF and XRD results. Relative elemental concentrations (%) produced by XRF analysis, are shown in Table 3.2 (Chapter 3), and indicate calcium is found to be present in samples T4.x, T2.3 and T8.2. The XRD PCA scores and loadings displayed in Figure 4.6 (Chapter 4), shows the grouping of samples T4.x and T2.3 due to calcium carbonate. T8.2 does not group with these samples in XRD PCA results but it is likely that another component is responsible. Samples T2.1 and T2.2 exhibit a similar band at 1466 cm^{-1}, however, XRF and XRD do not support the presence of calcium carbonate in these samples. It is assumed that the band is due to another material component not examined in this study.

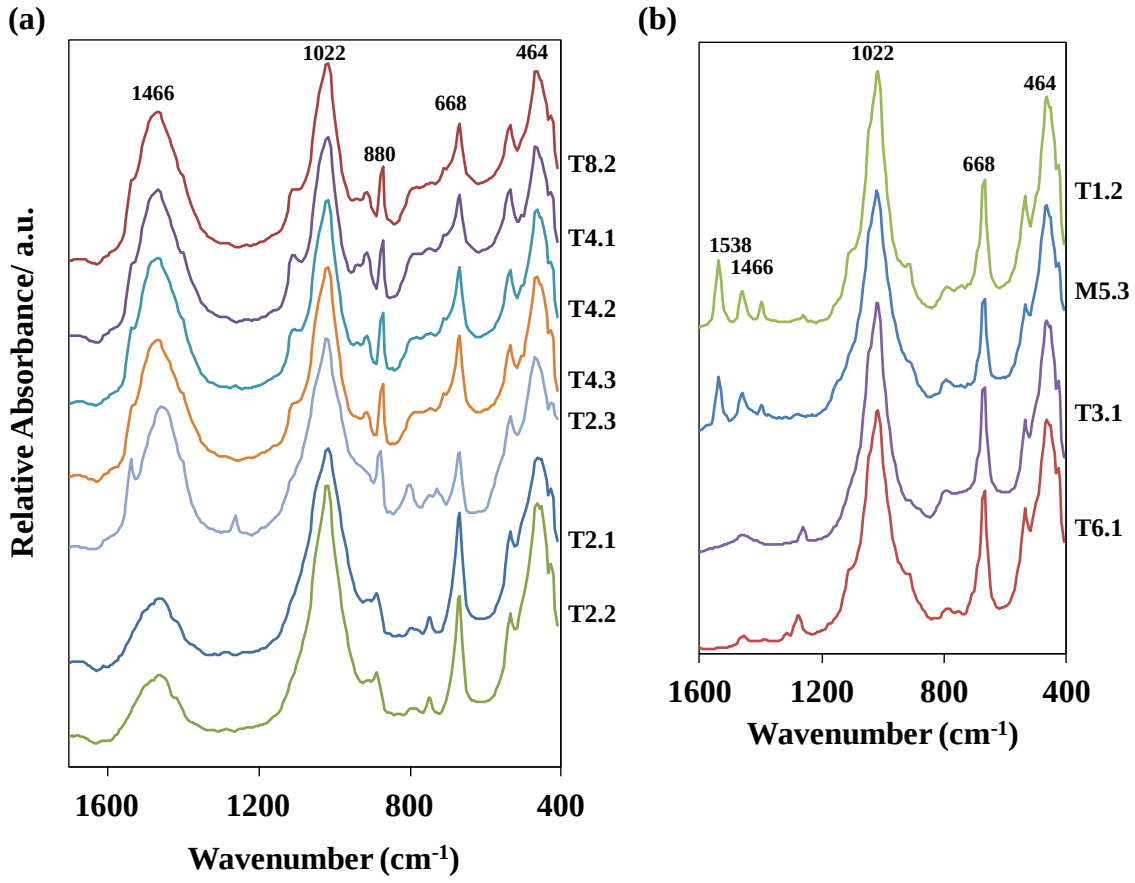

Figure 5.4 Comparison of spectra of traditional-based samples (a) T8.2, T4.x and T2.x and (b) T1.2, M5.3, T3.1 and T6.1 in the 1600-400cm^{-1} spectral region.

Samples T1.2, M5.3, T3.1 and T6.1 are shown in Figure 5.4(b) to highlight the differences in bands present in samples due to stearate at 1538 and 1466 cm^{-1}. Samples M1.x, M5.x and T1.x show characteristic bands of stearate near 2900, 1538 and 1466 cm^{-1}, whereas samples T3.x and T6.x do not exhibit a band at 1538 cm^{-1}. The MIR spectra of zinc stearate exhibits a band near 1537 cm^{-1} due to carboxylate vibrations [26]. It can be assumed that samples that exhibit a band at 1538 cm^{-1} contain zinc stearate and those without contain magnesium stearate or another form of stearate. XRD analysis could not support the presence of stearate in all cases. The X-ray powder diffraction patterns of zinc and magnesium stearate are similar. Patterns consist of peaks at 3°, 6°, 21.3° and 37.8° 2θ angles [27&28]. These peaks are only visible in diffraction patterns of samples M5.x. This indicates that absorbance bands could be due to another component besides stearate or XRD analysis was not an appropriate technique for the identification of stearate. Although samples M1.x, M5.x and T1.x contain traces of zinc determined by XRF analysis, elemental concentrations could not be used to confirm MIR results, as zinc is also present in cosmetic foundations as zinc oxide and was unable to be identified through FT-IR.

In comparison, the reflectance spectra of the mineral-based samples displayed in Figure 5.5 have less obvious spectral features and overlapping of component bands. The characteristic CH_2 stretching bands of stearate at 2924 and 2852 cm^{-1} are observed in some of the mineral-type foundations, M4.x and M6.x. The mineral-based sample spectra display major difference in the 1100 to 450 cm^{-1} compared to the traditional-based samples and lack of C=O bond at 1466 cm^{-1}. The mineral-based foundations feature absorbance characteristic of mica near 1000, 570 and 430 cm^{-1}. There are clear differences between the sample manufacturers. There are differences in spectra in the 840 to 560 cm^{-1} region. Figure 5.6 shows the comparison of MIR spectra of mineral-based samples for each manufacturer. It should be noted that samples produced from the same manufacturer gave very similar spectra and one

sample from each manufacturer is used as an example. The region from 1200 to 400 cm^{-1} displays spectral differences between samples due to mica. Samples M3.x exhibit bands at 1058 and 980 cm^{-1} and at 548 and 482 cm^{-1}, like those in the MIR spectra of pearl mica. In contrast, samples M2.x, M4.x, M6.x and M7.x display bands characteristic of sericite mica at 1004 and 914 cm^{-1} and then at 530 and 470 cm^{-1}. This indicates that the form of mica used may differ between manufacturers.

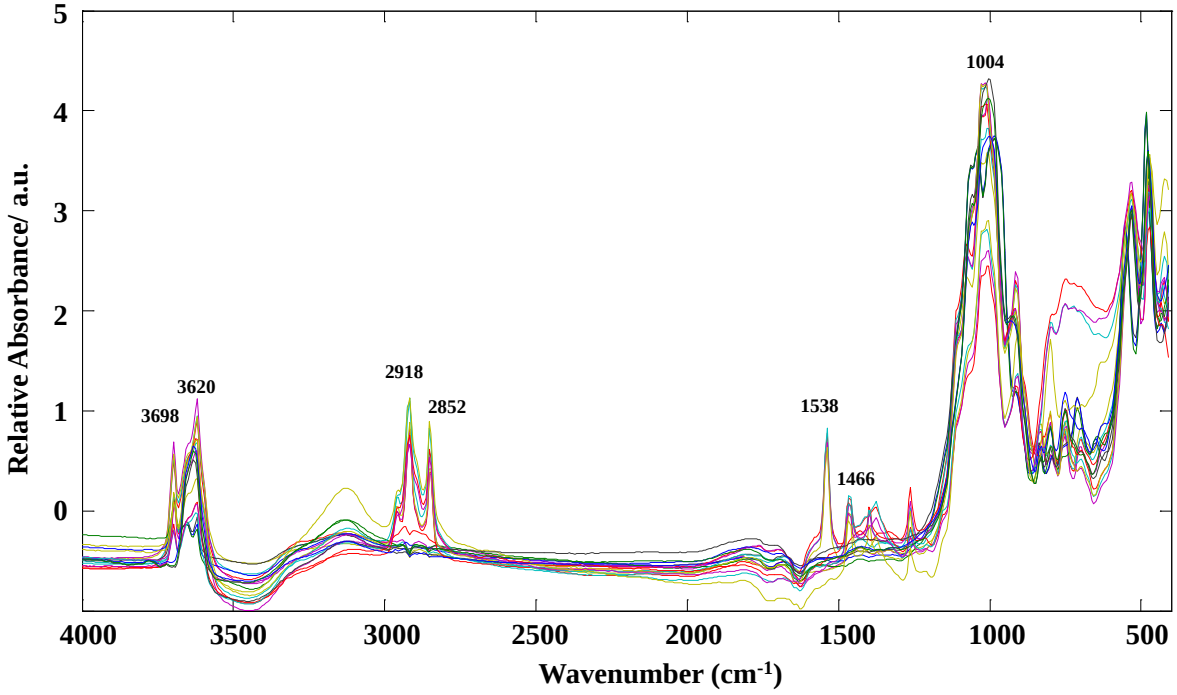

Figure 5.5 FTIR spectra of the 18 mineral-based foundation formulations recorded in the mid-infrared region.

Samples M6.x differs from the other mineral samples. M6.4 exhibits a band near 800 cm^{-1} that is not visible in the other samples from M6.x. These samples display a broad band near 750 cm^{-1}, seen in Figure 5.5. The MIR spectra of magnesium stearate features a band near 722 cm^{-1} but it is not clear whether it is responsible for the band present in samples M6.x.

Differences in spectral features between samples occur in the 4000 to 1200 cm^{-1} region. Samples from M4.x and M6.x exhibit bands near 2900 cm^{-1}, typical of CH_2 bands of stearate. Samples M4.x contain a sharp band at 1538 cm^{-1} and another at 1466 cm^{-1}. However, the band at 1538 cm^{-1} is absent in the spectra of samples M6.x. This indicates samples M4.x contain zinc stearate and samples M6.x contain another form of stearate. The presence of stearate in these samples is supported by XRD analysis and differences can be seen in their diffraction patterns. Both M4.x and M6.x show diffraction peaks at 21.3° but only samples M4.x have visible peaks at 3°, indicating differences in the form of stearate used between manufacturers.

Samples M7.x exhibit a broad band at 3620 cm^{-1}, that is similar to a band visible in the spectra of pearl mica. However, it does not display other spectral features of pearl mica in the 1200 to 400 cm^{-1} region.

Due to the complexity of the sample mixtures, not all spectral features could be identified visually because of band overlap.

Iron oxides, titanium dioxide, zinc oxide and bismuth oxychloride could not be identified visually, as characteristic features of these materials could not be seen within samples. Principal component analysis was employed to further investigate the components present in the foundation samples and the differences between samples.

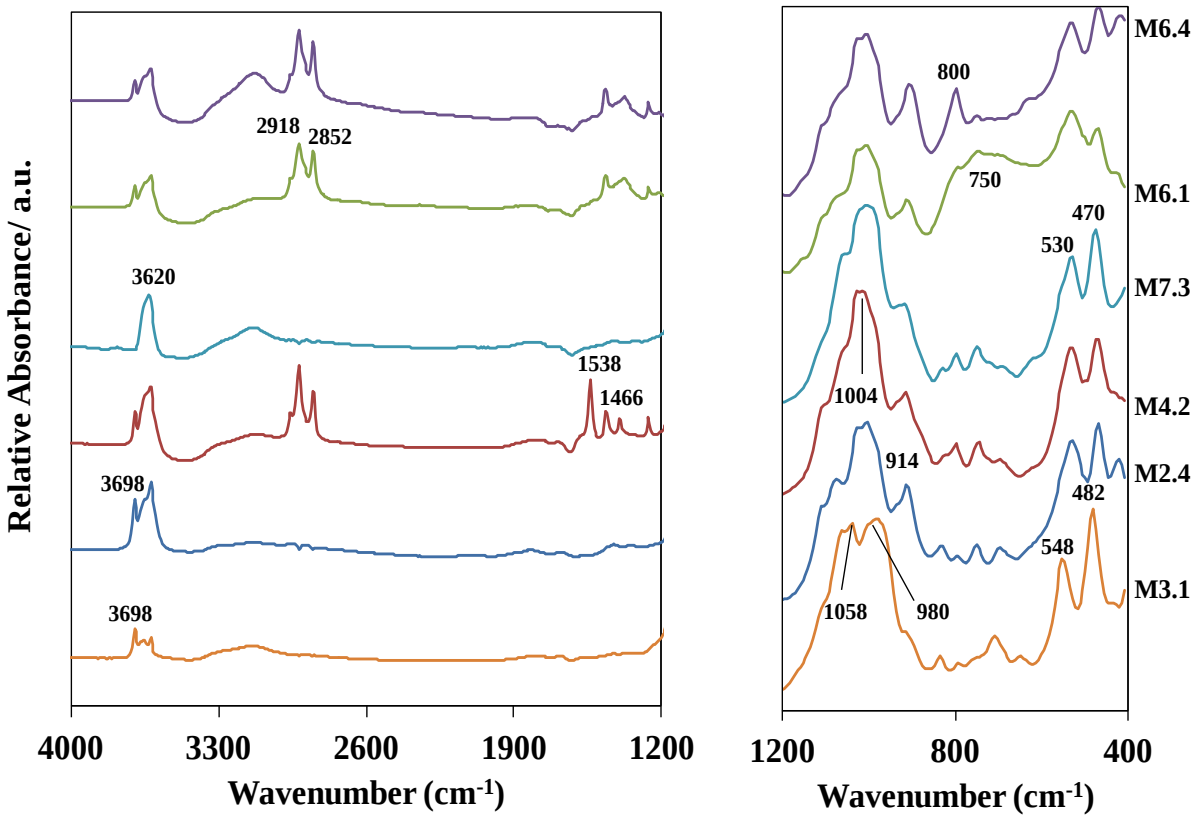

Figure 5.6 Comparison of MIR spectra of mineral-based samples from each manufacturer.

5.3.3 PCA of DRIFT spectra in the mid-infrared region

Principal component analysis was applied to 39 (samples) x 599 (absorbance at each wavelength) spectral data, scatter corrected by SNV. A plot of principal components and the variance of PCA scores (percentage of total variance) and the cumulative variance can be seen in Figure 5.7. The variances retained by PC1, PC2 and PC3 account for only 83% of the total variance contained in the spectral data. This value indicates that the first 3 PC's are not sufficient in providing enough information to describe the distribution of the samples, and additional PC's must be investigated. The first nine principal components accounted for near 98% of the spectral variance, however PC's with small variance may only reflect noise in the data. Therefore, the first 6 PC's accounting for 95% of variance will be considered.

A scores plot of the first two PCs is shown in Figure 5.8(a). Once again, there is a clear distinction between the mineral-based and the traditional-based formulations, with samples M1.x and M5.x consistently grouping with the traditional samples. The separation occurs mainly along the PC1 axis, and can be interpreted by the factor loading plot of Figure 5.8(b). The factor loadings show separation along PC1 is due to bands between 2900-2800 cm^{-1} and a band at 1466 cm^{-1} representative of stearate and calcium carbonate respectively.

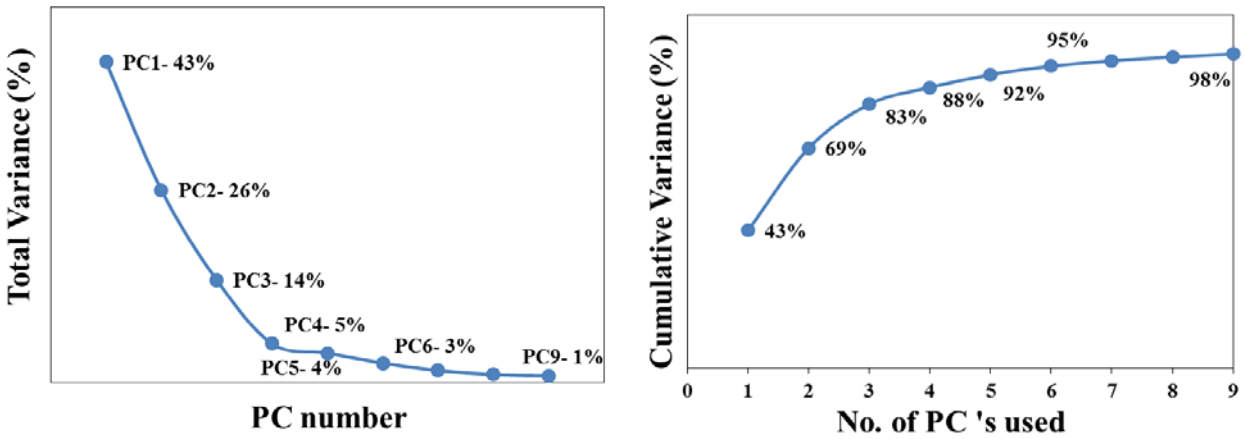

Figure 5.7 Scree plot of variance of PCA scores (percentage of total variance) of MIR spectral data for 39 cosmetic foundation samples.

Like PCA results from XRF and XRD data, separation of mineral and traditional-based samples is due to the presence of talc and calcium carbonate. Grouping of samples in the positive PC2 region is due to talc (distinct bands near 1022, 668 and 452 cm^{-1}), calcium carbonate in the positive PC1 region (absorbance band near 1466 cm^{-1}), and mica in the negative PC1 region. Samples T4.x, T2.3 and T8.2 have consistently grouped due to calcium carbonate. Samples M6.x is grouped away from the other mineral foundation samples. A band near 752 cm^{-1} seems to be responsible for the separation. The spectra of M6.x have a region that reflects the MIR spectra of titanium dioxide. XRF analysis found significant amounts of titanium in these samples and XRD analysis also displays titanium dioxide diffraction peaks in these patterns.

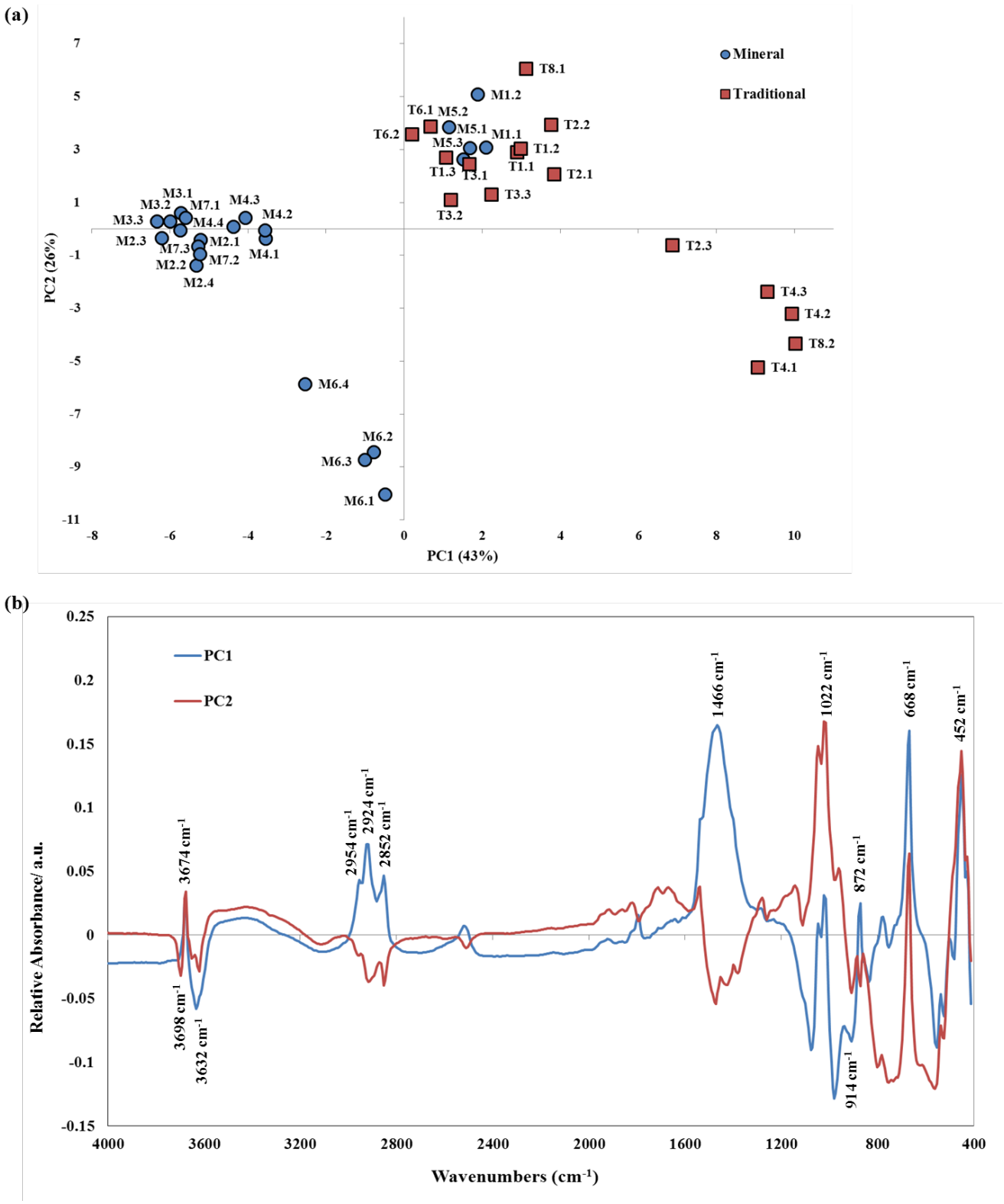

Figure 5.8 The scores plot (a) and the loadings plot (b) associated with PC1 and PC2 from principal component analysis of data obtained through diffuse reflectance spectroscopy in the mid-infrared region of the 39 foundation samples.

It cannot be confirmed that titanium dioxide is the cause of separation and further investigation of PC's is required. Sericite bands occur near 3698, 1010, 914, 530 and 470 cm^{-1} and in the 850 to 600 cm^{-1} region but not all are distinguishable due to overlap with other components such as kaolin and talc. Sericite mica is separating samples in the negative region of the PC1 axis. These samples have higher mica content but are not reflected by the loadings plot. There is no separation of samples M2.x, M3.x, M4.x and M7.x and differences may be apparent in other PC scores and loadings. Interpretation of MIR spectra of samples revealed that mineral-based samples M4.x and M6.x contain a form of stearate, however these samples grouping in the positive PC1 region.

Further information can be provided in PC1 and PC3, shown in scores and loadings plot of Figure 5.9. The scores plot (Figure 5.9(a)) shows grouping of samples due to calcium carbonate along the PC1 axis and talc along the PC3 axis. Samples M6.x is separated along the PC3 axis with a majority of the traditional-based formulations that contain talc. Absorbance bands for talc can be found at 3674, 1022, 668 and 452 cm^{-1} shown in the loadings plot of Figure 5.9(b). The loadings plot shows the absorbance bands near 3674 and 1022 cm^{-1} to have loadings close to zero in PC1 and PC3. However, the bands near 668 and 452 cm^{-1} have positive loadings in the PC1 and PC3 region. This indicates that overlapping of components is occurring and a component other than talc has caused samples M6.x to cluster with the group of traditional-based samples. Once again, stearate seems to have little effect on the separation of samples and there is little separation between mineral-based samples and PCA was undertaken on mineral-based formulas separately. In Figure 5.10(a) the samples identified as belonging to the mineral-type have been investigated by PCA. The associated loadings plot of Figure 5.10(b) show the separation is due to the presence of pearl mica, sericite mica and a form of stearate in the samples. The absorbance bands that appear

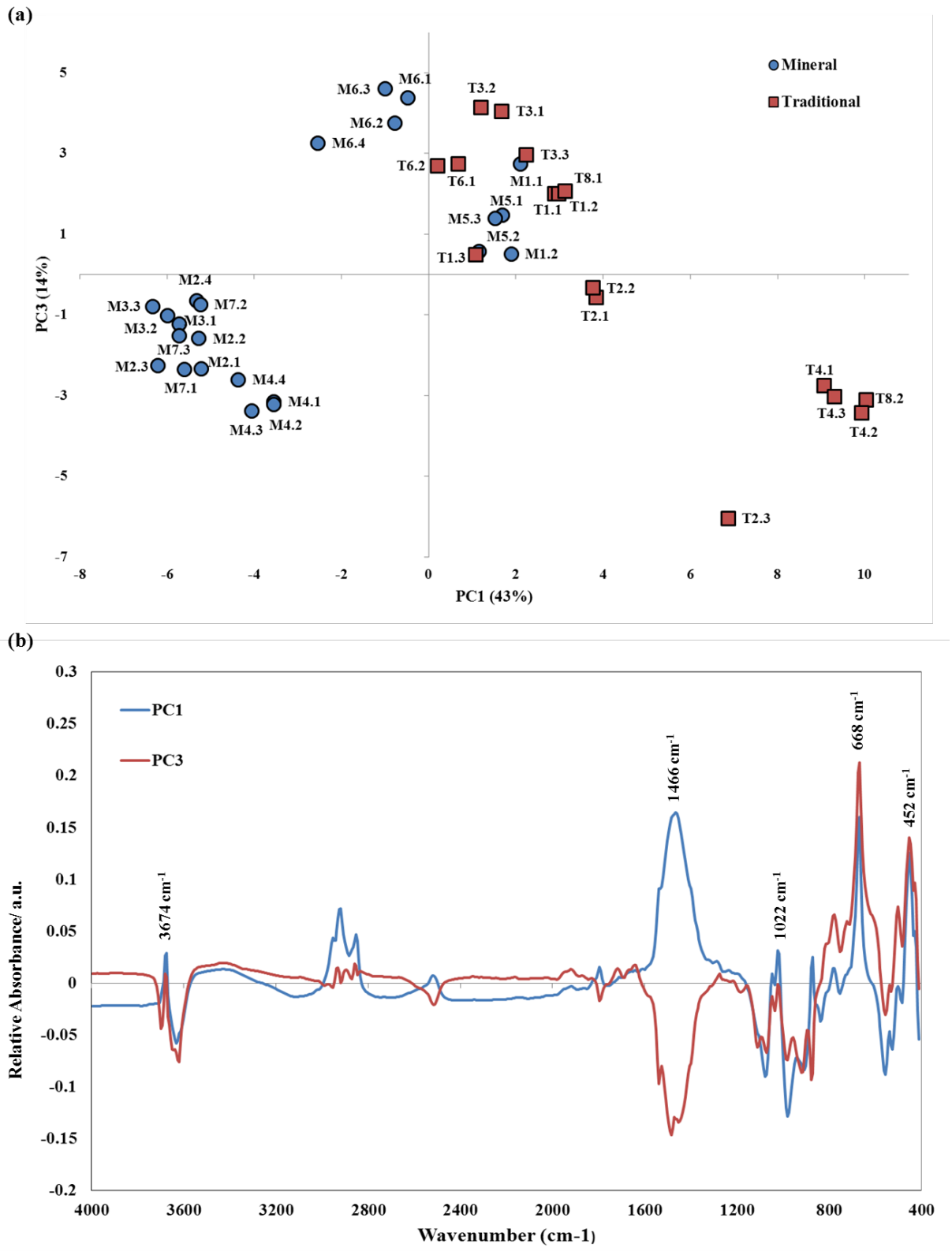

Figure 5.9 The scores plot (a) and the loadings plot (b) associated with PC1 and PC3 from principal component analysis of data obtained through diffuse reflectance spectroscopy in the mid-infrared region of the 39 foundation samples.

near 3698 and 3626 cm^{-1} are characteristic of bands that occur in this region in the DRIFT spectrum of sericite mica. Sericite mica is separating samples M2.x and M4.x along the negative axis of PC2. Samples M3.x are grouping in the positive PC2 region, which seems to be defined by the presence of pearl mica in these samples. Bands occurring in the loadings plot near 1058 and 986 cm^{-1}, resemble those in the DRIFT spectrum of pearl mica. Samples M7.x is grouping in the positive PC2 region but close to zero as it has characteristic spectral features from both pearl and sericite mica. There is an identifiable difference of separation of samples M6.x from the other mineral-based formulas. These samples are grouping to the left in the negative PC1 region, it is assumed due to a form of stearate, either magnesium or zinc. This is visible from the CH_2 stretching in the loadings plot at 2924 and 2852 cm^{-1}. However, samples M4.x were found to contain stearate and it would be expected that these samples would group with M6.x, but this is not the case. It is clear that another component is separating samples M6.x towards the positive PC2 region. The bands at 722 cm^{-1} are influencing samples M6.x to be grouping in the positive PC2 region, which could be due to titanium dioxide, however due to band overlap it is too difficult to identify the component responsible.

Further investigation of PCA with all 39 cosmetic foundations was undertaken to try to identify the distinct separation of samples M6.x. Figure 5.11 displays samples projected across PC3 and PC4 with the associated loadings vectors. The score plot in Figure 5.11(a) shows that samples are not distinctly separating based on foundation-type but still grouping according to manufacturer. Separation is occurring across PC3 axis due to talc in the positive PC3 region and $CaCO_3$ in the negative PC3 region. Once again samples high in calcium carbonate, MT2.3, M4.x and T8.2 are grouping together and M1.x and M5.x with other traditional-based formulas with high talc content. The effect of PC4 of samples is causing separation in the positive PC4 region due to stearate (bands at 2918, 2846 and 1538 cm^{-1}) and

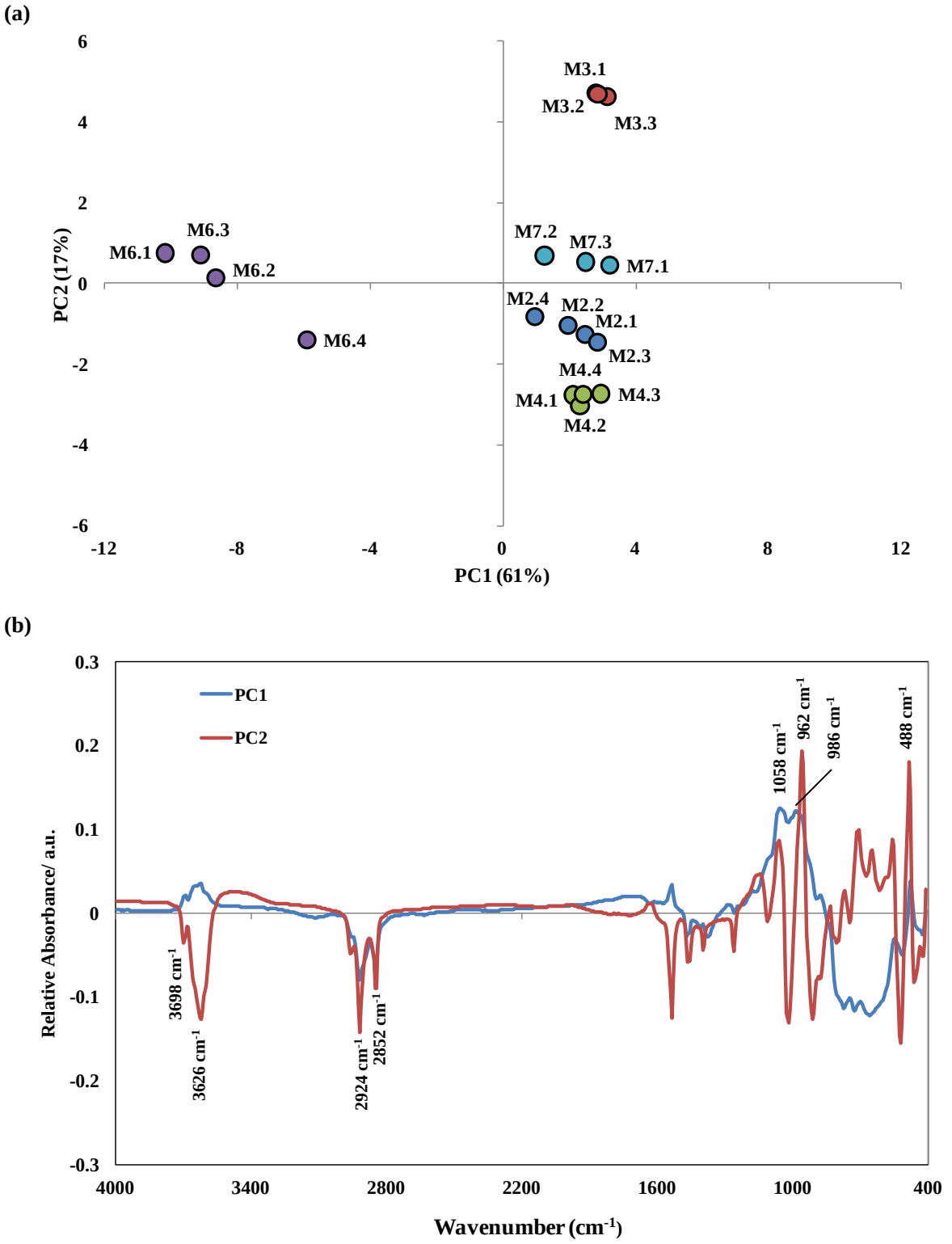

Figure 5.10 The scores plot (a) and the loadings plot (b) associated with PC1 and PC2 from principal component analysis of data obtained through diffuse reflectance spectroscopy in the mid-infrared region of the 18 mineral-based samples.

sericite mica due to bands at 3620, 914 and 524 cm^{-1}. There is a distinct separation of the mineral-based samples M2.x, M3.x, M4.x and M7.x, and depends on the form of mica present. Those samples that contain pearl mica, e.g. M3.x are grouping in the negative PC4 region due to pearl mica bands at 962 and 488 cm^{-1}. While samples M2.x and M4.x are grouping in the positive PC4 region due to sericite bands at 3620, 914 and 524 cm^{-1}. Samples M7.x is once again grouping in between as its MIR spectra displays characteristics from both pearl and sericite mica. Samples M4.x and M6.x are not grouping even though they both contain stearate. Comparison of their MIR spectra reveals M4.x contains a higher amount of sericite mica than samples M6.x. Unlike samples M4.x, M6.x have no band at 1538 cm^{-1} representative of zinc stearate, which indicates M6.x could contain another form of stearate. The band at 1538 cm^{-1} is grouping samples M4.x to the top left along the PC3 axis. This explains the separation based on the type of stearate but another component is grouping samples M6.x in the positive PC3 region. A band near 750 cm^{-1} in the loadings plot could be responsible for the grouping of M6.x, which once again could be due to titanium dioxide.

Principal components 5 and 6 were investigated but did not reveal any new trends and loadings began to reflect noise within data. Principal component analysis results successfully separated samples based on the manufacturer and the components present. However, the interpretation on which components were causing the separation in each case was not as clear as PCA results of XRF and XRD data, as overlapping bands of components caused confusion. It is assumed that samples M6.x were separating due to titanium dioxide but MIR analysis did not provide enough evidence to support this.

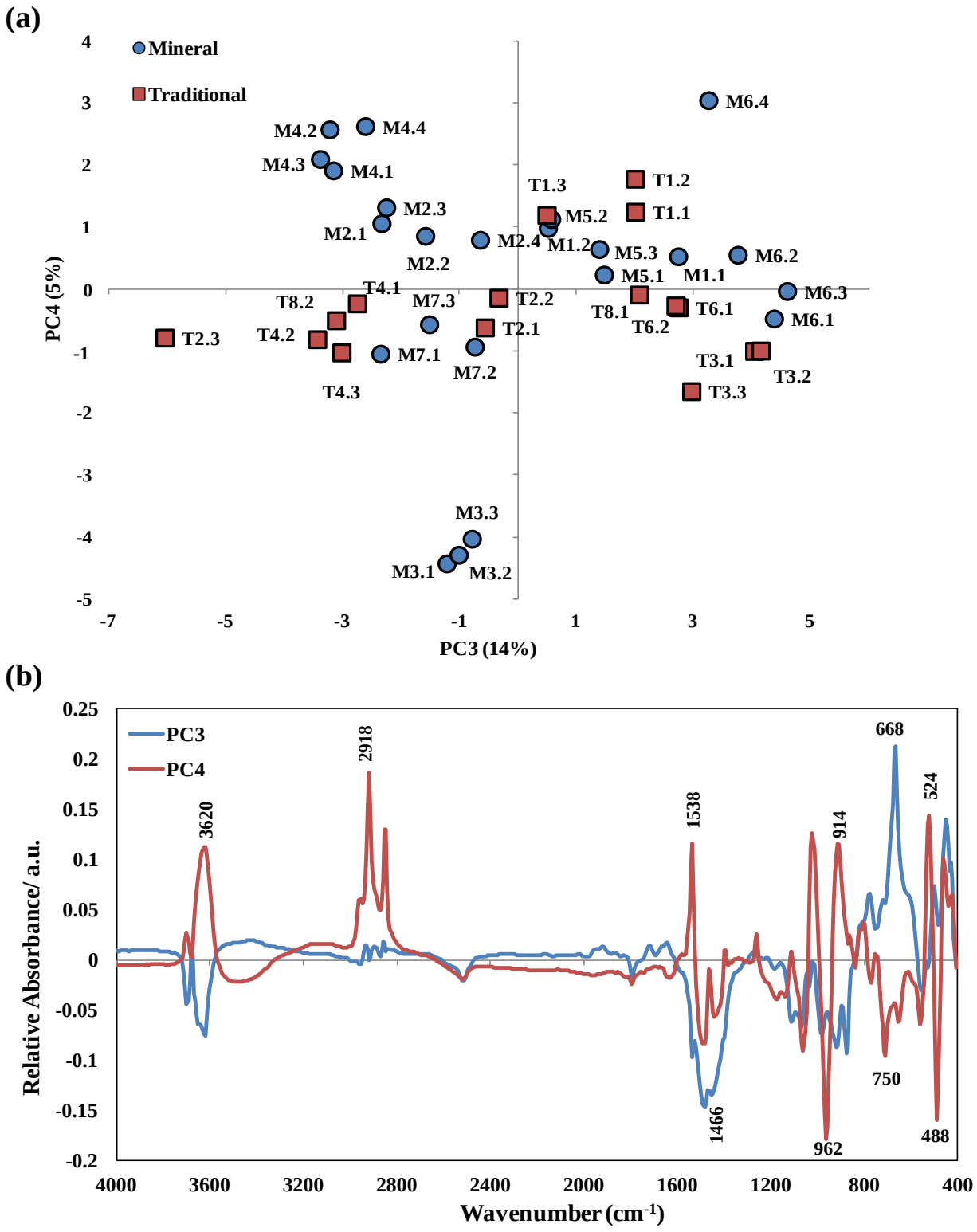

Figure 5.11 The scores plot (a) and the loadings plot (b) associated with PC3 and PC4 from principal component analysis of data obtained through diffuse reflectance spectroscopy in the mid-infrared region of the 39 foundation samples.

5.3.4 Covariance and correlation (MIR and XRD)

XRD phase data were correlated with MIR spectral data to aid interpretation and to confirm the presence of the material components in powder foundation samples. This method uses the correlation coefficient to estimate the degree of similarity between variables, in this case, XRD peak intensities and MIR absorbance bands.

A 2D covariance matrix was produced with MIR spectral data and XRD phase data for all samples given by,

$$\mathbf{\Phi} = \mathrm{MIR}^{T}.\mathrm{XRD} \qquad \text{(Equation 5.2)}$$

where MIR and XRD are the mean-centred data matrices obtained from diffuse reflectance spectra data (39 x 599) in the mid-infrared region and diffraction data (39 x 783) respectively. Figure 5.12 shows a 2D covariance contour map of MIR vs. XRD, in which positive and negative correlations are displayed. The red colour indicates a positive correlation of XRD component peaks with absorption bands of the MIR spectral data. A positive correlation indicates that XRD diffraction peak intensities and MIR absorbance bands are changing simultaneously. The covariance map shows positive correlations for the diffraction peaks of mica and talc with the characteristic absorbance bands of these components.

Two-dimensional correlation was employed to aid in the interpretation of the 2D map. A correlation slice of each component was taken from the XRD data at a selected 2θ with the highest peak intensity across mineral-based samples. For example, the diffraction pattern of sericite mica displays a characteristic diffraction peak at 26.6°. The correlation slice for sericite mica was taken at this angle. The correlation slice for each component was then cross-correlated with

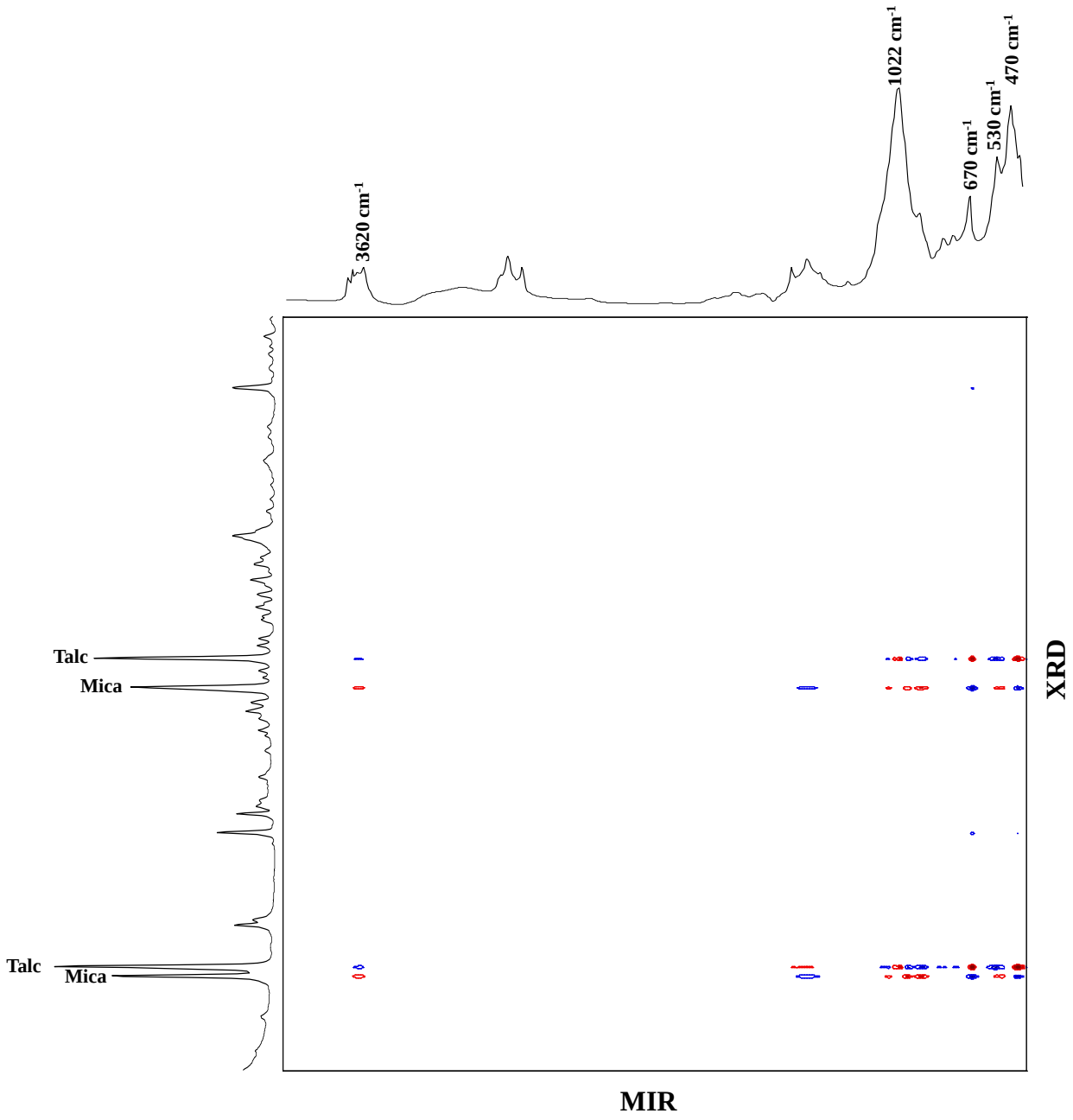

Figure5. 12 The covariance contour plot of MIR vs. XRD. An average spectrum of each technique is presented along each axis to aid in interpretation, showing positive (red) and negative (blue) correlations of XRD component diffraction peaks with MIR spectral bands of all foundation samples.

the entire MIR spectral data set to determine correlation coefficients to 2θ diffraction peaks that correlated with the absorbance bands. Iron oxides were not selected for this study as their

analysis using XRD produced such poor results due to the Cu Kα source. Two-dimensional correlation of MIR and XRD data was first undertaken across the whole sample set. As with the study of correlation with XRF and XRD data, the correlation method worked more successfully with the mineral-based formulations due to the similarity of components between manufacturers.

However, correlation coefficients using all samples produced for talc and calcium carbonate were higher than 0.8. Other components produced poor results. The covariance slices for talc (slice taken at 9.44°) and calcium carbonate (slice taken at 29.42°) are shown in Figure 5.13. It is clear that the 2θ peak positions of talc and calcium carbonate have highly correlated with the absorbance bands present in the reference spectra. The covariance slice of talc, displayed in Figure 5.13(a), produced correlation coefficients of 0.8 and 0.86, with absorption bands at 668 and 452 cm^{-1} respectively. These are consistent with absorption bands recorded in the reference spectra of talc. The correlation of the calcium carbonate diffracted peak resulted in a correlation coefficient value 0.81 with the strong broad characteristic band of calcium carbonate at 1466 cm^{-1}.

Two-dimensional correlation was investigated with mineral-based sample data to see whether higher correlation coefficients could be produced for other components present in cosmetic foundations.

A 2D covariance matrix was produced with MIR spectral data and XRD phase data for mineral-based samples given by,

$$\mathbf{\Phi} = \text{MIR(mineral)}^{T}.\text{XRD(mineral)} \qquad \text{(Equation 5.3)}$$

where MIR and XRD are the mean-centred data matrices obtained from diffuse reflectance spectra data (18 x 599) in the mid-infrared region and diffraction data (18 x 783) respectively.

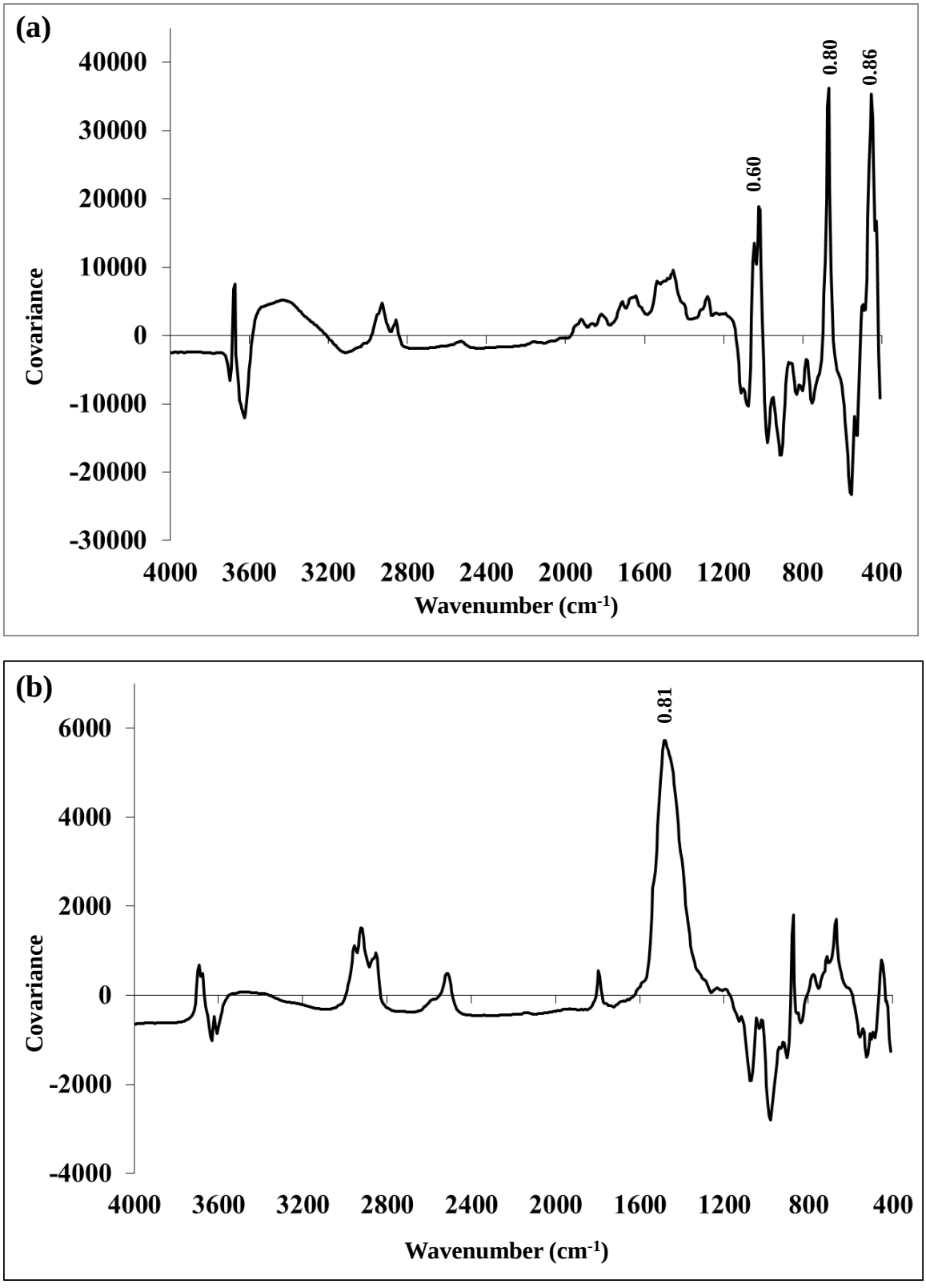

Figure 5.13 Covariance slices obtained from correlation of MIR and XRD data. The correlation coefficients relating to correlation of (a) Talc & (b) CaCO3 diffraction peaks with MIR spectral data of all samples.

Samples M1.x and M5.x were not included in this correlation study. Figure 5.14 shows a 2D covariance contour map of MIR vs. XRD, in which only positive correlations are displayed. The red colour indicates a positive correlation of XRD component peaks with absorption bands of the MIR spectral data. However, the 2D map is much more complex than in comparison to Figure 5.12 and is difficult to interpret by eye.

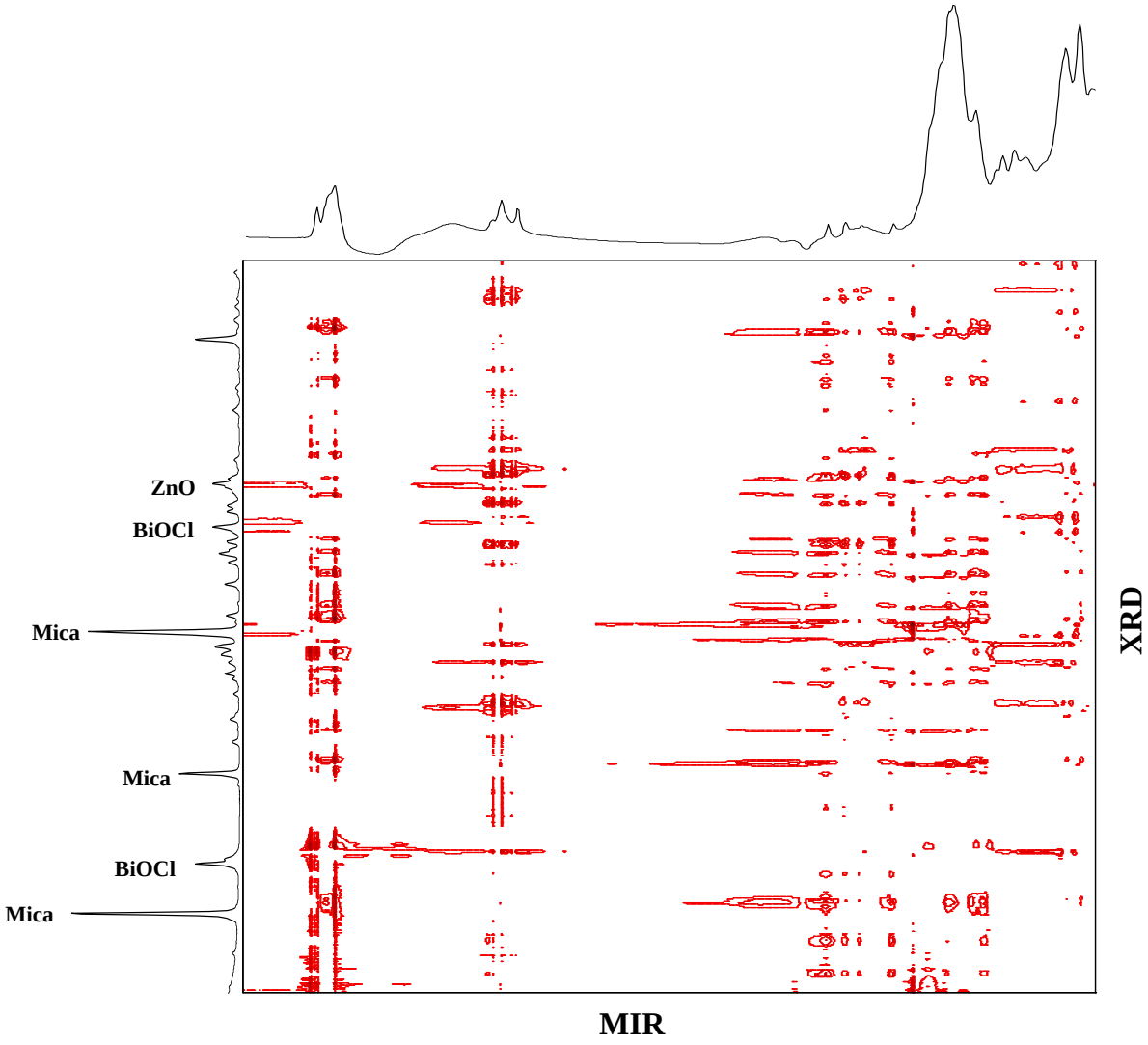

Figure 5.14 The covariance contour plot of MIR vs. XRD of mineral-based formulations. An average spectrum of each technique is presented along each axis to aid in interpretation, showing positive correlation of XRD diffraction peaks with MIR absorbance bands.

Two-dimensional correlation was employed to aid in the interpretation of the 2D map. The correlation coefficients of kaolin, pearl mica and sericite mica, with slices taken at 12.32°, 26.72° and 26.9° respectively are shown in Figure 5.15. It is clear that the 2θ peak positions of each component that have highly correlated with bands in the MIR data, match with the absorbance bands present in the reference component spectra. Kaolin, pearl mica and sericite mica returned correlation coefficients values close to 1. The diffraction peak of kaolin produced correlation coefficients ranging from 0.93 to 0.60, with absorbance bands found in its reference spectra.

Correlation of magnesium diffraction peak at 21.3° returned poor correlation values with MIR data. XRD analysis of magnesium stearate may have produced diffraction peaks that were too minor and insignificant to show differences between samples that have stearate present and those that did not, hence why poor correlation coefficient values were produced. The diffraction peaks for pearl and sericite mica matched consistently with most of the absorbance bands found in the reference spectra, with correlation coefficients ranging from 0.8 to 0.95.

2D correlation was successful in confirming absorbance in MIR spectral data using the mineral-based sample set. There was overlap of bands in the 400 to 1000cm^{-1} region which made interpretation particularly difficult. Mica and talc both exhibit Si-O absorbance bands in this region and when the mineral and traditional-based samples are combined for analysis, it is hard to determine which components are responsible with each absorbance band.

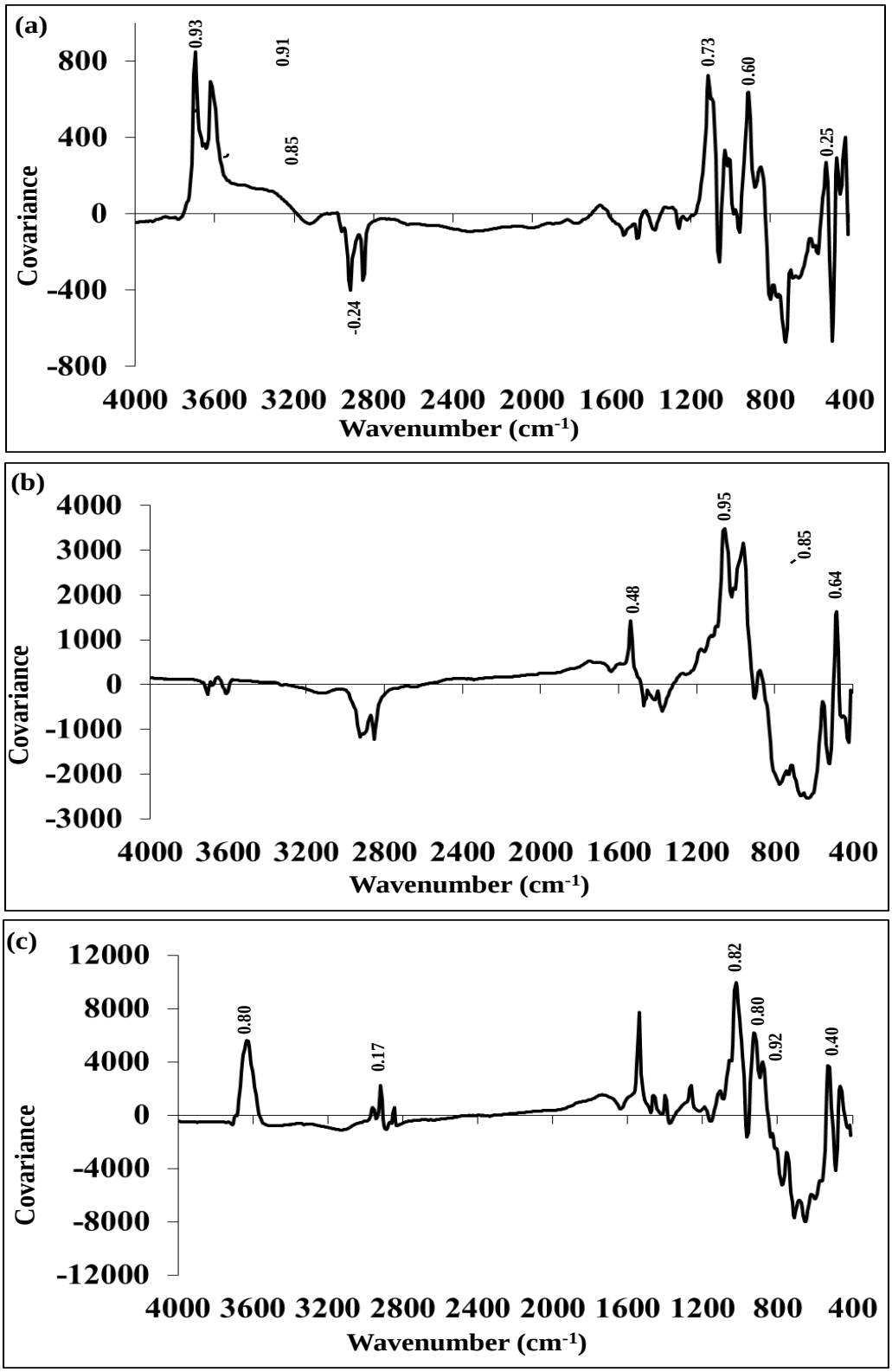

Figure 5.15 Covariance slices obtained from correlation of MIR and XRD data. The correlation coefficients relating to correlation of (a) Kaolin (b) Pearl Mica & (c) Sericite Mica diffraction peaks with MIR spectral data of mineral-based samples.

Eliminating the traditional-based samples, eliminated the presence of talc and hence highlighted absorbance bands representing mica. There is a possibility of overlapping of bands due to kaolin and mica in the 400 to 800 cm^{-1} region which have produced low correlation coefficient values. However, the method was still successful in finding a relationship between the two techniques and highlighted the range of components present in the mineral-based samples.

5.3.5 Spectral Analysis of Reference Materials in the Near-Infrared Region

Diffuse reflectance infrared fourier transform spectra in the mid-infrared region of some mineral components are presented in Figures 5.16. The DRIFT spectra of the cosmetic grade iron oxides were not analysed as the spectra were too noisy, and hence will not be discussed in this section.

Kaolin displays absorbance bands in the 4000 and 7000 cm^{-1} region due to the first overtone region near 7170, 7152, 7116 and 7068cm^{-1} corresponding to the outer and inner surface hydroxyl groups [29]. Bands at 4620 and 4530 cm^{-1} are assumed to be combination bands due to the addition of the inner hydroxyl stretching and the Si-O stretching [30]. The NIR spectrum of calcium carbonate did not exhibit any characteristic bands or features. Talc spectrum shows a sharp characteristic peak around 7188 cm^{-1} corresponding to the first overtone OH stretching [17]. The most notable feature of the IR spectra of pearl and sericite mica are the bands observed near 4530 cm^{-1} due to the Al-OH groups present in the structure of mica [20]. Magnesium stearate exhibits a strong absorbance observed near 5780 cm^{-1}, corresponding to the first overtone of CH_2 stretching, while the band near 4340 cm^{-1} is observed due to combinations of CH_2 stretching frequencies [31].

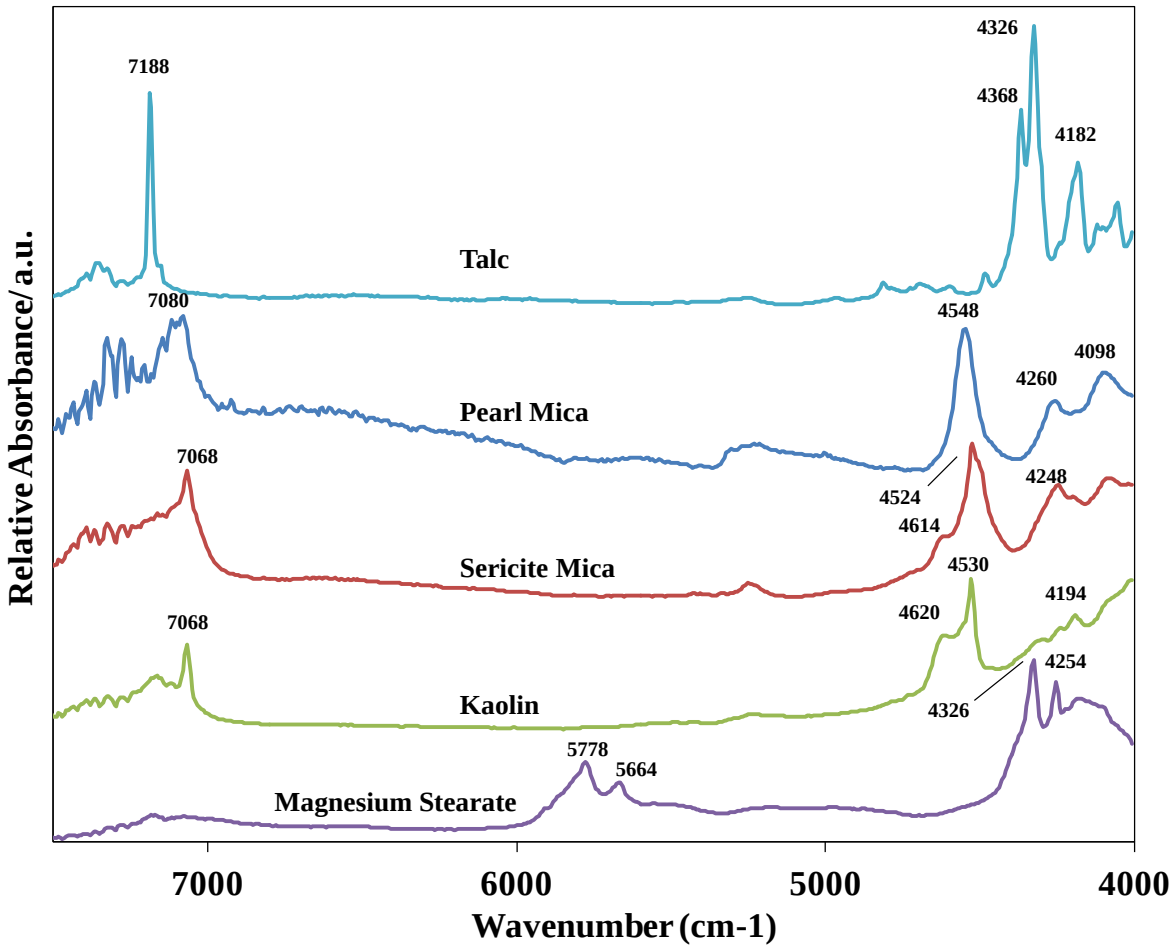

Figure 5.16 DRIFT spectra of mineral components used in production of cosmetic foundation powders in the near-infrared region.

The NIR spectra of titanium dioxide, bismuth oxychloride and zinc oxide displayed no significant characteristic features.

5.3.6 Comparison of Spectral Data in the near-infrared region using reference materials

The DRIFT spectra of, SNV corrected, mineral and traditional-based foundation powders in the near-infrared region (4000-7200 cm^{-1}) are presented in Figure 5.17 and 5.18. There are visible differences between the mineral and traditional foundation types, as well as by manufacturer. The spectra of traditional foundation samples (Figure 5.17) contain a sharp absorbance band characteristic of talc at 7180cm^{-1}. The traditional samples also display two

sharp bands at 4368 and 4326 cm^{-1} that mimic those recorded in the reference spectra of talc. Sample T2.3 shows a band near 4550 cm^{-1}, resembling a band in the reference spectra of pearl mica. There are notable differences between spectra of the two foundation types in the 4600 to 4000 cm^{-1} region. The mineral-based samples (Figure 5.18) contain a strong Al-OH group band found in mica at 4530 cm^{-1}. There is little visible difference between the spectra of the traditional samples. On closer inspection of the mineral-type samples, it is clear a form of stearate is present in samples M6.x. These samples exhibit an absorbance bands near 4320 and 5770 cm^{-1}, characteristic of the CH_2 stretching found in the reference spectra of magnesium stearate. This is seen more clearly in Figure 5.19, highlighting spectral differences between manufacturers M2.x, M3.x, M4.x, M6.x and M7.x. Samples M4.x also

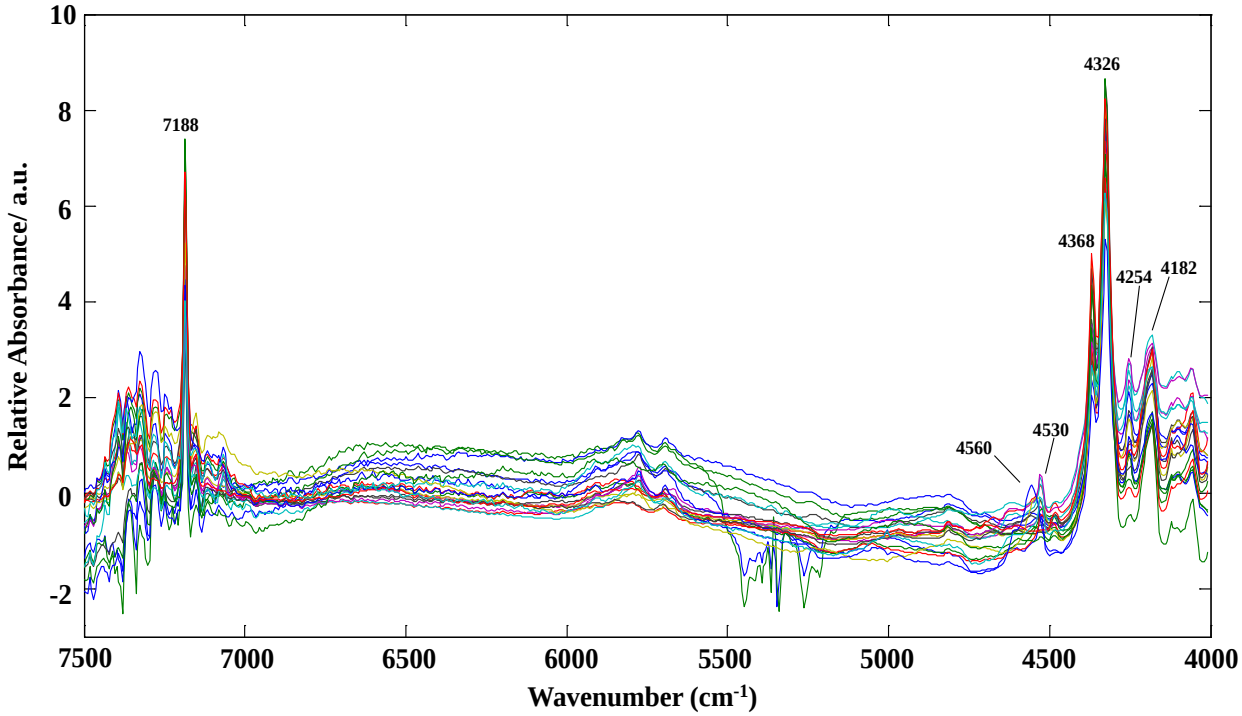

Figure 5.17 FTIR of the 21 traditional-based foundation formulations recorded in the near-infrared region.

exhibit characteristics of stearate, with bands observed near 4326 and 4254 cm^{-1} but not near 5772 cm^{-1}. Like the MIR spectra of M6.x, the NIR spectra of these samples displays bands at 4188 and 4098 cm^{-1} which are not present in the other true-mineral formulations. This could be due to titanium dioxide, however analysis of reference materials by NIR could not confirm this. Samples M2.x display a bands near 7068, 4524 and 4248 cm^{-1}, characteristic of bands found in the reference spectra of sericite mica. Whereas, M7.x shows a band at 4548cm^{-1}, characteristic of pearl mica. Mid-infrared spectra of M4.x clearly indicated the presence of sericite mica, however bands are not as clearly visible in the NIR spectra. This is also the case with M3.x, as pearl mica bands are not visible in the NIR spectra. Principal component analysis seeks to further investigate the components present in the foundation samples.

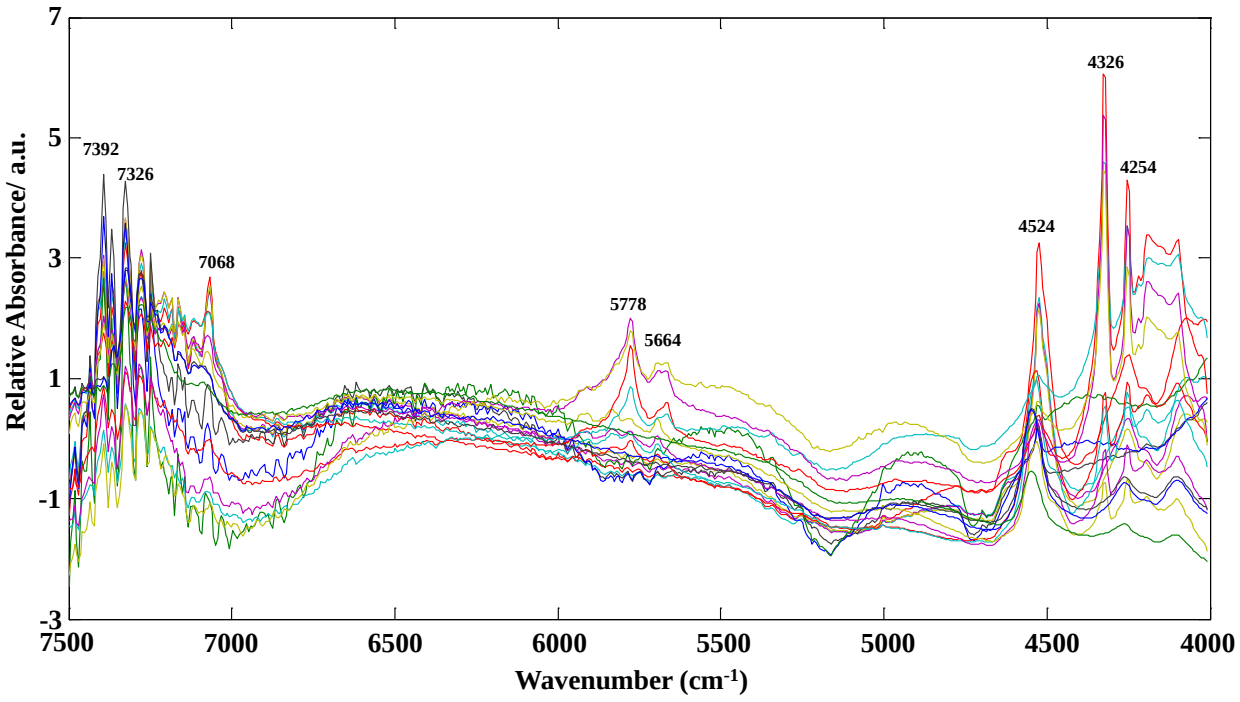

Figure 5.18 FTIR spectra of the 18 mineral-based foundation formulations recorded in the near-infrared region.

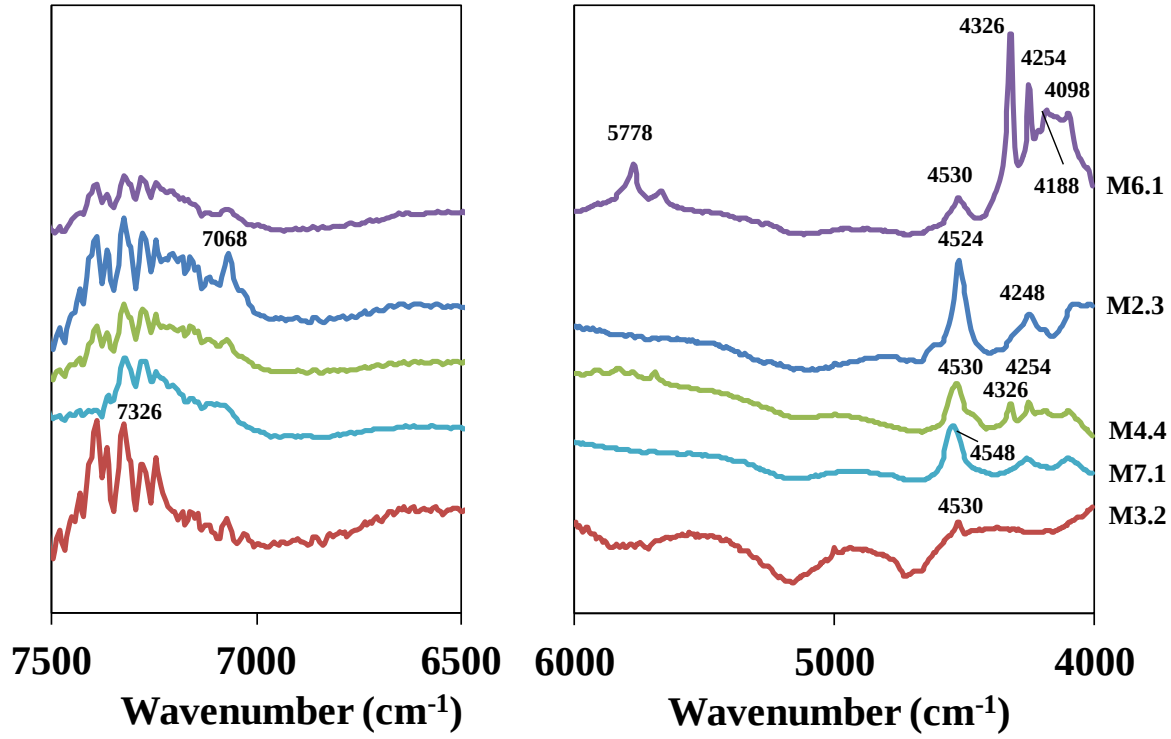

Figure 5.19 Comparison of NIR spectra of mineral-based samples from each manufacturer.

5.3.7 PCA of DRIFT spectra in the near-infrared region

Principal component analysis was applied to 39 (samples) x 533 (absorbance at each wavelength) spectral data, scatter corrected by SNV. Spectral data in the 7500 to 400cm^{-1} region was used as recorded spectra beyond this point was noisy and may have effected multivariate analysis results. A plot of principal components and the variance of PCA scores (percentage of total variance) and the cumulative variance can be seen in Figure 5.20. The variances retained by PC1, PC2 and PC3 account for only 85% of the total variance contained in the spectral data. This value indicates that the first 3 PC's are not sufficient in providing enough information to describe the distribution of the samples, and additional PC's must be investigated. The first nine principal components accounted for near 99% of the spectral variance, however PC's with small variance may only reflect noise in the data. Therefore, the first 6 PC's accounting for 96% of variance will be considered.

It must be noted that NIR analysis was unable to identify as many components as XRF, XRD and MIR, due to limitations of the technique and the high noise recorded. It was expected that separation of samples by PCA analysis would be due to very few components. The first three principal components contained approximately 85% of the spectral variance, with results summarized in Figures 5.21 and 5.22. A scores plot of the first two PCs is shown in Figure 5.22(a), accounting for 74% of the total variance contained in the spectral data. Once again, there is a clear distinction between the mineral-based and the traditional-based formulations, however, samples M1.x and M5.x are not grouping as closely with the traditional samples rather in comparison with XRF, XRD and MIR PCA results. As with MIR results samples M6.x are once again not grouping with the other mineral-based formulations.

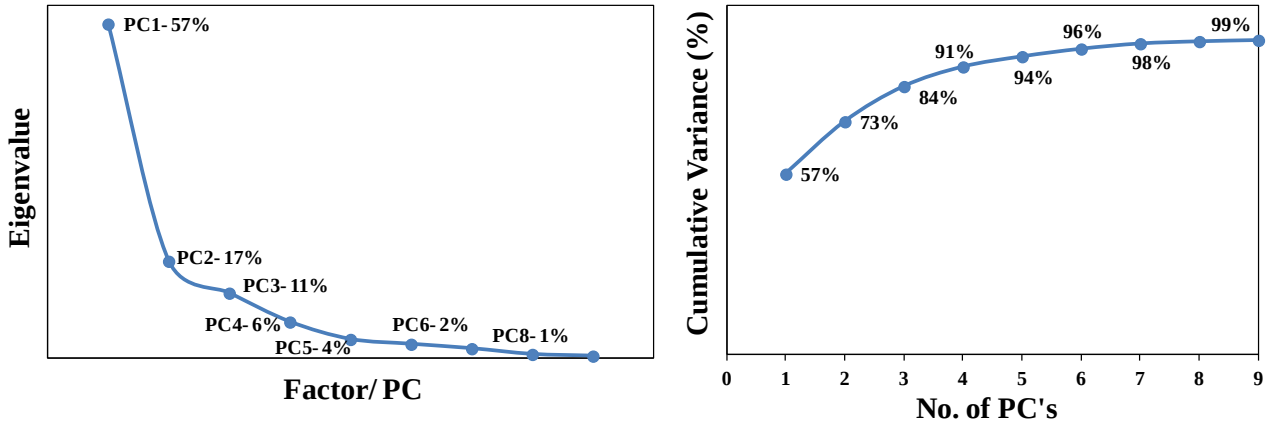

Figure 5.20 Scree plot of variance of PCA scores (percentage of total variance of NIR spectral data for 39 cosmetic foundation samples.

Separation occurs along the PC1 axis due to talc and mica, and can be interpreted by the factor loading plot of Figure 5.21(b). The NIR spectra of cosmetic grade components, previously discussed were used to aid in the interpretation of the loadings. The separation of mineral-based samples, M2.x, M3.x, M4.x and M7.x is due to an Al-OH stretching in mica at 4530 cm^{-1}. The traditional samples are grouping in the positive PC2 region and this is clearly due to the sharp band of OH group in talc at 7180 cm^{-1}. Other bands observed near 4368,

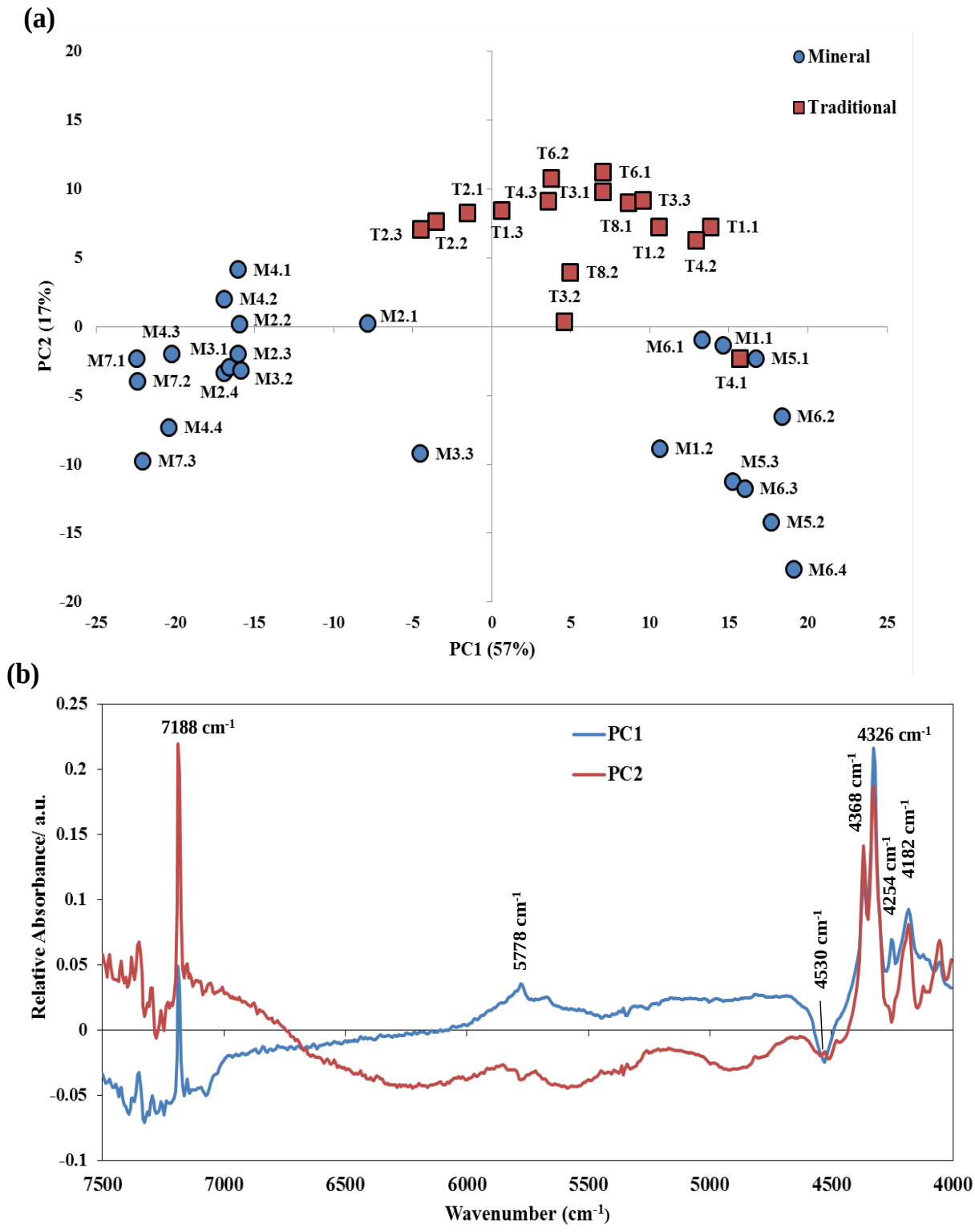

Figure 5.21 The scores plot (a) and the loadings plot (b) associated with PC1 and PC2 from PCA analysis of phase data obtained through diffuse reflectance spectroscopy in the near-infrared region of the 39 foundation samples.

4326 and 4182 cm^{-1} match those of the reference spectra of talc, shown in Figure 5.16. The loadings for the OH band at 7180 cm^{-1} is not distinctly positive in PC1 and PC2 as with bands at 4368, 4236 and 4182 cm^{-1} that are characteristic of talc. This indicates that scatter effects or noise may be influencing PCA results. The variation between individual sample NIR spectra may be large and SNV did not sufficiently correct for scatter effects. Samples M1.x, M5.x , M6.x and T4.1 seem to be grouping in the positive PC1 region due to bands at 5778 and 4257 cm^{-1} representative of stearate. It was expected that samples M1.x, M5.x and T4.1 would group closely with the remaining traditional samples due to the presence of talc. The presence of stearate is not a determining factor as it is also present in other traditional samples and does not explain the separation. Principal components 1 and 2 do not provide enough information.

The separation of the two foundation types is better illustrated in PC1 and PC3 shown in scores and loadings plot of Figure 5.22. Again we see samples M6.x grouping with traditional formulations but unlike PC1 versus PC2, samples M1.x, M5.x and T4.1 are grouping with traditional-based formulations. It is clear that the band at 4254 cm^{-1} is grouping these samples in the negative PC3 region, with the other traditional samples that also contain a form of stearate. Once again OH vibration of talc at 7180 cm^{-1}, is responsible for separation of traditional samples to the positive region of the PC1 and PC3 axis. Mineral-based samples are separating from traditional samples due to mica bands at 7068 and 4530 cm^{-1}. Principal component 1 vs principal component 3 shows the separation of samples M2.x, M3.x, M4.1 and M4.2 from M4.3, M4.3 and M7.x along the PC3 axis. It is assumed that mineral formulations would separate based on the form of mica present but noise in individual spectra seems to be the cause of the separation. Mid-infrared PCA results determined separation due to pearl mica in samples M3.x and M7.x and sericite in samples M2.x and M4.x.

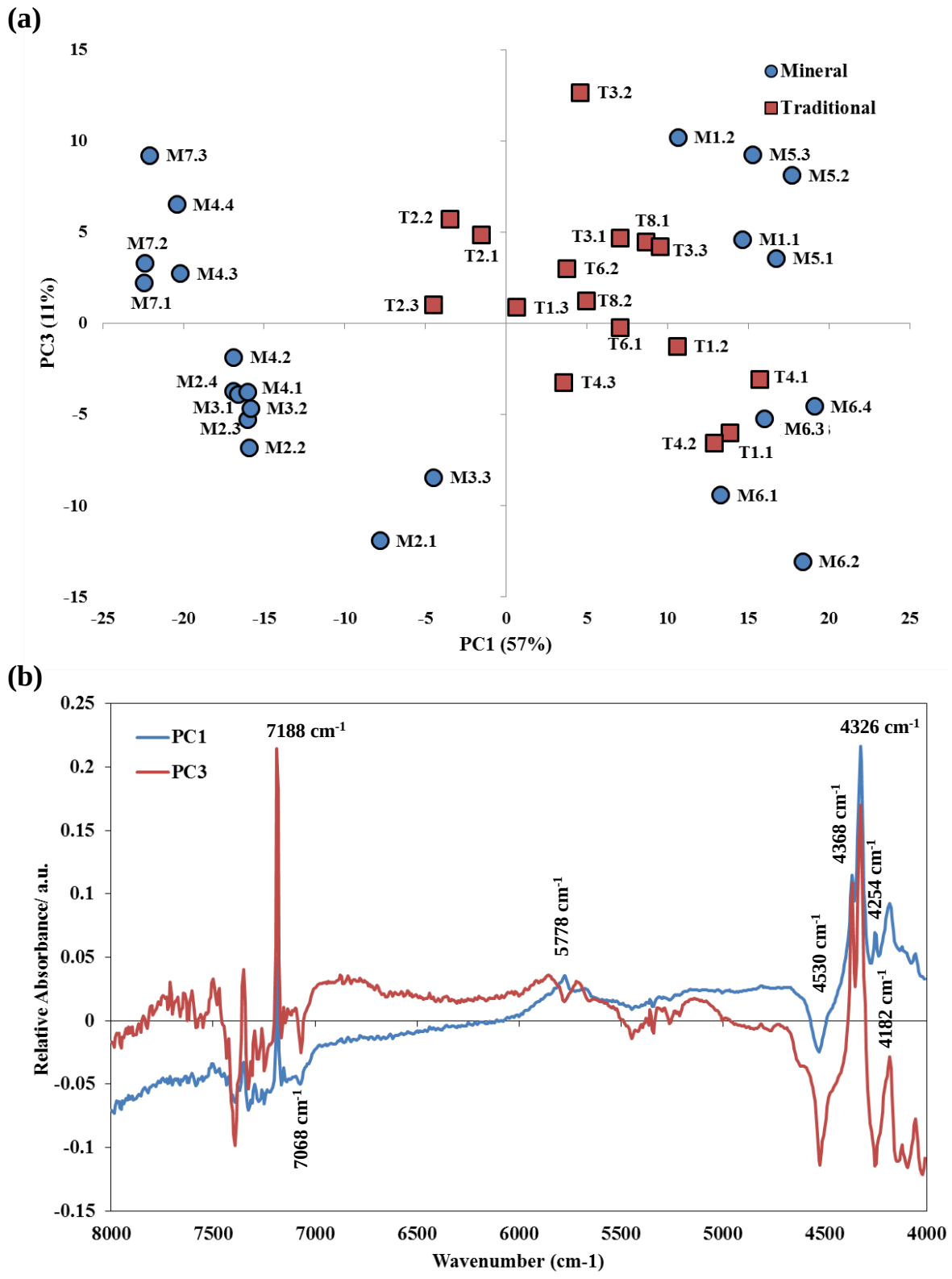

Figure 5.22 The scores plot (a) and the loadings plot (b) associated with PC1 and PC3 from PCA analysis of phase data obtained through diffuse reflectance spectroscopy in the near-infrared region of the 39 foundation samples.

Principal component 3 versus principal component 4 was investigated for further interpretation, with scores and loadings displayed in Figure 5.23. Mineral and traditional samples are grouping together. Talc bands at 7188 cm^{-1} are separating traditional samples positive PC3 region. Loadings show bands at 4368 and 4326 cm^{-1} in the positive PC3 region but are pulling samples into the negative PC4 region. While the band 4182 cm^{-1} has negative PC3 loadings. Because the loadings of talc are different across all bands, it is causing traditional-based samples to spread rather than group. Mineral-based samples are separating across PC4 due to sericite bands at 7068 and 4530 cm^{-1}. The NIR spectra of M3.x do not show many characteristic features of mica and hence are projected across the negative PC4 region.

Principal component analysis of NIR spectral data show separation of foundation-type due to talc. Mineral-based samples separated due to the presence of mica. Loadings for PC's were affected by scatter effects and noise in data that inhibited the interpretation of results. PCA results may be improved if other scatter correction techniques such as normalization were investigated.

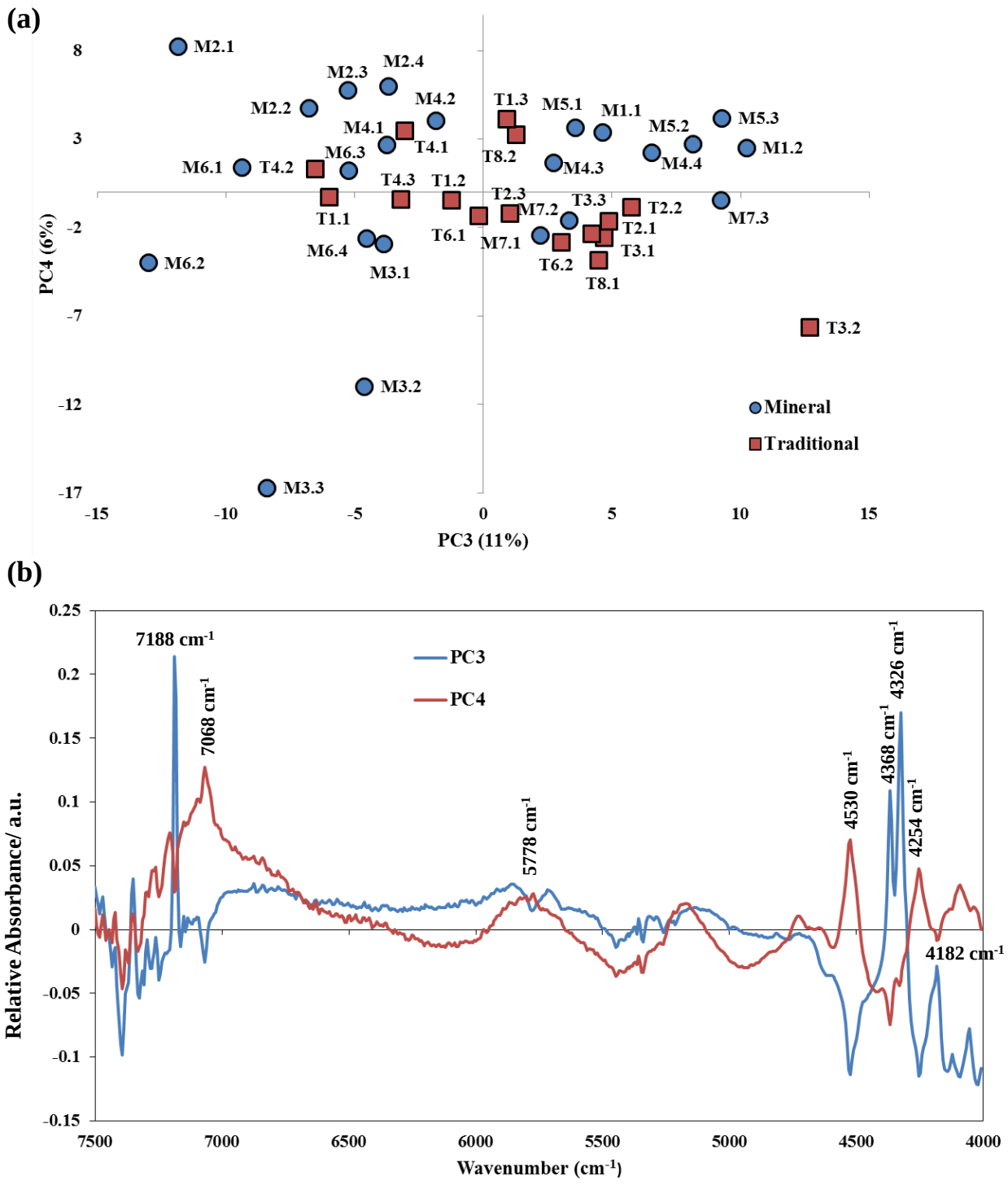

Figure 5.23 The scores plot (a) and the loadings plot (b) associated with PC3 and PC4 from PCA analysis of phase data obtained through diffuse reflectance spectroscopy in the near-infrared region of the 39 foundation samples.

5.3.8 Covariance and correlation (MIR and NIR)

Near-infrared spectral data was correlated with MIR spectral data to determine whether patterns could be found between the two data sets. A 2D covariance matrix was produced with MIR spectral data and XRD phase data for all samples to give,

$$\mathbf{\Phi} = NIR^{T}.MIR \qquad \text{(Equation 5.4)}$$

where NIR and MIR are the mean-centred data matrices obtained from spectra data (39 x 533) in the near-infrared region and spectral data in the mid-infrared region (39 x 599) respectively. Figure 5.24 shows a 2D covariance contour map of NIR vs. MIR, in which positive and negative correlations are displayed. The red colour indicates a positive correlation of NIR with absorption bands of the MIR spectral data. There is a positive correlation between the OH stretching of the Mg-OH bonds in talc at 1022 cm^{-1} in the mid-infrared region and 7180 cm^{-1} in the near-infrared region. Talc bands at 670 and 470 cm^{-1} positively correlate with talc bands at 4368, 4326 and 4182 cm^{-1}. Stearate band at 4326 cm-1 shows a correlation with a band at 1538 cm^{-1}, characteristic of zinc stearate. Positive correlation in the fingerprint and combination band regions was difficult to interpret due to overlap of component bands. It was expected the mica band at 4530 cm^{-1} in the NIR region would show correlation with mica bands in the MIR region, however, overlap of mica with talc and kaolin may be the cause.

Two-dimensional correlation was employed to aid in interpretation of the 2D contour map. A correlation slice of component was taken from the MIR data at a particular wavenumber, relating to a characteristic absorption band across all samples. For example, talc shows a characteristic band at 452 cm^{-1} and the correlation slice taken at this wavenumber. A correlation slice was taken for each component was then cross-correlated with the entire

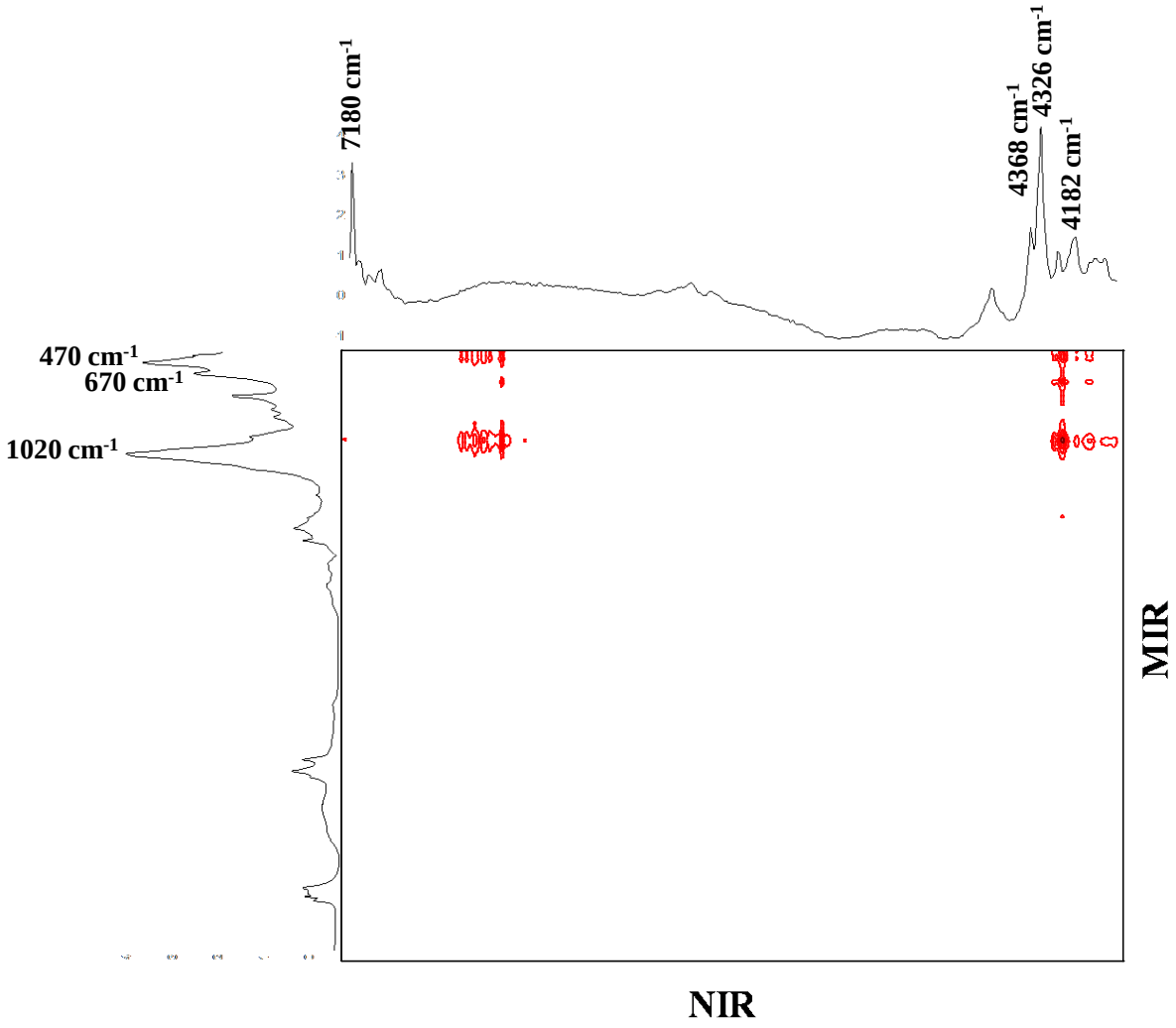

Figure 5.24 The 2D covariance contour plot of NIR vs. MIR. An average spectrum of each technique is presented along each axis to aid in interpretation, showing positive (red) correlations spectral bands of all foundation samples.

NIR spectral data to determine correlation coefficients. Initially, 2D correlation was conducted across all samples, and like the previous studies using this method, it produced poor results for certain components. However, relatively high correlation coefficients were produced for talc and magnesium stearate. The covariance slices for talc and magnesium stearate are displayed in Figure 5.25. Correlation of OH stretching band observed in the MIR

region, produced correlation coefficients of 0.85 and 0.90 with bands near 7180 and 4320 cm^{-1} respectively. Magnesium stearate produced a coefficient value of 0.73, correlating with the first overtone CH_2 stretching band of stearate at 5770 cm^{-1}. It was expected that magnesium stearate would highly correlate with bands near 4320 cm^{-1}, characteristic of combination CH_2 stretching of the NIR reference spectra of magnesium stearate. This was not the case, and the presence of other component band overlap may have contributed to this.

2D correlation was conducted using mineral samples. Once again it produced poor results for certain components, however, relatively high correlation coefficients were obtained for mica and kaolin. The covariance The MIR spectra of pearl and sericite mica exhibit similar characteristic features, therefore an absorbance band that was representative of both forms of mica was chosen to correlate with NIR spectra. The covariance slice of kaolin and mica with corresponding correlation coefficient values are displayed in Figure 5.26. Mica produced a correlation coefficient of 0.88 with a band near 7068 cm^{-1}, relating to a band observed in the reference spectra of pearl and sericite mica. The MIR absorbance band of kaolin correlated with a band near 4524 cm^{-1}, in which a coefficient value of 0.79 was obtained, due to Si-O stretching visible in the NIR reference spectra of kaolin.

Two-dimensional correlation using MIR spectral data was successful in confirming components in the NIR region. Once again, correlation across the entire sample set did not produce sufficient coefficient values for all components and to achieve the best results, mineral-based samples had to be analysed separately. Performing 2D correlation on the mineral-based sample set eliminated talc and hence highlighted absorbance bands of mica and kaolin. Generally, poor correlation coefficient values were obtained for absorbance bands in the 5000-4000 cm^{-1} region and not all bands could be successfully confirmed. Overlapping of component bands may have contributed to poor results in this region.

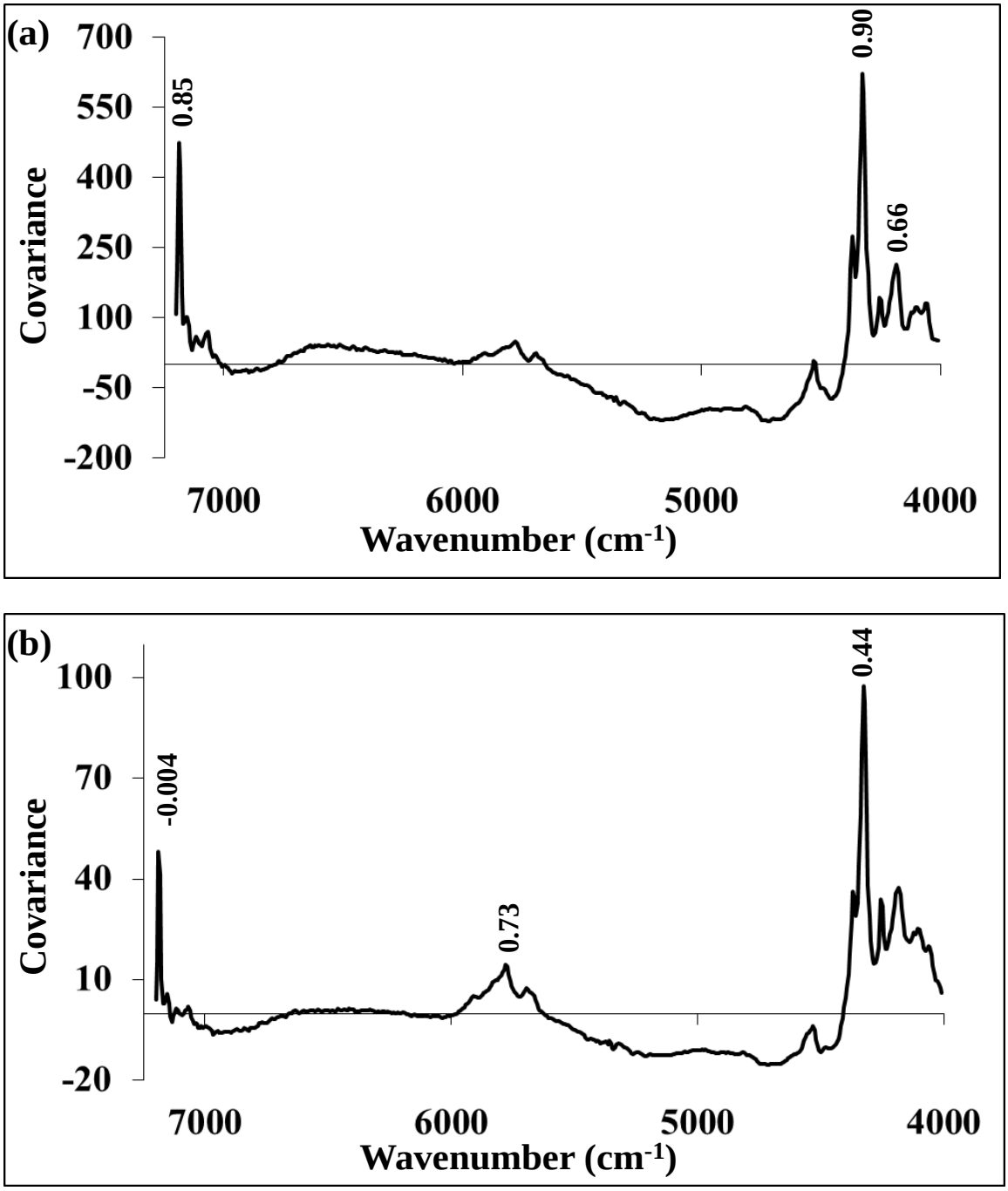

Figure 5.25 Covariance slices obtained from correlation of NIR and MIR data. The correlation coefficients relating to correlation of (a) Talc & (b) Magnesium stearate MIR absorbance bands with NIR spectral data of all samples.

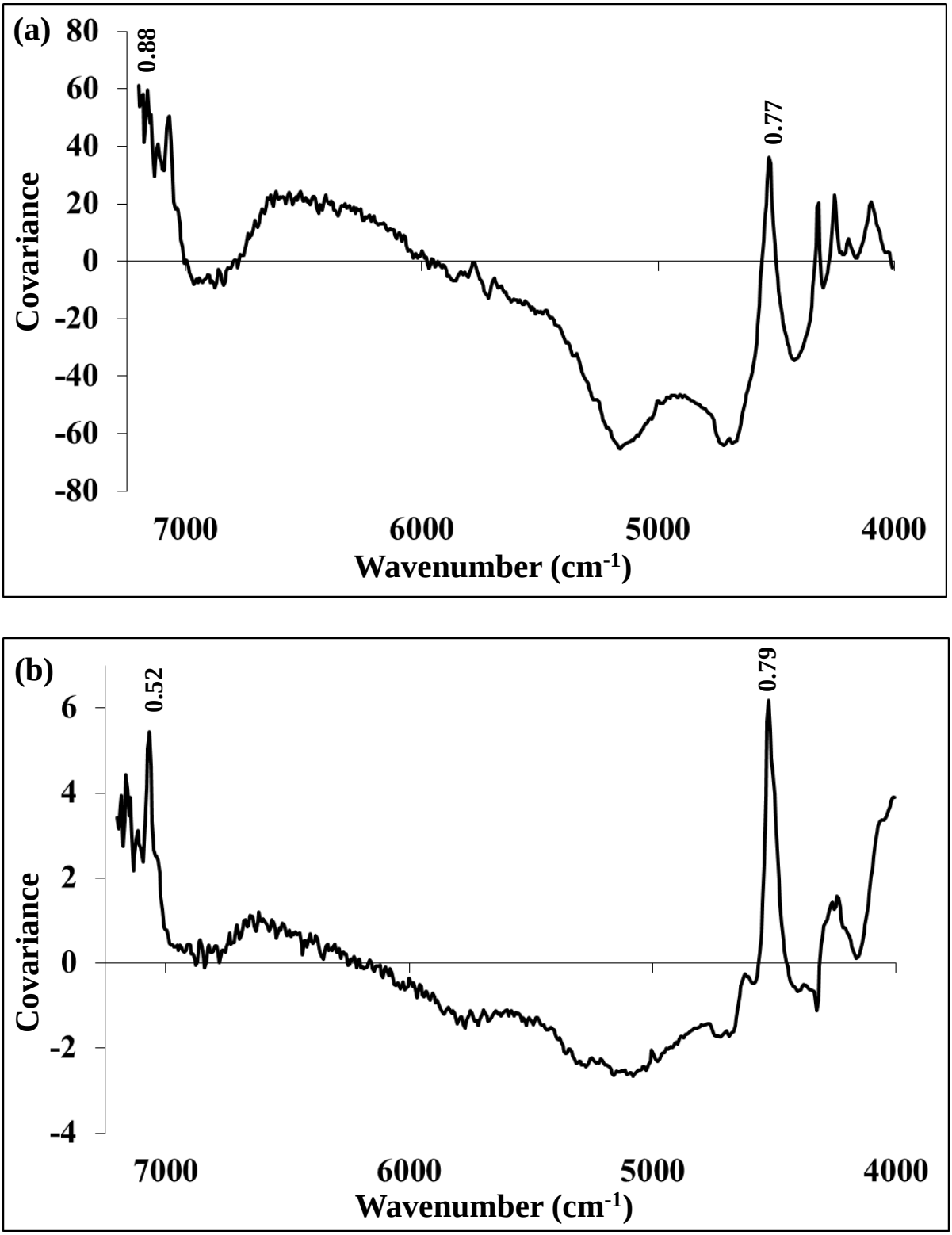

Figure 5.26 Covariance slices obtained from correlation of NIR and MIR data. The correlation coefficients relating to correlation of (a) Mica & (b) Kaolin MIR absorbance bands of mineral-based samples.

5.4 Conclusion

Application of FTIR to cosmetic foundation samples was successful in providing additional structural and chemical information, concerning the components used in their production. Spectral data obtained in the mid and near infrared regions gave a more complete analysis of samples. Analysis of reference spectra of known materials used in foundation production, verified chemical bonding of components within samples and spectra could be interpreted by eye.

Principal component analysis was effective in separating samples based on their structural and chemical composition.

Two-dimensional correlation of XRD phase data and MIR spectral data proved successful in finding a relationship between the two techniques. Correlation demonstrated that XRD data could aid in the interpretation of MIR spectra and validated the presence of components in samples that could not be visually identified.

Two-dimensional correlation of NIR and MIR displayed positive correlation of absorbance bands representative of talc. However, it was unsuccessful in highlighting positive correlation of the other components present due to overlap of bands.

5.5 References

1. V. C. Farmer, *The Infrared Spectra of Minerals*, Mineralogical Society, London, UK, **1974**.
2. K. W. Raymond & J. A. Corkhill, *Diffuse Reflectance Infrared Spectroscopy*, J. Chem. Educ, 1994, **71**(8): pA204.

3. T. T. Nguyen, L. J. Janik, M. Raupach, *Diffuse Reflectance Infrared Fourier Transform (DRIFT) Spectroscopy in Soil Studies*, Aust. J. Soil Res., 1991, **29**: p.49-67.
4. M. P. Fuller & P. R. Griffiths, *Diffuse Reflectance Measurements by Infrared Fourier Transform Spectrometry*, Anal. Chem., **50**(13): p.1906-1910.
5. G. W. McCarty, J. B. Reeves, V. B. Reeves, R. F. Follett and J. M. Kimble, *Mid-Infrared and Near-Infrared Diffuse Reflectance Spectroscopy for Soil Carbon Measurement*, Soil Sci. Soc. Am. J., 2002, **66**: p.640-646.
6. H. Cen & Y. He, *Theory and application of near infrared reflectance spectroscopy in determination of food quality*, Trends in Food Science & Technology, 2007, **18**: p.72-83.
7. M. Kransiz, A. Dominguez-Vidal, D. McNaughton and B. Lendl, *Fourier-transform infrared (FTIR) spectroscopy for monitoring and determining the degree of crystallisation of polyhydroxyalkanoates*, Anal. Bianal. Chem., 2007, **388**(5-6): p. 1207-1213.
8. T. Naes, T. Isaksson, T. Fearn, and T. Davies, *A user-friendly guide to Multivariate Calibration and Classification*, NIR Publications, Chichester, UK, **2002**.
9. M. S. Dhanoa, S. J. Lister, R. Sanderson and R. J. Barnes, *The link between Multiplicative Scatter Correction (MSC) and Standard Normal Variate (SNV) transformations of NIR spectra*, J. Near Infrared Spectrsc., 1994, **2**: p. 43-47.
10. M.U. A. Bromba and H. Ziegier, *Application Hints for Savitzk-Golay Digital Smoothing Filters*, Analytical Chemistry, 1981, **53**: p.1583-1586.
11. I. S. Helland, T. Naes, T. Isaksson, *Related versions of multiplicative scatter correction method for preprocessing spectroscopic data*, Chemometrics and Intelligent Systems, 1995, **29**(2): p.233-241.

12. R. J. Barnes, M. S. Dhanoa, S. J. Lister, *Standard Normal Variate Transformation and De-trending of Near-infrared Diffuse Reflectance Spectra,* Applied Spectroscopy, 1989, **43**(5): p. 722-777.
13. R. L. Frost & U. Johansson, *Combination bands in the infrared spectroscopy of kaolins- A DRIFT Spectroscopy study*, Clays and Clay Minerals (1998), **46**(4): p. 466-477.
14. J. Madejova, *FTIR techniques in clay mineral studies*, Vibrational Spectroscopy, 2003, **31**: p.1-10.
15. R. W. Berry, A. C. Rule, S. Guggenheim, *Teaching Clay Science*, The Clay Mineral Society, Colorado, USA, **2002**.
16. S. D. Wightman & A. Murray, *The identification of pigments in paper coatings by infrared spectroscopy*, The Internet Journal of Vibrational Spectroscopy, 1998, 3(3): p. 1-17.
17. S. Petit, F. Martin, A. Wiewiora, P. De Parseval, A. Decarreau, *Crystal-chemistry of talc: A near infrared (NIR) spectroscopy study*, American Mineralogist, 2004, **89**: p. 319-326.
18. P. A. Schroder, *Infrared Spectroscopy in clay science: in CMS Workshop Lectures, Vol. 11 Teaching Clay Science*, The Clay Mineral Society, Aurora, CO, **2002**.
19. M. Gilbert, I. Sutherland, A. Guest, *Characterization of coated particulate fillers*, Journal of Materials Science, 2000, **35**(2): p.391-397.
20. X. Luo, Z. Zhang, Y. Liang, *Structure of Cobalt Stearate & Cobalt Sulfide- Stearic Acid Langmuir- Blodgett Films*, Langmuir, 1994, **10**: p.3213-3216.
21. J. L. Post & L. Borer, *Physical properties of selected illites, beidellites and mixed-layer illite-beidellites from southwestern Idaho, and their infrared spectra*, Applied Clay Science, 2002, **22**: p.77-91.

22. H. Namduri and S. Nasrazadani, *Quantitative analysis of iron oxides using Fourier transform infrared spectrophotometry*, Corrosion Science, 2008, **50**: p.2493-2497.
23. P. Cambier, *Infrared Study of Goethites of varying crystallinity and Particle size: 1. Interpretation of OH and lattice vibration frequencies*, Clay Minerals, 1986, **21**: p. 191-200.
24. R. M. Cornell and U. Schwetmann, *The Iron Oxides: Structure, Properties, Reactions, Occurrences & Uses (2nd Ed.)*,Wiley-VCH Verlag Gmblt & Co., Weinheim, Germany, **2003**.
25. M. Jarlbring, L. Gunneriusson, B. Hussmann, W. Forsling, *Surface complex characteristics of synthetic maghemite and hematite in aqueous suspensions*, Journal of Colliod & Interface Science, 2005, **285**(1): p.212-217.
26. A. Rittermeier, S. Miao, M. K. Schroter, X. Zhang, M. W. E van den berg, S. Kundu, S. Schimpf, E. Loffler, R. A. Fischer and M. Muhler, The formation of colloidal copper nanoparticles stabilized by zinc stearate: one-pot single-step synthesis and characterization of the core-shell particles, Physical Chemistry Chemical Physics, 2009, 11(37): p.8358-8366.
27. R.D. Vold and G. S.Hattiangdi, *Characterization of Heavy Metal Soaps by X-Ray Diffraction*, Industrial and Engineering Chemistry, 1949, **41**(10): p.2311-2321.
28. V. Swaminathan and D. O. Kildsig, *An Examination of the Moisture Sorption Charcateristics of Commercial Magnesium Stearate*, AAPS PharmSciTech, 2001, **2**(4): p.73-79.
29. S. Petit, A. Decarreau, M. Martin, R. Buchet, *Refined relationship between the position of fundamental OH stretching and the first overtones for clays*, Phys Chem Mineral (2004), **31**: p.585-592.

30. R. L. Frost & U. Johansson, *Combination bands in the infrared spectroscopy of kaolins- A DRIFT Spectroscopy study*, Clays and Clay Minerals (1998), **46**(4): p. 466-477.

31. R. L. Green, M. D. Mowery, J. A. Good, J. P. Higgins, S. M. Arrivo, K. McColough, A. Mateos and R. A. Reed, *Comparison of Near-Infrared and Laser-Induced Breakdown Spectroscopy for Determination of Magnesium Stearate in Pharmaceutical Powders and Solid Dosage Forms*, Applied Spectroscopy, 2005, **59**(3): p.340-347.

Chapter 6: Conclusion and Future Work

6.1 Conclusion

X-ray diffraction and spectroscopic methods proved to be useful tools in the examination of material components in cosmetic foundation samples. The techniques employed provided information on the elemental, crystalline content, chemical composition and structure of cosmetic foundations, resulting in an extensive characterisation of their composition. These techniques were successful in confirming the material components of samples and were used complementary to provide a more complete means of analysis, with each technique interpreting or supporting the other.

Two-dimensional correlation was effective in highlighting relationships between analysis techniques. It was able to aid in interpretation of diffraction and spectral data, hence confirming the presence of material components in samples. Two-dimensional correlation of XRF and XRD use is limited as it is only successful for components that may have a single element that can be represented by a crystal phase. It was successful using bismuth, titanium and zinc Kα emission lines interpret diffraction peaks and confirm the presence of bismuth oxychloride, titanium dioxide and zinc oxide in samples. However, these components could not be confirmed in FTIR data using diffraction peaks. 2D correlation of MIR and XRD was better suited to confirming absorbance bands of talc, calcium carbonate, kaolin and mica. Near-Infrared versus Mid-Infrared confirmed the presence of components such as talc and stearates.

Principal component analysis was useful in visually displaying the similarities and differences between samples based on their composition. Through all characterization methods, foundation samples grouped consistently according to foundation-type and manufacturer. This indicates differences in the raw components incorporated into formulas between manufacturers. These components are from differing sources and that formulations vary in differing amounts of each component.

Cosmetic foundation samples could be discriminated by manufacturer based on the raw materials and the amount present in each sample. Certain so-called 'mineral' samples were classified as traditional samples, having the same raw components as traditional samples. This was consistent throughout all analysis techniques and separation of sample type was due to the presence of talc in traditional samples and larger amounts of mica in mineral-based formulations. There was a considerable variation in components between the foundation types. Traditional-based samples contained a larger variety of potential components. For example, calcium carbonate was only present in certain samples. Analysis of traditional samples could not determine the source/manufacturer but it could determine whether two samples were similar or not. The mineral-based samples exhibited similar components throughout the sample set, generally only varying in the amounts of each component. However, certain samples differed and contained bismuth oxychloride. Samples could be discriminated based on manufacturer.

The presence of iron oxides in samples was not thoroughly investigated in this study. X-ray Fluorescence was successful in determining the relative concentration of iron in foundation powders. However, XRD and FTIR could not confirm the presence of iron oxide and could not discriminate chemical form of iron oxide present in each sample.

6.2 Future Work

The current research has the possibility of expansion. Characterisation of the red, yellow and brown iron oxides would be beneficial and provide further knowledge on the material composition of cosmetic foundation powders. X-ray Diffraction could be employed for this analysis, using Co Kα radiation source to overcome the problem of fluorescence when recording iron.

Use of the powder diffraction beamline at the Australian Synchrotron could potentially be useful in identification of iron oxides. Mössbauer Spectroscopy could be used complementary to XRD, to identify iron oxides by examining the valence state of iron in each sample.

Far-infrared spectroscopy could be investigated to see whether it could provide structural information for bismuth oxychloride and other metal oxides, such as zinc and titanium dioxide, as those were not successfully identified in samples in the mid and near-infrared regions.

The analytical methods, procedures and data analysis protocols could be used to characterise other powder inorganic mixtures, whether they be other cosmetic products or not.